The Development of GFRP Bridge Deck Modules

A Project Report
Presented to
The Department of Civil Engineering
Faculty of Engineering
University of Manitoba

In Partial Fulfillment
of the Requirements for the Degree
Masters of Science in Civil Engineering (M.Sc.)

THE UNIVERSITY OF MANITOBA

FACULTY OF GRADUATE STUDIES

*****

COPYRIGHT PERMISSION PAGE

The Development of GFRP Bridge Deck Modules

BY

Brea Kelly Williams

A Thesis/Practicum submitted to the Faculty of Graduate Studies of The University of Manitoba in partial fulfillment of the requirements of the degree of Master of Science

Abstract

The highway infrastructure industry must meet a critical demand for the repair or replacement of thousands of bridge decks. These decks are reaching the end of their service lives and are suffering the effects of cracking and spalling concrete and corroding steel reinforcement.

This project investigates the replacement of these bridge decks with glass fibre reinforced polymer (GFRP) deck modules. These innovative modules offer lightweight, ease of installation and durability.

Wardrop Engineering Inc. designed prototype GFRP decks modules, which were then fabricated by Faroex Ltd. These were tested under a simulated truck wheel load to failure. All modules in this test phase surpassed the required AASHTO HS30 design truck loading for which they were designed.

Based on the promising results from the prototype specimens, full-scale specimens were produced. These specimens incorporated several design changes intended to improve their behaviour over the prototype modules. These modules performed well, demonstrating enhanced load capacity and stiffness.

An analytical model was also developed to predict the load-deflection behaviour of the decks in service load ranges. Measured behaviour appears to agree well with that predicted by the model.

Table of Contents

List of Figures

Chapter One

Chapter Two

Chapter Three

Chapter Five

List of Tables

Chapter Two

Chapter Three

Chapter Four

$A_{ellipse}$ = area of elliptical portion of filler bar in deck cross section

A_{total} = total area of filler bar in deck cross section

A_i = area of element of deck cross section

$[A]$ = extensional stiffness matrix of laminate

$[B]$ = coupling stiffness matrix of laminate

$[D]$ = bending stiffness matrix of laminate

E_{11} = modulus of elasticity of lamina in direction of fibre length

E_{22} = modulus of elasticity of lamina in direction transverse to fibre length

$E_{composite}$ = modulus of elasticity of composite (matrix and fibres)

E_f = modulus of elasticity of fibres

E_m = modulus of elasticity of matrix

$E_{xx-effective}$ = effective modulus of elasticity of a laminate in the x-direction

$E_{yy-effective}$ = effective modulus of elasticity of a laminate in the y-direction

G_{12} = longitudinal shear modulus of lamina

G_f = shear modulus of fibres

G_m = shear modulus of matrix

$G_{xy-effective}$ = effective shear modulus of a laminate

h = total thickness of laminate

h_{j-1} = distance from midplane of laminate to the top of the j^{th} lamina in consideration

h_j = distance from midplane of laminate to the bottom of the j^{th} lamina in consideration

I_{bar} = local moment of inertia about x-axis of filler bar in deck section

$I_{ellipse}$ = local moment of inertia about x-axis of elliptical portion of filler bar in deck section

I_{global} = moment of inertia about x-axis of overall deck cross section

I_{rect} = local moment of inertia about x-axis of rectangular portion of filler bar in deck section

I_x = local moment of inertia about x-axis of elements in deck cross section

k_{xx} = bending curvature in the x-direction in the laminate

k_{yy} = bending curvature in the y-direction in the laminate

k_{xy} = twisting curvature in the laminate

L = span of bridge deck

M_{xx} = bending moment resultant in the yz-plane (per unit width of laminate)

M_{yy} = bending moment resultant in the xz-plane (per unit width of laminate)

M_{xy} = twisting moment resultant (per unit width of laminate)

N = total number of laminas in a laminate

N_{xx} = normal force resultant in the x-direction (per unit width of laminate)

N_{yy} = normal force resultant in the y-direction (per unit width of laminate)

N_{xy} = shear force resultant (per unit width of laminate)

n = equivalence factor to account for different stiffness in elements of deck cross section

P = load applied to bridge deck

$[Q]$ = intermediate lamina stiffness matrix (assumes $\theta = 0°$ or $90°$)

$[\overline{Q}]$ = global lamina stiffness matrix

$[S]$ = laminate stiffness matrix
$T_{composite}$ = tensile strength of composite (matrix and fibres)
T_f = tensile strength of fibres
T_m = tensile strength of matrix
t_{lamina} = thickness of lamina
$\{U\}$ = angle invariant properties of lamina
v_f = fibre volume ratio of composite = (volume of fibres)/(total composite volume)
v_m = matrix volume ratio of composite = $1 - v_f$
x-y-z: global axis system of a lamina
$\bar{y}_{bar}$ = centroid of filler bar in deck cross section, with respect to bottom of bar
$y_{centroid}$ = centroid of overall deck cross section, with respect to bottom of section
$\bar{y}_{ellipse}$ = centroid of elliptical portion of filler bar in deck cross section
$\bar{y}_i$ = centroid of element in deck cross section, with respect to bottom of section
1-2-z: principal axis system of a lamina
Δ = theoretical deflection of FRP deck at midspan
ε_{fail} = tensile strain at failure of laminate
ε°_{xx} = midplane normal strains in the x-direction of the laminate
ε°_{yy} = midplane normal strains in the y-direction of the laminate
γ°_{xy} = midplane shear strains in the laminate
ν_f = Poisson's ratio of fibres
ν_m = Poisson's ratio of matrix
ν_{12} = major Poisson's ratio of lamina
ν_{21} = minor Poisson's ratio of lamina
θ = fibre orientation angle; angle between the 1-axis and the x-axis

CHAPTER ONE:

INTRODUCTION

1.1 General

The demand for the development of more efficient and durable bridge decks is at the forefront of the priority of highway authorities worldwide. This need stems from the fact that many bridge structures are reaching the end of their service lives, many have succumbed to the effects of deterioration of concrete and steel and many cannot meet the new code's truck load demands. A typical example of a deteriorated deck is shown in Figure 1.1. This severely deteriorated bridge structure was constructed in 1926 in New York State at Bennetts Creek.

The two possible solutions to the problem are repair or replacement. The cost associated with the replacement of such a large number of bridges is estimated to be in the billion-dollar range around the world. To reduce cost, the current trend is to retain the existing substructure and repair or replace the crumbling bridge decks.

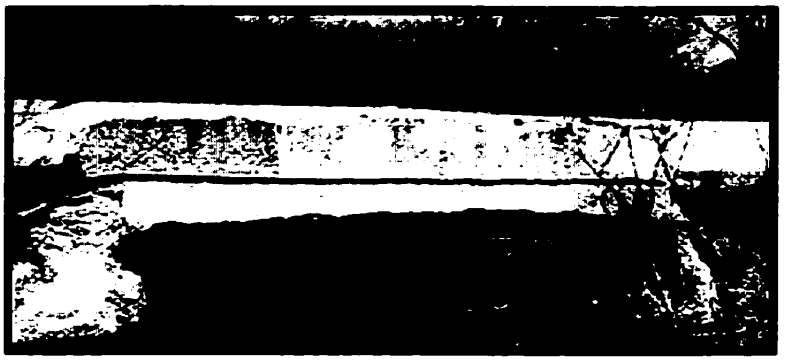

Figure 1.1: Bennetts Creek Bridge in New York State (Black, 2000)

The initial approach for many civil engineers would be to repair the deck with more reinforced concrete. However, this solution would only delay the inevitable deterioration before the same repair would be required again. As well, repairing with concrete would significantly increase the dead load of the structure. The disadvantages associated with using reinforced concrete are not only limited to material aspects. The installation of the concrete deck itself is a time-consuming, laborious task that will delay traffic for a significant period of time while the concrete is prepared, cast and cured.

A new alternative, which has been developed in recent years, is to use fibre reinforced polymer (FRP) modular bridge decks to reduce the large structural self weight as well as to avoid durability problems due to corrosion.

1.2 Objective

The main objective of this thesis is to examine the structural performance of GFRP bridge decks that have been designed and fabricated with industrial partners. The research focusses on the fabrication process using filament winding technology to

produce durable, safe and economical GFRP bridge decks. The research also includes an experimental and analytical phase to study various parameters believed to affect the deck behaviour.

1.3 Scope

This thesis investigates the development of FRP modular bridge decks. In particular, it follows the development of a deck designed by Wardrop Engineering Inc. and fabricated by Faroex Ltd. The deck modules were tested by ISIS Canada at the McQuade Structural Lab at the University of Manitoba.

Chapter Two begins with an extensive discussion of the material characteristics of FRPs, including the manufacturing process. Review of the current activities in this field in the United States is discussed in Chapter Two along with some of the field application of this technology for pedestrian and rural highway bridges.

Chapter Three introduces the concept of the bridge deck developed during the course of this thesis. The experimental program, test setup and instrumentation are presented. Step-by-step description of the patented fabrication process is included.

Chapter Four discusses the results and analysis of the test results. Major areas of focus include the behaviour of the deck modules under simulated wheel loads, the mode of failure of the decks as well as an in-depth analysis of the strain behaviour of the decks.

This extensive analysis was performed in order to establish the FRP deck modules as a safe, efficient and high performance structural technology.

Chapter Five introduces an analytical model developed to predict the load-deflection behaviour of the FRP decks in the service load range. The theory and assumptions used in the model are also reviewed. A comparison of theoretical versus the measured values is presented to verify the model prediction capability. Finally, test results from similar research are compared against the results from this test program in order to evaluate the viability of this particular deck product on the market.

Major conclusions and observations are highlighted in Chapter Six, with a brief discussion of the future direction of the research work needed for this project.

1.4 Acknowledgements

I would like to thank the following groups for their collaboration and financial support on this project.

- ISIS Canada;
- Wardrop Engineering Inc.;
- Faroex Ltd.;
- NSERC;
- NRC – IRAP; and,
- Manitoba Industry, Trade and Mines.

I would also like to thank the following people for their contribution to the research.

• Dr. Rizkalla for his perpetual support and guidance, and for always challenging me to surpass my own expectations;

• Moray McVey for his technical expertise, patience and sense of humour, which proved essential to my successful work in the lab; and,

• Scott Sparrow and the graduate students of the McQuade Structural lab for their invaluable assistance with the lab work.

CHAPTER TWO:

LITERATURE REVIEW

2.1 Infrastructure Challenges

The highway infrastructure industry faces a large task to repair and/or replace thousands of bridge decks across North America. This task must be met with ingenuity and innovation in order to efficiently tackle the matter and prevent future infrastructure crises.

It has been documented that over half of the United States' 600 000 state, county and city bridges were built prior to 1940 (Zureick et al, 1995). Naturally these bridge decks are now reaching the end of their useful service lives. The expected deterioration processes associated with conventional materials have occurred – corrosion of steel structural members and steel rebar (Salim et al, 1997), and spalling and cracking of concrete related to sulfate attack and other chemical processes. The heavy weight of the concrete and steel decks has also led to a reduced load capacity, yielding many decks inadequate for

the standard live load demands of today. The combination of material deterioration and substandard load ratings has led to 200 000 US bridge structures being classified as structurally deficient or functionally obsolete (Zureick et al, 1995).

The typical response to this problem is to replace the deteriorated deck with the same traditional materials - the conventional material that by virtue of its weight is difficult to place and leads to long traffic delays; the same heavy steel-reinforced concrete which is susceptible to corrosion; the "safe" material that continues to be specified because of its familiarity in the civil engineering community (Owens Corning, 1999).

Some attempts have been made to alleviate the corrosion problem. In fact, much money has been dedicated to research of delaying the onset of corrosion through use of cathodic protection, epoxy-coated reinforcement and galvanized steel reinforcement. However, employing these methods only delays the inevitable outcome of reinforcement corrosion and the subsequent spalling and deterioration of the concrete bridge deck.

In recent years the use of fibre reinforced polymer (FRP) bars for concrete reinforcement has been investigated and found to yield promising results. The FRP material is lightweight, high strength and does not corrode. Use of FRP reinforced concrete would appear to be a possible solution to the deterioration problem of the rebar. However, there still exists the concrete's susceptibility to durability attack as before.

As an innovative alternative, which completely eliminates the durability issue of the concrete, this project proposes the use of a bridge deck system consisting entirely of FRP The light weight of the FRP deck allows for an increased load rating and the bridge no longer being labeled as functionally obsolete. The corrosion resistance of the deck extends the service life beyond what would have been possible with conventional materials. In short, FRP bridge decks could be a long-term solution to the infrastructure crisis facing the world today.

2.1.1 Problems with Current Materials

For years, steel and concrete have been the preferred building materials of civil engineers. Although these materials perform satisfactorily, using them means dealing with their disadvantages.

Placement of steel reinforcement in the bridge deck can be an awkward job given the cumbersome nature of the elements. Added to this are the many hours of labour required to prepare, cast and cure the concrete. The disadvantages are not limited to installation either. Concrete is highly susceptible to many combinations of attacks from moisture, chloride penetration and sulfate attack. All of these lead to cracking and spalling of the concrete, which only enhance further material degradation.

While the concrete undergoes deterioration, the elements necessary for initiation of steel rebar corrosion move in towards the steel. Oxygen, water and chlorides react at the steel surface causing corrosion of the rebar, reducing its cross section. As a result of the

deterioration of concrete material and steel rebar, the bridge deck can no longer be expected to resist the original loads for which it was designed and the deck becomes substandard.

This scenario is occurring all over North America: aging and deteriorating bridges are in need of repair or replacement. Clearly, solving the problem by using the same materials that contributed to the problem in the first place is not using engineering technology to its full capacity. The degradation would only be delayed for a number of years until the same situation was revisited.

2.1.2 Aspects of a New Material

A different material should be used in construction which meets the original material concerns directly.

First, the lightweight properties of an FRP bridge deck would solve several problems. It would allow for easier handling and installation, consequently minimizing the required manpower. There would also be the potential for more rapid installation, thus reducing disruption to traffic. Overall, the cost of placement would be driven down due to the efficiencies of installation. A final advantage of a low weight deck is that with the reduced self-weight of the structure, the load capacity could be increased so that the deck can resist current load demands.

Second, a deck with lasting durability would eliminate many of the problems discussed in the previous section. Without steel corrosion and concrete cracking, a structure retains its structural integrity much longer. In addition, its service life is extended, therefore the associated life cycle costs are spread over a longer period and are reduced. Finally, with durable and reliable decks in service, repairs and maintenance to the structure will be drastically reduced.

2.1.3 Concept of Proposed Deck

This project introduces a new generation of bridge decks designed as a solution to bridge deck deterioration. The FRP deck is designed by Wardrop Engineering Inc. and produced by the filament winding technique by Faroex Ltd. in Gimli, Manitoba. Further details as to manufacturing process of the deck follow in the Experimental Program.

Goals of the deck concept are to produce a repeatable set of deck modules which can be installed within hours of arriving at the bridge site. The deck must be durable, lightweight and capable of withstanding a load comparable to an HS30 design truck as specified by AASHTO. Most importantly, this must be achieved at a cost competitive with conventional methods of replacement.

As with any relatively new material, advanced composites have been judged with more perception than with data (Owens Corning webpage, 1999). The uneasiness to use the material has been compounded by the initial high cost associated with the advanced material. Throughout this research, then, the vital aspect of cost minimization has been

kept at the forefront of production considerations. Any deck produced must be considered cost competitive in order to appear attractive to the engineering community (Bernetich et al, 1996). Otherwise, the end product that was so heavily researched will be too expensive to be feasibly applied anywhere.

At the same time, despite the importance of cost reduction one must look at the bridge deck as more than its constituent materials. The initially higher materials costs can be offset by factors including extended service life, reduced maintenance and a much higher load capacity (Owens Corning webpage, 1999).

It is this fine balance between structural performance and production costs that was so carefully considered and reassessed throughout the duration of this project.

2.2 FRP Materials

This section provides an overview of fibre reinforced polymer (FRP) materials, from their components to their manufacturing process.

FRPs consist of two components: fibres and matrix. The fibres possess high strength and modulus, and are the main source of load resistance in any composite material. The matrix is the medium in which the fibres are embedded, holding them in place and protecting them from harsh environmental conditions like humidity, extreme temperatures and UV. In addition, the matrix transfers applied load to the fibres through shear force interaction.

There are various types of fibres available to manufacturers including aramid, kevlar, glass and carbon, the latter two being most prevalent in recent years. As well, there are several matrix varieties available, all of which fall into one of two groups: thermoset or thermoplastic. A thermoset matrix is one that is permanently set once heated, while a thermoplastic matrix becomes soft and malleable upon reheating and only hardens once cooled.

Due to their composition, FRPs possess several advantages over conventional materials. First, they are capable of attaining a high strength, depending on the type of matrix and fibres used and the fibre to matrix volume ratio. In fact, some FRP bridge decks have reportedly displayed six to seven times the load capacity of reinforced concrete decks (Owens and Corning, 1999). One of the unique properties of FRPs related to strength is that they display linear-elastic stress-strain behaviour up until failure, as shown in Figure 2.1.

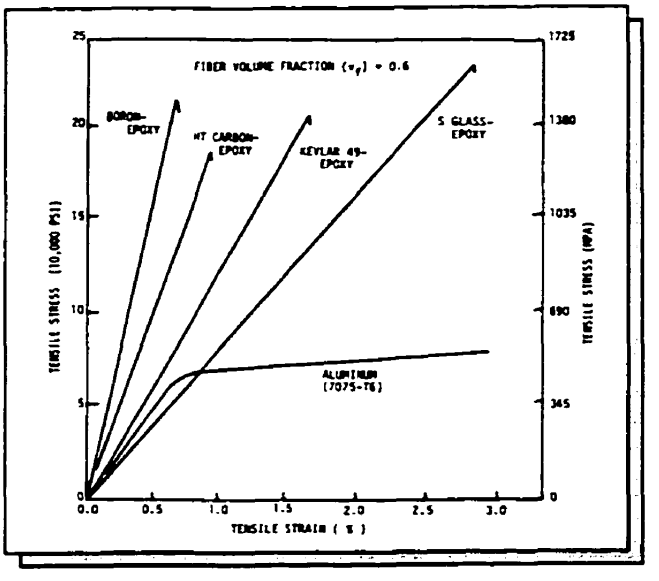

Figure 2.1: Stress-Strain Comparison Between FRP and Steel *(Mallick, 1993)*

Another valuable quality of FRPs is that they are lightweight. The low-density matrix allows for this to be possible. The low material weight of FRP components means that less labour is involved and that faster installation is possible. The end result is a reduced traffic delay on-site, and lower installation costs overall.

A third and very significant advantage of FRPs is that they are essentially corrosion resistant. The matrix contains several chemicals which protect the fibres from most chemical and temperature aggressors. With a durable construction material, costly maintenance and repairs over the life of a structure are eliminated.

FRPs also offer design flexibility to the engineer. The various composite manufacturing processes available allow for composites to be produced into almost any shape and size imaginable. This means that FRP components can meet the demands and specifications of a wide range of civil engineering projects.

Finally, FRPs do indeed have a proven reputation – a fact that is sometimes lost on those unfamiliar with the material. FRP technology has been used successfully in the boat manufacturing and aerospace industries for over 40 years (MMM webpage, 1999). This wide base of experience should provide the confidence necessary to use composites in construction.

The initial cost of FRP materials is relatively higher than steel or concrete. However, initial materials costs cannot be the single deciding factor in a construction project.

Overall life cycle costs must instead be considered, as well as the additional advantages gained from using FRP materials. Figure 2.2 summarizes the key advantages gained from FRP use.

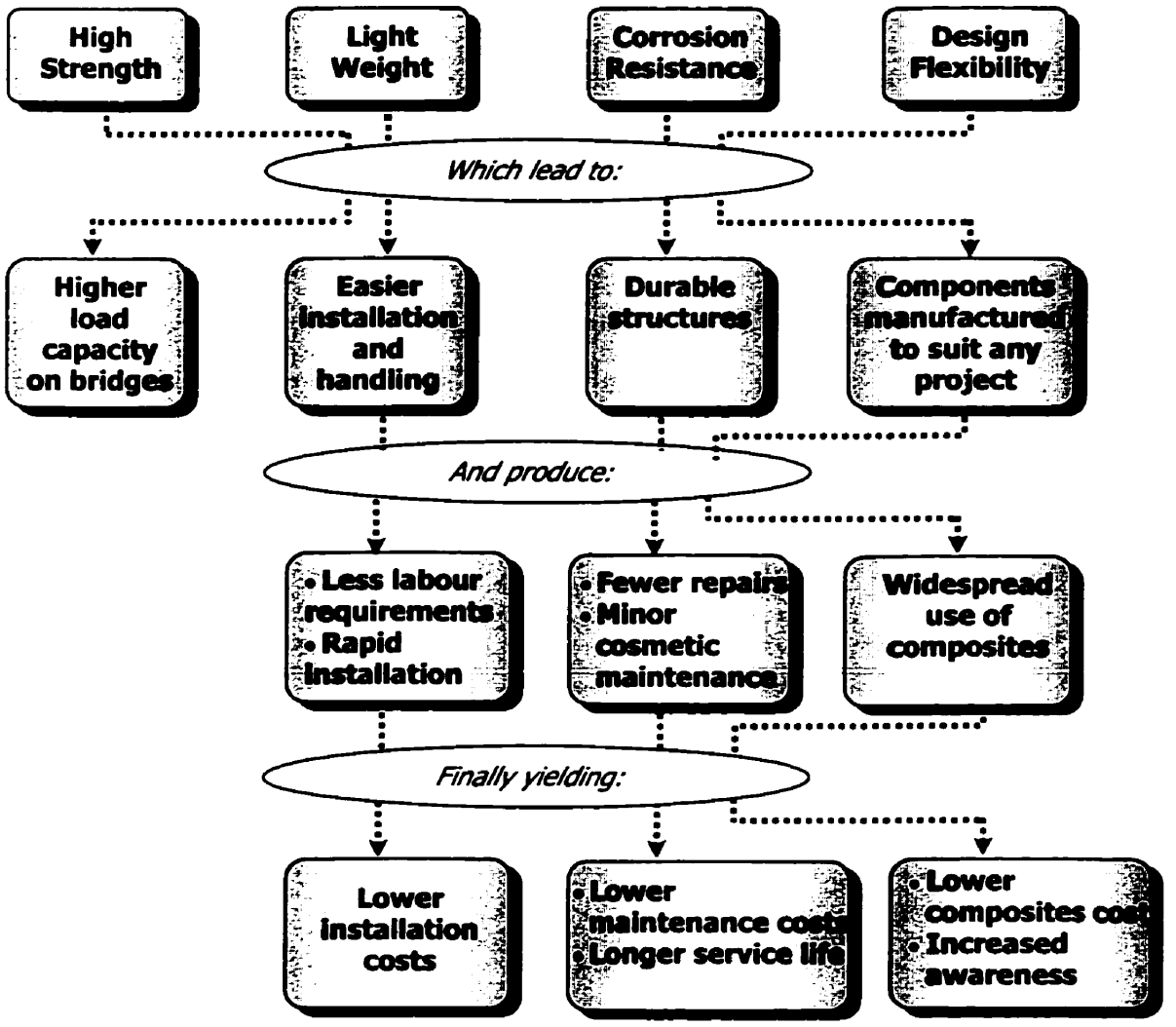

Figure 2.2: Advantages of FRP Use

2.2.1 Composite Matrix

The matrix of any composite material plays various roles in its performance. It protects fibres from mechanical abrasion, it transfers stresses to and between fibres, and it protects fibres from adverse environmental conditions.

When selecting the matrix material, several key issues must be considered. First, interaction between the chosen matrix and fibres is very important, therefore compatibility between the two is a necessity. The processability of the composite component depends to a large degree on the matrix properties, which in turn affect the physical and thermal characteristics of the end product. Finally, the selected matrix has a major influence on a composite's interlaminar shear strength as well as affecting its inplane shear strength. By providing lateral support, the matrix can even prevent fibre buckling, thus influencing compressive strength as well.

There are several properties desired in a matrix, including:

- high tensile modulus, which influences compressive strength of the composite;
- high tensile strength, which controls cracking between laminas;
- high toughness, which affects ply delamination and crack growth;
- dimensional stability in adverse environments; and,
- resistance to moisture and solvents, such as antifreeze, gasoline and deicing fluids.

Given the wide range of influences a matrix has, it is clear that its selection is very important in the overall composite design.

The matrix material can be metallic, ceramic or polymeric, however only the latter is considered in this discussion. By definition, a polymer is a long-chain molecule containing one or more repeating units of atoms joined together by strong covalent bonds.

Polymers possess a number of unique qualities. Their mechanical properties depend strongly on ambient temperature and loading rate. For instance, with increases in temperature, the matrix becomes rubber-like and undergoes large elastic deformations. As the temperature approaches the glass transition temperature (T_g), the matrix transforms from hard (glass-like) to soft (leather-like) with a low surface hardness. When high loading rates are applied, polymeric matrices display brittle behaviour, while at lower loading rates, they behave in a ductile manner as shown in Figure 2.3.

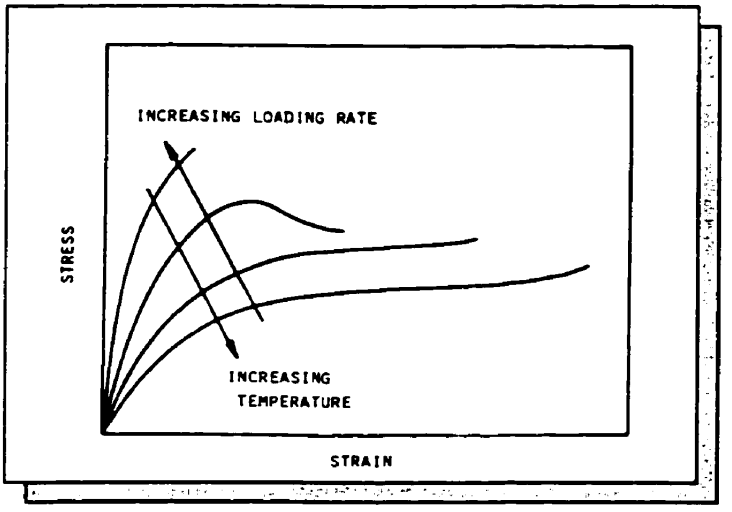

Figure 2.3: Stress-Strain Behaviour of Polymers Under Varying Loading Rates *(Mallick, 1993)*

Within the polymeric matrix classification, a further division can be made between thermoplastic and thermoset materials.

2.2.1.1 Thermoplastic Polymers

Thermoplastic materials are processed so that they set upon cooling but can be remolded and reshaped when reheated. This is because the individual polymeric molecules forming the material are linked only by weak hydrogen bonds and van der Waals forces. Therefore, when heat is applied, the bonds are easily overcome allowing the polymer to be reshaped.

Thermoplastic polymers possess a number of positive attributes not available with the other polymeric matrix alternative. These include:

- unlimited shelf life;
- shorter fabrication time;
- ease of handling due to lack of tackiness;
- high impact strength;
- low moisture absorption; and,
- good dimensional stability at elevated temperatures.

Despite these good qualities, thermoplastic polymers have not been the choice material for composite construction. Because of their high viscosities, it is difficult to incorporate continuous fibres into thermoplastic matrices. Also, thermoplastic matrices demonstrate lower creep resistance and thermal stability than thermoset polymers (Mallick, 1993). As

a result, much engineering development has been applied to thermoset polymers, as explained in the next section.

2.2.1.2 Thermoset Polymers

After being heated to their cure temperature and cooled, thermoset polymers become permanently set and cannot be remolded. This is due to the polymeric molecules being chemically bonded with cross-links, forming a rigid structure.

Thermoset polymers are the preferred material in commercial use for these reasons:

- low viscosity in production, allowing fibres to get fully wet;
- thermal stability;
- chemical resistance; and,
- less creep and stress relaxation.

However, they also possess some disadvantages, including:

- limited shelf life;
- low strain to failure; and,
- low impact strength.

Three of the most prominently used thermoset polymers are described in more detail below.

a. Epoxy

This material begins as a low molecular weight organic liquid resin. Dilutants are added to reduce viscosity and improve impact strength. The curing reaction is initiated just prior to addition of fibres and is achieved by addition of a curing agent. The type of agent used determines whether curing can be done at room temperature or if elevated temperatures are required.

If the cross-link density between polymeric molecules can be increased, the resulting epoxy resin will have a higher tensile modulus and thermal stability, but its toughness will be reduced. This cross-link density can be affected by the resin composition at the start of the reaction, as well as the temperature and length of cure.

Epoxy resins undergo a low shrinkage during curing, and possess excellent resistance to chemicals and solvents. In addition, they have very good adhesion to fillers and fibres, which is a highly desirable quality in composite design. Drawbacks include higher material costs, and a longer cure time than other matrix varieties.

b. Polyester

Polyester starts as an unsaturated polyester resin. It is similar to epoxy resin in that its properties are dependent on its cross-link density. The cross-link density is affected by the number of unsaturation points in the uncured polyester material, which can be varied by altering the weight ratio of different ingredients making up the polyester. As such, polyesters are available in a wide range from hard and brittle to soft and flexible.

Low viscosity, rapid cure and low cost are among the advantages of using polyester resin. However, this material does display a large amount of shrinkage at curing. Although this does allow for easier release of the parts from the mold, the amount of resin shrinkage is significantly different from that of the fibres. This incompatibility creates unsightly depressions in the surface of the finished product.

c. Vinyl Ester

This material begins as an unsaturated vinyl ester resin. It has fewer cross-links than polyester resin, providing it with more flexibility and higher toughness.

The advantage of vinyl ester is that it combines the positive aspects of epoxy and polyester. Vinyl ester has the good chemical resistance and high tensile strength of epoxy resin, as well as the low viscosity and fast cure of polyester resin without the high shrinkage. Electrical and thermal insulation properties are excellent, in addition to its high impact resistance and low permeability to water. Although vinyl ester has only a moderate adhesive strength to fibres, it has very good compatibility with both glass and carbon fibres. The next table summarizes the properties of the materials discussed.

Material	Tensile Strength [MPa]	Elastic Modulus [GPa]	Poisson's Ratio	Specific Gravity	Thermal Expansion [10^{-6}/°C]	Cure Shrinkage [%]	Heat Deflection Temperature [°C]
Epoxy	55-130	2.75-4.10	0.20-0.33	1.2-1.3	50-80	1-5	103
Polyester	34.5-103.5	2.1-3.45	-	1.1-1.4	-	5-12	60-205
Vinyl Ester	73-81	3-3.5	-	1.12-1.32	-	5.4-10.3	93-135

Table 2.1: Typical Properties of Polymeric Resins
(Mallick, 1993)

2.2.2 Fibres

The principal component of a composite is fibres. They may be present in the form of long continuous fibres or short discontinuous fibre mats. Whatever form they take, fibres resist the majority of the applied structural load.

The fibres themselves, also referred to as filaments, are very small in diameter. A single filament has a diameter of only 10μm. The small size of filaments makes them difficult to handle, so instead a large number of them are placed together in bundles called strands.

Fibres on their own display linear stress-strain behaviour. They fail in a brittle mode at very low strains, without displaying any yielding prior to this point. The lack of fibre yielding makes them prone to damage due to handling or contact with other surfaces. In addition to handling difficulties, fibres also break easily during composite production, resulting in frequent manufacturing slowdowns.

When long continuous fibres are used, the highest strength and modulus is achieved in the direction along the fibre, while the lower strength and modulus is attained transverse to it. Fibre mats, with a random distribution of short fibres, always display a lower strength than continuous fibre mats. With the random fibre orientation though, there is the possibility that the mat will provide a strength nearly equal to that of continuous fibres.

As is the case with the composite matrix, proper selection of fibre type, amount and orientation is crucial to the processability, performance and economy of the final composite. The choice of fibres directly affects the composite's:

- specific gravity, and consequently the weight;
- tensile strength and modulus;
- compressive strength and modulus;
- electrical and thermal conductivities; and,
- cost.

Fibres available for manufacturing include glass, carbon, and aramid, however only the first two are discussed in detail.

2.2.2.1 Glass Fibres

Glass fibres are the most common of all commercially available fibres for polymeric composites. The main reason for their widespread us is the low material cost coupled with a high tensile strength, high chemical resistance and excellent insulating properties. Glass fibres do suffer some drawbacks such as a low tensile modulus, relatively high specific gravity, low fatigue resistance and sensitivity to abrasion during handling and high hardness. The abrasion problem leads to a reduction in tensile strength while the high hardness results in excessive wearing on cutting tools used on the composite.

Internally, the glass fibre structure is a three-dimensional, long network of silica, oxygen and other randomly oriented atoms. The random orientation implies that glass fibres are

amorphous and isotropic. It is important to note the low content or absence of two compounds from the glass fibre composition, namely Na_20 and K_20. The presence of Na^+ and K^+ ions would lower the pH of the composite environment, creating a situation conducive to corrosion. Therefore, the absence of these ions in glass fibres means that the fibres have enhanced corrosion resistance to water (Mallick, 1993).

There are two subgroups of glass fibres, denoted E-glass and S-glass. E-glass has the lowest cost of all commercially available fibres, and is the most widely used. S-glass, on the other hand, has higher tensile strength, but its compositional differences from E-glass and its higher manufacturing costs make it more expensive than E-glass. Although E-glass appears very attractive to users, there is the warning that is should not be used in environments where the pH is less than 3 or greater than 10, for fear of corrosion. This claim has been disputed in literature (Marshall Industries, 1997).

Commercially, glass fibres are available as unidirectional roving or in woven roving form. An example is shown in Figure 2.4.

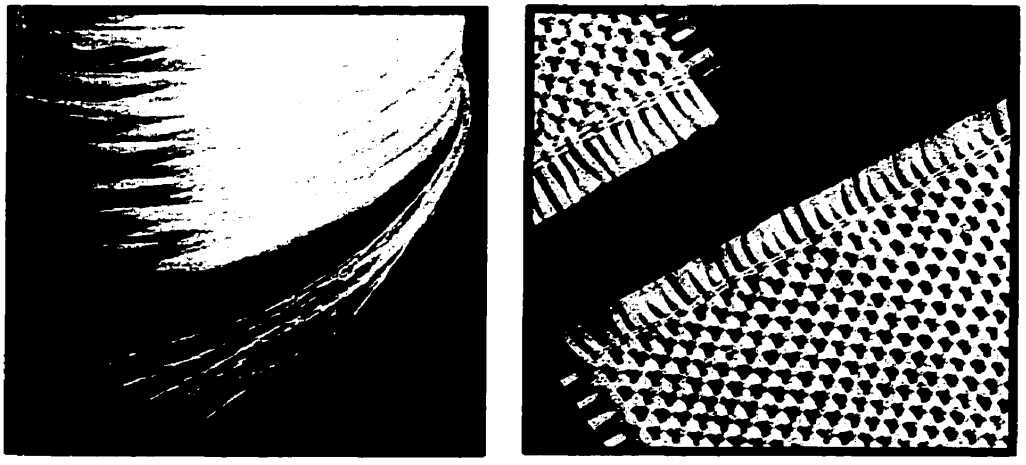

Figure 2.4: Glass Fibre Roving and Woven Roving (Mallick, 1993)

The woven roving is formed from unidirectional continuous roving laid in two perpendicular directions to create a coarse fabric. Further, woven roving can even be bonded with a layer of chopped fibres to produce a woven roving mat.

As mentioned earlier, glass fibres experience some unique problems. When they are first produced, the fibres have a strength of around 3.45 GPa. However, surface damage produced by abrasion, either by rubbing the glass fibres against each other or by contact with processing equipment, reduces this strength to 1.72 to 2.07 GPa.

Another element that causes a reduction in strength is water and fatigue loading. Water leaches alkalis out from the fibre surface and deepens flaws already present from processing. Under sustained loading, growth of flaws is accelerated and the tensile strength reduced with increased duration of loading. Figure 2.5 illustrates this concept.

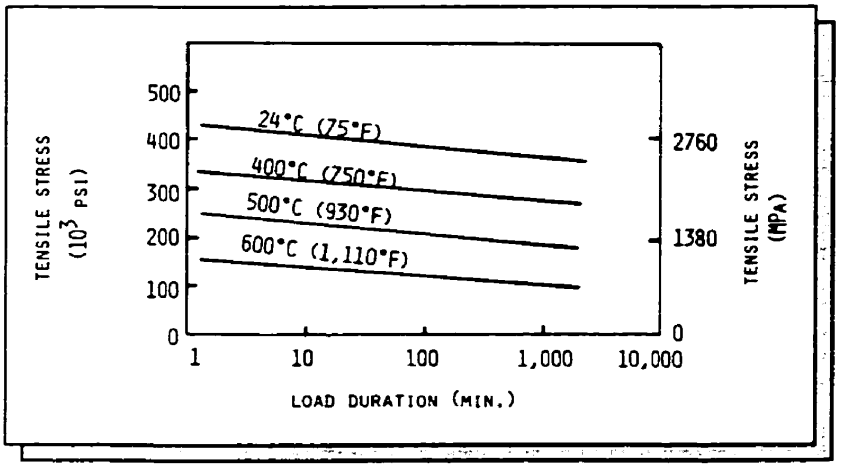

Figure 2.5: Loss of Tensile Strength with Time and Temperature *(Mallick, 1993)*

2.2.2.2 Carbon Fibres

Carbon fibres are a second type of fibre whose use is relatively widespread. They are available with an extremely wide range of tensile moduli, from 2.07 GPa to 1035 GPa.

The low modulus fibres have considerably different properties. The low modulus fibres have low specific gravity, higher tensile and compressive strengths and a lower cost than the high modulus fibres.

Some of the advantages of carbon fibres in general are:

- very high strength-to-weight ratio;
- very low coefficient of expansion, providing good dimensional stability in extreme conditions; and,
- fatigue resistance.

The disadvantages of carbon fibres are:

- low impact resistance;
- high electrical conductivity; and,
- high cost, preventing widespread use.

The cost of any type of fibre is key because it is responsible for determining a material's commercial viability.

Carbon fibres consist of a blend of amorphous carbon and graphitic carbon. The carbon atom planes are held together by weak van der Waals forces, while strong covalent bonds hold the atoms in plane. This unbalanced bonding results in anisotropic properties in carbon fibres.

Carbon fibres may be produced from one of two precursors: textile or pitch. The most common textile used is polyacrylonitrile (PAN), which contains highly polar carbon-nitrile groups that are randomly arranged on either side of the PAN chain. Filaments are wet spun from PAN and stretched at an elevated temperature, at which point the polymer chains are aligned in the filament direction.

Pitch is a by-product of petroleum refining or coal coking, and is therefore lower in cost than PAN. The carbon atoms are arranged in low molecular weight aromatic ring patterns. Heating them to temperatures above 300°C stabilizes the molecules in long, two-dimensional, sheet-like structures. Table 2.2 summarizes properties of some typical glass and carbon fibres.

Fibre Type	Specific Gravity	Tensile Modulus [GPa]	Tensile Strength [GPa]	Strain at Failure [%]	Poisson's Ratio	Coefficient of Expansion [10^{-6}/°C]
E-glass	2.54	72.4	3.45	4.8	0.2	5
S-glass	2.49	86.9	4.30	5.0	0.22	2.9
PAN carbon [T-300]	1.76	231	3.65	1.4	0.2	-0.6
Pitch Carbon [P-55]	2.0	380	1.90	0.5	-	-1.3

Table 2.2: Properties of Typical Fibres (Mallick, 1993)

2.2.3 Other Constituents

Although fibres and matrix constitute the major volume of composites, there are additional components that may be added to improve performance. Coupling agents and coatings, when applied to fibres, promote bonding across the fibre-matrix interface, thus

improving load transfer between the two. Fillers, on the other hand, do exactly what the name indicates: they take up volume in the matrix. Each constituent is described below.

2.2.3.1 Coupling Agents and Coatings

The primary role of surface treatment is to improve fibre surface wettability with the matrix and to create strong bonds between fibres and matrix.

Coupling agents are used with glass fibres to create additional physical and chemical bonds and also to protect the fibres from moisture and fluids. Before treatment, the surface of the fibre is cleaned by heating it in an air oven for 15 to 20 hours. The fibres are then immersed in a solution of the coupling agent, which bonds chemically to the fibres. When the fibres come into contact with the matrix, the coupling agent reacts to form chemical bonds with it.

Without coupling agents, glass fibres would still have a bond with the matrix, except it would be physical. The bond would result from mechanical interlocking arising from shrinkage of the matrix, since the matrix has a coefficient of thermal expansion 10 times that of the fibres. However, at elevated temperatures or under high applied loads the difference in expansion between the fibres and matrix may relieve the mechanical interlocking. Therefore, mechanical bonds are unreliable, while chemical ones are preferred.

Coatings are used with carbon fibres, since the fibres are chemically inactive. The coatings improve bonding by supplying a media with which the matrix can chemically

bond, as well as by creating micropores along the fibre surface. This increase in surface area provides more locations where the matrix can bond.

The addition of coupling agents and coatings typically improves the tensile and interlaminar shear strengths of the composite. The extent of improvement, though, depends closely on the compatibility of the agents with the resin.

2.2.3.2 Fillers

As stated earlier, the main use of fillers is to take up volume in the composite, as well as:

- to reduce cost, since it is less expensive than resin;
- to increase the modulus;
- to control viscosity; and,
- to create a smoother composite surface.

Common fillers include calcium carbonate ($CaCO_3$), clay and mica. Although not intended, fillers reduce the strength of the matrix as well as decreasing impact resistance.

Finally, additional composite constituents are not limited to those described above. Other components include colourants, flame-retardants and UV absorbers.

2.3 Composite Manufacturing

Prior to describing the composite production process, it is useful to review the basic structure of a composite. First, a single layer, or lamina, of fibres is created which will

consist of long continuous or short discontinuous fibres. In the case of long fibres, they are placed in the lamina either as unidirectional or bi-directional plies. Laminas with unidirectional fibres display their highest strength and modulus parallel to the longitudinal axis of the fibres while their strength in the transverse direction is low. The strength and modulus of bi-directional laminas can be varied by changing the amount of fibres in the longitudinal and transverse directions.

A single lamina cannot withstand an applied load alone, as its thickness is only in the range of 0.1 to 1.0 mm. Therefore, the manufacturing of composites begins with stacking a number of laminas together to form a single laminate. The laminas themselves can be oriented in the same direction, but they are most likely oriented in different directions in order to achieve specific physical and mechanical properties. These properties may also be altered by simply changing the lamina stacking sequence.

Once the laminas are stacked, proper curing must be provided. This is a very important step common to all composite manufacturing methods. The two conditions required for curing are elevated temperature and pressure. An elevated temperature initiates the chemical reaction which causes the material to cure into a solid component. The pressure provides the force required to cause flow of the highly viscous resin within the composite structure, as well as providing consolidation for the individual plies to become a single laminate.

Several techniques are available to produce composite components, though only a few are described in detail here. These include hand lay-up, pultrusion and filament winding. The key to successful production is cost-effective and reliable manufacturing methods. Thus, for each unique composite component, the most efficient method of production must be selected and its manufacturing costs minimized. Every aspect of the process, from materials and equipment to rate of production, has a significant effect on the overall efficiency. For this reason, it is pivotal to select the most suitable manufacturing process for the composite component.

2.3.1 Hand Lay-up

The hand lay-up method of composite production is the oldest method available. Though it does reliably produce the required components, the process can be very slow and labour intensive.

The method involves applying successive layers of resin and fibre fabric onto a mold, which dictates the final shape of the component. After each resin-fibre layer is applied, a roller is used to press the resin into the fabric. This allows fibre wetout and impregnation, as well as removal of entrapped air (Karbhari, 1996). The roller is not always successful, so voids and resin-rich areas are common in components produced by this method.

Upon completion of lay-up, the composite is cured at ambient or elevated temperature. The curing process is enhanced by applying a vacuum during this period. By covering

the component with bagging film and applying a vacuum inside the bag, a better quality product results.

2.3.2 Pultrusion

Pultrusion is a continuous molding process where long straight structural members are produced, such as solid rods, hollow tubes and flat sheets. These members are restricted in size by the capacity of the pulling apparatus and size of the deck (Karbhari, 1996). It is a low-cost alternative which allows fabrication with automated machines as opposed to manpower.

Longitudinally oriented continuous strand rovings are most commonly used with the pultrusion process. Layers of mats or woven rovings are sometimes added to the outer surface to enhance transverse strength, as shown in Figure 2.6.

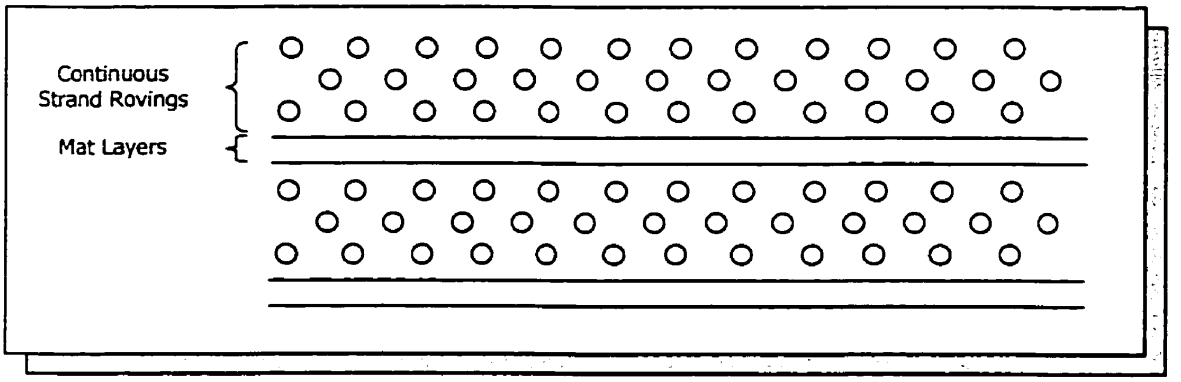

Figure 2.6: Composition of Pultruded Laminate *(Mallick, 1993)*

In addition to fibre rovings, polyester or vinyl ester resins are usually used as well. Epoxies could be employed, but they take longer to cure and do not release easily from the dies.

The following figure illustrates the pultrusion process and a step-by-step description is provided as well.

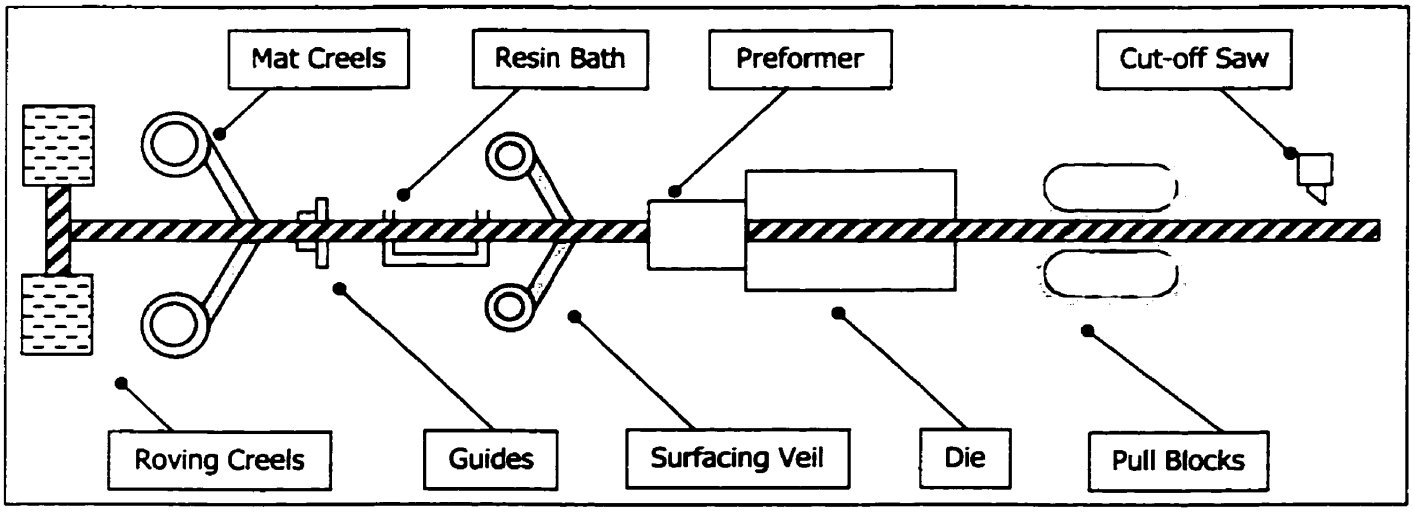

Figure 2.7: Schematic of Pultrusion Process *(Mallick, 1993)*

- continuous strand roving is pulled from one end of the line;
- the roving is pulled into a resin bath which contains liquid resin and curing agent
    - the viscosity of the resin and amount of time in the bath are adjusted to ensure complete wet-out of the fibres
- fibres enter the preformers, which distribute the fibres evenly, squeeze out the excess resin and bring the material into its final configuration;
- upon entering the die, the fibres undergo their final shaping, compaction and curing
    - the entrance is cooled to prevent premature gelling of the resin
    - the remaining length of the die is heated to aid curing

- the die length, die temperature and pull speed are controlled to allow the resin to cure completely prior to exiting the die

- the composite component is then pulled out of the die and cooled with air or water; and,
- the part is cut into desired lengths with a diamond blade saw

(Mallick, 1993).

The most important factor affecting a composite's mechanical performance is the degree of fibre wet-out achieved during pultrusion. Uniformly coating each bundle of fibres with resin determines how well the laminas will act as one unit. Varying several parameters attains the desired degree of fibre wet-out as listed below:

- initial resin viscosity
- resin bath temperature
  - a higher bath temperature provides increased wet-out
- amount of time fibres spend in bath
  - the more time spent in bath enhances wet-out
- mechanical action applied to fibres while in bath
  - increased mechanical working improves wet-out

Within the die, a complex temperature process is evolving. The curing reaction occurs at an increasing rate as the fibre-resin stream moves towards the die exit. With this increased reaction rate comes a large amount of heat evolved from the exothermic reaction, which consequently raises the die temperature. By the time the composite nears

the exit, cooling is applied in order to reduce the material's temperature. Without this action, the composite would exit the die at a temperature much higher than that of its surroundings, resulting in rapid cooling and leads to interlaminar cracking.

It may be expected that increasing the speed of the pultrusion line would increase productivity. However, increasing the speed could cause reduction of the fibre wet-out, consequently causing poorer quality of the composite. It is suggested to use multiple dies instead of high line speed to increase productivity.

2.3.3 Filament Winding

Another popular technique use for composite production is filament winding. In short, filament winding involves wrapping a band of continuous resin-impregnated rovings around a rotating mandrel. This well-established and very repeatable process is typically used to produce axisymmetric hollow parts such as oxygen tanks, hydro poles and pipelines (Karbhari, 1996). However, with the advancement of computer-controlled winding systems, irregular and complex shapes without an axis of symmetry can now be produced. The filament winding process is illustrated in Figure 2.8.

- a large number of fibre rovings is pulled into a liquid resin bath containing resin, catalyst and other ingredients
    - fibre tension is controlled by fibre guides located between the roving creel and the resin bath

- before entering the bath, fibres are gathered into a band by passing them through a steel comb

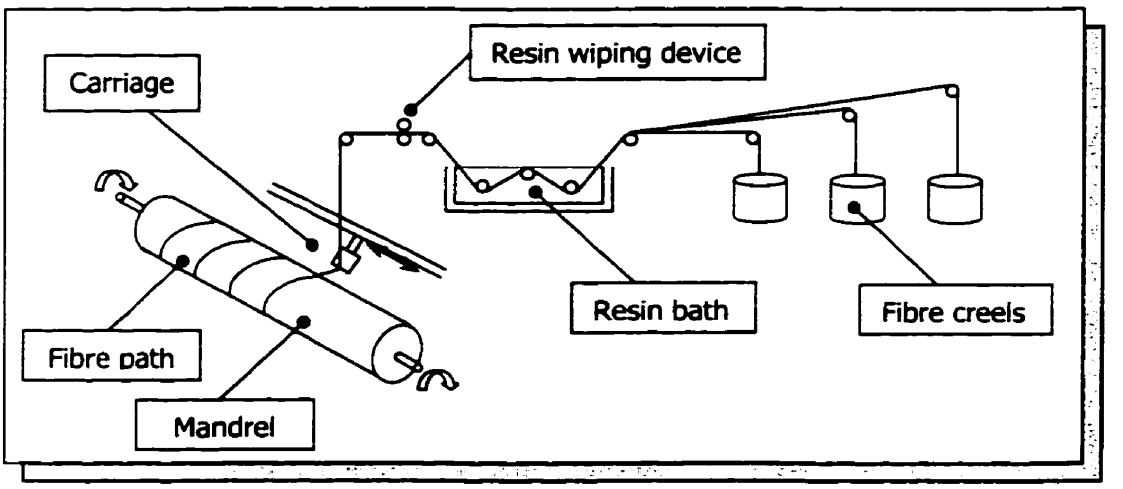

Figure 2.8: Schematic of Filament Winding Process *(Mallick et al, 1993)*

- after leaving the resin tank, the rovings are pulled through a wiping device (usually a set of rollers) to remove excess resin and to control the thickness of the resin coating
- the fibres are gathered in a flat band and positioned on the mandrel
  - the band traverses back and forth along the mandrel length
  - the traverse speed of the carriage and wind speed of the mandrel determine the wind angle patterns
- once the desired composite thickness is reached, the component is cured
  - curing can take place on the mandrel (stay-in mandrel) or with the mandrel removed (collapsible mandrel)

It should be noted that the process described is referred to as "wet winding." There is a similar process that can be used called "dry winding" where dry preimpregnated fibres are wound around a mandrel then later impregnated with resin. This modified method provides for better, more uniform resin distribution than achievable with the wet wind method.

A critical design aspect in filament winding is the angle of the fibres with respect to the mandrel's longitudinal axis. By adjusting the traverse speed of the carriage and the wind speed of the mandrel, angles from near 0° (longitudinal) to near 90° (transverse) can be achieved. Mechanical properties of the final composite depend very much on the winding angle, as demonstrated in the figure below.

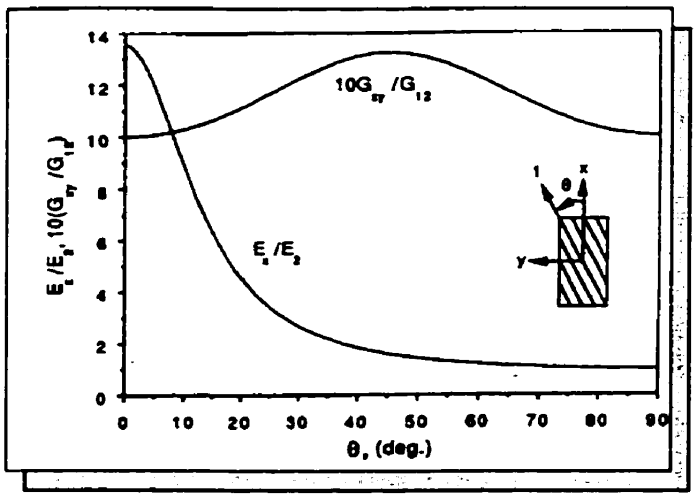

Figure 2.9: Variation of Mechanical Properties of Composite with Wind Angle
(Daniel et al, 1994)

One advantage of the filament winding technique is that as the feed carriage traverses back and forth across the mandrel, it creates a criss-cross pattern at plus and minus the wind angle, thus creating an interlocking effect between fibres.

Other important parameters specific to the process include:

- fibre tension
  - tension must be sufficient to maintain fibre alignment
- fibre wet-out
  - proper wet-out must be achieved in order to eliminate voids in the final composite
- resin content
  - viscosity of the resin must be low enough to impregnate the moving fibre strands in the bath, but not so low as to allow resin to drip and run off of the fibres
  - pot life must be long enough so that large components don't have premature gelation, which indicates initiation of curing

When any of the above parameters is not adjusted properly, flaws will occur in the final composite. Voids may appear due to poor fibre wet-out, presence of air bubbles in the resin bath or excessive resin squeeze-out caused by high fibre tension. Delaminations will occur in large parts where there is an extended period of time between two consecutive wind layers, and where the resin pot life is limited. Finally, wrinkles will result when an improper winding tension is applied, or when the rovings are misaligned. These conditions cause unstable fibre paths, leading to fibre slippage on the mandrel and improper fibre orientation.

The versatility of filament winding has been improved drastically in past years because of the use of computer-controlled machines. The computer software allows most wind designs to be numerically generated using the robotic teaching capabilities of the machine. With these added capabilities, better process control and more reproducible parts are possible. In fact, complex and irregular shapes can now be manufactured using filament winding with the use of these computer processes.

In terms of expense, filament winding could be an economical fabrication alternative. There is an initial startup cost for the mandrels and computer equipment, but the material cost is one of the lowest of all production options. This is especially true when comparing material costs with pultrusion products, whose material cost is 60-75% of the finished product cost (Karbhari, 1996).

2.4 Related Research

Although GFRP deck technology is a relatively new concept, a considerable amount of research has been done over the past 20 years (Zureick et al, 1995). For over 40 years, a reliable composite research base bas been formed in the areas of boat manufacturing and aerospace technology. However, it takes ingenuity and innovation to apply this same technology to bridge decks.

Bridge decks are expected to withstand several loading conditions during its service life; long service life demands; long periods of time between repair and maintenance, and

exposure to moisture and UV. Each issue must be considered carefully and resolved in order for composites to be successful as an alternative structural material.

Each research group discussed in this section attempts to achieve a high performance, reliable FRP deck. The various groups do have differing specific goals, such as minimal deck weight, low production cost, or small deflection, but each test competed adds to knowledge and experience. The experimental programs performed are important because they validate predictions and aid in the creation of models. It would be ideal to test various FRP deck configurations, but this is unrealistic. With models in place, parameters can simply be varied in the computer program and their effect on strength and stiffness known almost instantly.

Due to the wide range of deck configurations and test methods used, it is difficult to make direct comparisons. Instead, several primary research programs are highlighted in this section.

2.4.1 Hardcore DuPont Composites

One of the leaders in composite deck technology has been Hardcore DuPont Composites (Bernetich et al, 1996; Composites Technology, 1999). They have produced several deck configurations using the Seeman Composite Resin Infusion Molding Process (SCRIMP) technique. This simply involves wrapping foam cores in off-the-shelf stitch-bonded glass fabric, laying up the deck by hand between face plates and infusing the unit with resin

under a vacuum. Initially, three different configurations were considered, as shown in Figure 2.10.

The triangular and cube sections were produced as described previously, while the trapezoid cores were produced by lying fabric plies between the cores, not wrapping them.

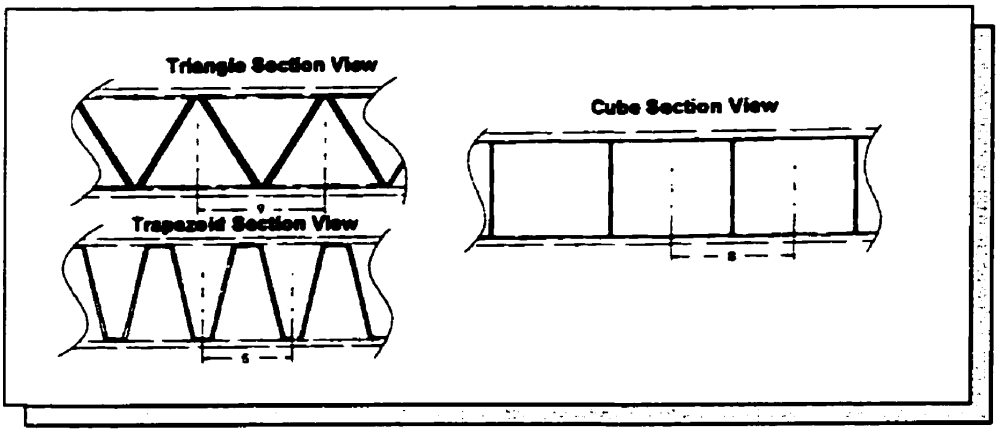

Figure 2.10: Trial Deck Configurations by DuPont (Bernetich et al, 1996)

Since each deck had the same face plates in its configuration, and because those plates would govern stiffness and bending strength, it was clear that the cores were used to provide the shear strength. Thus, the performance characteristics studied were focused on the shear strength of the core and the overall deck production cost.

Test results indicated that the longitudinally oriented triangular and trapezoidal decks performed best. Failure of the core in shear occurred at load levels of 894 kN and 1219 kN, respectively. Significantly lower load capacity was achieved with the cores oriented

perpendicular to the span. This implies that the triangular and trapezoidal decks would be suitable for applications with the load path in one direction: bridge decks. The box decks resisted high load levels in both directions (436 kN to 700 kN). However, their performance was outweighed by the excessive hours of labour required for production.

In the case where the cores were running transverse to the beam axis, the core webs exhibited truss action. This created significant tensile stresses at the bond line between the face plate and web, which could lead to premature failure. With the continuous bond line formed by the continuous wrap around the triangular core, this problem was alleviated. When the cores were oriented parallel to the span, they simply acted as flexural members.

One problem associated with FRPs is their potential for brittle and catastrophic behaviour. All decks in this test program exhibited significant load capacity even after substantial cracking and failure.

2.4.2 North Carolina State and California State University

These two institutions have also focused much attention on composite deck research (Zureick et al, 1995). The decks tested are shown in Figure 2.11.

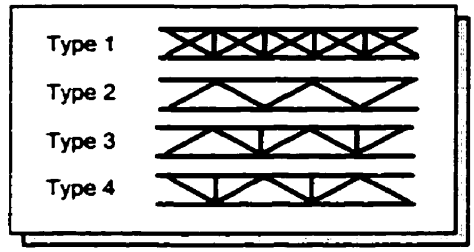

Figure 2.11: Cross Section of Decks Considered by N. Carolina State and California State Universities *(Zureick et al, 1995)*

For both, the simply supported and continuous span testing conditions, the design was always controlled by deflection limit state and not strength. The only deck to satisfy the AASHTO deflection requirement of L/800 was of the "X" type. As a result, this was the only deck pursued for further research.

The deck consisted of 10 layer laminate shapes produced with filament winding and the hand lay-up process. Filament wound diamond and triangular-shapes were bonded together using hand lay-up, which was followed by the application of unidirectional tapes to create a deck unit. This tape consists of prepregnated unidirectional fibres, which is tacky on both sides. Since the tape already contains resin, the component is wrapped and the tape is cured using a vacuum and heat.

The deck underwent fatigue testing of 2 million cycles with only minor stiffness losses. When subjected to an additional 2 million cycles, the deck showed 34% stiffness losses and failed at the tape/filament wound interface due to delamination.

2.4.3 University of Illinois

Aref et al (1999) believe that much focus has been on composite bridge components rather than an entire bridge structure. As such, they have tried to design an entire structure that uses the inherent properties of FRP to their fullest.

The system has two components, as shown in Figure 2.12; inner oval cells lying parallel to traffic flow, and an outer shell. Note that the deck cores lie parallel to traffic, whereas most other decks discussed position the deck cores perpendicular to traffic.

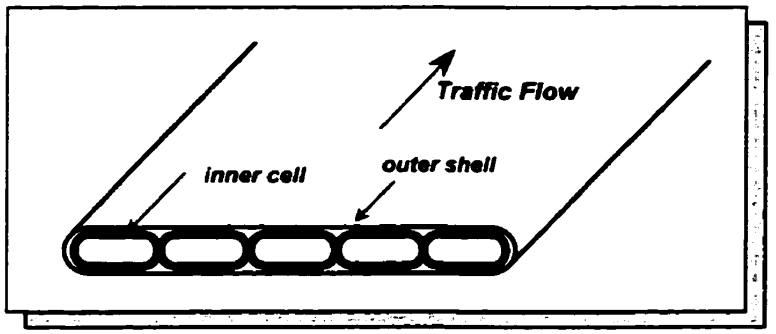

Figure 2.12: Deck Configuration of Aref et al (1999)

At this stage, the deck's fabrication is purely conceptual. The inner cells will be filament wound individually, cured, then assembled in a chuck coupling device. This device allows for the cells to have an outer layer filament wound about them.

Much thought has gone into every aspect of design and production. Filament winding will be used because it offers reliable, rapid fabrication cycles. The inner oval cells were designed to have a large contact area with the outer shell in order to reduce the shear stress to acceptable values. Finally, the outer shell will be filament wound around the entire section to create shell behaviour and increase the structural stiffness.

Instead of taking the testing approach, the deck was studied extensively using computer modeling. The exact specifications of the deck had yet to be determined, such as number of cells, wind angles, number of laminas and lamina thickness. To optimize the deck overall, an optimization procedure was used to determine these values in order to produce the lowest deck weight possible while meeting the L/800 criteria set by AASHTO.

Comparison of the output design parameters with those of a deck already produced by another manufacturer yielded excellent agreement. Though very little lab testing has occurred in this program, the computer modeling approach appears to have efficiently provided an initial "optimal" deck from which to begin lab testing.

2.4.4 University of Missouri and West Virginia University

FRP deck development goes beyond just testing in the lab. At the University of Missouri and West Virginia University, thin pultruded box sections were produced and tested in the lab. In addition to this, an analytical method was developed to aid in analysis of the composite deck and girders.

The pultrusion process was used to produce GFRP box tubes which were then bonded side-by-side and placed transversely over FRP girders. When tested in shear, torsion and bending the thin-walled sections usually buckled before reaching the material strength. This failure mode appears to be common behaviour in most decks.

Upon testing the initial sections, the analytical model was used to optimize the section with respect to deflection, material failure and elastic buckling. Once again, the combination of experimental and analytical seems the most efficient approach to composite research.

2.4.5 Virginia Tech

Virginia Tech, in collaboration with Strongwell, have developed modular deck sections consisting of pultruded square tubes and plates (Hayes et al, 2000), as shown in Figure 2.13. The tubes are connected with Fibrebolt studs and nuts, while the plates are adhered to the section with epoxy resin. Fibrebolt studs and nuts are a standard item available from Strongwell, manufactured by pultruding glass roving through resin and subsequently machining the threads.

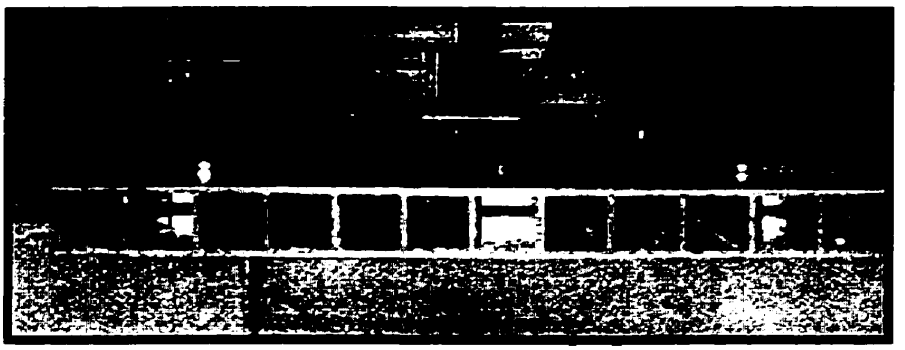

Figure 2.13: Cross Section of Box Core Deck by Strongwell (Hayes et al, 2000)

Testing of the 1.22m spans under simply supported conditions has revealed an *L/270* deflection response at HS20 service loads. Failure of these decks was due to punching shear along the long side of the 508 x 305 mm loading patch. Fatigue testing was also performed for 3 million cycles between 11.1 and 111 kN (20% above service loads). No

significant loss of stiffness or strength was observed after cycling. Overall, it appears that deflection controls the design.

2.4.6 Other Universities

Other universities have developed optimization or objective functions as presented earlier (Salim et al, 1997). The parameters of local buckling, deflection, weight and strength constitute the objectives of most functions.

All of the decks mentioned consisted of glass fibres only. There are some projects ongoing that study the concept of hybrid decks using a combination of carbon and glass fibre to achieve the deflection limits. It may be true that carbon stiffens a structure considerably, however, the drastic material cost increase must be taken into account.

2.4.7 Summary

At first glance, it appears that each research group is focussing on very different areas of composite deck research. However, the common goal of those involved in this technology is the production of a cost-efficient, structurally reliable, durable FRP deck. This goal can be attained with the optimization of deck weight, geometry and strength through experimental and analytical studies.

2.5 Field Application

No matter how much laboratory research is done, FRP bridges must prove their reliability and functionality with demonstration projects. These projects are becoming more

numerous each year as manufacturers see the opportunity for a new market in the infrastructure industry. Several of these projects are highlighted here.

2.5.1 Owens Corning and Fiberline, 1999

A pedestrian bridge composed solely of composites was constructed in Denmark using the Fiberline Design Manual, shown in Figure 2.14. Only the bolts and clamps in the foundation were not FRP.

Figure 2.14: Fiberline Bridge in Kolding, Denmark (Owens Corning webpage, 1999)

The 13m long 3m wide bridge was erected in 18 hours and weighed only 12 000 kg, which is an impressive improvement over the 28 000 kg the bridge would weigh if it were made of steel. A sheet of GFRP composite was added on the deck floor and coated with silicate sand to enhance skid resistance.

2.5.2 Hardcore DuPont Composites, 1999

Hardcore DuPont Composites is clearly a leader in this area, with 10 composite bridge decks installed and many more on the way. Their decks employ the SCRIMP fabrication

process, which allows design features, such as highway crown and skew, to be easily incorporated.

While the deck is being built in the plant (two days production), the contractor is demolishing and preparing the bridge site. When preparation is complete, the deck is simply dropped in place and a polymer concrete wearing surface applied. Total installation time is less than one day.

2.5.3 Atlantic Research Corp. and Georgia Institute of Technology, 1999

These groups have collaborated to produce a 6 x 6m deck panel which has been installed in the pavement of a truck weigh station on the Virginia Interstate (Black, 2000). The fully instrumented deck consists of pultruded triangular tubes, which have pultruded top and bottom face plates bonded to them. Both components are produced by Creative Pultrusions. The panels, also know as the EZSpan deck, are designed to resist HS25 loads. To date, the average deflection is unchanged compared with initial installation data.

2.5.4 New York State and Hardcore Composites, 1998

The state of New York needed to upgrade a crumbling concrete bridge in order to resist increasing truck loads on the Bennetts Creek Bridge (Black, 2000). They found it was too expensive to replace the bridge, and replacing the bridge deck with concrete would not allow the project objective to be met. Instead, they commissioned Hardcore Composites to design a 610-mm deep deck that could withstand HS25 loading. The

honeycomb core consisted of blocks of foam wrapped with E-glass fibre and infused with vinyl ester resin. The process used to do this is called Vacuum Assisted Resin Transfer Molding (VARTM). A 3/8" polymer concrete wearing surface was applied prior to transport. The deck installation is shown in Figure 2.15.

Figure 2.15: Installation of Deck Panels in New York (Black, 2000)

The 5 x 7.6m modules were secured to the abutments with 1-inch stainless steel dowels, held in place with non-shrink grout. After the one-day installation, the deck was found to meet the *L/800* deflection limit specified by AASHTO.

2.5.5 Owens Corning and Creative Pultrusions, 1997

This joint venture produced two pedestrian bridges in 1997, each with an AASHTO load rating of HS25. The structures had 6-7 times the capacity of reinforced concrete at only one-fifth the weight. Each bridge was installed in less than 5.5 hours. A typical installation by Creative Pultrusions is shown in Figure 2.16.

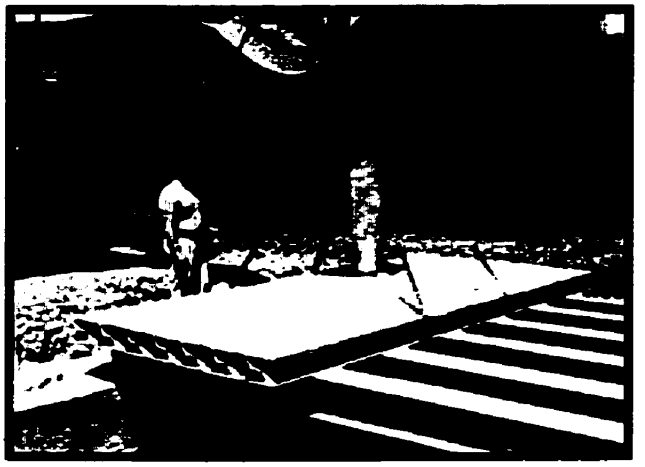

Figure 2.16: Installation of Deck by Creative Pultrusions (Creative Pultrusions webpage, 1999)

2.5.6 Martin Marietta Materials and Glassforms, 1997

These companies collaborated to construct composite bridges in both Idaho and Ohio. The bridge decks employ a trapezoidal cross section, as shown in Figure 2.17. The installation took less than eight hours, four crew and lightweight equipment. These bridges are both performing very well to date. Discussions with New York and other states are currently underway to secure future projects.

Figure 2.17: Deck Cross Section Used by Martin Marietta (Martin Marietta webpage, 1999)

2.5.7 Kansas State and KSCI, 1997

The state of Kansas and Kansas Structural Composites Inc. (KSCI) have also repaired two bridges using FRP decks (Black, 2000). These decks were of honeycomb sandwich construction, hand layed-up with skins on the top and bottom. A cross slope of 2% was even incorporated in the fabrication process. Instead of bolting the modules to the girders, clamps were used to hold the modules in place. This eliminated localization of stress in the glass fibre. Both decks are capable of withstanding HS25 loads.

2.6 Future Work

The National Composite Center in the US is hoping to build 100 composite bridges in Ohio over the next 12 years. This mass production of composite bridges could be what the technology needs to drive down its cost and build up its reputation.

Before composite bridges can be used on a widespread basis, several challenges must be met.

- affordable manufacturing methods must be developed that produce high performance FRP bridge decks of complex geometry;
- in-depth studies (analytical and experimental) must be done to determine every aspect of behaviour of the decks; and,
- practical aspects of FRP decks must be considered.
    - i.e., connection of modules to each other, connection of modules to girders, incorporation of curbs and railings

Each of these issues is important to the application of this technology. FRP decks will appear attractive only when they are cost-competitive with conventional methods. The in-depth studies will allow composite behaviour to be documented and predicted through modeling. With models in place, design standards and guidelines can be developed which allow FRP design to be accessible and accountable. Finally, with the practical issues resolved, composite bridge decks could be a feasible, innovative alternative to reinforced concrete decks. As our experience and confidence grows, so will the application of FRP decks in highway bridges.

CHAPTER THREE:

EXPERIMENTAL PROGRAM

3.1 Introduction

The main objective of the experimental program is to determine the structural behaviour of GFRP bridge deck modules subjected to simulated loading conditions satisfying the requirements of AASHTO specifications. The GFRP bridge deck is expected to resist HS-30 according to AASHTO specifications for design truck loads.

The testing program was organized into several phases. The first phase involved testing of three intact three-tube deck modules. The specimens were tested using two orientation schemes, and with and without the outer plates to provide an in-depth understanding of the behaviour of the different components constituting the bridge deck.

The second phase consisted of specimens closer to the proposed full-scale bridge deck. These deck specimens were the same span as those in Phase I, but consisted of seven tubes and were fabricated using a different manufacturing process aimed at improving outer plate behaviour.

3.2 Test Specimens for Phase I

The decks used in Phase I consisted of three equilateral triangular filament wound tubes approximately 200 mm in height, as shown in Figure 3.1. A filament winding process was used to manufacture each tube due to its relatively low material costs in comparison to pultruded products. Each tube was wrapped with eight layers of roving, in a [90/±45/±10/±45/90] wrapping sequence producing tubes with a fibre volume ratio of 42.6%.

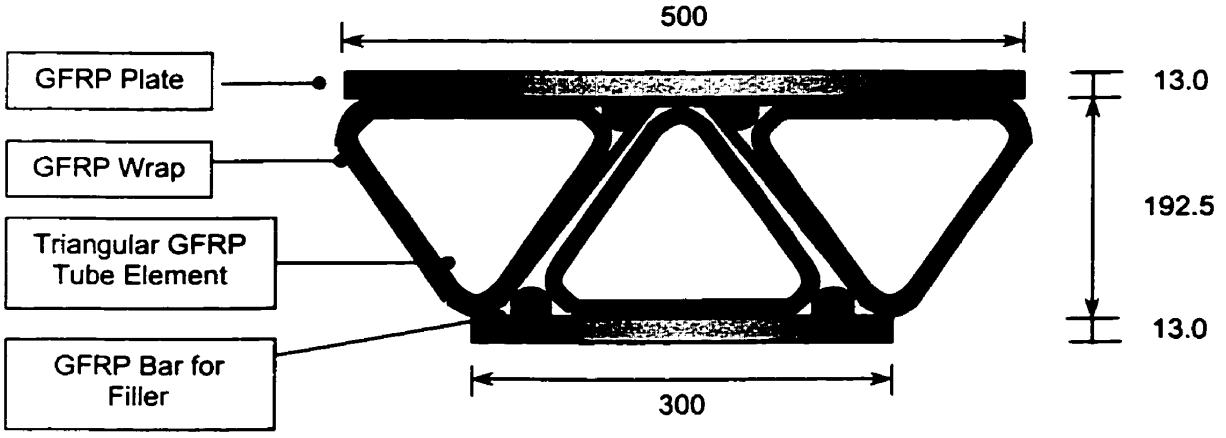

Note: GFRP Mat used in only one deck specimen in Phase I

Figure 3.1: Cross Section of Phase I Modules

The tubes were adhered together with epoxy resin from the filament winding process as well as additional epoxy which was added during the lay-up process. The rounded shape configuration of the tubes created large voids at the interconnecting nodes. To eliminate weaknesses associated with these large epoxy-filled voids, pultruded GFRP bars were placed in the section as filler as shown in Figure 3.1.

In one of the three deck specimens, a bi-directional glass fibre mat was wrapped around the three tubes in order to examine its effect on enhancing the interlaminar shear interaction between the tubes as well as the overall deck performance.

The final component of the section was the pultruded glass fibre plates, which were bonded to the top and bottom of the tubes to create one modular unit. The plates were made from GFRP laminates which were available at Faroex, however they were not specifically designed for this purpose. Each 13-mm plate consisted of five individual pultruded laminas that were stacked and bonded with resin under a vacuum. Three laminas with fibres in the longitudinal direction (0°) were stacked alternately with two laminates with fibres in the transverse direction (90°). This provided a fibre volume ratio in the plates of 41.4%. The 0- or 90-degree laminas were sandwiched between two outer random or omni-directional mats of 0.5 mm. The composition of each lamina, and in turn, the overall deck plate, is provided in Figure 3.2.

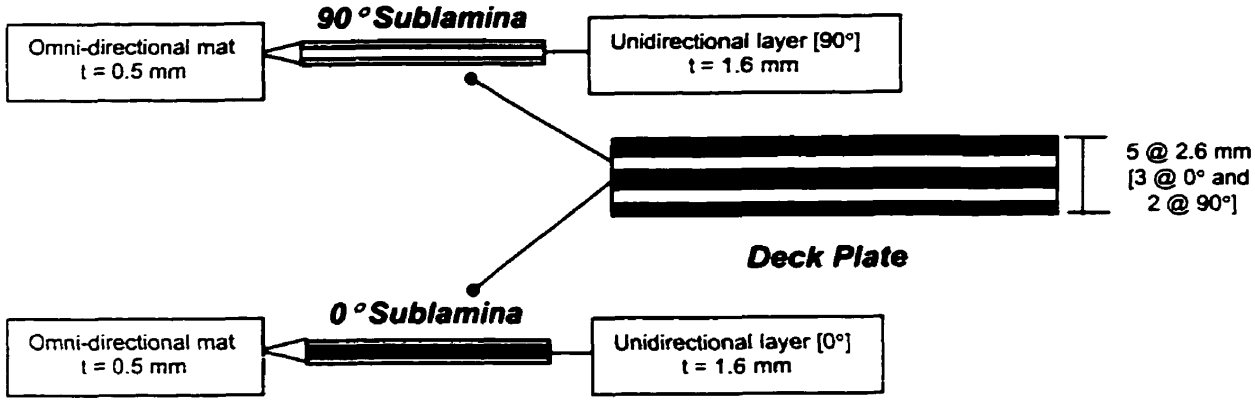

Figure 3.2: Schematic of Phase I Deck Plate Composition

3.3 Test Specimens for Phase II

The cross section of the deck modules used in Phase II is shown in Figure 3.3.

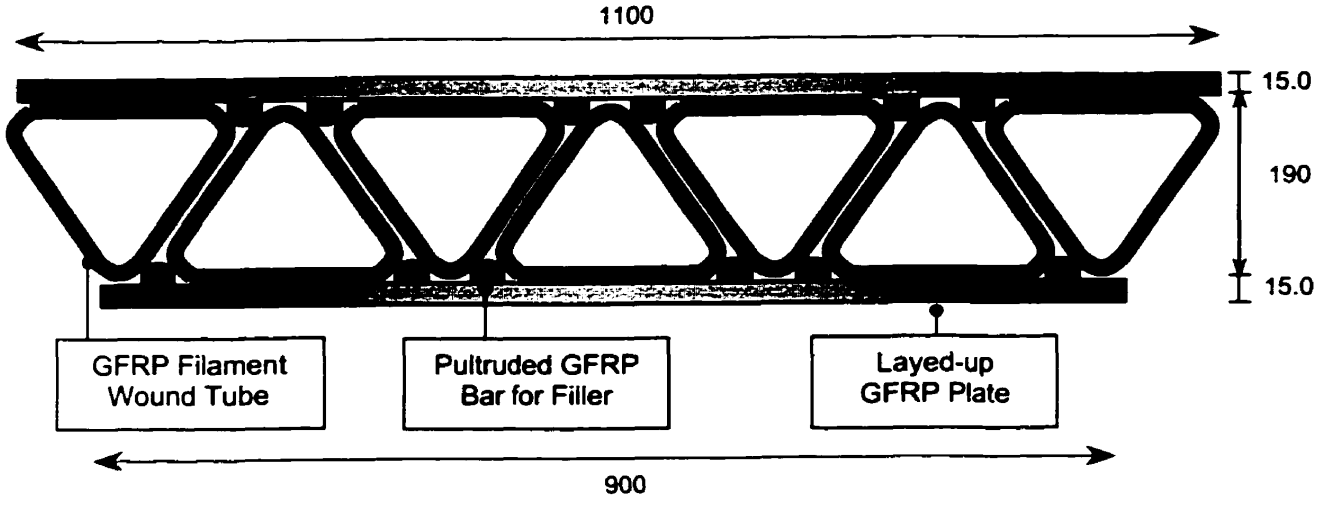

Figure 3.3: Cross Section of Phase II Modules

The specimens consisted of the same equilateral-shaped, filament wound tubes used in Phase I. The tubes were wound using the same layering sequence of

[90/±45/±10/±45/90], except that the inner six layers were only half the thickness. This reduced the tube thickness from 5 mm to 4 mm. The altered winding pattern produced 42.6% fibres by volume in the 90° layers and 28% fibres by volume in the remaining layers.

The same pultruded bars were used for filler at the nodes of the triangular tubes. To enhance the mechanical interaction within the different components of the deck, 3 mm deep by 3-mm wide grooves were cut every 25 mm along the length of the bars. The second deck specimen produced for Phase II incorporated bars with a reduced cross section in order to provide for a more compact fit within the voids. This modification reduced the bar cross sectional area by approximately 32 percent.

The second generation of specimens was also enhanced by using a different manufacturing process from those in the first phase. Instead of using pultruded plates, it was planned to use the filament winding technique to overwrap the entire section. At the time of production, this method had not yet been mastered. Thus, in order to simulate the process, an equivalent filament winding technique was used. The plates were fabricated using unidirectional glass fibre mats, layed-up on the top and bottom of the decks. In one deck, 38 layers were used in each plate in a sequence of $[90/(\pm45/\pm10/\pm10/\pm10)_2/45/\pm10/-45/(\pm10/\pm10/\pm10/\pm45)_2/90]$, while in the second deck 42 layers were used in a sequence of $[90/(\pm45/\pm10/\pm10)_3/45/\pm10/-45/(\pm10/\pm10/\pm45)_3/90]$.

3.4 Parameters

The main objective of testing was to study the flexural behaviour of composite decks. The seven tests performed for the first phase are summarized in Table 3.1. The various parameters included are:

- orientation of the deck during testing;
- condition of deck plates;
- presence of fibre mat wrapping around tubes; and,
- presence of filler bars

Phase	Specimen Designation	Orientation During Testing	Plate Condition	Filler Bar Condition
1	F1-TB *Basic Module*		Top: Intact Bot.: Intact	Top: Intact Bot.: Intact
1	F1-TB-a *Deck F-1 Retested*		Top: Intact Bot.: Delaminated	Top: Intact Bot.: Intact
1	F2-TB-a *Basic Module*		Top: Intact Bot.: Intact	Top: Intact Bot.: Intact
1	F2-T-a *Deck F-2 Retested*		Top: Intact Bot.: Removed	Top: Intact Bot.: Removed
1	FR-TB-a *Basic Module with mat wrapping*		Top: Intact Bot.: Intact	Top: Intact Bot.: Intact
1	Deck FR-T *Deck F-3 Retested*		Top: Intact Bot.: Removed	Top: Intact Bot.: Intact
1	Deck FR-a *Deck F-3 Retested*		Top: Removed Bot.: Removed	Top: Intact Bot.: Intact

Table 3.1: Phase I Specimen Designation

Key:

F: *flexural testing*
R: *tubes wrapped with bi-directional GFRP mat*

T: *top plate present*
B: *bottom plate present*

a: *tested with wide edge on top (no designation implies that deck was tested with the wide edge on the bottom)*

1,2...: *identifies specimen number where more than one deck of a specification exists*

The second phase of bridge decks consisting of seven-tube modules both were designed with the same dimensions and properties. However, because the manufacturing process was evolving as the project progressed, there were small manufacturing details that varied between these decks. The essential differences between the two specimens are summarized in Table 3.2.

Phase	Specimen Designation	Orientation During Testing	Bar Cross Section	Number of Plate Layers
1	F7-1			38
2	F7-2			42

Table 3.2: Phase II Specimen Designation

The differences between Phase I and II decks, in addition to the manufacturing techniques, are provided in Table 3.3.

Phase	Tubes	Plates	Bars
1 *(all decks)*	• filament wound • eight layers • sequence: [90/±45/±10/±45/90] • 41.4% fibres by volume	• pultruded • five layers • sequence: [0/90/0/90/0] • 42.6% fibres by volume	• pultruded
2 *(F7-1)*	• filament wound • eight layers (45/10 are half layers) • sequence: [90/±45/±10/±45/90] • 90°: 41.4% fibres by volume 10/45°: 28% fibres by volume	• layed-up • 38 layers • sequence: [90/(±45/±10/±10/±10)$_2$/45/±10/-45/(±10/±10/±10/±45)$_2$/90] • 45% fibres by volume	• pultruded • grooved every 25 mm
2 *(F7-2)*	• filament wound • eight layers (45/10 are half layers) • sequence: [90/±45/±10/±45/90] • 90°: 41.4% fibres by volume 10/45°: 28% fibres by volume	• layed-up • 42 layers • sequence: [90/(±45/±10/±10)$_3$/45/±10/-45/(±10/±10/±45)$_3$/90] • 49.7% fibres by vol.	• pultruded • grooved every 25 mm • cross section area reduced by 32%

Table 3.3: Technical Differences Between Phases I and II

3.5 Material Properties

The material properties of the Owens Corning Type 30 glass fibre roving used for filament winding of the tubes are provided in Table 3.4.

Property	Value
Specific Gravity	2.624
Tensile Strength [MPa]	1700
Tensile Modulus [GPa]	72.4
Strain at Failure	4.6%
Poisson's Ratio	0.22
Thermal Expansion [10-6/°C]	5.8

Table 3.4: Glass Fibre Roving Properties

The material properties of the custom-made epoxy resin are given in Table 3.5. This resin was based on Shell Chemical's EPON 828 resin for composites.

Property	Value
Specific Gravity	1.163
Tensile Strength [MPa]	64.8
Tensile Modulus [GPa]	3.15
Poisson's Ratio	0.27
Percent Elongation	9.9
Heat Deflection Temperature [°C]	103

Table 3.5: Epoxy Resin Properties

Table 3.6 summarizes the products used for each component of the deck in each phase. Other component properties are available from Faroex.

Phase	Tubes	Plates	Bars
I	• Owens Corning Type 30 glass fibre roving • custom epoxy resin based on Shell Chemical's EPON 828 resin for composites	• 5-lamina plates custom-made at Faroex	• Pultruded GFRP bars (full cross section used)
II	• Owens Corning Type 30 glass fibre roving • DOW Chemical D.E.R. 388 Epoxy Resin	• Knytex unidirectional woven fabric A130A, by-product of Owens Corning • DOW Chemical D.E.R. 330 epoxy resin	• Pultruded GFRP bars (grooved for F7-1; grooved and cross section reduced for F7-2)

Table 3.6: Material Products Used in Each Phase

3.6 Fabrication

The deck modules were fabricated by Faroex Ltd. in Gimli, Manitoba. The process used to produce the three- and seven-tube GFRP modules is in the following sections.

3.6.1 Three-Tube Module Production

1. Fabrication of the custom-made triangular-shaped styrofoam mandrels is shown in Figure 3.4. Chopped glass fibres were applied to strengthen the surface of these mandrels.

Figure 3.4: Styrofoam Mandrels

2. A filament winding technique was used to fabricate the individual tubes with Owens Corning Type 30 glass fibre rovings as shown in Figure 3.5 at the ISIS Canada-Faroex Filament Winding Facility. As described earlier, eight lamina layers were wound around the tubes in a [90/±45/±10/±45/90] sequence. A specific mix design was used for the epoxy to allow for a 24-hour pot life.

Figure 3.5: Filament Winding Machine

3. When all of the tubes were wrapped, they were laid out on the deck plate and the pultruded filler bars were placed in position. The components were bonded by adding epoxy resin. In the case of Deck FR, a GFRP mat was wrapped around the tubes, as shown in Figure 3.6. Again, additional resin was added and worked into the fabric to aid in fibre wet-out and to eliminate the voids.

Figure 3.6: Wrapping of Tubes with GFRP Mat

Figure 3.7: Placement of GFRP Filler Bars

4. The top plate was adhered with added resin
5. Upon completion of assembly, the entire deck was wrapped in a plastic bag and sealed as seen in Figure 3.8.

Figure 3.8: Sealing Phase I Deck Module in Bag for Curing

6. The deck module was cured for 8-10 hours at 180°F, while a vacuum pump worked to remove excess resin from the deck. The final Phase I deck specimen is shown in Figure 3.9. The ends were cut off of the module. Although the final deck product shown in Figure 3.9 is a three-tube module, full-scale modules are expected to consist of at least 7 to 12 tubes.

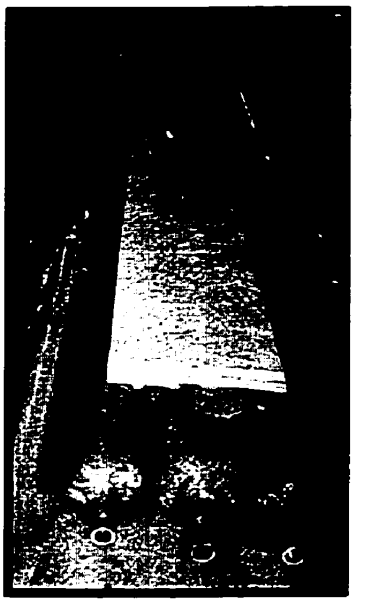

Figure 3.9: Final Deck Specimen

3.6.2 Seven-Tube Module Production

1. The resin infusion tubing was laid out on the surface where the deck was to be constructed, as shown in Figure 3.10.

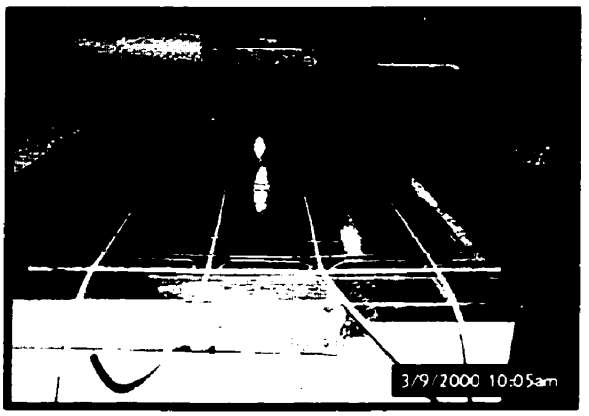

Figure 3.10: Layout of Resin Infusion Tubing

2. A layer of PET 200 (Polyethylene Terephthalate) was placed down on the bed, which helps the resin travel during infusion. This was followed by placement of a polyurethane sheet on the bed as well.

3. The inner seven layers of the triangular tube elements were wet-wound onto styrofoam mandrels using Owens Corning Type 30 fibre roving and Dow Chemical D.E.R. 383 epoxy resin. This was followed by curing of the triangle at room temperature while rotating in the filament winding machine. The completed tubes are shown in Figure 3.11.

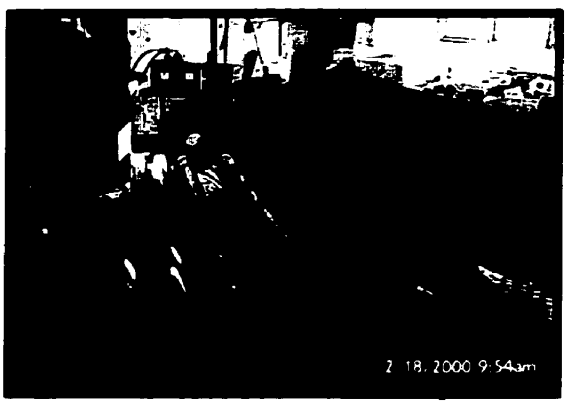

Figure 3.11: Tubes After Winding and Curing

4. When curing was complete, the final circumferential layer was dry-wound onto each of the tubes as shown in Figure 3.12.

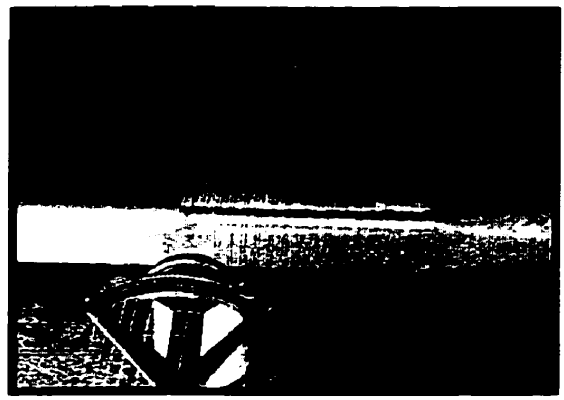

Figure 3.12: Winding Final Layer of Tubes

5. The pultruded GFRP bars were modified to enhance deck behaviour. First, 3 mm deep by 3 mm wide grooves were cut 25 mm apart along the length of the bars in order to enhance mechanical bonding. As well, the bars in the second deck of Phase II were cut from their original semi-elliptical shape to triangular shape in order to fit compactly in the section. This resulted in a 32% reduction in cross section area. The grooved filler bars are shown in Figure 3.13.

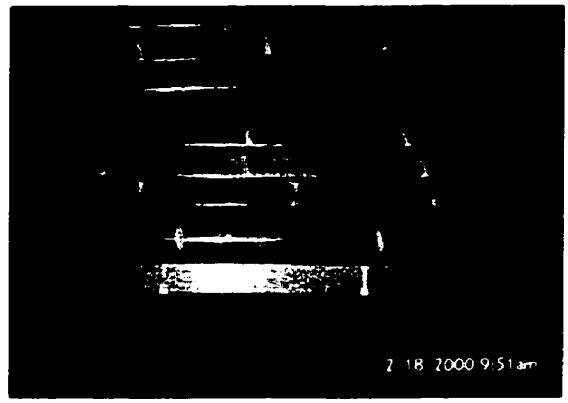

Figure 3.13: Grooved Filler Bars

6. The lower deck plate was layed-up dry by hand and positioned on the bed. The mat used was Knytex unidirectional woven fabric A130A, a by-product of Owens Corning.

7. The tubes and bars were positioned on the lower plate, followed by lay-up of the upper deck plate, shown in Figures 3.14 and 3.15.

Figure 3.14: Assembly of Deck Components

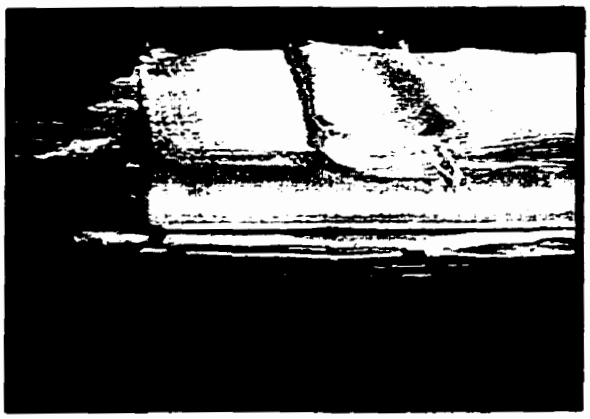

Figure 3.15: Lay-up of Upper Deck Plate

8. When deck assembly was complete, the resin infusion ports were positioned on the upper plate of the deck, shown in Figure 3.16.

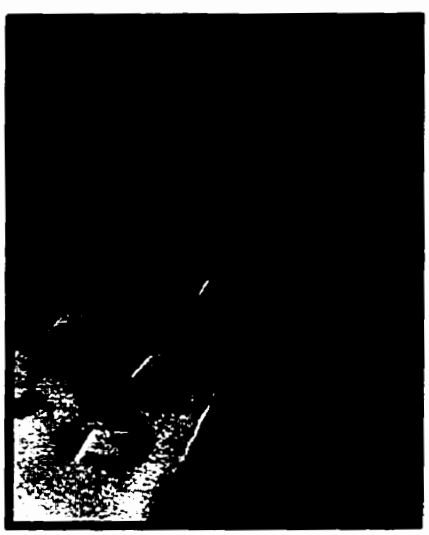

Figure 3.16: Resin Infusion Ports

9. The deck was wrapped in plastic sheeting and the sheeting sealed around the deck, as shown in Figure 3.17.

Figure 3.17: Sealing of Plastic Wrap Around Deck

10. A vacuum was applied to the deck for approximately one hour to remove all air and to compress the glass fibres.

11. The deck was infused with Dow Chemical D.E.R. 330 epoxy resin for approximately 2 hours, shown in Figure 3.18. The resin was then left to gel for 4 hours.

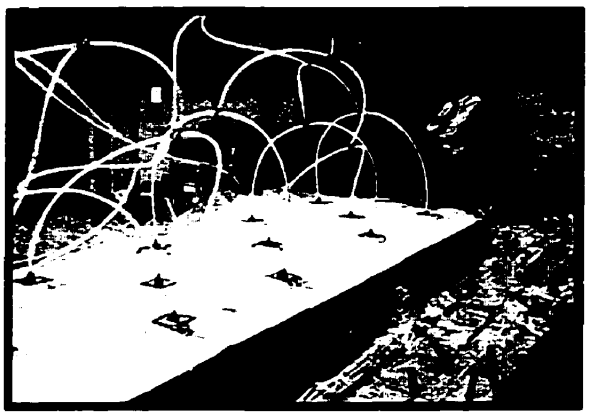

Figure 3.18: Deck During Infusion Process

12. The deck was cured at room temperature for 24 hours, followed by post-curing at 160°F for 4-6 hours. Cross section and elevation views of the deck modules upon completion are provided in Figures 3.19 and 3.20.

Figure 3.19: Phase II Deck at Completion (Cross Section View)

Figure 3.20: Phase II Deck at Completion (Full View)

3.7 Instrumentation

The specimens were instrumented with between 13 to 28 electrical resistance strain gauges placed axially and transversely along the upper and lower plates to determine strain behaviour. Several gauges were also located axially along the side of the tubes closest to the plates for comparison purposes. The gauges were 6 mm long with preattached long lead wires made by Tokyo Sokki Kenkyujo Co. Ltd. In preparation for

instrumentation, the deck was sanded lightly to remove the outer epoxy layer. Gauges were glued with M-Bond adhesive.

Earlier specimens were more heavily instrumented than later specimens, in order to ensure measurement of any type of deck behaviour that might occur. As testing progressed and deck behaviour became more predictable, fewer gauges were required.

An average midspan deflection was measured using a number of linear voltage displacement transducers (LVDTs) placed on either side of the width at midspan. Another LVDT was placed at the west support to determine deflection of the neoprene pad at this location. This measurement was recorded to determine the net midspan deflection.

After the plates had been removed in certain Phase I decks, PI gauges were used to measure strains at midspan instead of using strain gauges.

The complete instrumentation layout for each deck specimen is found in the Figures 3.21 through 3.29.

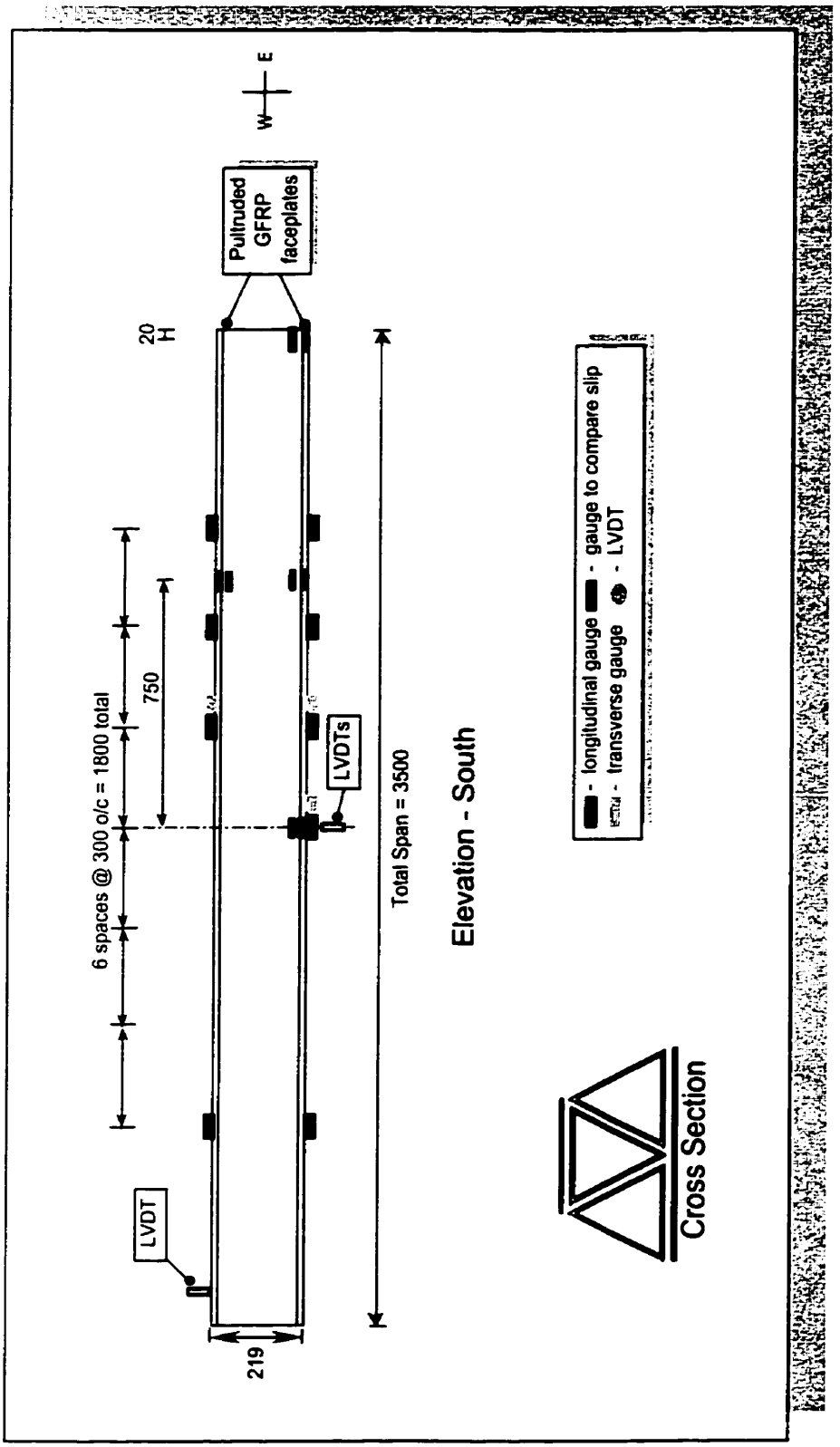

Figure 3.21a: Instrumentation for F1-TB (Elevation)

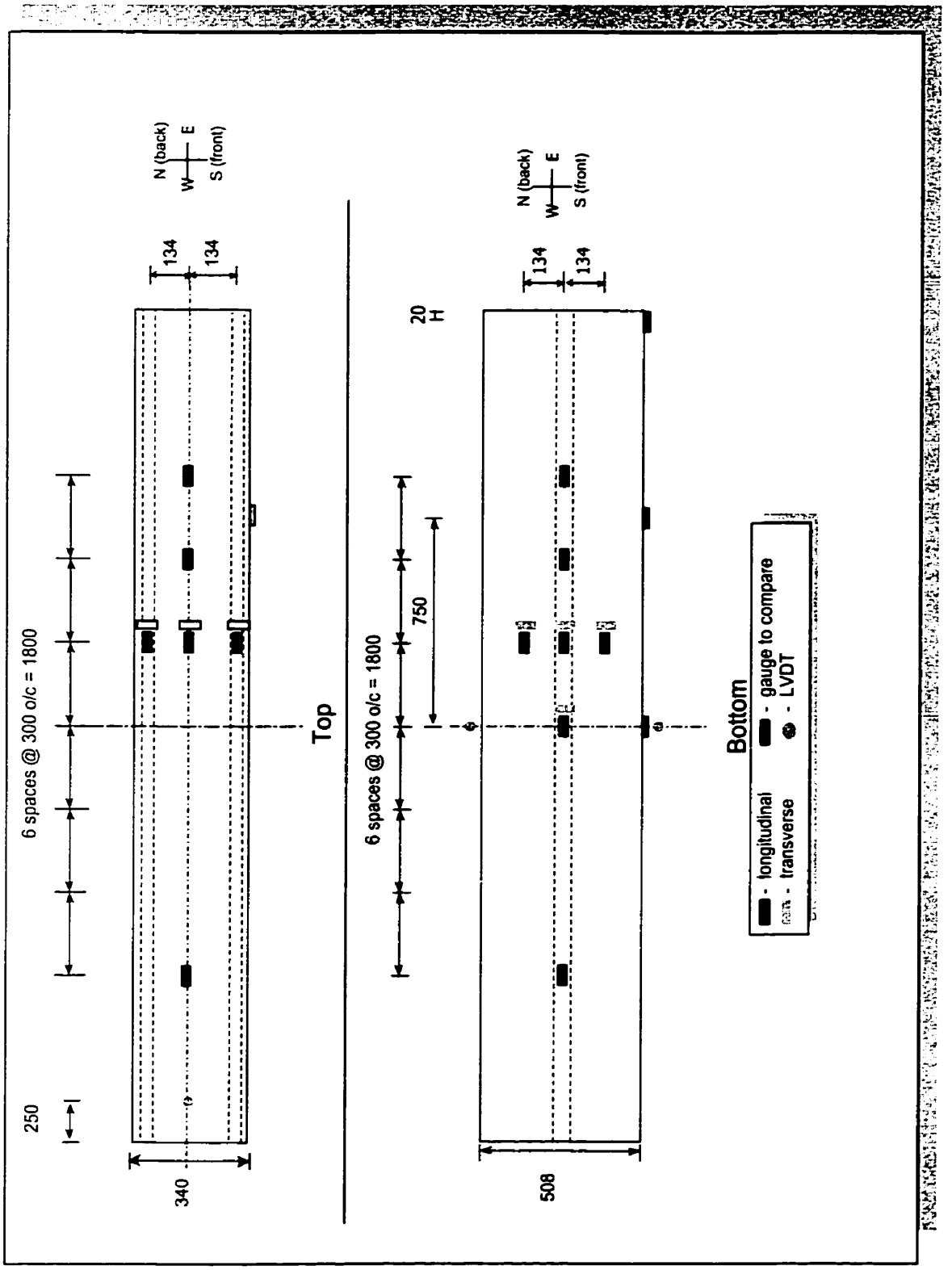

Figure 3.21b: Instrumentation for F1-TB (Top and Bottom)

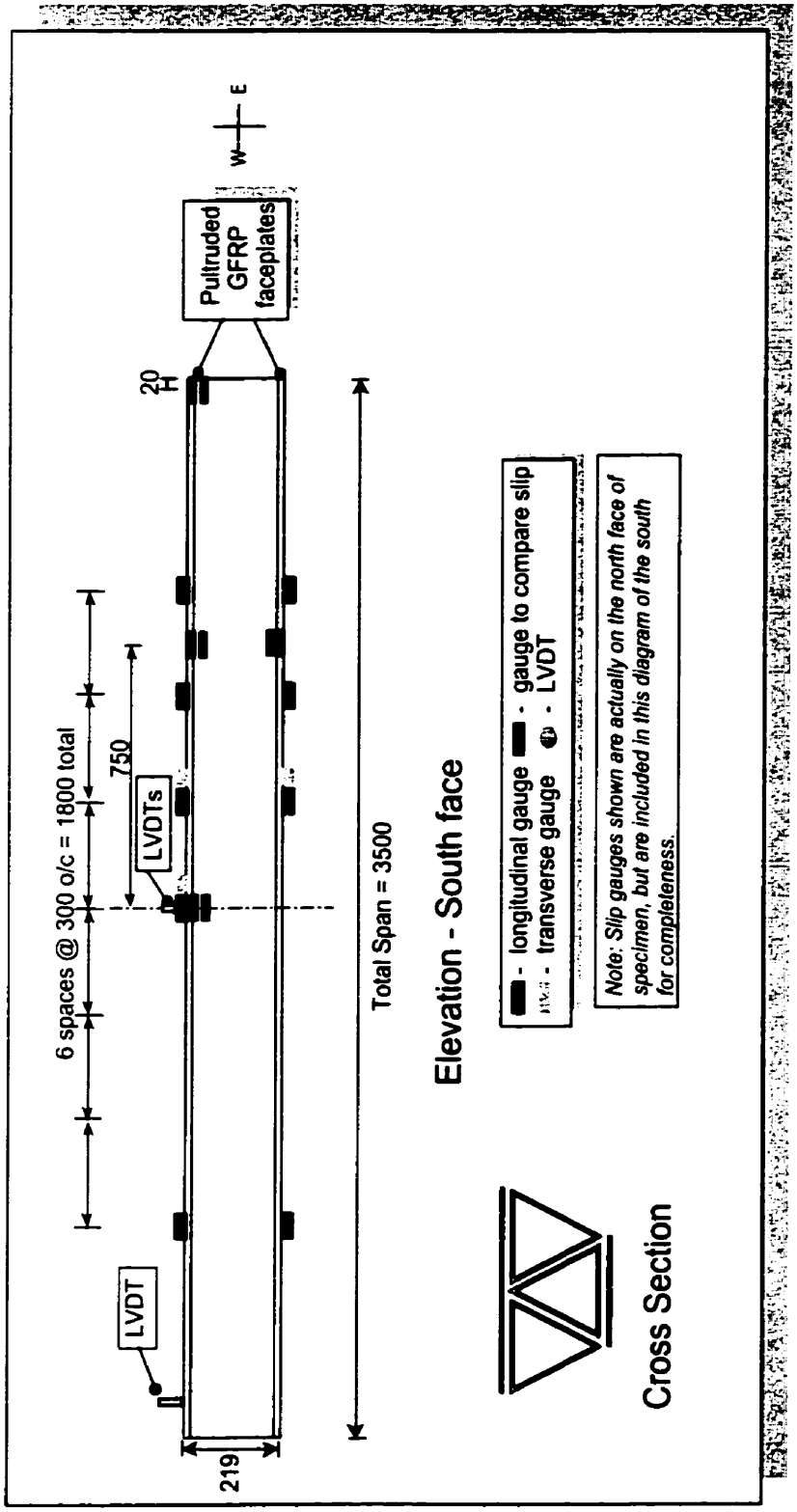

Figure 3.22a: Instrumentation for F1-TB-a (Elevation)

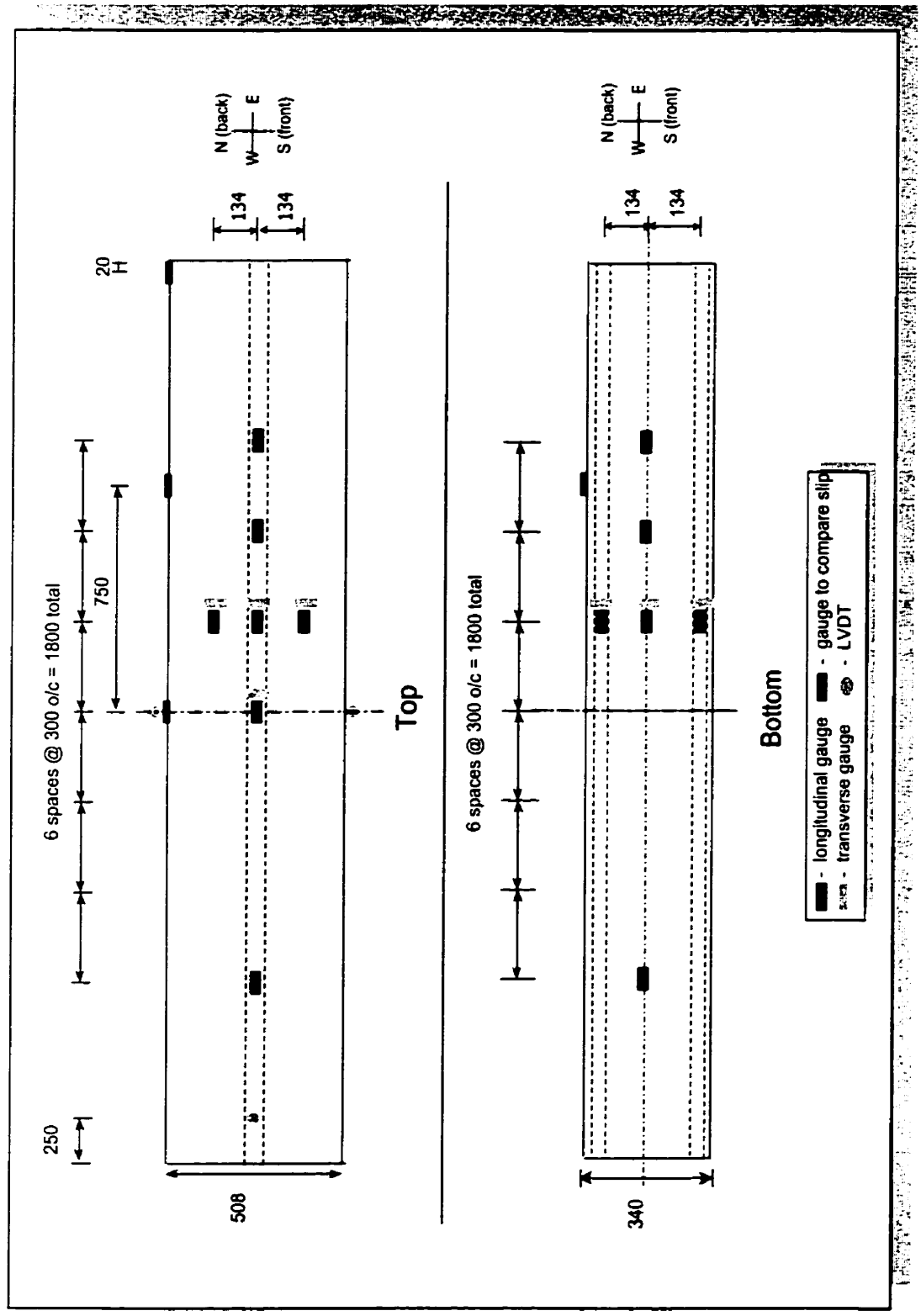

Figure 3.22b: Instrumentation for F1-TB-a (Top and Bottom)

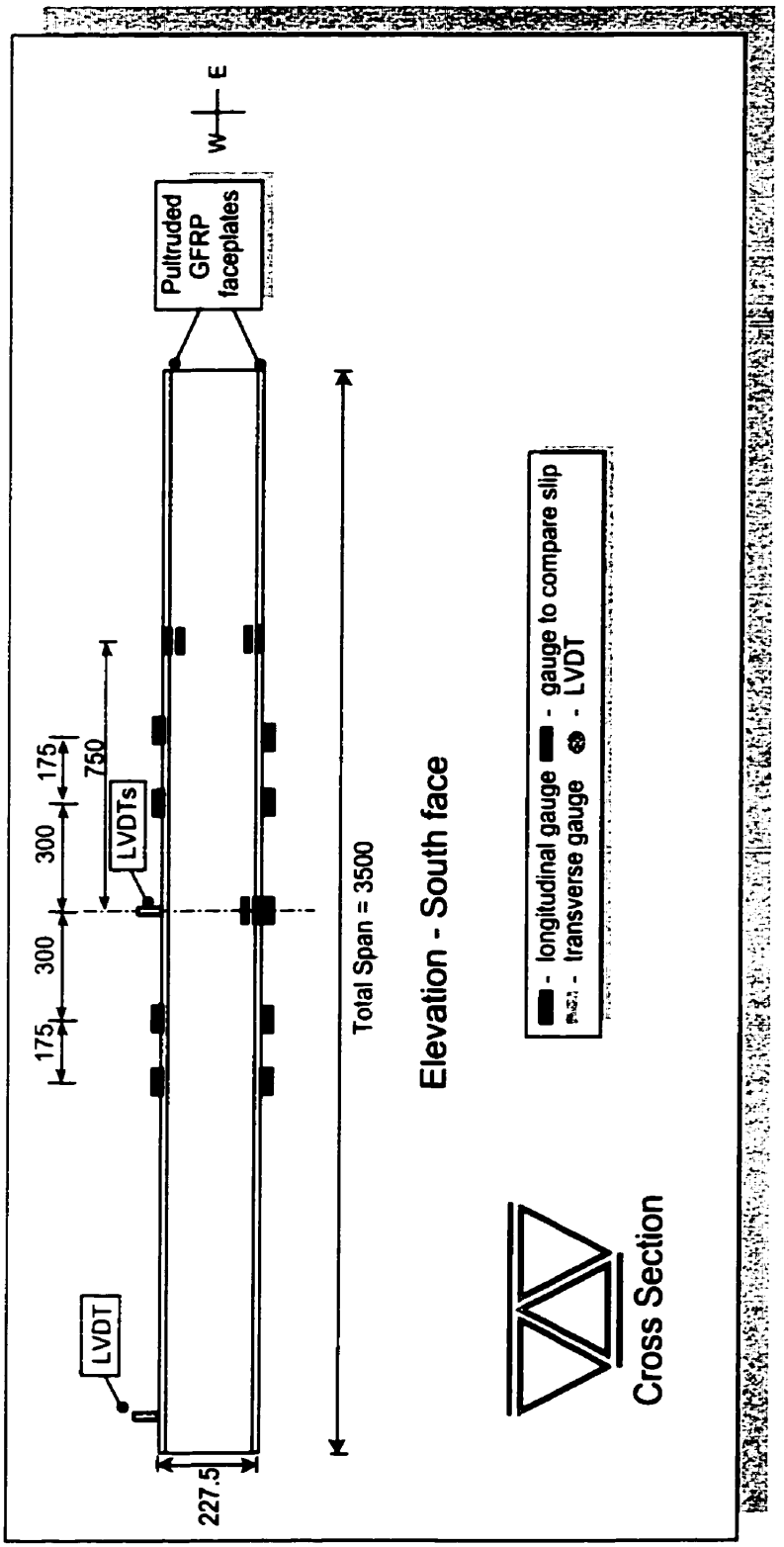

Figure 3.23a: Instrumentation for F2-TB-a (Elevation)

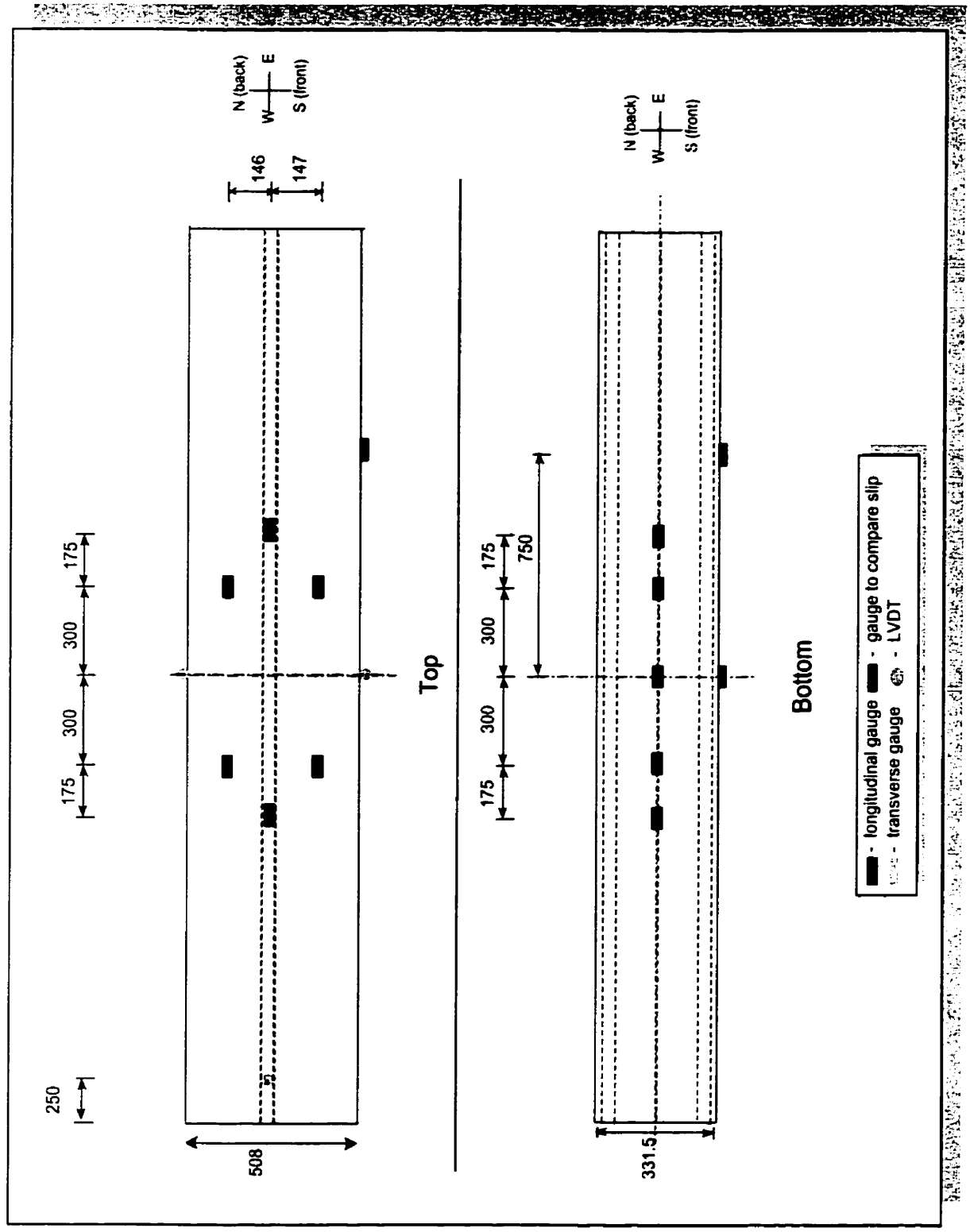

Figure 3.23b: Instrumentation for F2-TB-a (Top and Bottom)

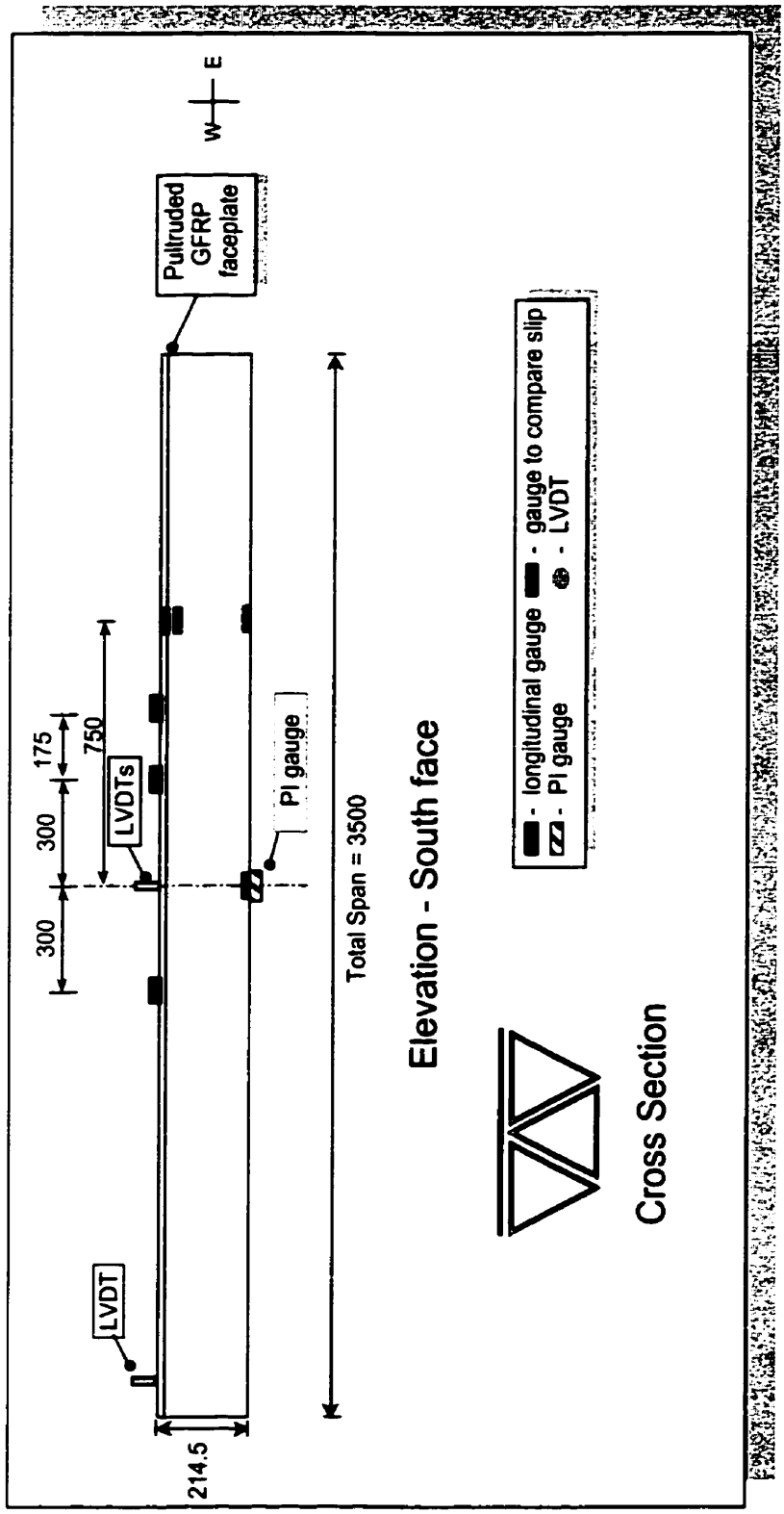

Figure 3.24a: Instrumentation for F2-T-a (Elevation)

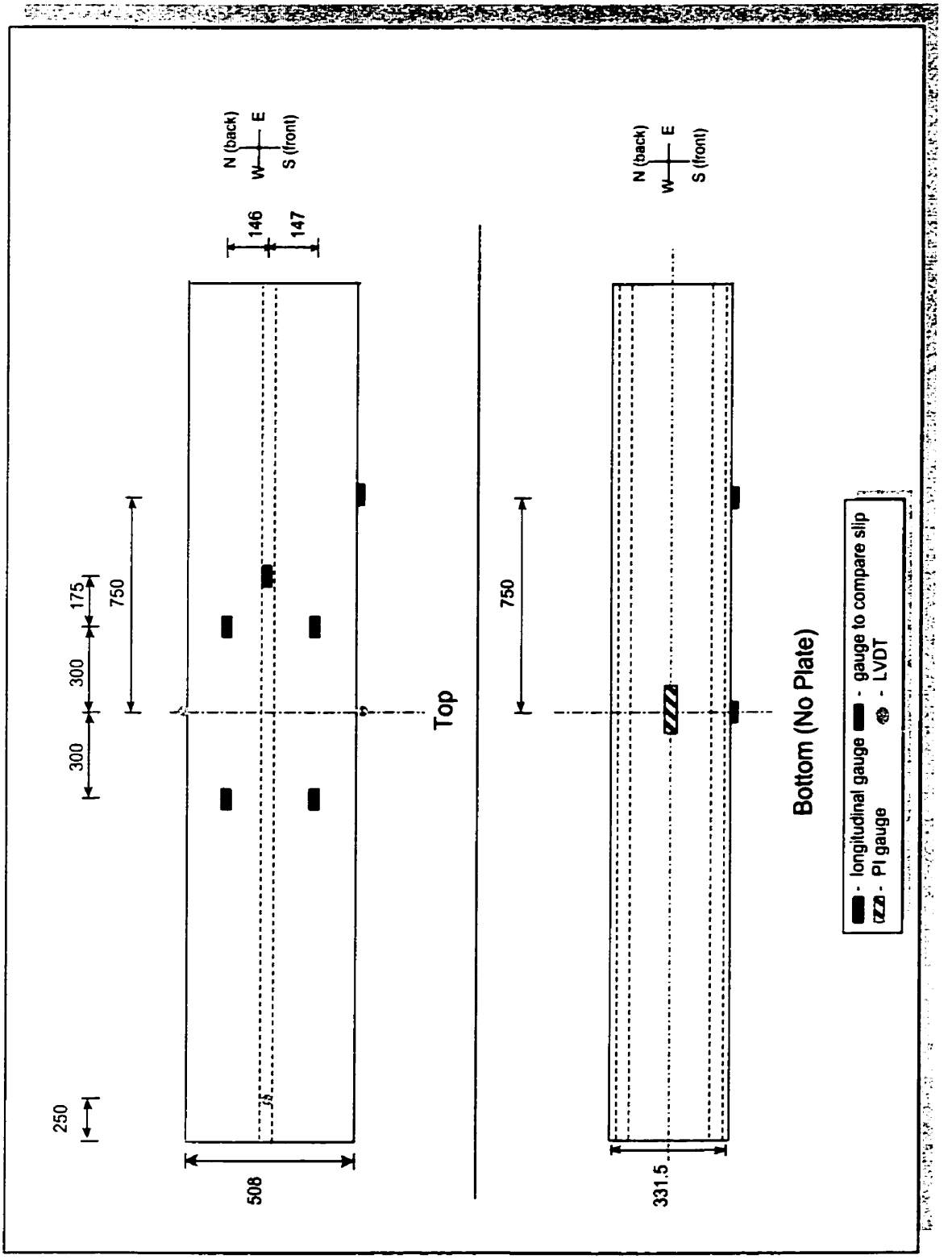

Figure 3.24b: Instrumentation for F2-T-a (Top and Bottom)

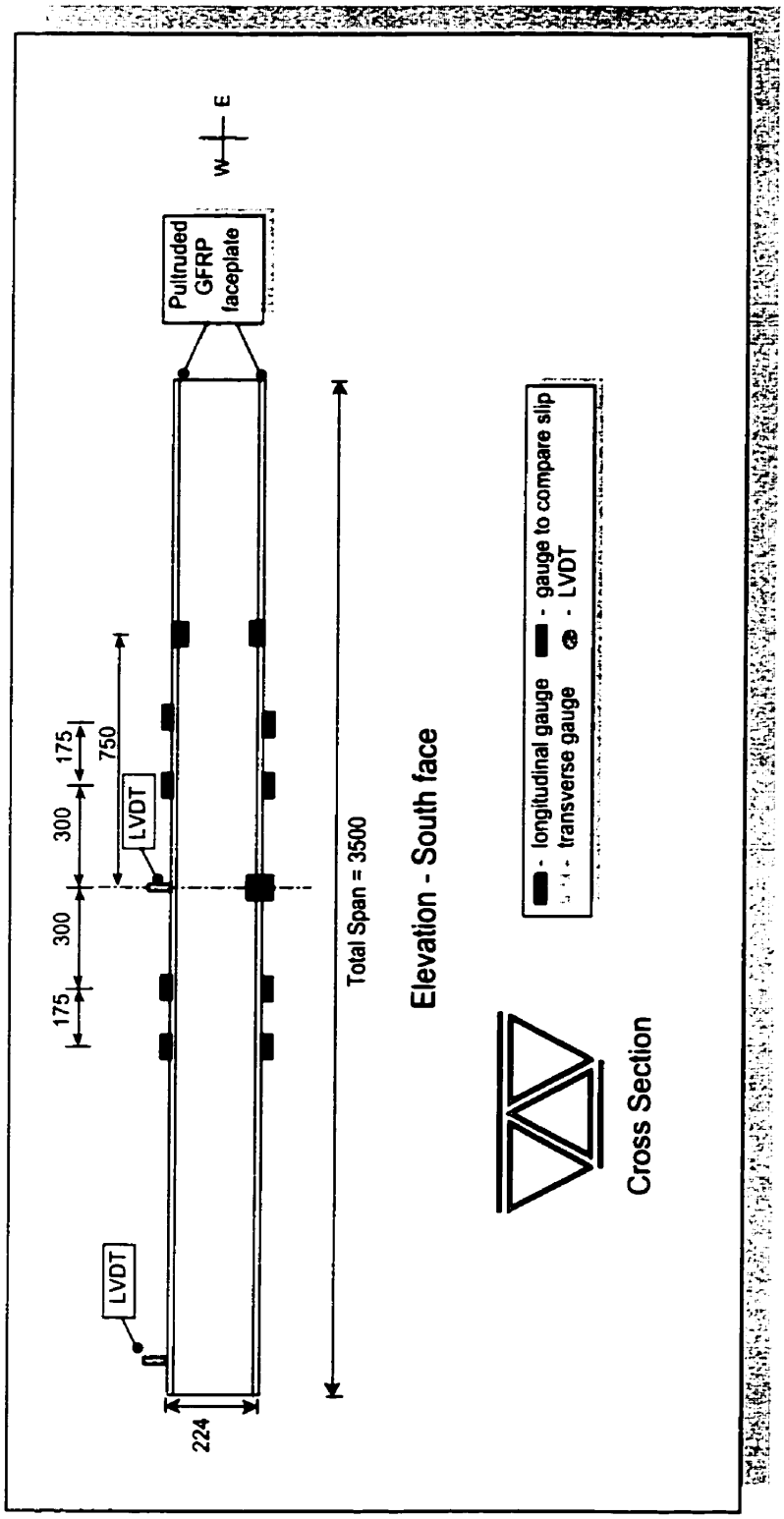

Figure 3.25a: Instrumentation for FR-TB-a (Elevation)

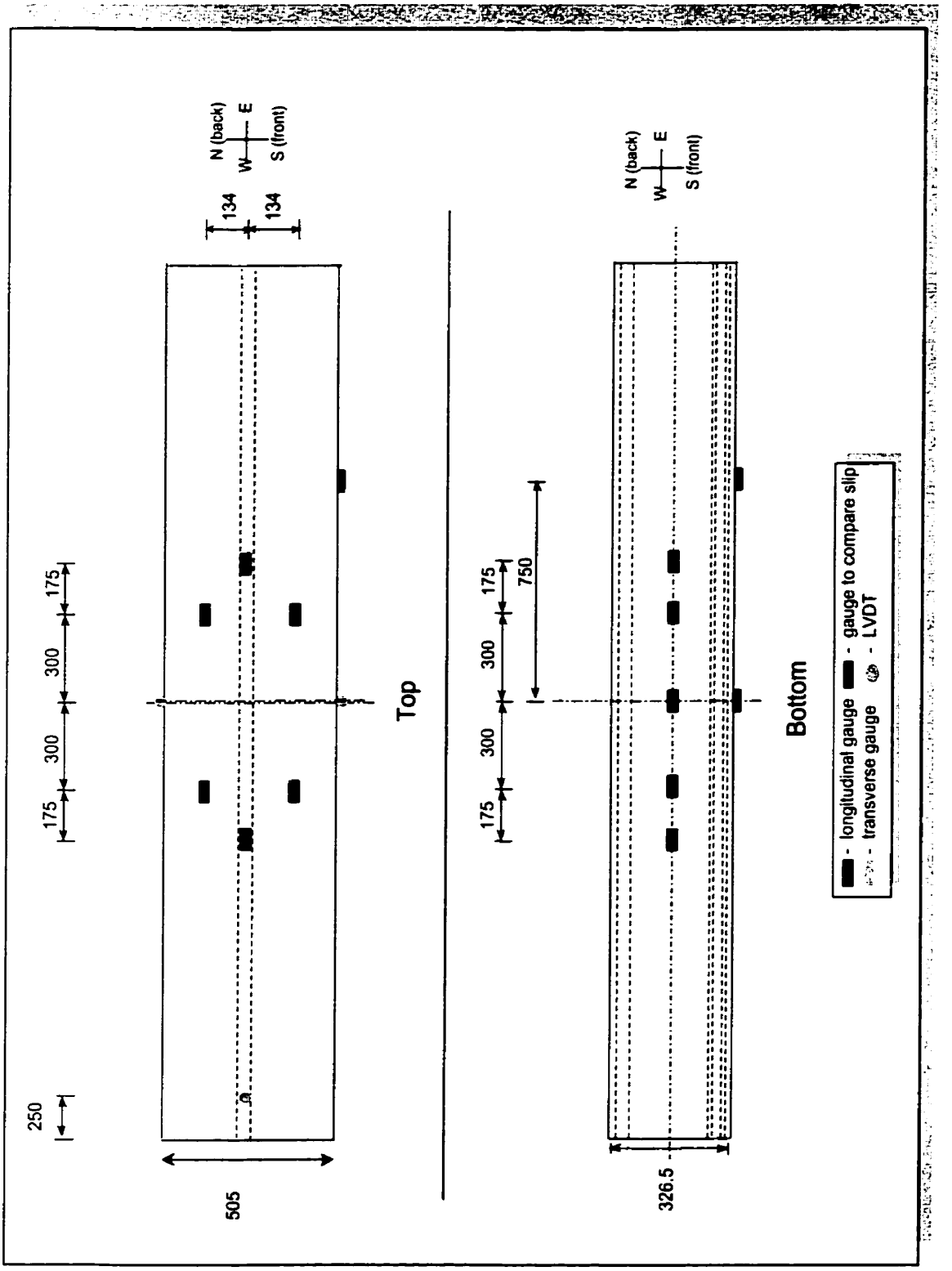

Figure 3.25b: Instrumentation for FR-TB-a (Top and Bottom)

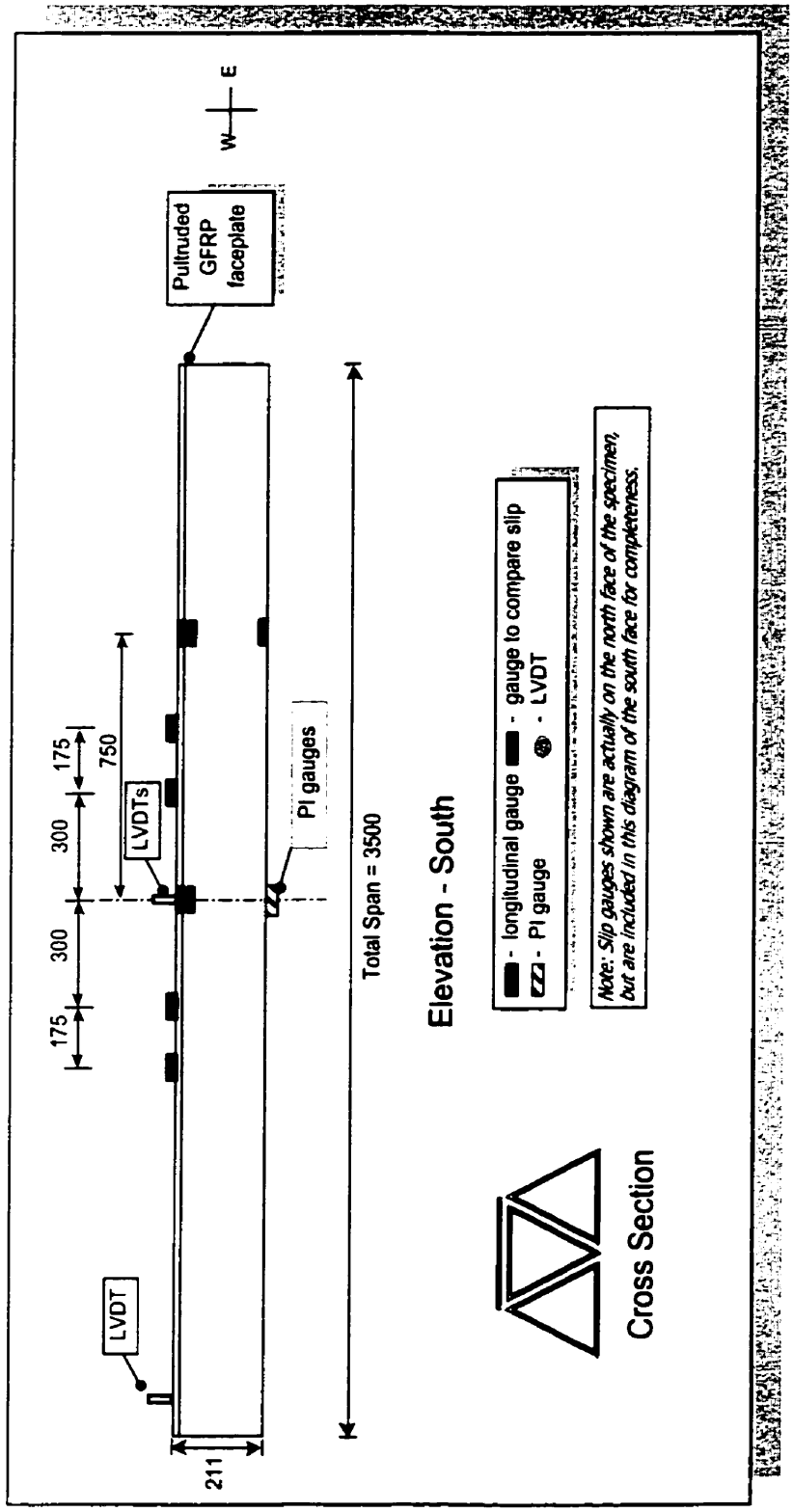

Figure 3.26a: Instrumentation for FR-T (Elevation)

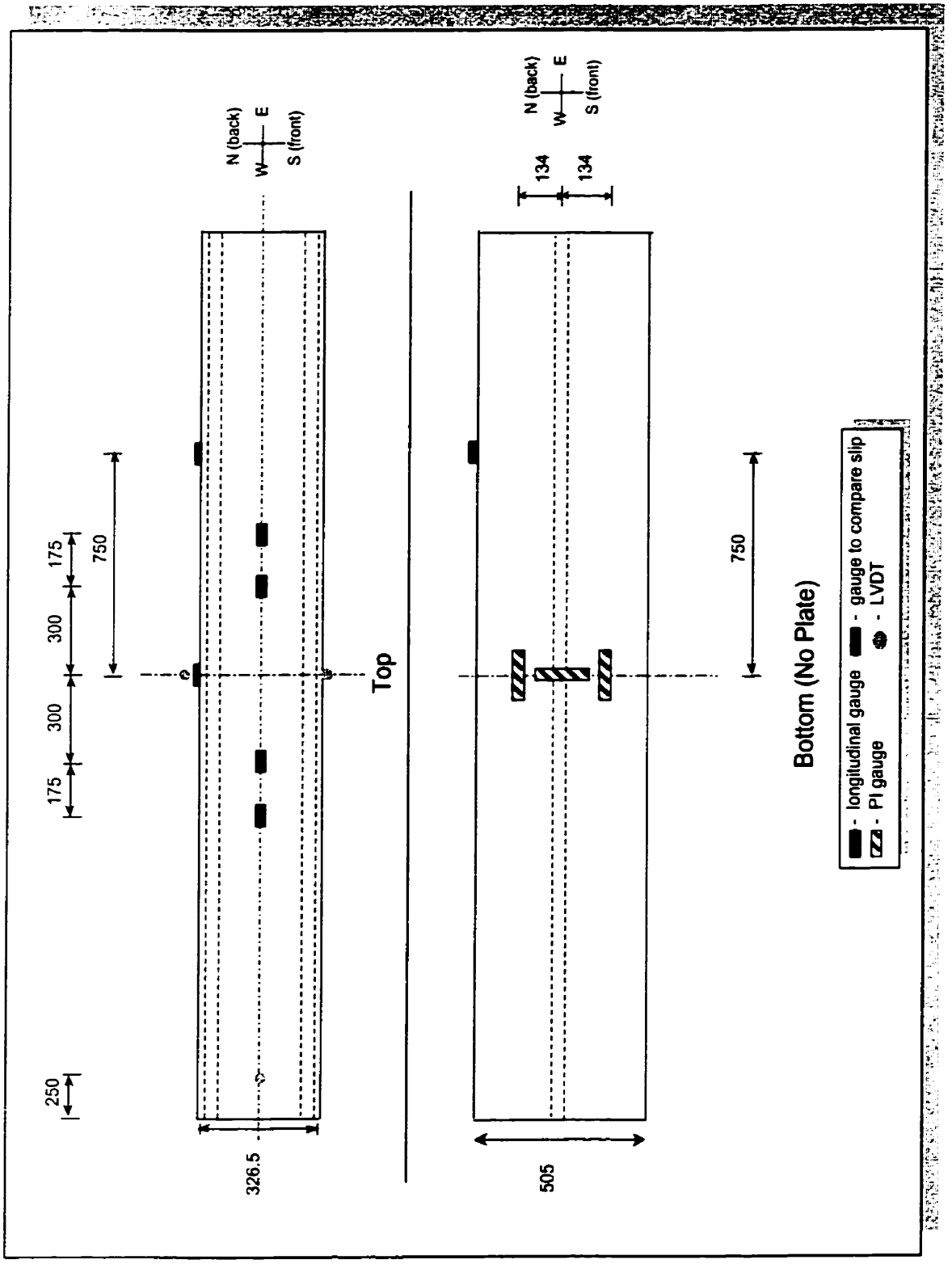

Figure 3.26b: Instrumentation for FR-T (Top and Bottom)

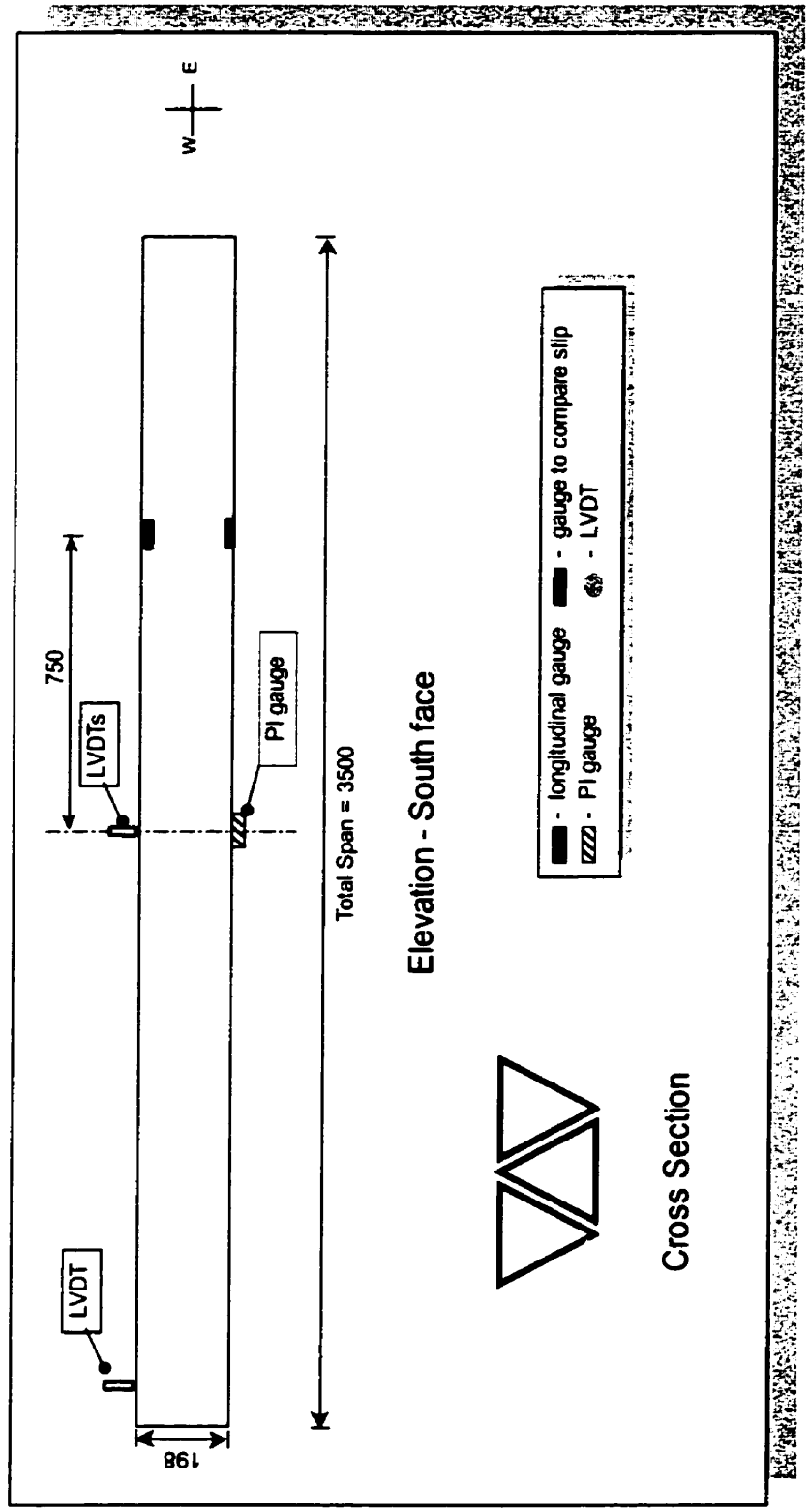

Figure 3.27a: Instrumentation for FR-a (Elevation)

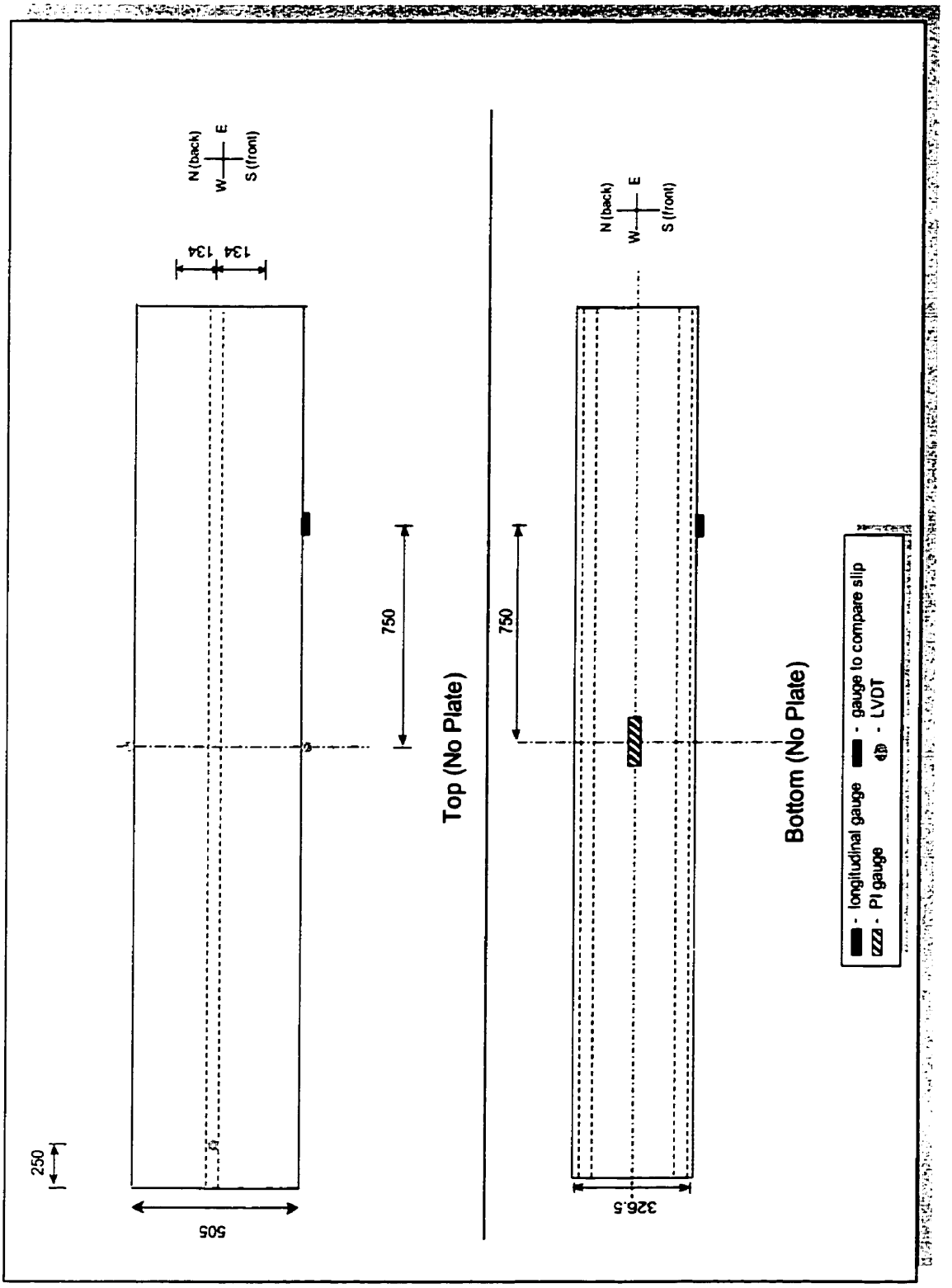

Figure 3.27b: Instrumentation for FR-a (Top and Bottom)

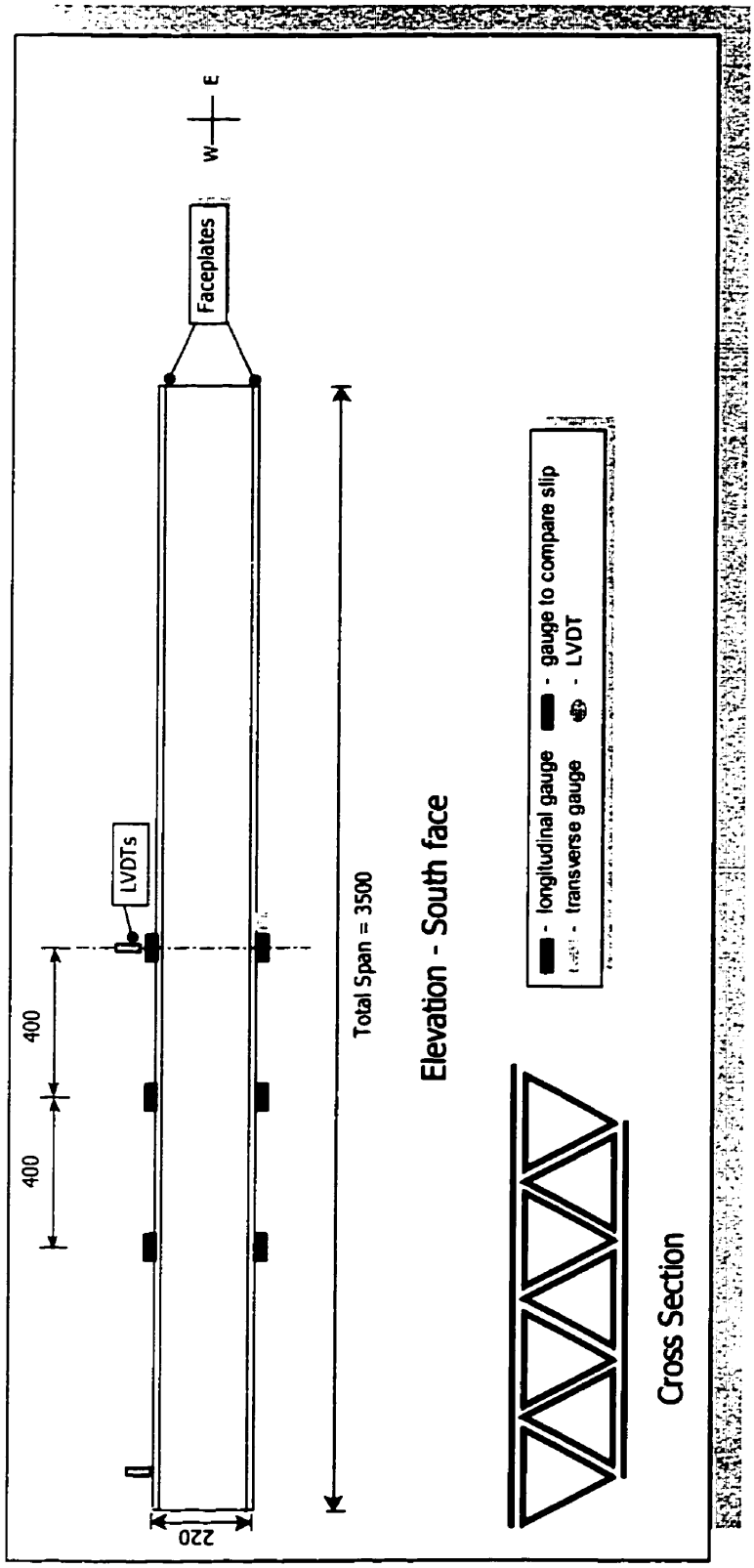

Figure 3.28a: Instrumentation for F7-1 (Elevation)

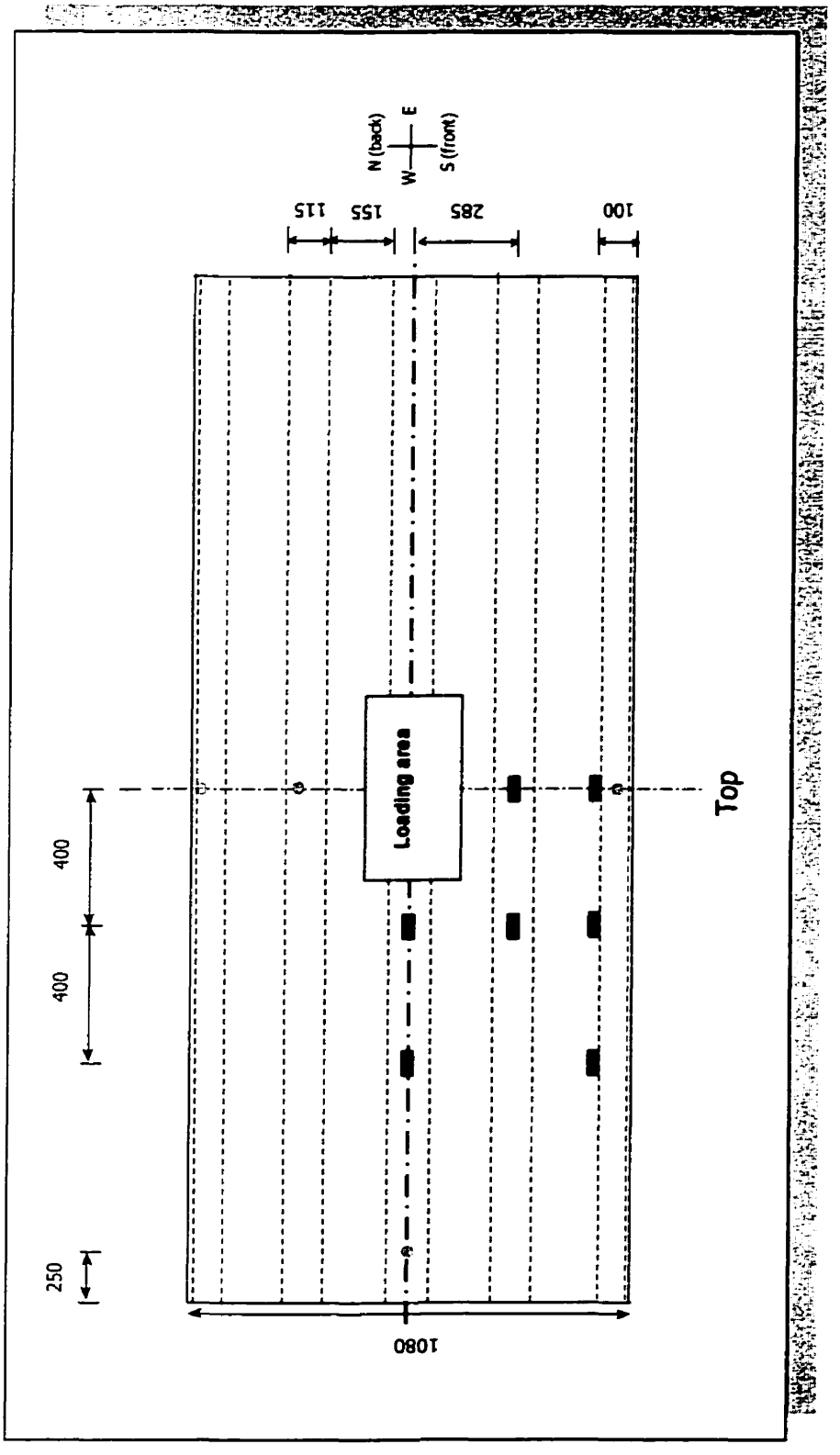

Figure 3.28b: Instrumentation for F7-1 (top)

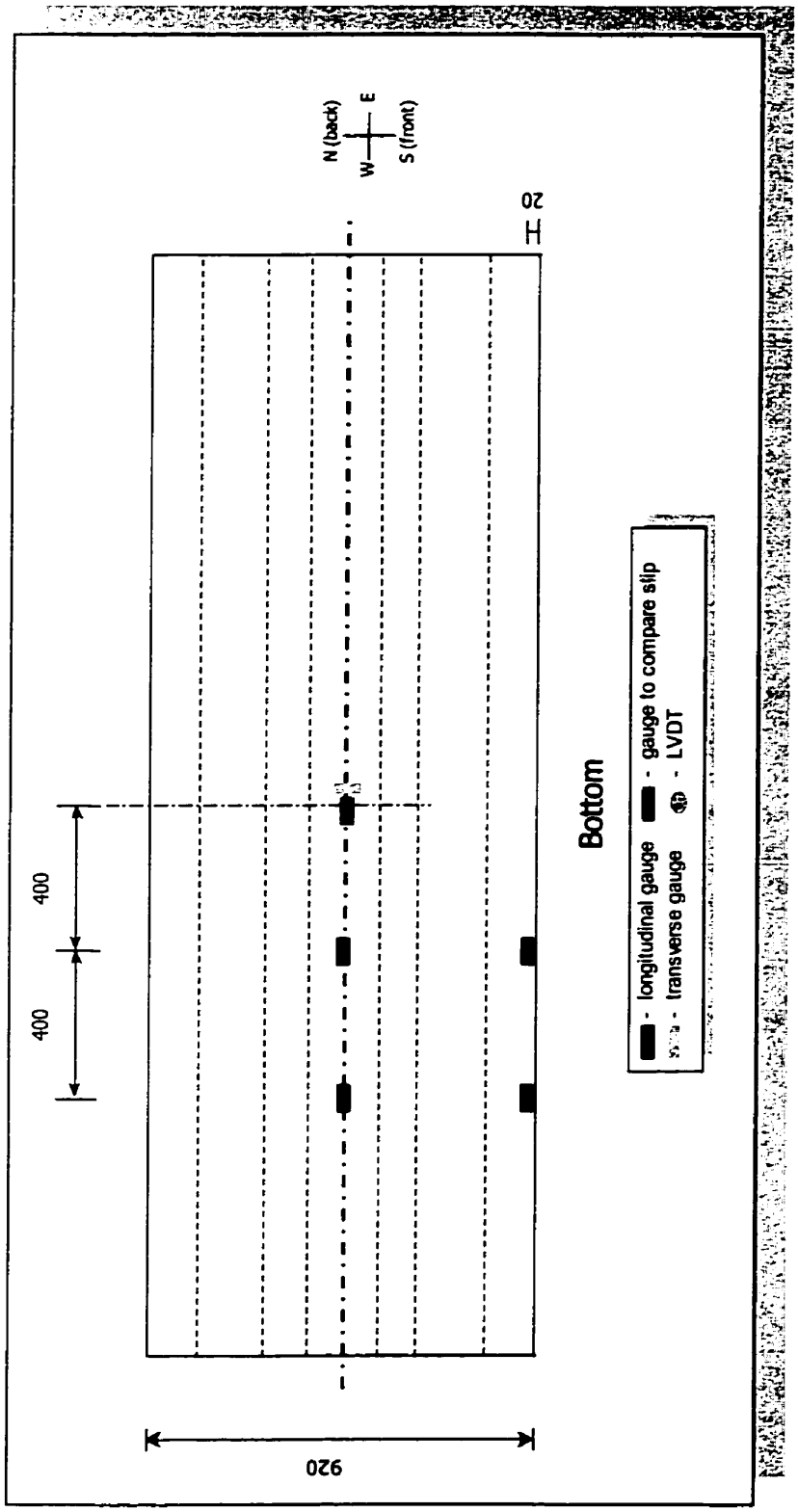

Figure 3.28c: Instrumentation for F7-1 (Bottom)

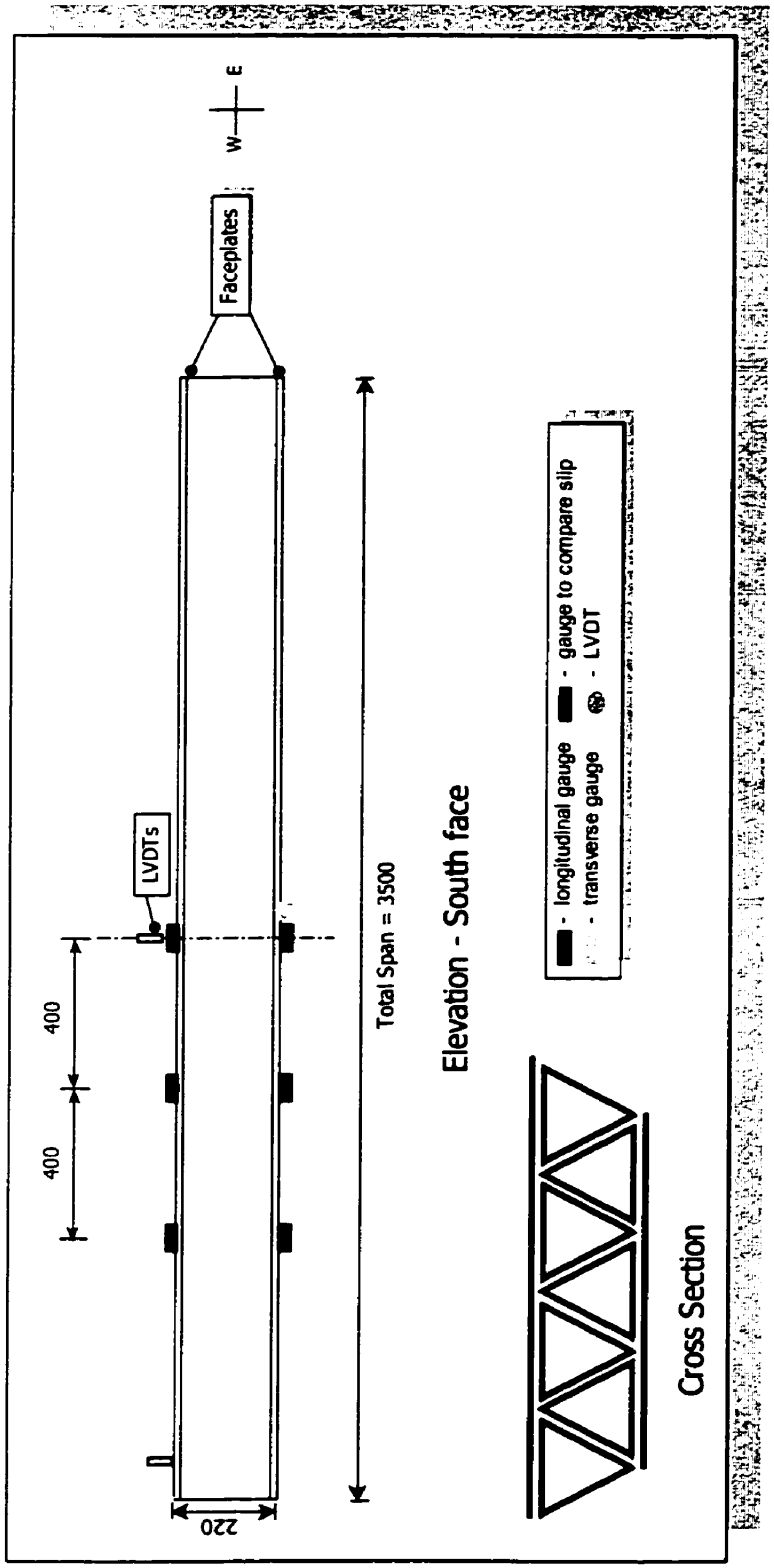

Figure 3.29a: Instrumentation for F7-2 (Elevation)

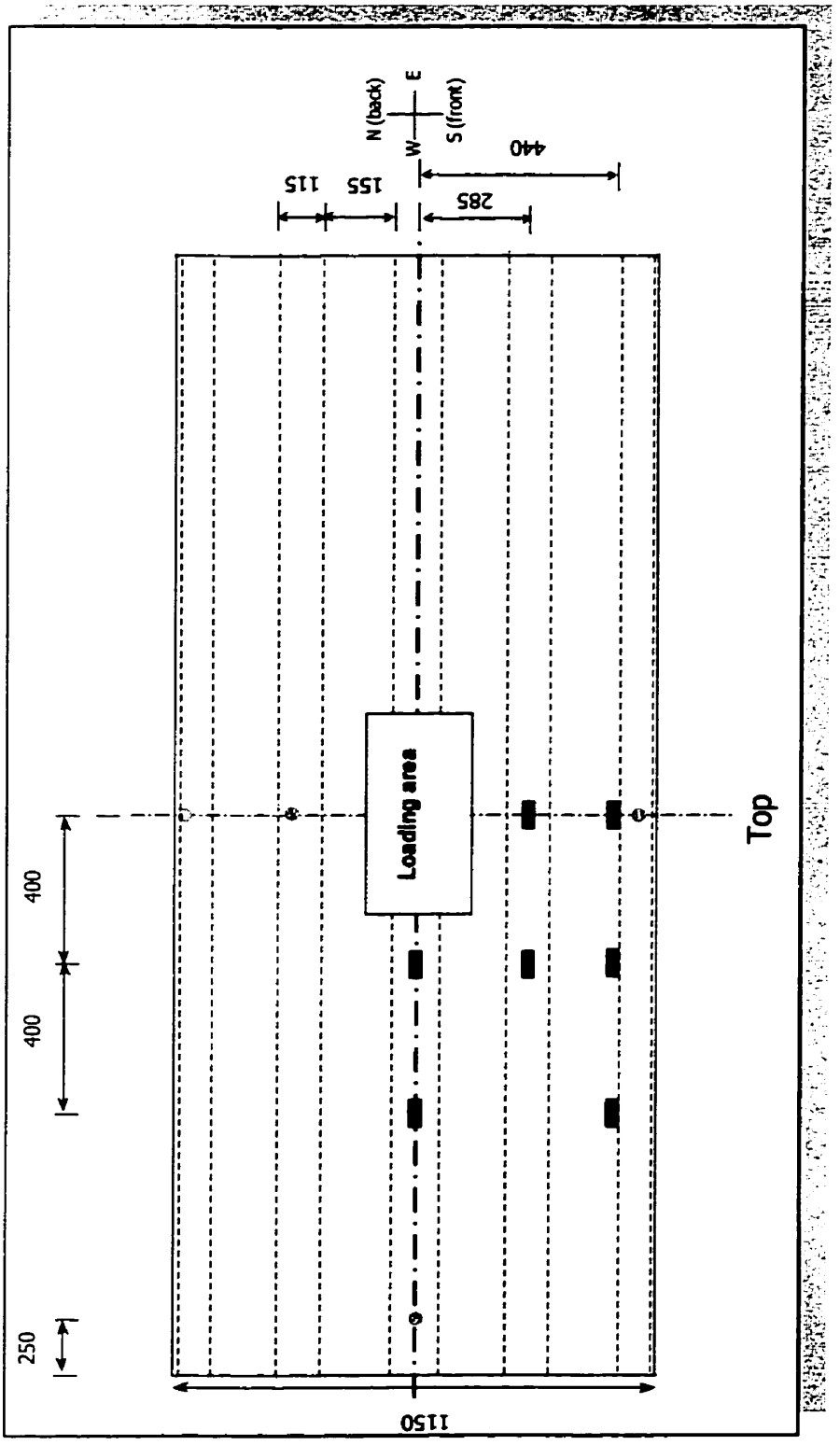

Figure 3.29b: Instrumentation for F7-2 (Top)

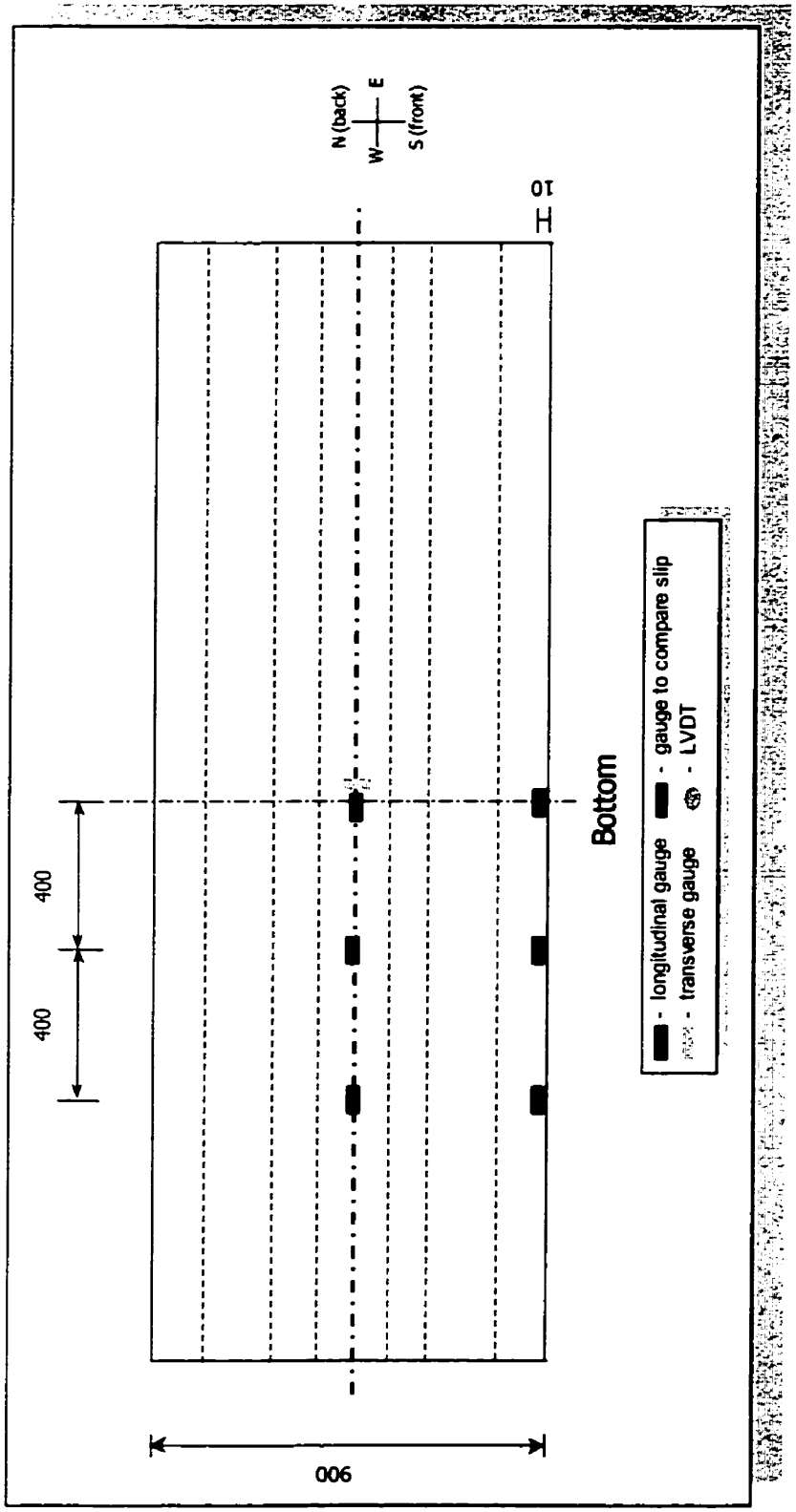

Figure 3.29c: Instrumentation for F7-2 (Bottom)

3.8 Test Setup

Testing was conducted at the McQuade Structural Lab at the University of Manitoba. Testing of the three-tube deck units (Phase I) was done using a 1000-kN capacity closed-loop MTS machine. A single 250 x 250 mm point load was applied using stroke control at the centre of the 3m span to simulate the wheel load of a truck. Figure 3.30 illustrates the flexure test setup where the deck is simply supported on roller supports.

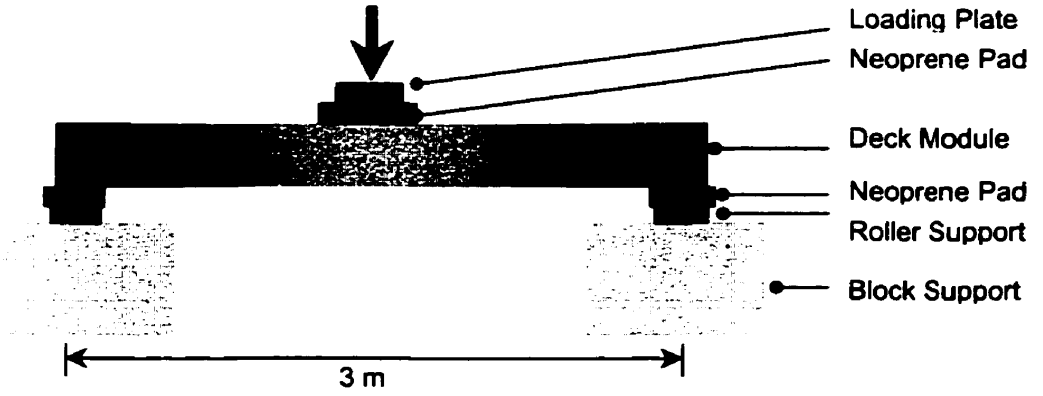

Figure 3.30: Schematic of Flexure Test Setup for Phase I Modules

At both the supports and the central loading point, neoprene pads of 15 and 25 mm thickness, respectively, were used. Figure 3.31 shows the test setup in the lab.

Figure 3.31: Test Setup for Phase I Modules

Testing of the larger deck units (Phase II) was performed using a 5000-kN capacity closed-loop MTS machine. A single point load of 570 x 225 mm was applied under stroke control at the centre of the deck's 3m span, as shown in Figure 3.32.

Figure 3.32: Test Setup for Phase II Modules

The 570 mm length of loading plate was located parallel to the 3m span of the deck. This ensured that the double wheel load area of an AASHTO design truck (250 x 600 mm) was properly represented in test conditions. A schematic diagram describing this concept is provided in Figure 3.33.

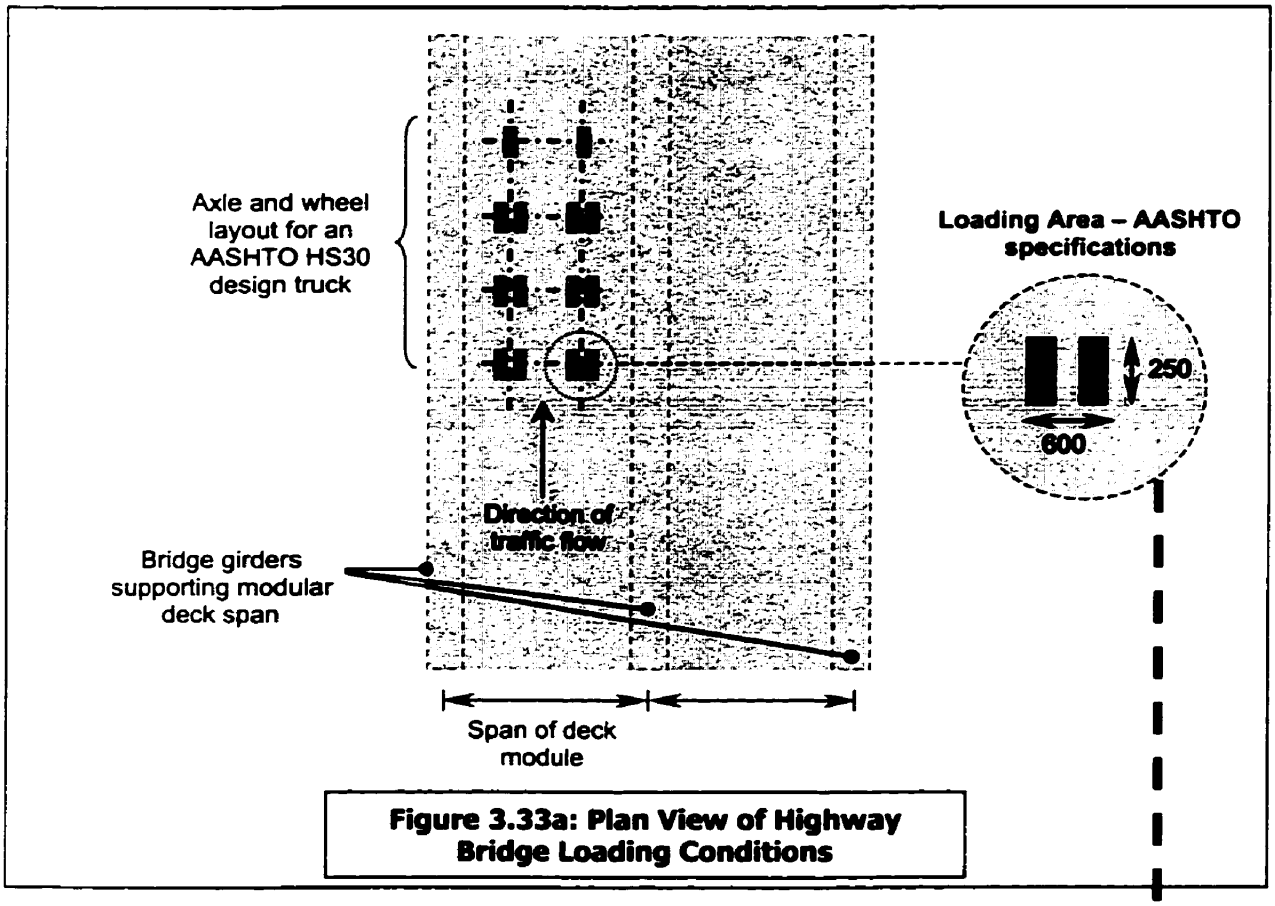

Figure 3.33a: Plan View of Highway Bridge Loading Conditions

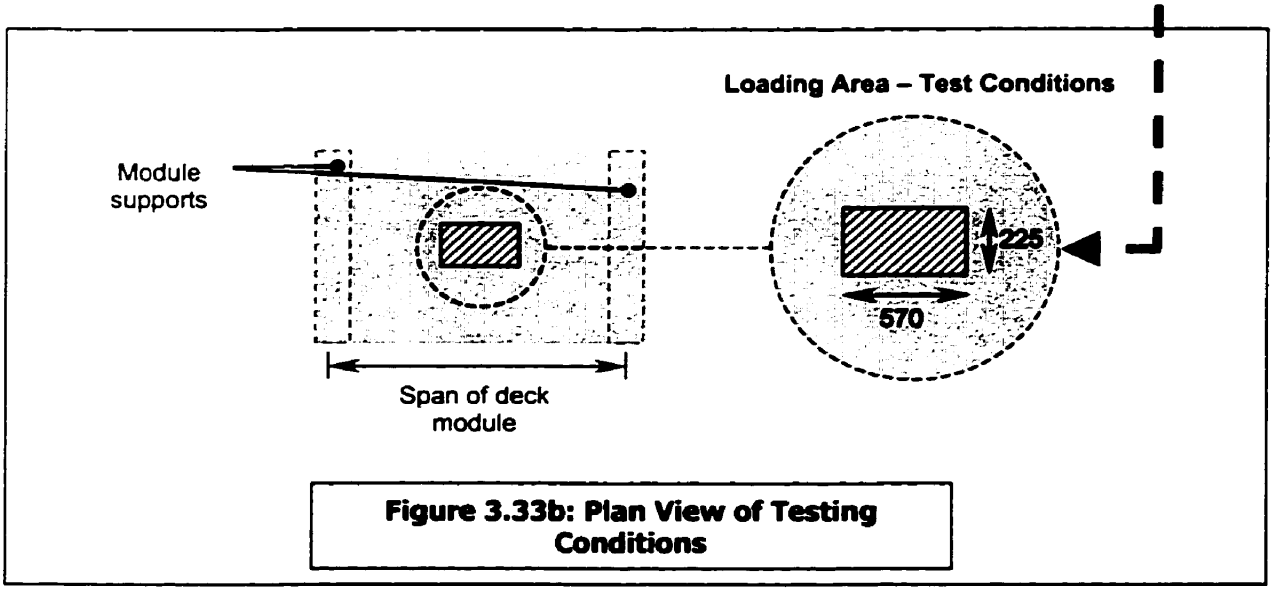

Figure 3.33b: Plan View of Testing Conditions

CHAPTER FOUR:

TEST RESULTS AND ANALYSIS OF THE EXPERIMENTAL PROGRAM

The test program consisted of two phases. The first phase included the first generation of decks, which consisted of three tubes. The second generation, which realized considerable improvement based on the experience from the first phase, consisted of seven-tube specimens. The results presented in this chapter are reported in the same sequence.

4.1 Load-Deformation Relationship and Mode of Failure

4.1.1 Three-Tube Specimens

The measured load-deflection relationship for tests performed on Deck F1 are shown in Figure 4.1.

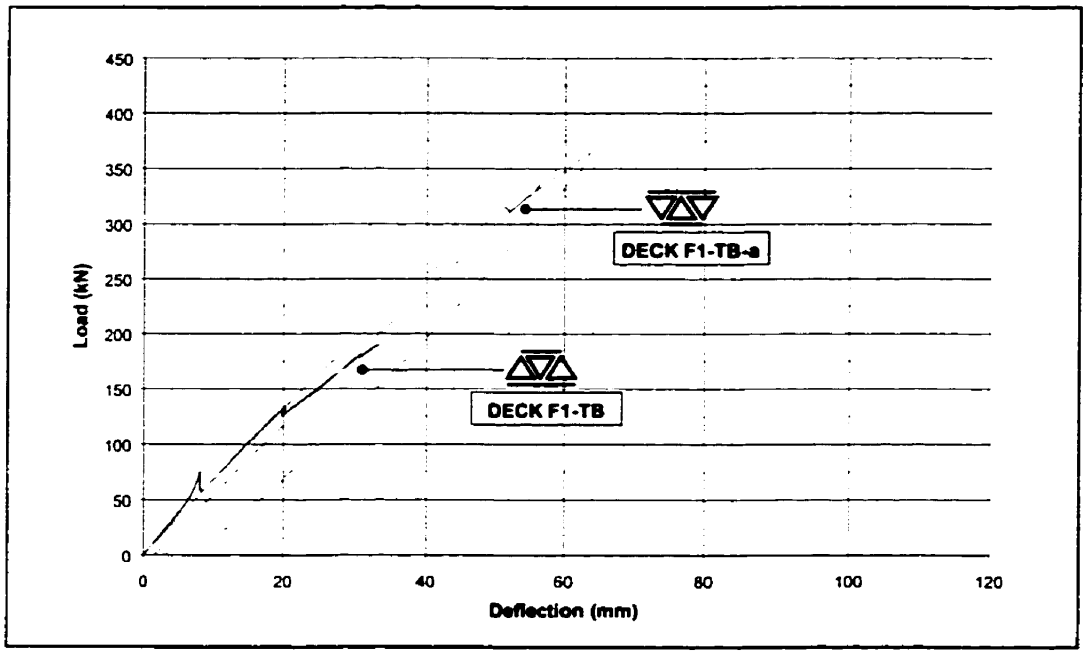

Figure 4.1: Load-Deflection for Deck F-1 Group

The first test done on this specimen was denoted *F1-TB*. The slight increase of the stiffness of *F1-TB* at a load level of 75 kN could be attributed to possible restraint of the deck at the interface with the neoprene supports, as evident by the observed sudden release of energy as the deck adjusted itself. The small drops of the load at the end of testing were associated with the sound of cracking. Neither the crack location nor its separation between the different components could be found externally. Test *F1-TB* reached a load level of 190 kN when the top plate buckled and failure was observed. This plate buckling was to be encountered again in future tests and was attributed to the fact that the five layers of the plate were not properly bonded, leading to premature local buckling. This feature was improved upon in the manufacture of the plates for Phase II decks. The local buckling failure in *F1-TB* is shown in Figure 4.2.

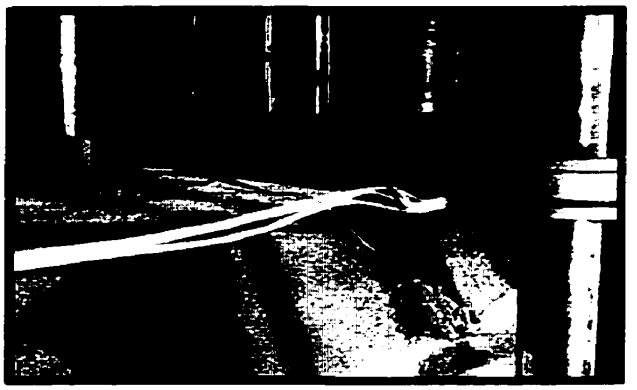

Figure 4.2: Plate Buckling in F1-TB

Upon completion of the first test of deck F1, the specimen had suffered minor damage other than the buckled upper plate. The same specimen was then rotated to a new orientation and retested as *F1-TB-a*. Deck F1 displayed virtually the same linear stiffness in the second test, reaching much higher loads. In the initial loading, the deck experienced some stiffness loss at higher loads, again due to resin cracking. At a load of 265 kN, the deck was unloaded and reloaded again. Unloading resulted in a permanent deformation of 2 mm. Upon reloading, the deck demonstrated stiffness similar to that of initial loading until failure at a load of 350 kN. The ability to recover deformation and retain original stiffness is considered a promising characteristic of the performance of the deck.

The failure of deck *F1-TB-a* came as the result of delamination of the lower plate. This mode of failure is reasonable, since the same plate had delamination initiated by buckling in the previous test. The delamination is shown in Figure 4.3.

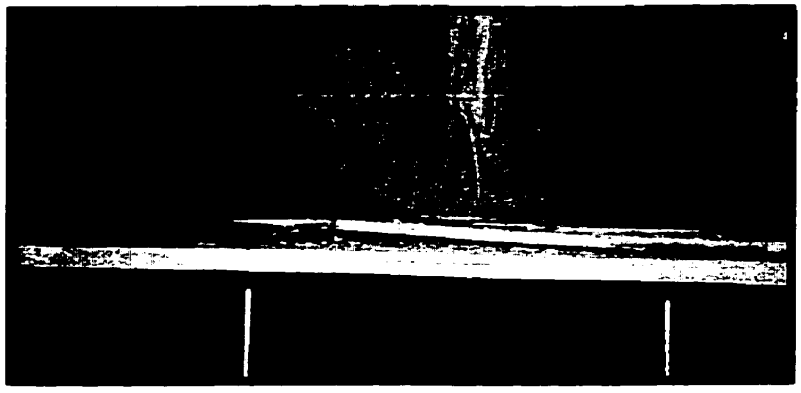

Figure 4.3: Plate Delamination in F1-TB-a

The load deformation behaviour for the Deck F2 group is shown in Figure 4.4.

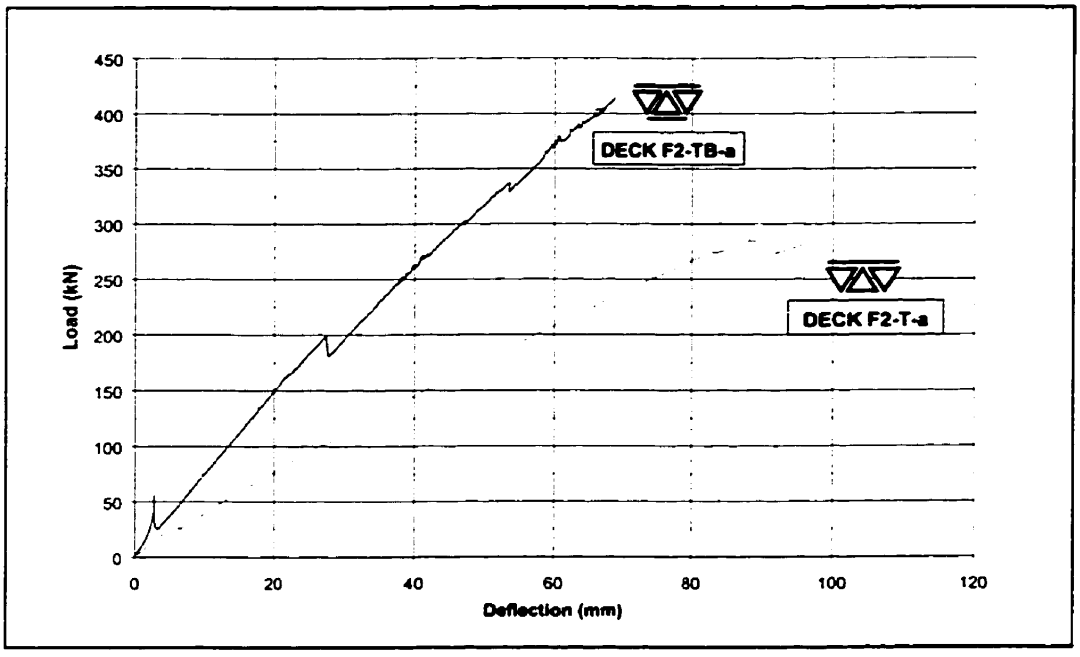

Figure 4.4: Load-Deflection for Deck F-2 Group

A linear behaviour was measured for the original test *F2-TB-a* and after removing the bottom plate in test *F2-T-a*. Support restraint of the deck was also observed for *F2-TB-a*, at early load levels of the test of 50 kN. The load drop at 200 kN in *F2-TB-a* is

associated with the slippage of the filler bars from this section. This behaviour was accompanied by a loud "pop" and was physically observed by protrusion of the bars from the deck, as shown in Figure 4.5.

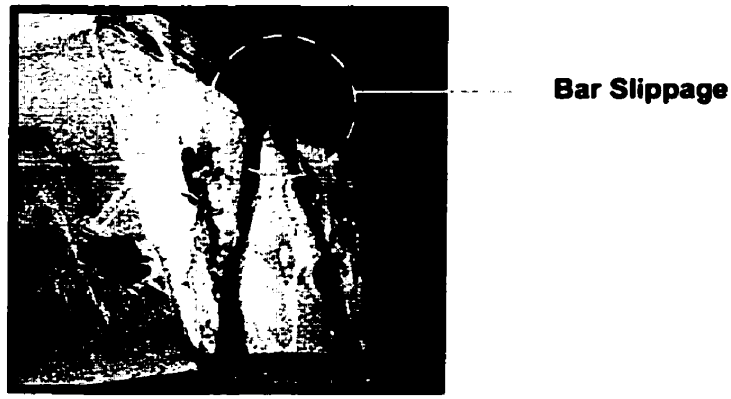

Figure 4.5: Bar Slippage in F2-TB-a

This localized failure did not significantly affect the load-deflection behaviour of *F2-TB-a*. At a load level of 300 kN, the upper ply of the top plate suffered local buckling without significantly affecting the behaviour and the specimen was able to continuously maintain the load. By increasing the applied load, further cracking and subsequent load deviations occurred until failure at 414 kN. The failure occurred as a result of delamination of the bottom plate from the tubes, as shown in Figure 4.6. The bond between these two components was expected to be weak due to manufacturing problems.

The lower plate of Deck F2 was removed and the deck tested in the same configuration for test *F2-T-a*. Therefore, its observed stiffness was significantly less than the original deck specimen. Due to the initial buckling of the upper plate, the buckling mechanism propagated across the width of the upper plates between the loads of 110 and 285 kN.

Upon buckling and complete delamination of the top plate from the tubes at midspan at a load level of 285 kN, the load capacity of the deck was slightly reduced. However, the tubes successfully maintained the load until failure occurred at 281 kN due to buckling of the tubes, as shown in Figure 4.7.

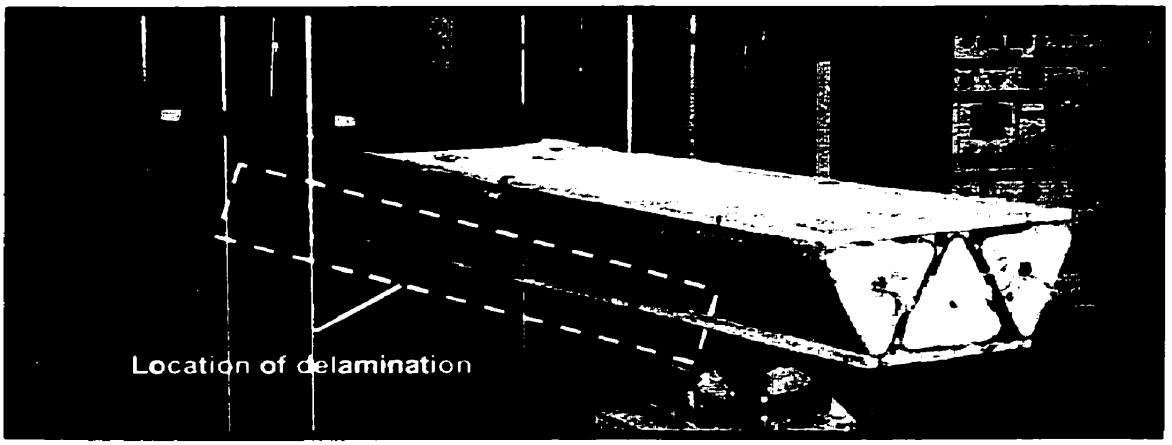

Figure 4.6: Plate Delamination in F2-TB-a

Figure 4.7: Tube and Plate Buckling in F2-T-a

The fact that the tubes picked up the load after the plate buckled and delaminated from the tubes is very important. It provides a sound safety factor for the deck. Should the plates, for whatever reason, become unable to resist bridge loads, the tubes can be relied on to carry almost the entire load safely.

Figure 4.8 shows the load-deflection behaviour for the Deck FR group of tests.

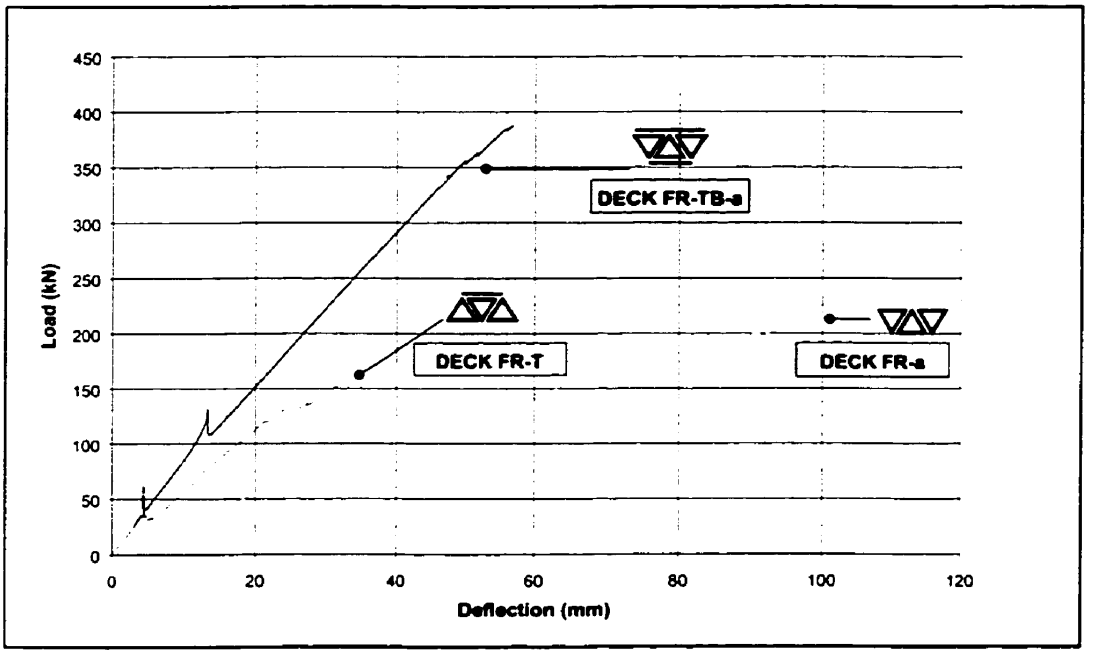

Figure 4.8: Load-Deflection for Deck FR Group

The FR series of tests also displayed linear behaviour throughout testing. Test *FR-TB-a* was the first done on the deck. The recurring support restraint problem appeared in the test, this time at a load level of about 125 kN. Apart from this anomaly, the *FR-TB-a* test displayed remarkable stiffness to significant load levels. Some stiffness was lost later in the test at a load of 261 kN when the filler bars slipped in the section. The deck finally failed at 387 kN when the top plate buckled, as shown in Figure 4.9. The buckling of the

plates was once again due to the poor bond between individual plies of the plates. In this test, the buckling was widespread across nearly the entire deck span.

Figure 4.9: Plate Buckling in FR-TB-a

The upper plate was removed and the deck rotated to a new configuration for the next test, *FR-T*. Due to the removal of the plate, the deck had a much reduced stiffness. The support restraint problem appeared again in this test around 50 kN. As well, slippage of the filler bars was evident at 143 kN, as marked by a drop in load resistance in Figure 4.8. The deck failed at 162 kN when the top plate buckled, as shown in Figure 4.10.

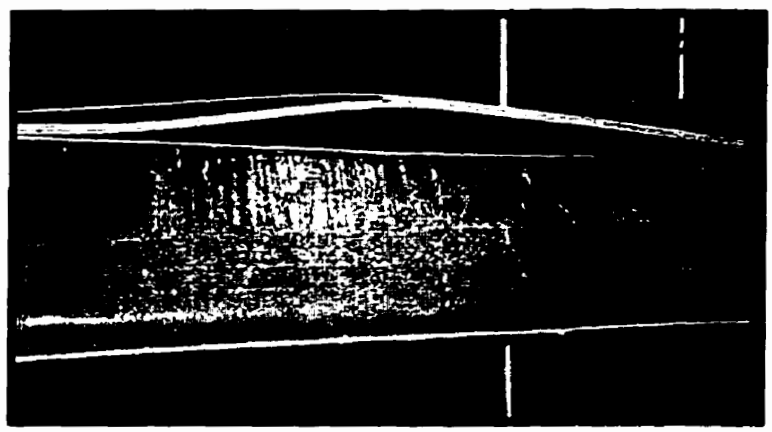

Figure 4.10: Plate Buckling in FR-T

With the removal of the last plate, the remaining tubes were tested as *FR-a*. This configuration led to the lowest stiffness and the highest ductility of all tests. Bar slippage occurred at 80 kN, leading to the load drop seen in Figure 4.8. The deck eventually failed due to buckling of the tubes at midspan at a load of 212 kN. The deck at failure is shown in Figure 4.11.

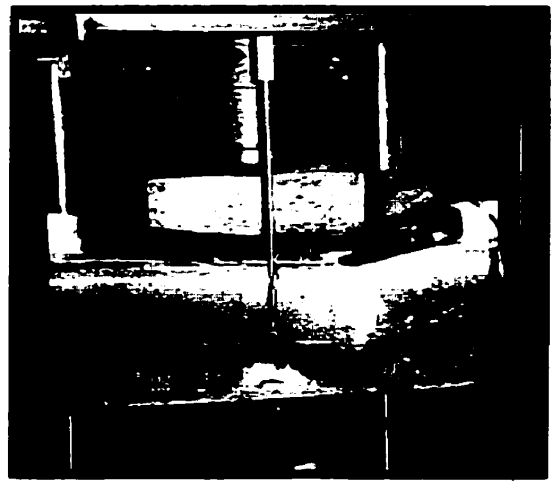

Figure 4.11: Tube Buckling in FR-a

The fact that *FR-a* failed due to tube buckling shows that the bond between the tubes is sufficient to resist separation of the tubes. Of course, this loading situation would not realistically occur on a bridge, as the plates will always be part of the modular unit. However, this test did validate that the deck components are reliable and provide the redundancy necessary for safety of the bridge.

It is also important to compare behaviour between decks. Table 4.1 summarizes failure characteristics for the Phase 1 specimens and Figure 4.12 compares behaviour of the

three intact specimens in Phase I, including the effect of the GFRP mat wrap on deck performance.

Deck	Failure Load (kN)	Failure Mode
F1-TB	190	Top plate buckled
F1-TB-a	365	Bottom plate delaminated
F2-TB-a	414	Bottom plate delaminated
F2-T-a	285	Top plate buckled and tube buckled
FR-TB-a	387	Top plate buckled
FR-T	162	Top plate buckled
FR-a	212	Tube buckled

Table 4.1: Summary of Failure Characteristics

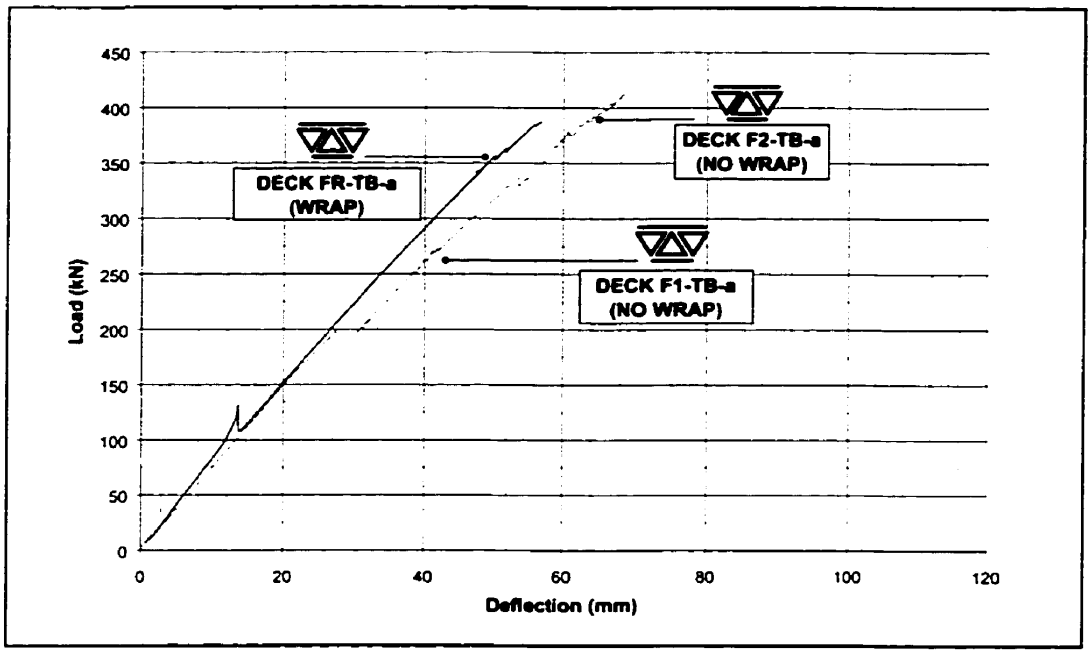

Figure 4.12: Comparison of Behaviour Between Decks

There were three modes of failure observed for the Phase I specimens: plate buckling, plate delamination and buckling of the tubes. While buckling of the plate was the most prominent mode of failure, it is not representative of a typical mode of failure for this deck. The plates used in the Phase I decks consisted of five layers which were not properly bonded together, causing premature local buckling. This feature was an area of improvement in Phase II.

It is also important to note that all decks sustained a load exceeding the wheel load of an HS30 design truck load as specified by AASHTO. This, again, provides an additional factor of safety in the performance of the deck.

With respect to the comparative load-deflection behaviour of the three intact decks, all of them displayed similar stiffness in the initial portion of the test. The load capacity of specimen *F1-TB-a* was relatively less than that of specimen *F2-TB-a* due to slippage of the filler bars. Overall, the absolute load capacity of the three decks was comparable. It appears that the addition of the GFRP mat wrap around the tubes did not enhance deck performance significantly. The stiffness was marginally improved, however the increase of ultimate load capacity was insignificant.

4.1.2 Seven-Tube Specimens

The load-deflection relationship for decks *F7-1* and *F7-2* is plotted in Figure 4.13. Load is plotted against the LVDT located closest to the load patch as depicted in the Figures 3.28b and 3.29b.

As was the case in previous tests, the *F7-1* deck displayed linear behaviour for a significant portion of the loading. Cracking between the fibre layers and internal shifting of the tubes and bars was heard around a load level of 300 kN. This corresponded to a gradual reduction in stiffness as shown in Figure 4.13. When the load exceeded a level of 500 kN a loud bang was heard from the deck, however no external damage was observed. The load then stabilized at about 400 kN and the specimen was capable of maintaining

the load even after the occurrence of internal failure. The test was subsequently stopped without observing a clear ultimate failure.

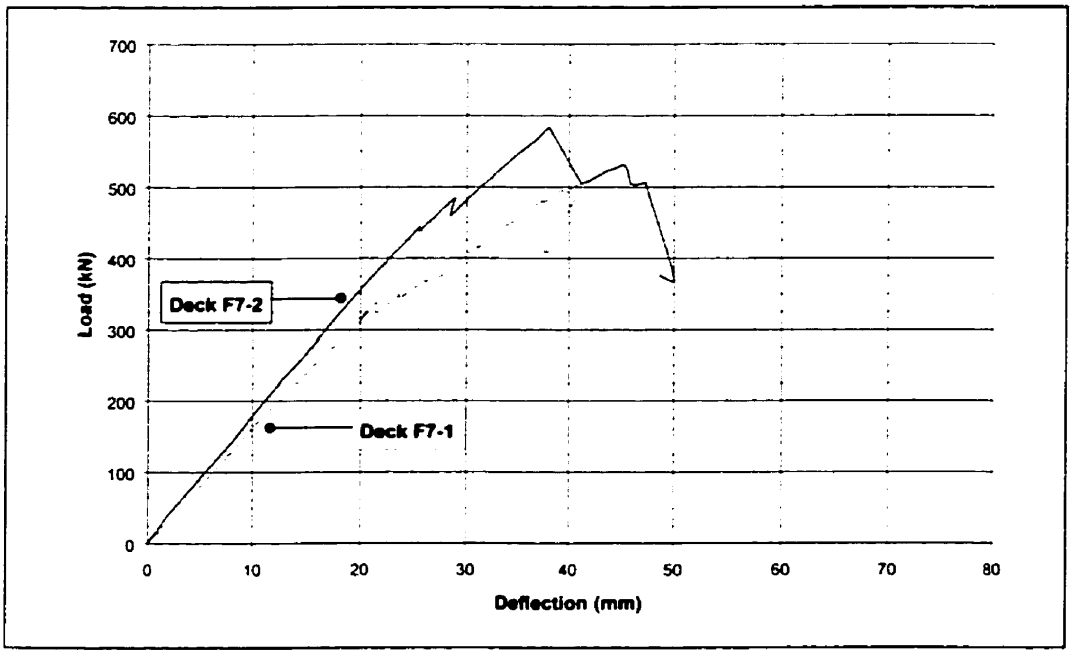

Figure 4.13: Load-Deflection for Phase II Decks

Although a definite mode of failure was not evident in the deck, several strain gauges near the loading patch displayed characteristics indicating local damage. As well, Figure 4.14 shows the deformation of the upper plate in the vicinity of the loading plate. Thus, it must be concluded that the deck suffered internal damage which did not allow an increase in the load carrying capacity above 500 kN.

Figure 4.14: Deformation Near Loading Plate of Deck F7-1

Since deck *F7-2* was the second made in the Phase II series, additional manufacturing improvements were introduced during the fabrication process. As a result, resin cracking and loss of stiffness did not occur until a higher threshold of about 450 kN. Initial failure of the deck occurred at 585 kN, signaled by delamination along the side of the tubes. This delamination occurred at the interface between the seventh wet-wound layer and the eighth dry-wound layer of the tubes, as shown in Figure 4.15. Following this, the load dropped to 400 kN prior to beginning its climb again. The final failure occurred when one of the triangular tubes at the west end of the deck slipped, as shown in Figure 4.16. Careful examination of the tube slippage showed that the bond between the two triangles was intact. That is, the outer dry-wound layers of the tubes remained bonded together. It was the bond between the inner wet-wound and the outer dry-wound layers that had failed.

Figure 4.15: Delamination of Tube Layers in Deck F7-2

Figure 4.16: Slippage of Tubes at End of Deck F7-2

The increase of the stiffness and performance of deck *F7-2* over that of deck *F7-1* is due to improvement of the manufacturing process. Since *F7-1* was the first deck made in the new series, some problems were encountered during its fabrication. This resulted in voids in the section as well as the geometry not matching the design. These problems were overcome in the manufacture of the second deck, creating a more uniform, consistent product.

Other than this difference in stiffness, the two decks generally behaved in the same manner. It is reasonable to assume that had the first deck been loaded further, it would have failed in the same manner as the second deck.

A summary of the failure data for the Phase II specimens is provided in Table 4.2.

Deck	Failure Load (kN)	Failure Mode
F7-1	507	Internal damage
F7-2	585	Tube delamination and slippage of tubes at end

Table 4.2: Failure Summary for Phase II Decks

Once again, the decks exceeded the required wheel load of an AASHTO HS30 design truck of 139 kN. With this second phase tested, a true verification of the strength capacity has been obtained.

A final important observation to make is the lack of certain failure modes in this second phase of decks. Bar slippage did not occur, proving that the grooves cut along the bar lengths did in fact improve mechanical interlocking. Buckling and delamination of the plates also did not appear. This indicates that filament winding the deck with an overwrap is a promising next step in deck production.

4.2 Deflection

4.2.1 Three-Tube Specimens

The service and maximum displacements varied in relation to the stiffness of the specimen tested. The intact specimens (i.e., those with both plates bonded to the tubes) experienced the least service and maximum deflection. It follows that the highest

deflections occurred in the decks with one or both plates removed. A summary of these deflections is provided in Table 4.3.

Deck	Maximum Deflection (mm)	Service Deflection (mm)
F1-TB	33.3	22.9 (L/131)
F1-TB-a	63.4	21.2 (L/142)
F2-TB-a	68.7	18.8 (L/160)
F2-T-a	95.7	38.7 (L/78)
FR-TB-a	56.8	18.4 (L/163)
FR-T	40.7	28.7 (L/105)
FT-a	100.0	58.0 (L/52)

Table 4.3: Deflection of Three-Tube Modules

GFRP is commonly perceived as being a brittle material, providing minimal advance warning of failure. However, based on the results above, the GFRP decks as a structural system appear to be sufficiently ductile. This implies that in actual bridge loading conditions there would not be any danger of catastrophic, brittle failure.

A second aspect of importance is the deflection at service loading of the FRP deck. AASHTO currently calls for maximum deflection of *L/800* at service (AASHTO, 1998). However, this is mainly intended for limiting bridge girder deflection. Thus, a more realistic limiting deflection should be determined. Concrete decks are usually stiff enough not to require deflection checks, and steel decks are rarely used in practice. Therefore, the best limitations to use for bridge decks are those that apply to timber decks, *L/450*. This value isn't directly applicable to a GFRP deck though, because it is desired to have a somewhat flexible deck that allows for some deformation of the wearing surface. Thus, it is reasonable to use a deflection limit of *L/360*, which is an accepted limiting value used by several deck researchers (Aref and Parsons, 1996).

The service loading conditions used for comparison are based on AASHTO's HS30 design truck, with a maximum service wheel load of 139 kN with impact. A detailed schematic of the specified loading layout is provided in Figure 4.17.

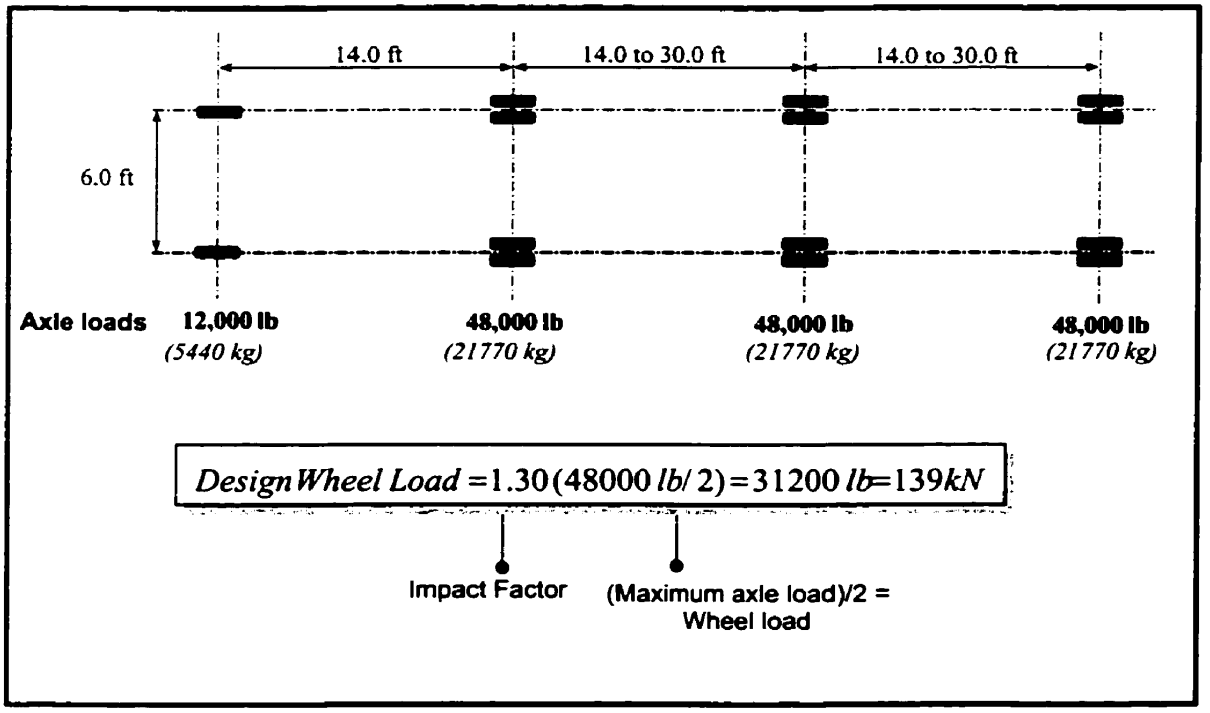

Figure 4.17: HS30 Truck Loading Specifications *(AASHTO, 1998)*

Comparison of the limiting deflection at service (*L/360*) against the actual behaviour of the decks given in Table 4.3 indicates that the intact decks did not meet the required standard. However, when these modules are used in the field, they will be installed in 7-12 tube modules, thus increasing the stiffness and allowing them to meet the AASHTO serviceability standard. In fact, this standard is met and exceeded by the seven-tube modules discussed in the following section.

4.2.2 Seven-Tube Specimens

Table 4.4 summarizes the maximum and service deflections for the decks of Phase II.

Deck	Maximum Deflection (mm)	Service Deflection (mm)
F7-1	41.2	8.7 (L/345)
F7-2	48.8	7.9 (L/380)

Table 4.4: Deflection of Seven-Tube Modules

Based on these results, it is clear that the second phase of decks was considerably stiffer than the first. This is in part due to the fact that the number of tubes in each module was increased. The change in plate lay-up sequence from 5 laminas to over 38 laminas also accounts for this improvement.

The maximum deflection of the decks was consistent with values obtained from the Phase I decks. It is the service deflection that improved greatly from the three-tube to seven-tube modules. Deck *F7-1* reached a deflection ratio of *L/345*, while deck *F7-2* surpassed the limiting ratio with *L/380*. As well, because the testing was done under simply supported conditions, the deflections obtained are overconservative compared with conditions the modules will experience in the field. It is most likely that the modules will be partially fixed at both ends, subjecting the deck to less extreme deflections than in the lab setting.

These results are significant in the overall scheme of deck development. It has now been established that the deck modules have sufficient stiffness to perform satisfactorily at service loads. Having met this standard in more than one instance signifies that a

uniform, consistent product has been created, and that the concept itself is successful. Further development of deck detailing may now take place based on this concept.

4.3 Strain Behaviour

4.3.1 Three-Tube Specimens

4.3.1.1 Axial Strain Distribution Along Span

Although seven tests were performed in this phase, the discussion will cover typical strain diagrams due to the close similarity in the behaviour for all of the tests. The behaviour of the three tests that are directly comparable, *F1-TB-a*, *F2-TB-a* and *FR-TB-a*, will be the main focus of discussion.

The axial strain distribution along top and bottom plates at various loads is shown in Figures 4.18 through 4.23.

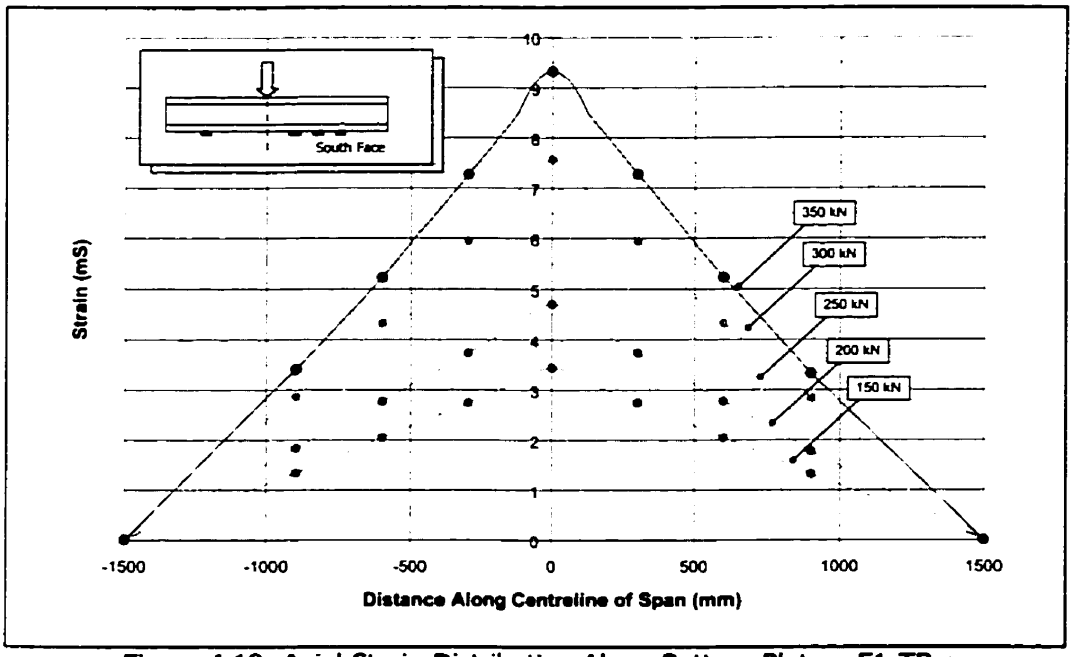

Figure 4.18: Axial Strain Distribution Along Bottom Plate – F1-TB-a

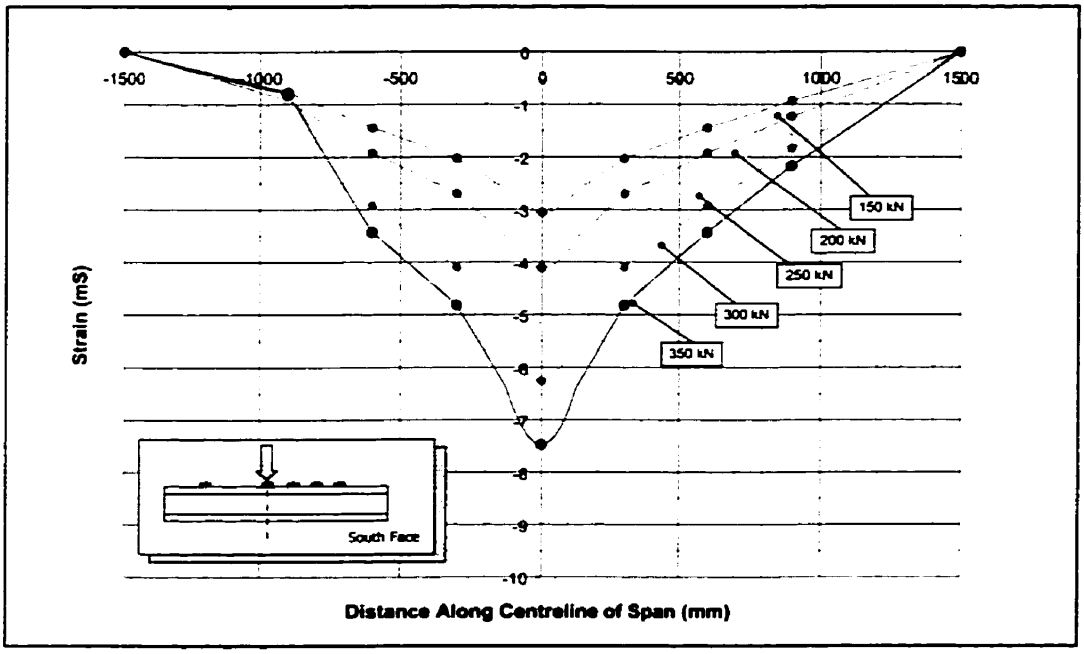

Figure 4.19: Axial Strain Distribution Along Top Plate – F1-TB-a

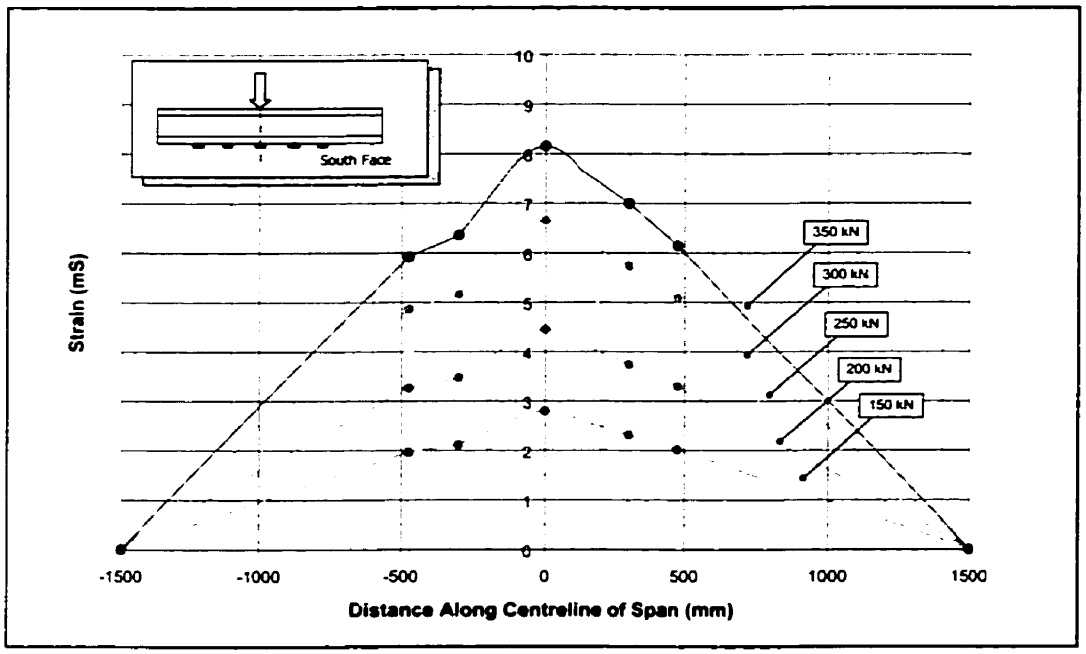

Figure 4.20: Axial Strain Distribution Along Bottom Plate – F2-TB-a

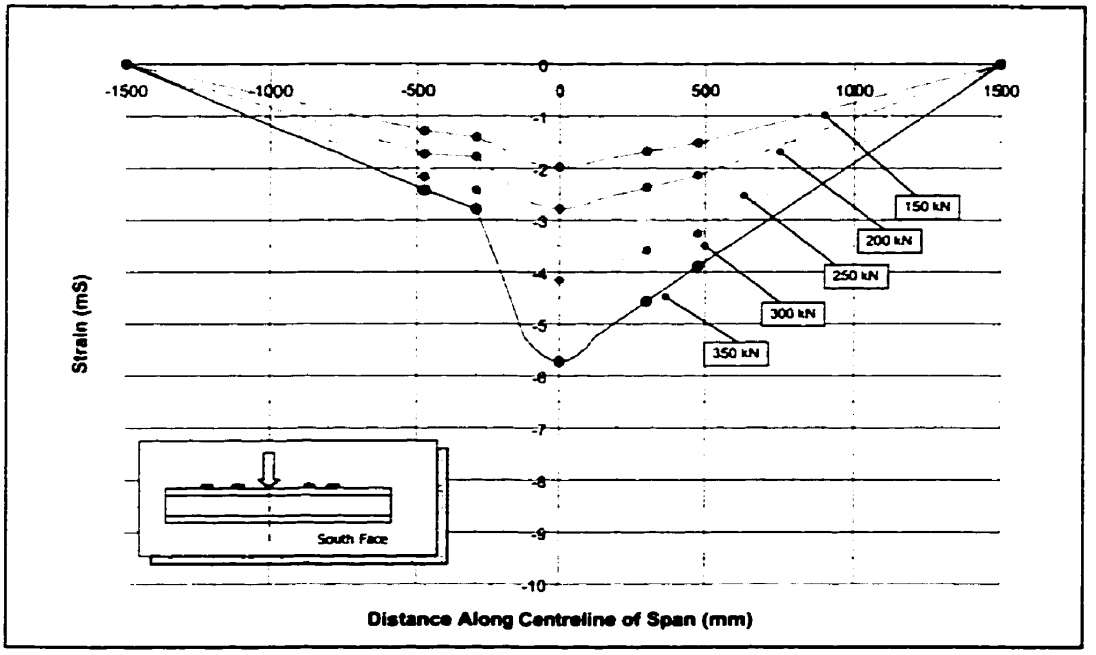

Figure 4.21: Axial Strain Distribution Along Top Plate – F2-TB-a

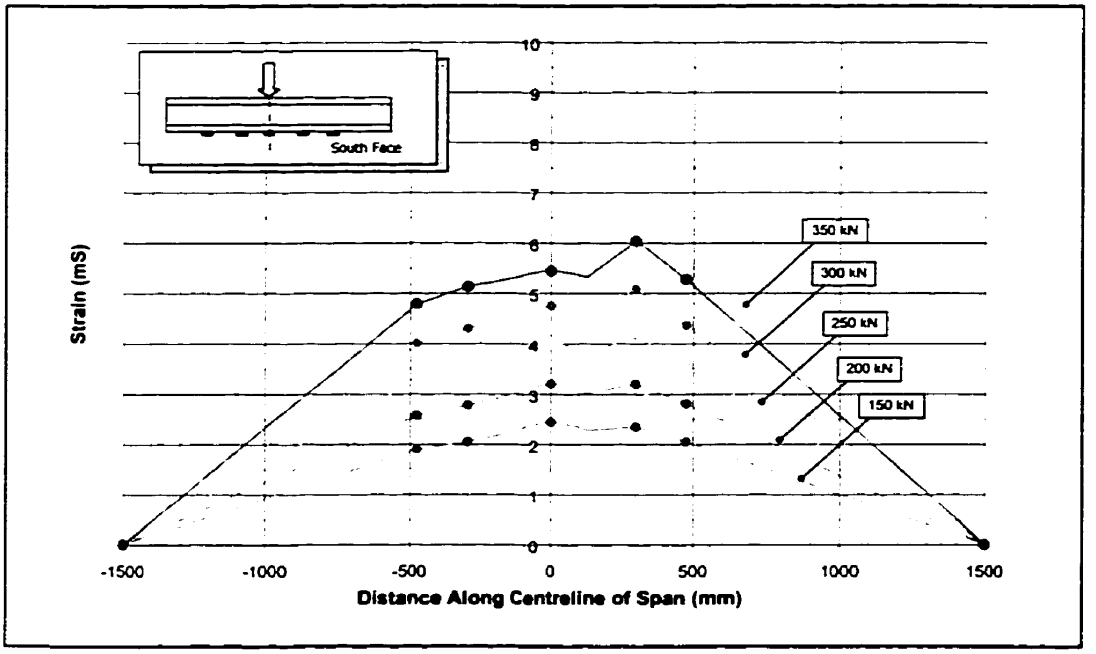

Figure 4.22: Axial Strain Distribution Along Bottom Plate – FR-TB-a

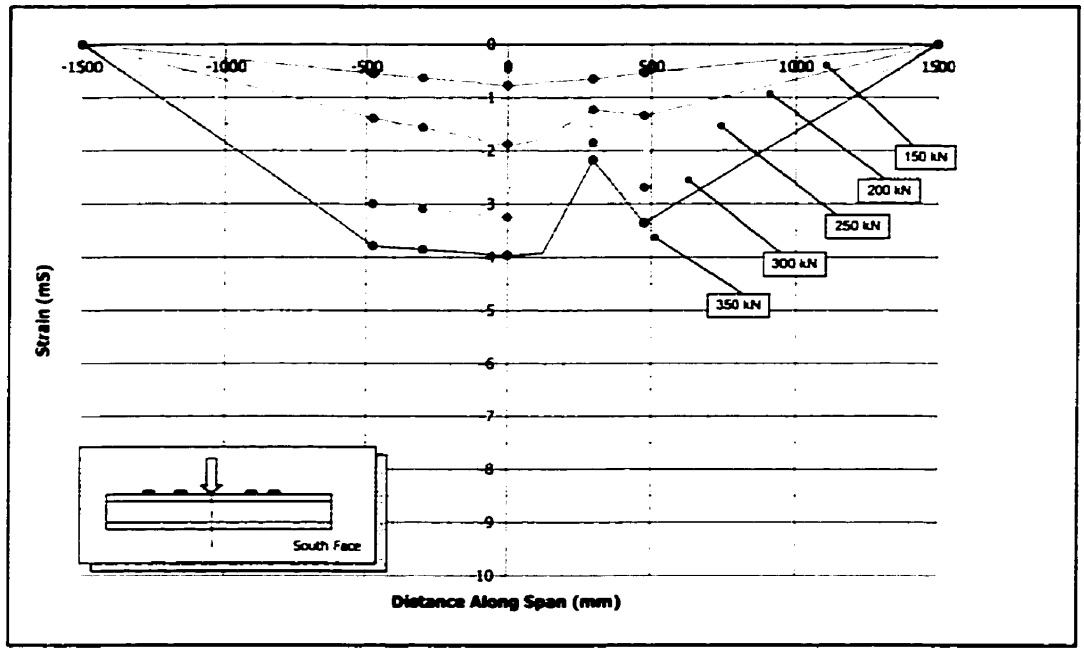

Figure 4.23: Axial Strain Distribution Along Top Plate – FR-TB-a

The results indicate that all of the decks displayed similar axial strain distributions. In most cases, the strain was well distributed along the span, with the maximum strain being at the midspan. The distribution along the bottom plate of deck *F1-TB-a* shown in Figure 4.18 is a model one, with all measured strains following a linear distribution. The corresponding distribution for the top plate, shown in Figure 4.19, was much the same with the exception of one measured point 600 mm from the left support. The fact that it continues to read virtually the same value throughout loading indicates malfunctioning of the strain gauge at this location.

The strain distributions along the span of deck *F2-TB-a*, shown in Figures 4.20 and 4.21, show that the left span of the deck was experiencing lower strains than that of the right

span. This behaviour could possibly be due to slight shifting of the loading plate from the centre of the span, or a possible problem with the alignment of the gauge itself.

The strain distributions along the span of deck *FR-TB-a*, shown in Figures 4.22 and 4.23, showed more symmetrical behaviour with the exception of one gauge just right of midspan, where compressive strain was lower than expected and tensile strain was higher than trend values would predict. The behaviour suggests that the upper plate may have suffered local buckling at this location early in the test. The loss of the compressive resistance at this point may have then caused increased tensile strains at the same location.

4.3.1.2 Maximum Strains

The maximum compressive and tensile strains attained in each test are provided in Table 4.5. The location of these extremes is marked in the schematic diagrams shown in Figures 4.24 through 4.26.

Test	Maximum Tensile Strain (mS)	Maximum Compressive Strain (mS)
F1-TB	4.2	-1.7
F1-TB-a	7.6	-7.8
F2-TB-a	9.7	-4.7
F2-T-a	7.0	-4.2
FR-TB-a	5.9	-8
FR-T	15.2	N/A
FR-a	16.0	-4.4

Table 4.5: Maximum Strains in Phase I Deck

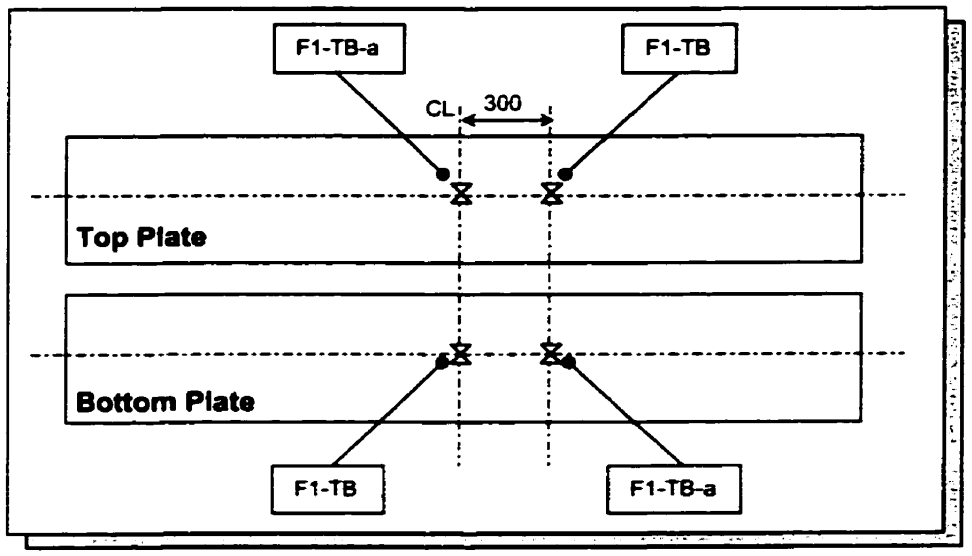

Figure 4.24: Location of Maximum Strains in Deck F1

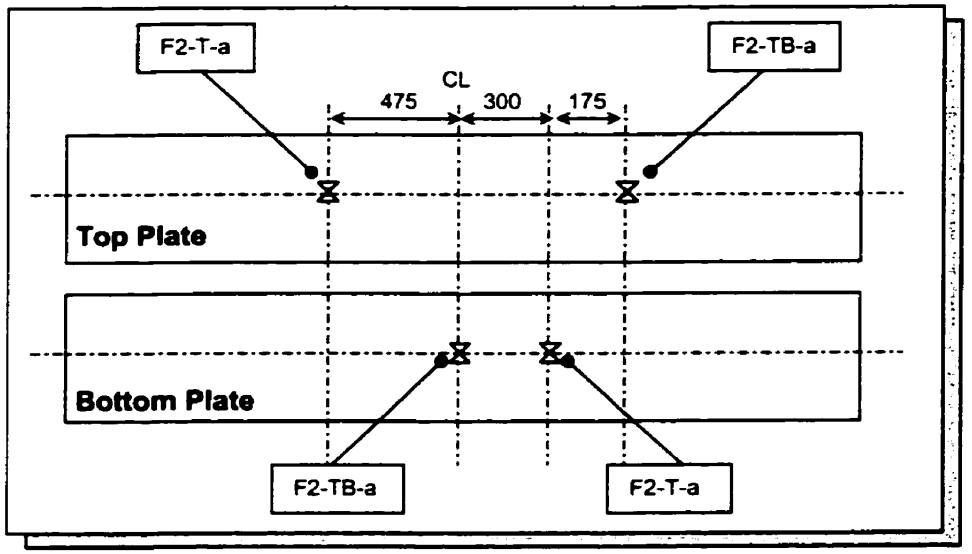

Figure 4.25: Location of Maximum Strains in Deck F2

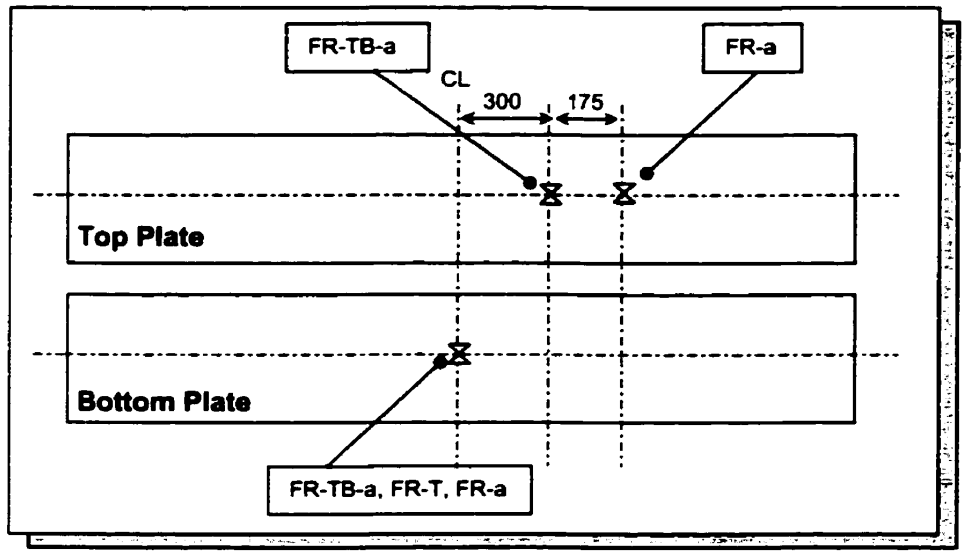

Figure 4.26: Location of Maximum Strains in Deck FR

In most cases, the maximum tensile strains were located directly beneath the loading point, which was to be expected. However, several of the maximum compressive strains occurred slightly away from midspan. This was due to one of two reasons: (a) localized buckling of a ply of the plate resulting in high strain; or (b) possible mislocation of the gauge to record the maximum strain.

The maximum strain envelope along the span of the deck is provided in Figure 4.27. This provides a visual representation of the overall maximum strains that were experienced across the plate of the three intact deck specimens. The shape of the envelope emphasizes two phenomena: a section within *L/4* distance from the support where strain increases slowly at a constant rate, and an area within *L/4* distance of the midspan where strain increases rapidly. This behaviour reflects the distribution of the truck load beyond the specified length used in the code.

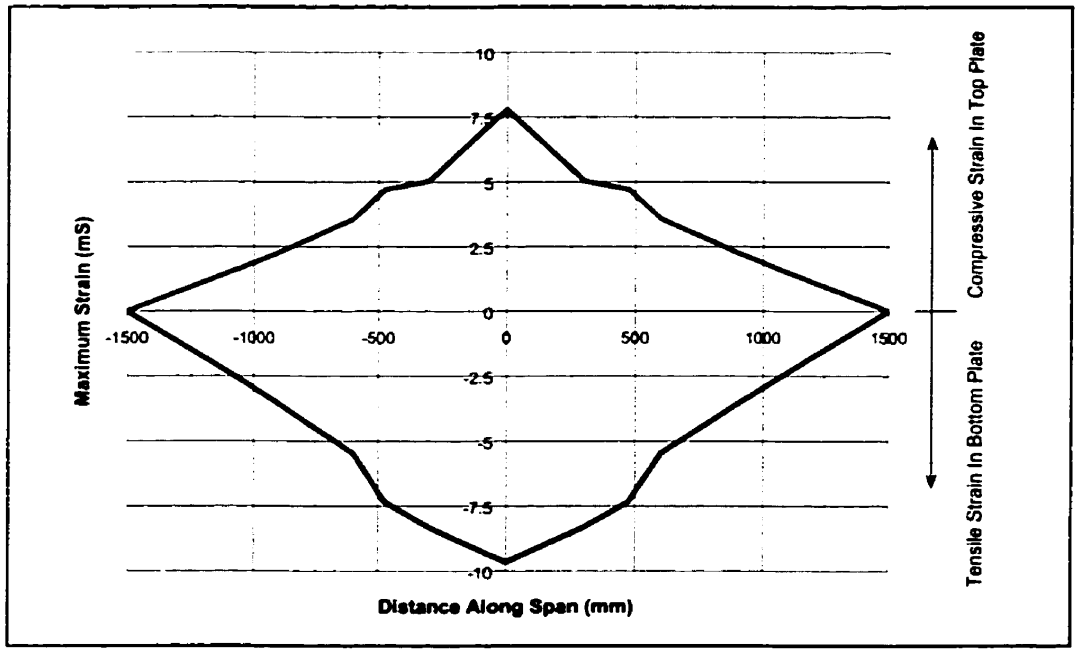

Figure 4.27: Maximum Strain Envelope for Phase I Intact Decks

Using a simple rule of mixtures (Mallick, 1993), the tensile strain capacity for the glass fibre composite plates can be calculated using the characteristics of the fibres and matrix as follows.

$$T_{composite} = T_f v_f + T_m (1 - v_f)$$
$$\text{where: } T_f = \text{tensile strength of fibres} = 1700\,MPa$$
$$v_f = \text{fibre volume ratio of plates} = 0.426$$
$$T_m = \text{tensile strength of matrix} = 64.8\,MPa$$
$$T_{composite} = \text{tensile strength of composite}$$
$$T_{composite} = (1700)(0.426) + (64.8)(1 - 0.426) = 761.4\,MPa \qquad \text{[E4.1]}$$

$$E_{composite} = E_f v_f + E_m (1 - v_f)$$
$$\text{where: } E_f = \text{modulus of fibres} = 72\,GPa$$
$$E_m = \text{modulus of matrix} = 3.15\,GPa$$
$$E_{composite} = \text{modulus of composite}$$
$$E_{composite} = (72)(0.426) + (3.15)(1 - 0.426) = 32.5\,GPa \qquad \text{[E4.2]}$$

$$\varepsilon_{fail} = {}^{T_{composite}}\!/_{E_{composite}}$$
$$= {}^{761.4}\!/_{32.5E3} \qquad \text{[E4.3]}$$
$$= 0.0234\% = 23.4\,mS$$

Based on this maximum material strength calculated above, the intact specimens (*F1-TB-a, F2-TB-a, FR-TB-a*) all have a reserve tensile strain capacity of at least 58 percent of the original capacity. It is therefore unlikely that the material strength will be exceeded. Allowable deflections and bond between elements will govern deck performance instead.

Another important aspect related to allowable strain is creep rupture. Under sustained loads, dead load and a percentage of live load, glass fibre composites will rupture if that load acts for a long period of time and enough strain is acting on the composite. In order to eliminate the possibility of this type of failure, limitations of strain have been set. Under service loads, the maximum sustained strain suggested is 10 percent of the ultimate strain of the composite. At ultimate loads, the maximum sustained strain suggested is increased to 30 percent of the ultimate composite strain.

Surveying the data from the three intact deck tests produced Figures 4.28 and 4.29 which compare the strains in the three intact decks to the maximum allowable strain at service and ultimate loading conditions.

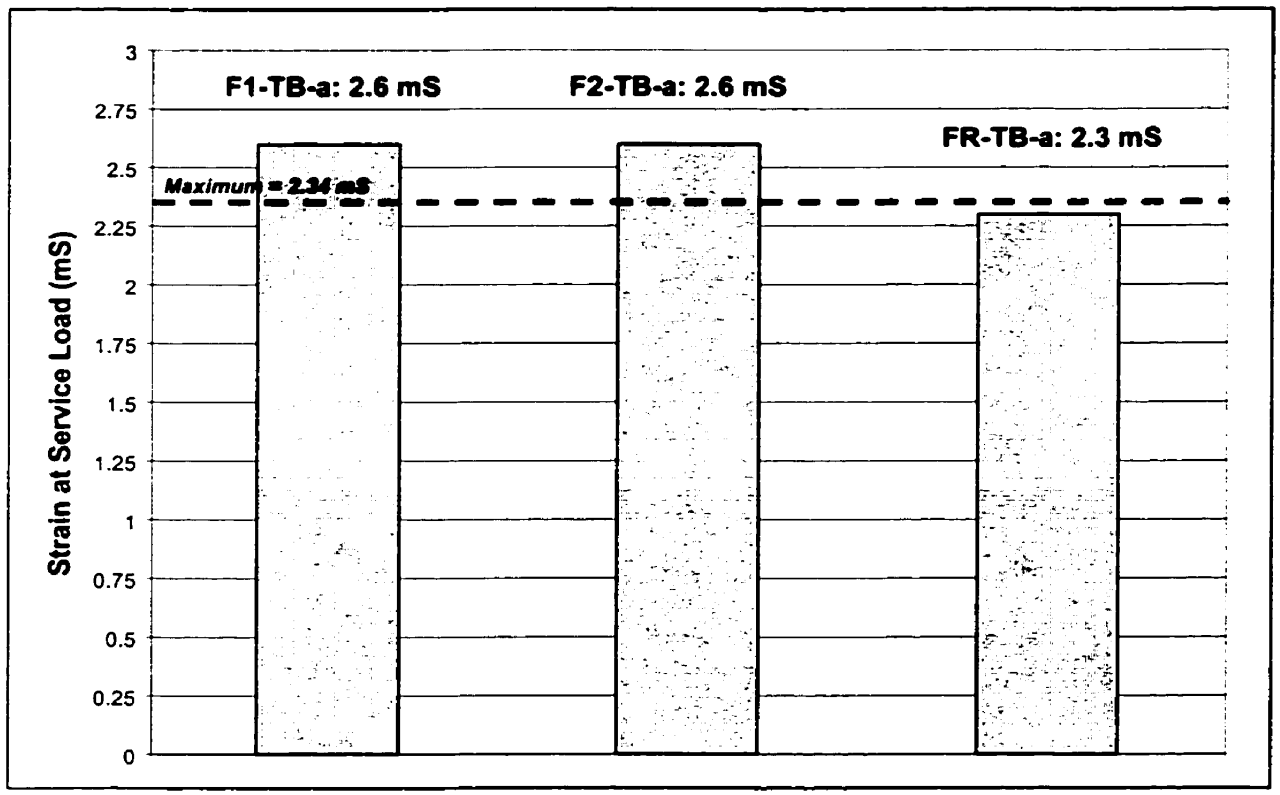

Figure 4.28: Comparison of Strain at Service Load with Maximum Allowable

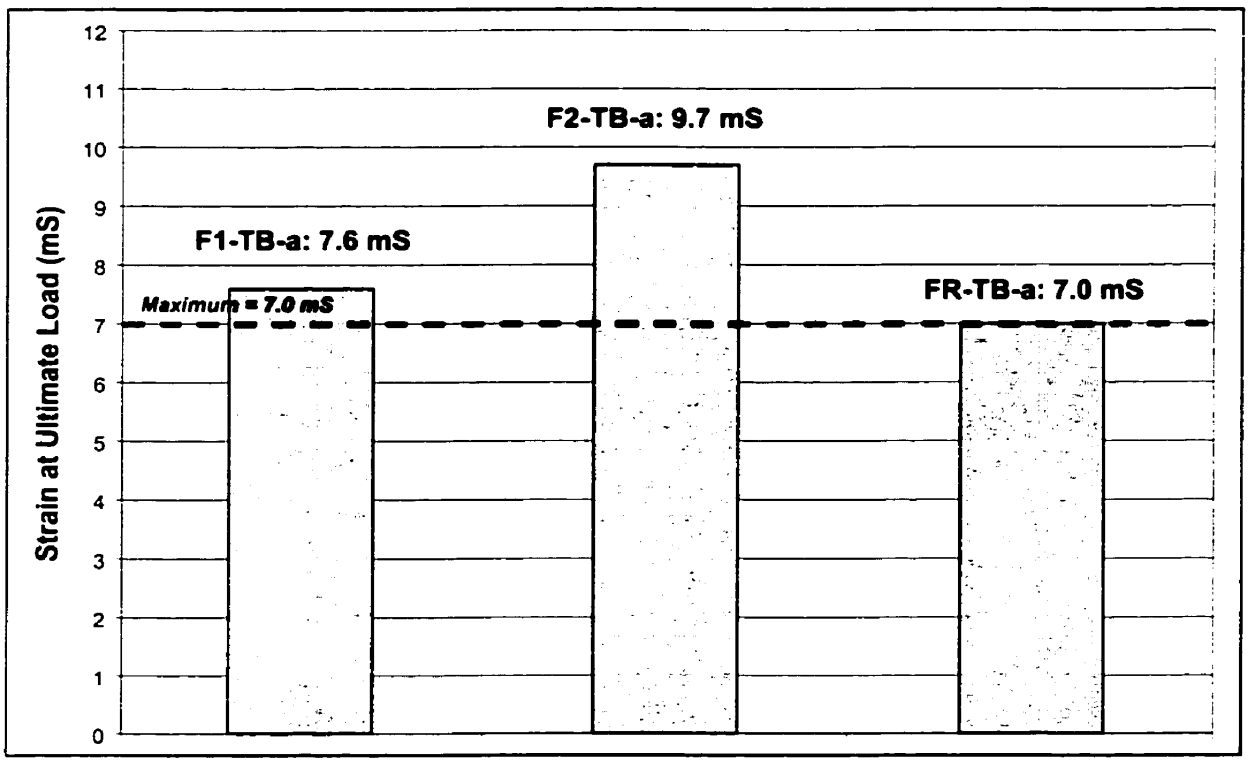

Figure 4.29: Comparison of Strain at Ultimate Load with Maximum Allowable

The data shows that while the strains in the deck are close to the recommended maximums, they still exceed these limits. In the interest of safety, it would be wise to modify the deck in the next phase in order to reduce these strains to a safe margin below the maximum.

4.3.1.3 Axial Strain Distribution Across Deck Width

The axial strain distributions across the width of the top deck plate for the three main specimens are provided in Figures 4.30 through 4.32. The bottom deck plates displayed similar trends and are therefore not included in analysis.

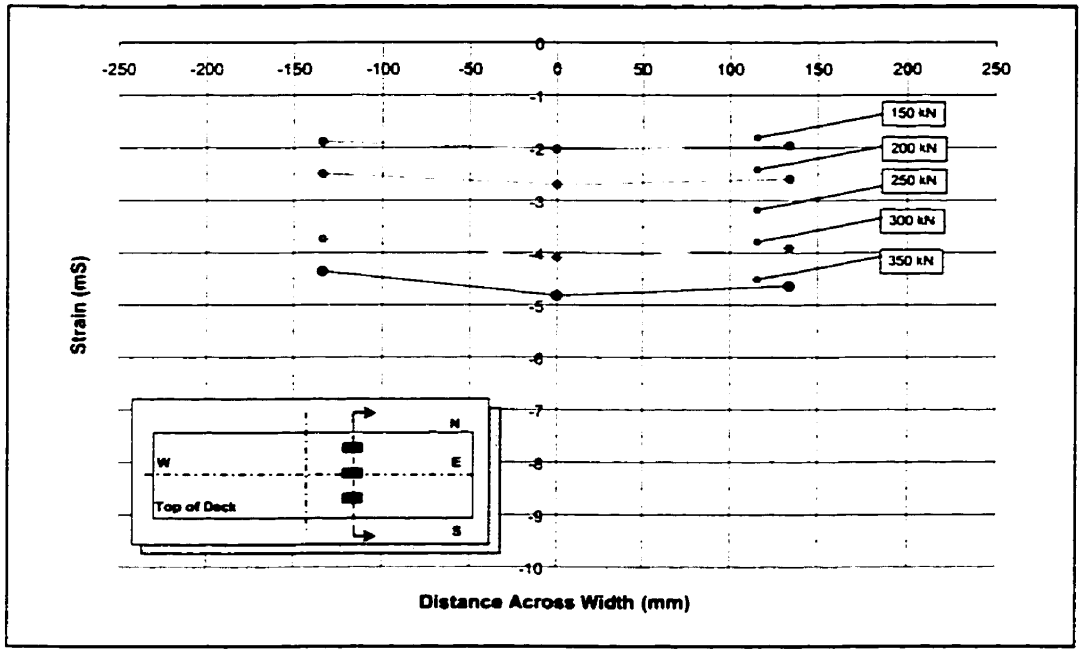

Figure 4.30: Axial Strain Distribution Across Top Deck Plate at 300 mm from Centreline – *F1-TB-a*

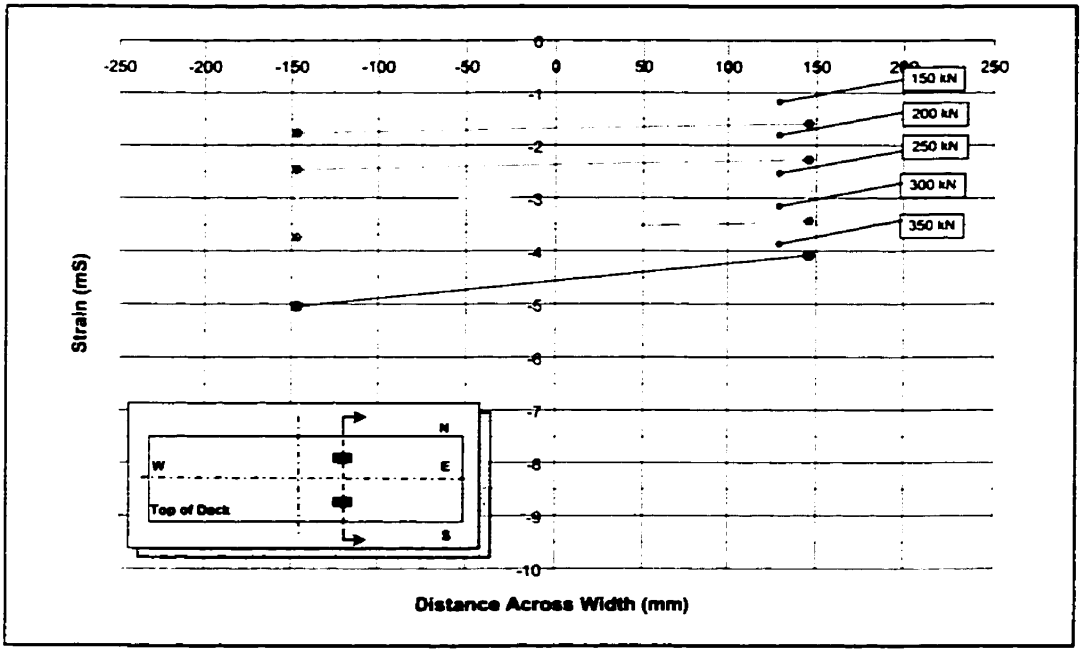

Figure 4.31: Axial Strain Distribution Across Top Deck Plate at 300 mm from Centreline – *F2-TB-a*

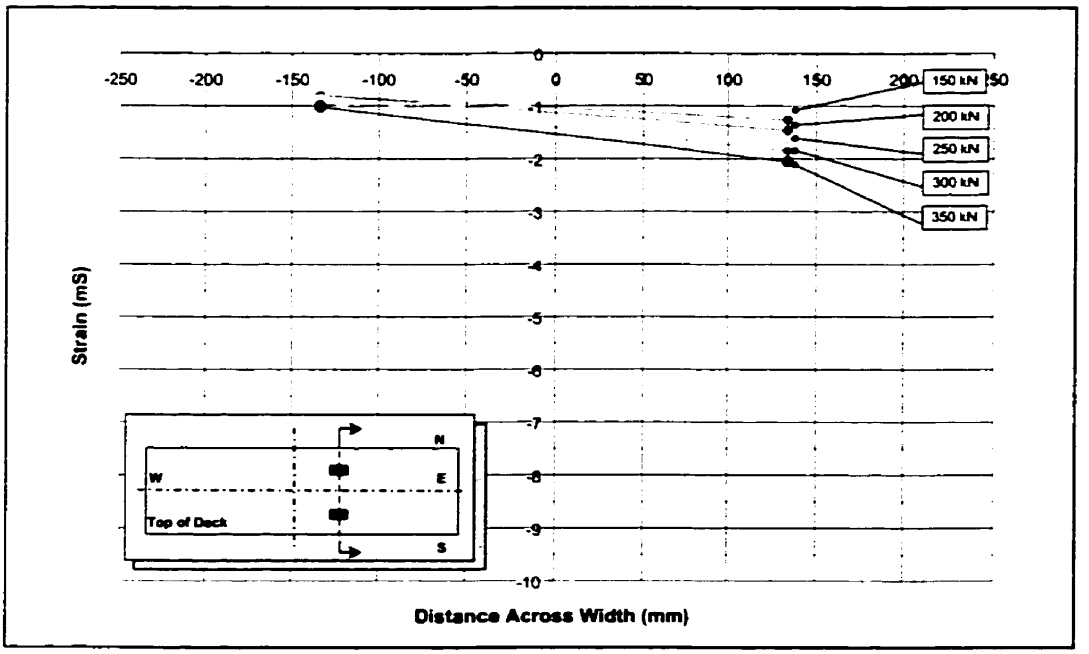

Figure 4.32: Axial Strain Distribution Across Top Deck Plate 300 mm from Centreline – *FR-TB-a*

Deck *F1-TB-a* displayed a uniform strain distribution across its width, as shown in Figure 4.30. The distribution is given for a section at a distance of 300 mm from the loading

point. Since the loading plate did not cover the entire deck width, the strains at the centre were slightly higher than at the edges. The uniformity of strain across the deck width indicates that the entire width was subject to the same strains, and that the tubes were resisting equal levels of load. This is desired behaviour, as it demonstrates efficient deck design and performance.

Deck *F2-TB-a*, shown in Figure 4.31, indicates a relatively uniform strain variation across its upper plate width. The difference of 1 mS across the plate could be due to eccentric location of the load. This behaviour could also be due to a possible poor bond between the laminas of the plate, which would lead to inability to distribute strain energy uniformly.

Deck *FR-TB-a*, shown in Figure 4.32, also showed the same lack of even strain distribution across its width. Again, this was attributed to poor bond between laminas. The maximum strains reached were much less than those attained in *F1-TB-a* and *F2-TB-a*, even though all of the decks reached comparable loads. As discussed previously, these reduced strains were likely due to early localized buckling of the upper lamina of the plate.

Analyzing the axial strain distribution across the deck plate is a useful tool for evaluating efficiency of deck behaviour. Based on the results of Phase I testing, it appeared that the decks had the potential to perform efficiently, with all tubes resisting equal loads. However, whether this efficiency had been achieved in all decks made up to this stage is

questionable. The plates, with their weak interlaminar bond, seemed to hinder the transmission of strain along and across the deck. Their premature localized buckling also created strain abnormalities. For these reasons, the deck plates were a major focus of improvement in the second phase of production.

4.3.1.4 Strain Distribution Along Depth of Deck

Along with strain measurements on the face of the plates, strain gauges were also located within the depth of the deck, midway between midspan and the supports. All three of the intact decks displayed similar strain behaviour at this location, so only one set of data is provided, as shown in Figure 4.33.

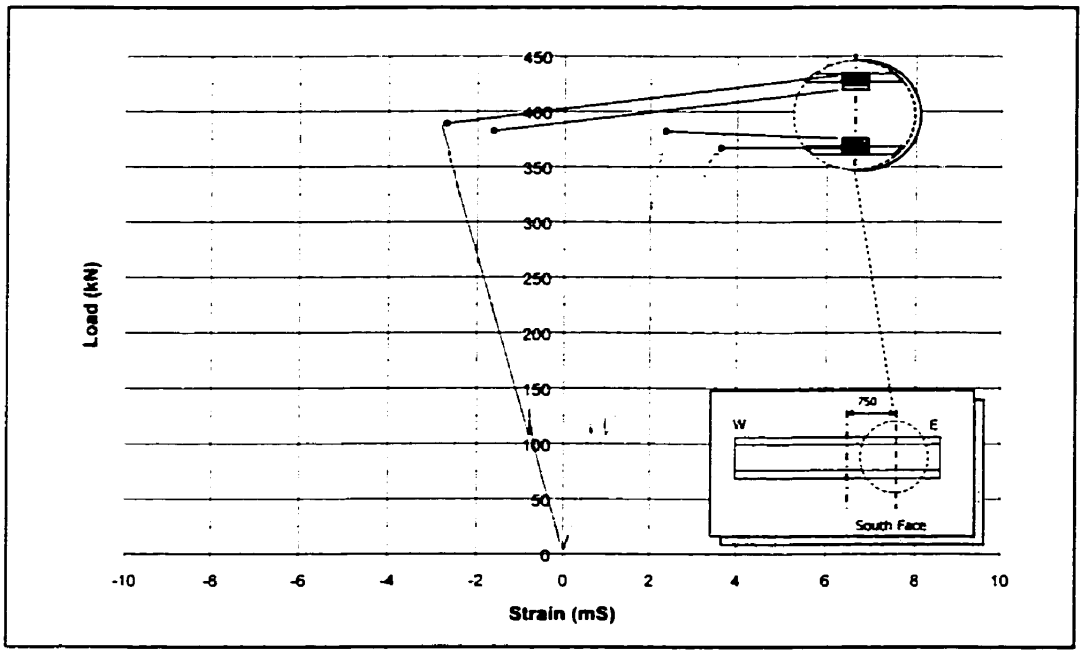

Figure 4.33: Strain Behaviour Within Depth for FR-TB-a

The plates experienced higher strain because of their outer location within the section. Both tubes and plates responded linearly to the load, which is expected of FRP material. In all three intact tests, the tensile strains were slightly greater than compressive strains.

Based on the strain behaviour in Figure 4.33, the cross section strain profile at 350 kN for the three main specimens was produced. The resulting diagrams are provided in Figures 4.34 through 4.36.

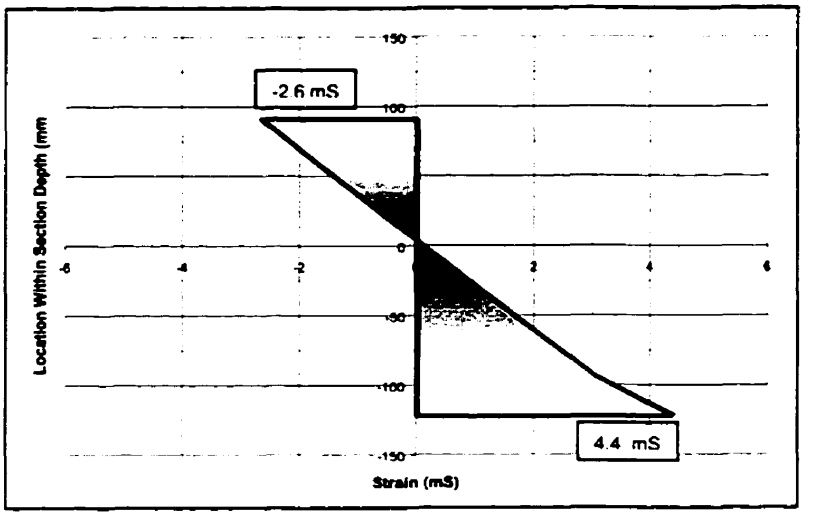

Figure 4.34: Strain Profile at 350 kN in F1-TB-a

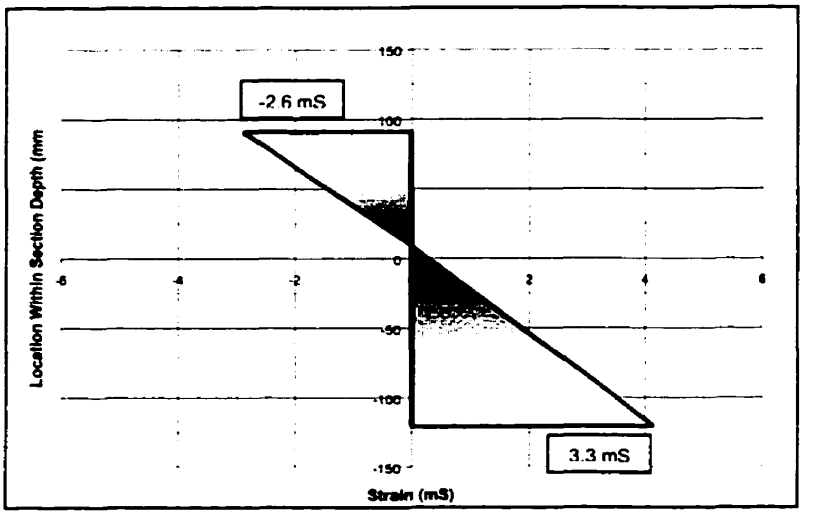

Figure 4.35: Strain Profile at 350 kN in F2-TB-a

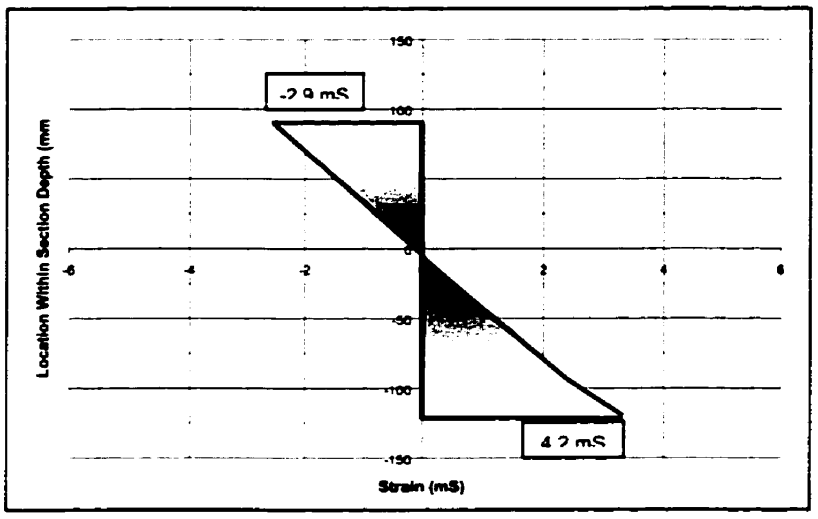

Figure 4.36: Strain Profile at 350 kN in FR-TB-a

Each strain diagram showed a smooth strain profile within the cross section. In all cases, maximum tensile strains were higher than the compressive strains reached. The analytical model, discussed later in Chapter 5, was used to predict the location of the neutral axis for these diagrams. Since the model applies to service loads prior to cracking and section degradation, the point of zero strain of the neutral axis did not coincide with that predicted value by the model. However, the location of the actual neutral axis with respect to the predicted location verified the observed deck behaviour. In *F1-TB-a* where extensive tensile cracking and delamination occurred, the neutral axis shifted upwards to account for this cracking. The same phenomenon was observed in deck *F2-TB-a*. Deck *FR-TB-a*'s neutral axis was positioned slightly below the predicted location, due to the excessive upper plate buckling that occurred along the entire span.

4.3.1.5 Transverse Strain Behaviour

Transverse strain gauges were only applied to the first deck, *F1-TB-a*. Plots of transverse strains at various loads are provided in Figures 4.37 and 4.38 for both top and bottom plates.

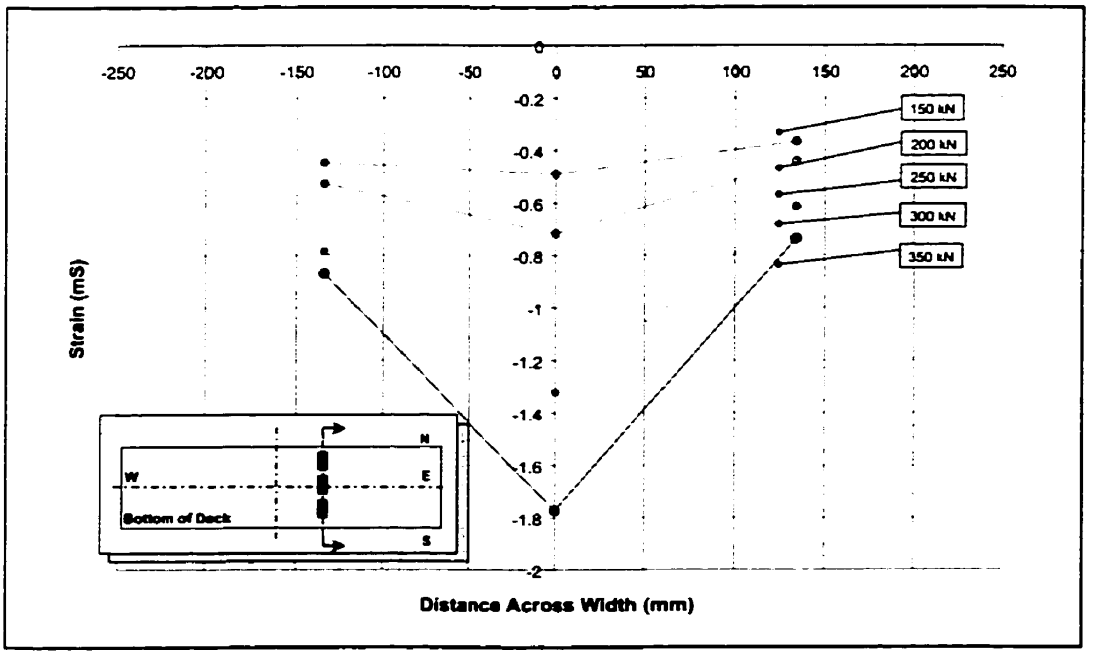

Figure 4.37: Transverse Strain Distribution Across Bottom Plate – F1-TB-a

Transverse strains were markedly lower than axial strains experienced in the same location. Maximum axial strains in the top and bottom plate reached -5.0 and 7.6 mS, respectively, whereas transverse strains reached only 0.4 mS in the top plate and -1.8 mS in the bottom plate.

Transverse strain in the bottom plate appeared to follow a definite pattern, as shown in Figure 5.20, with higher strains near the centreline and reduced strains further from the centreline of the plate. In addition, the strains were relatively symmetric on both sides of

the plate centreline at earlier stages of loading, again indicating efficient and well-distributed transmission of strain.

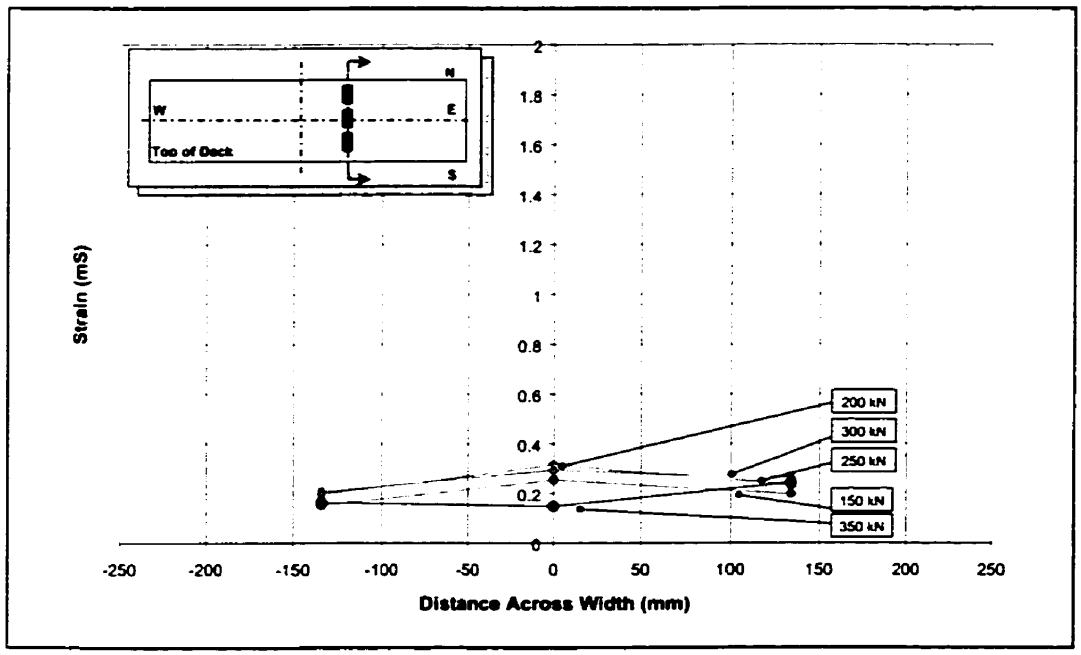

Figure 4.38: Transverse Strain Distribution Across Top Plate – F1-TB-a

Unlike the bottom plate strain distribution, there was almost a constant transverse strain across the top plate at all load levels, as shown in Figure 4.38. At the highest load level, the strain dropped off, indicating that perhaps local lamina buckling at this location had occurred.

Due to the small, insignificant transverse strains observed, transverse strains were not monitored further in the Phase I tests.

4.3.2 Seven Tube Specimens

4.3.2.1 Axial Strain Distribution Along Span

The axial strain distributions along the centre and edge of the top plate of the seven-tube modules are given in Figures 4.39 through 4.42.

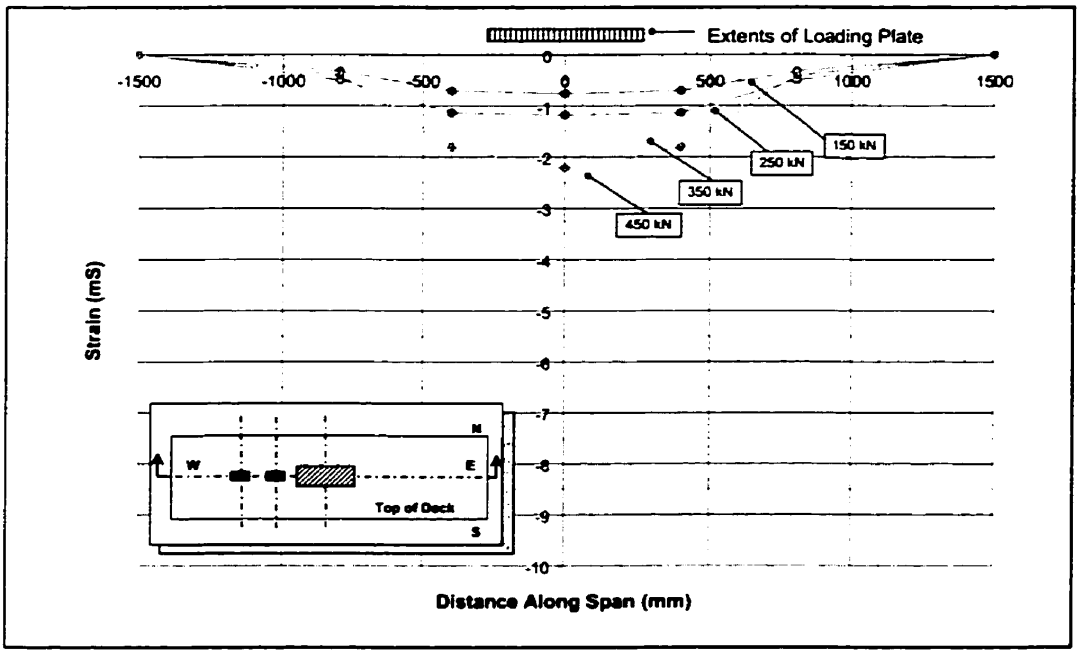

Figure 4.39: Axial Strain Distribution Along Centreline of Top Plate – F7-1

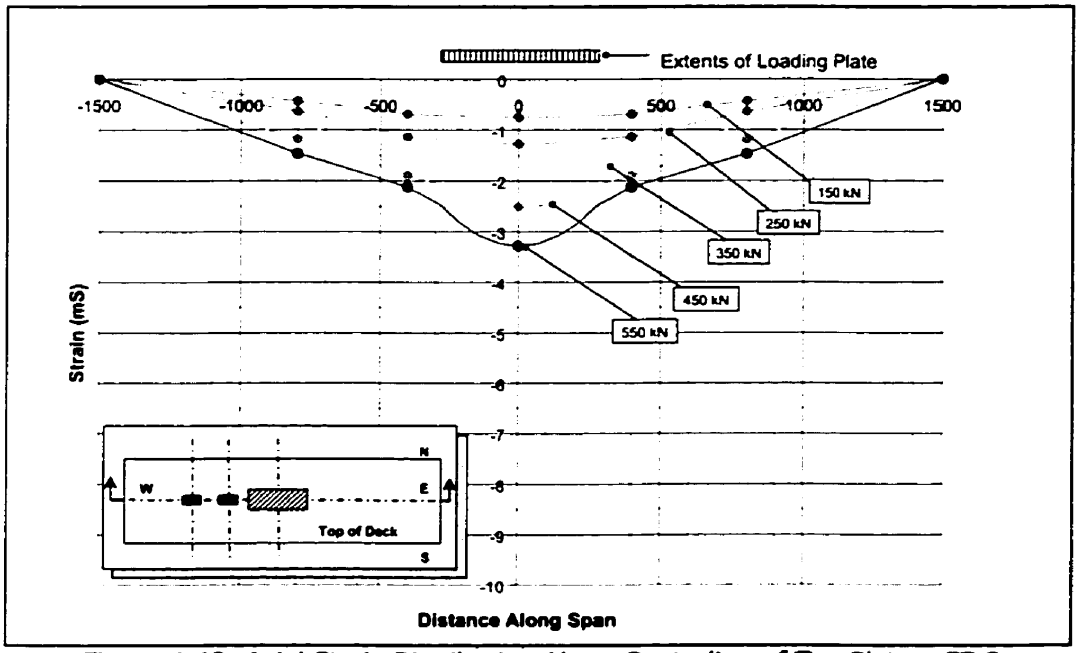

Figure 4.40: Axial Strain Distribution Along Centreline of Top Plate – F7-2

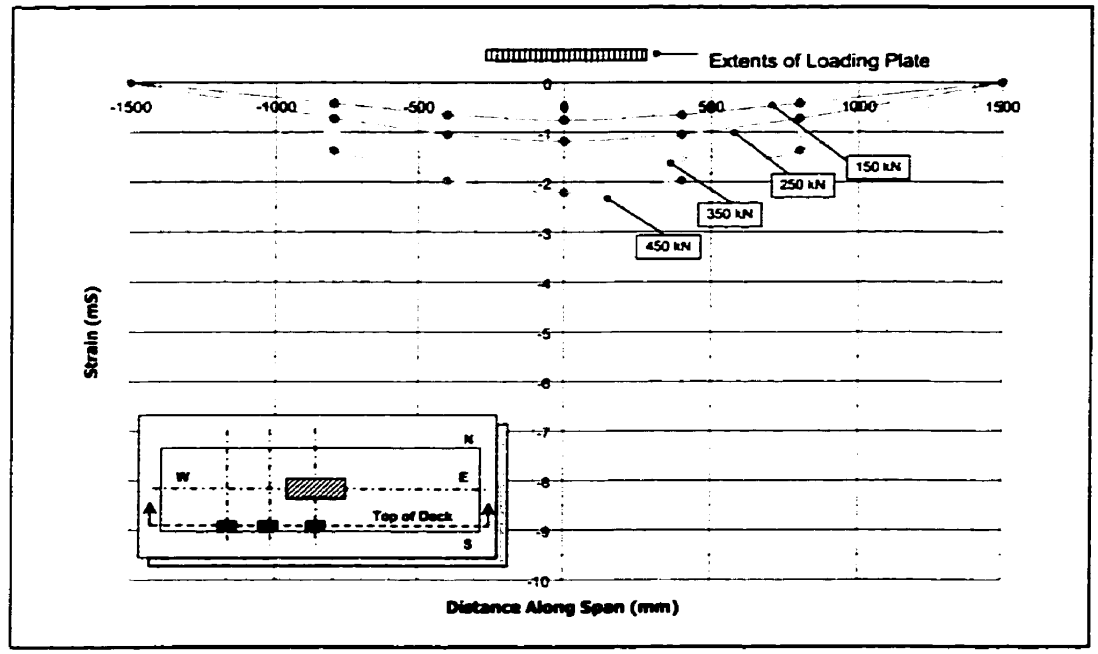

Figure 4.41: Axial Strain Distribution Along Edge of Top Plate – F7-1

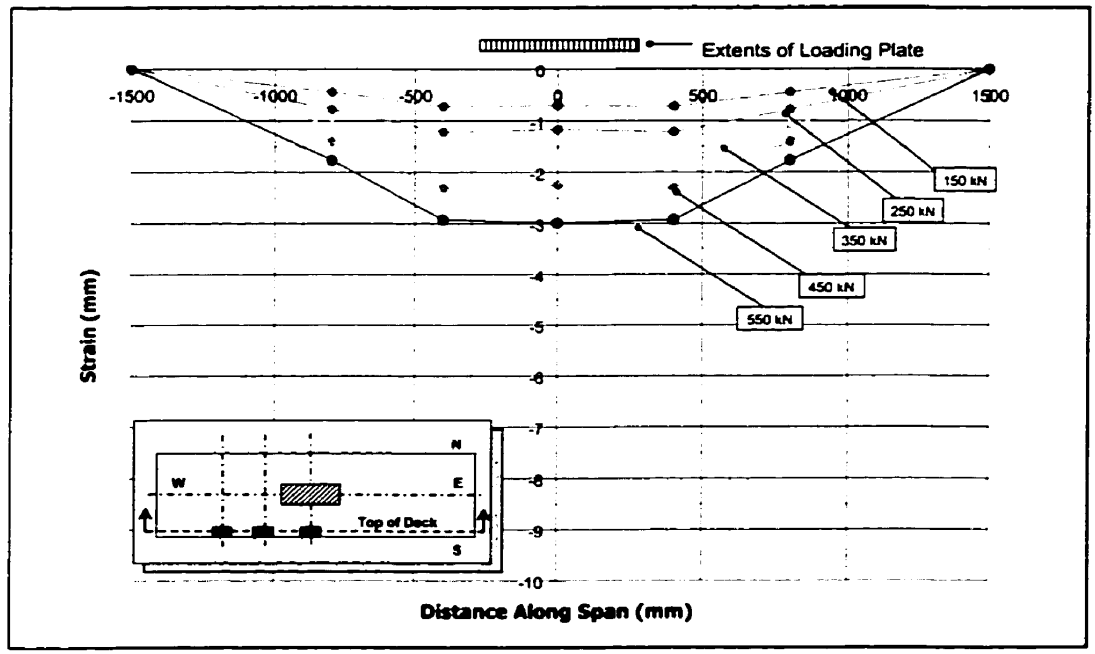

Figure 4.42: Axial Strain Distribution Along Edge of Top Plate – F7-2

The seven-tube modules showed well-distributed strains along the span. In contrast with the three-tube decks, where plate buckling and delamination was a problem, these decks displayed no plate buckling whatsoever. The smooth strains distributions and lack of strain build-up anywhere along the plates reflect this.

Both decks experienced virtually the same strain levels at the selected load levels. This indicates comparable performance between the two specimens, which is the result of consistent manufacturing.

The strain distributions along the edge of the upper plates showed that a similar strain distribution is being obtained across the entire deck. This, again, is an indication of consistent deck behaviour.

Figures 4.43 and 4.44 show the axial strain distributions along the bottom plate of the Phase II decks.

These distributions display the expected trends: well-distributed strain along the span, with the maximum strain occurring directly beneath the load. Once again, the level of strain experienced by each deck was very much comparable.

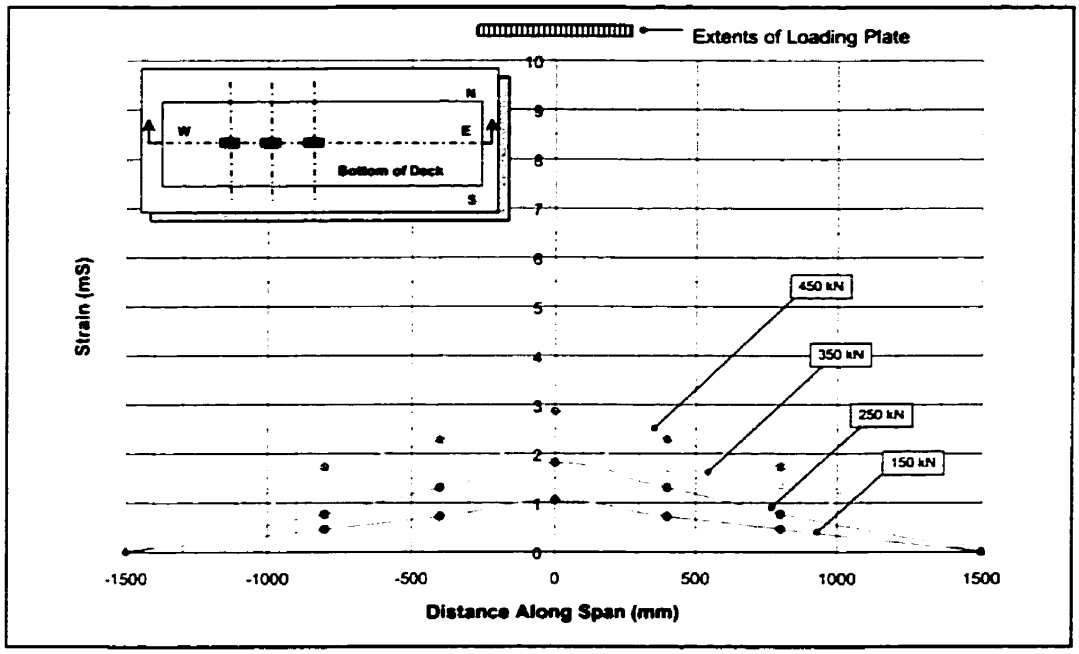

Figure 4.43: Axial Strain Distribution Along Centreline of Bottom Plate – F7-1

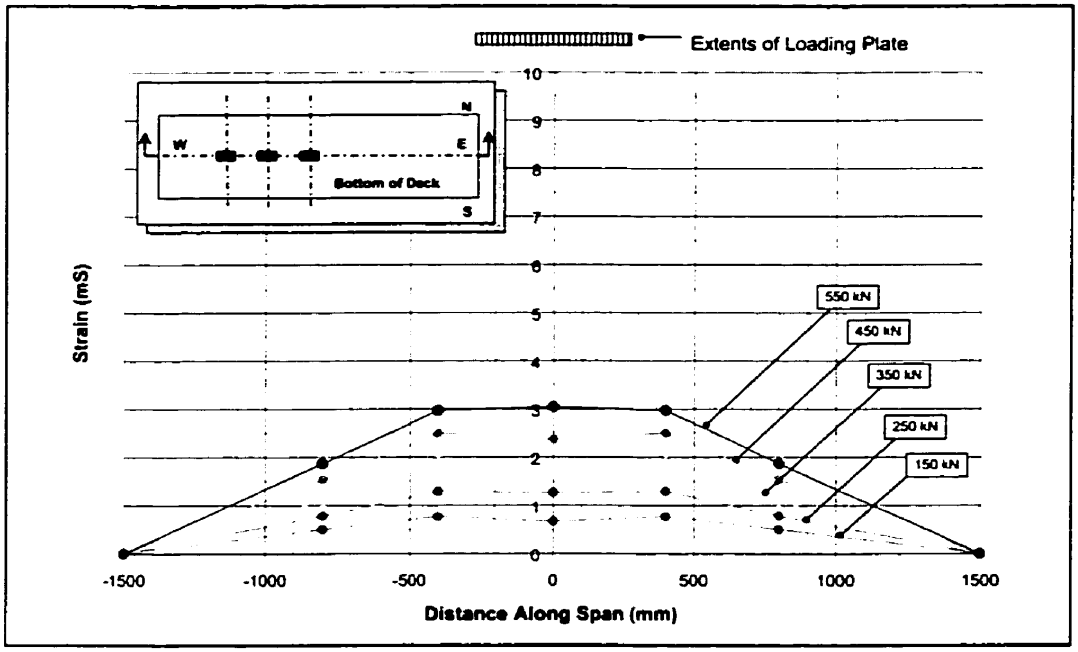

Figure 4.44: Axial Strain Distribution Along Centreline of Bottom Plate – F7-2

4.3.2.2 Maximum Strains

The maximum compressive and tensile strains attained in each test is provided in Table 4.6.

Test	Maximum Tensile Strain (mS)	Maximum Compressive Strain (mS)
F7-1	3.20	-2.77
F7-2	3.52	-3.88

Table 4.6: Maximum Strains in Phase II Decks

In all cases, the maximum strains occurred directly beneath the load. The maximum strain envelope is provided in Figure 4.45.

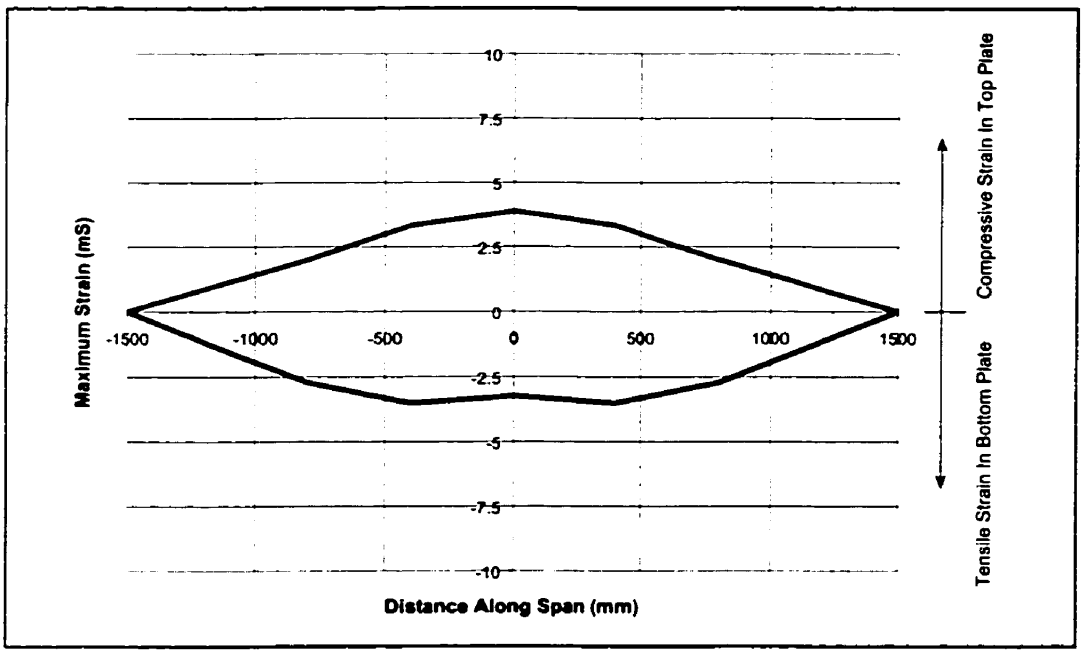

Figure 4.45: Maximum Strain Envelope for Phase II Decks

The maximum strains experienced follow much the same pattern as that of the three-tube modules. The maximum strain increases from the supports to about *L/3* where the maximum strain becomes somewhat constant. Therefore, changing the loading plate to meet AASHTO standards did not change strain behaviour significantly.

Applying *[E4.1]* through *[4.3]* allows the reserve strain capacity of the Phase II decks to be calculated.

$$T_{composite} = T_f v_f + T_m (1 - v_f)$$

$$\text{where: } T_f = \text{tensile strength of fibres} = 1700\ MPa$$

$$v_f = \text{fibre volume ratio of plates} = 0.426$$

$$T_m = \text{tensile strength of matrix} = 64.8\ MPa$$

$$T_{composite} = \text{tensile strength of composite}$$

$$T_{composite}(F7-1) = (1700)(0.45) + (64.8)(1-0.45) = 800.64\ MPa$$

$$T_{composite}(F7-2) = (1700)(0.50) + (64.8)(1-0.5) = 882.4 MPa$$

$$E_{composite} = E_f v_f + E_m (1 - v_f)$$

$$\text{where: } E_f = \text{modulus of fibres} = 72\ GPa$$

$$E_m = \text{modulus of matrix} = 3.15\ GPa$$

$$E_{composite} = \text{modulus of composite}$$

$$E_{composite}(F7-1) = (72)(0.45) + (3.15)(1-0.45) = 34.13\ GPa$$

$$E_{composite}(F7-2) = (72)(0.5) + (3.15)(1-0.5) = 37.575\ GPa$$

$$\varepsilon_{fail}(F7-1) = {}^{T_c}\!/_{E_c} = {}^{800.64}\!/_{34.13e3} = 0.0257\% = 25.7\ mS$$

$$\varepsilon_{fail}(F7-2) = {}^{T_c}\!/_{E_c} = {}^{882.4}\!/_{37.575} = 0.0235\% = 23.5\ mS$$

Based on these calculated values, the decks have a reserve strain capacity of at least 85 percent of the original material capacity. This reserve material strength is over and above that calculated for the three-tube modules, indicating that the method of manufacturing used for Phase II specimens created a safer, more efficient product.

Once again, the strain values are compared against the limiting 10 percent of ultimate composite strain at service load and 30 percent of ultimate composite strain at ultimate load in order to avoid creep rupture. Figures 4.46 and 4.47 detail these results.

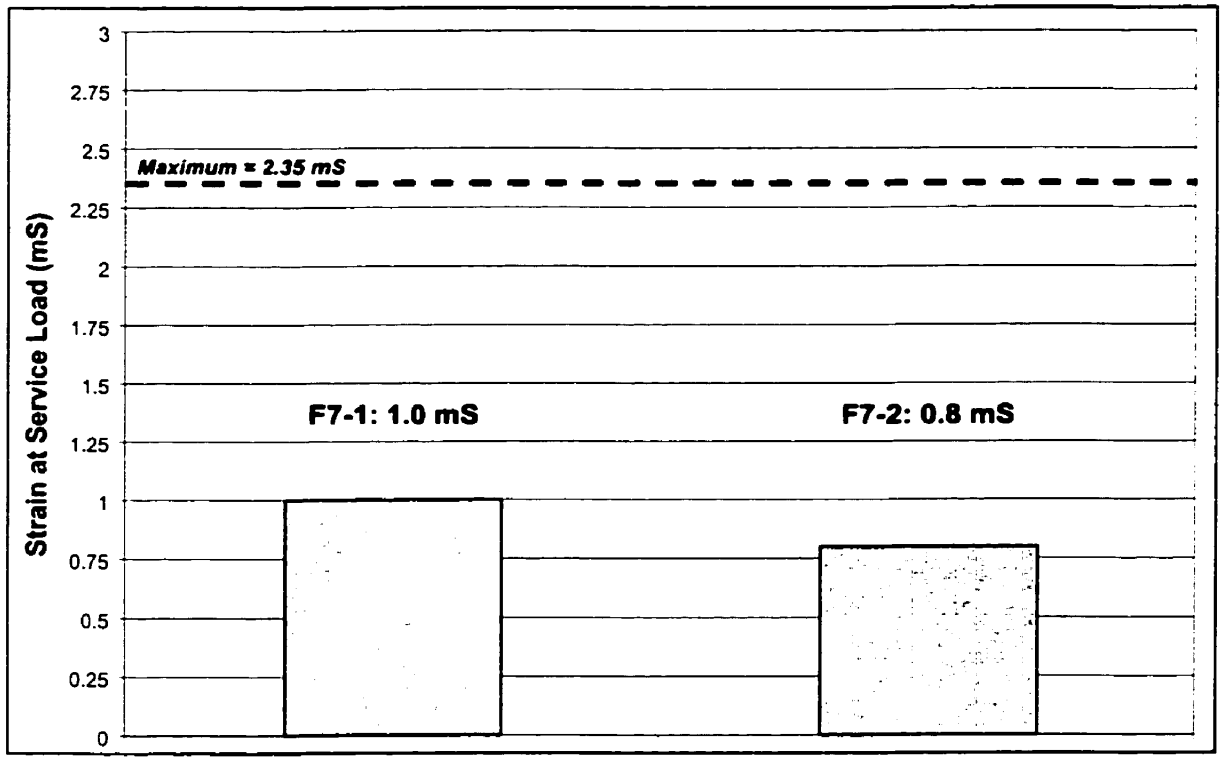

Figure 4.46: Comparison of Strains at Service Load with Maximum Allowable

Upon modification of the deck design and manufacturing technique, the FRP deck modules now display strains well under the maximum allowable values. This improved behaviour adds to the safety of the structural system and eliminates the possibility of catastrophic failure due to creep rupture.

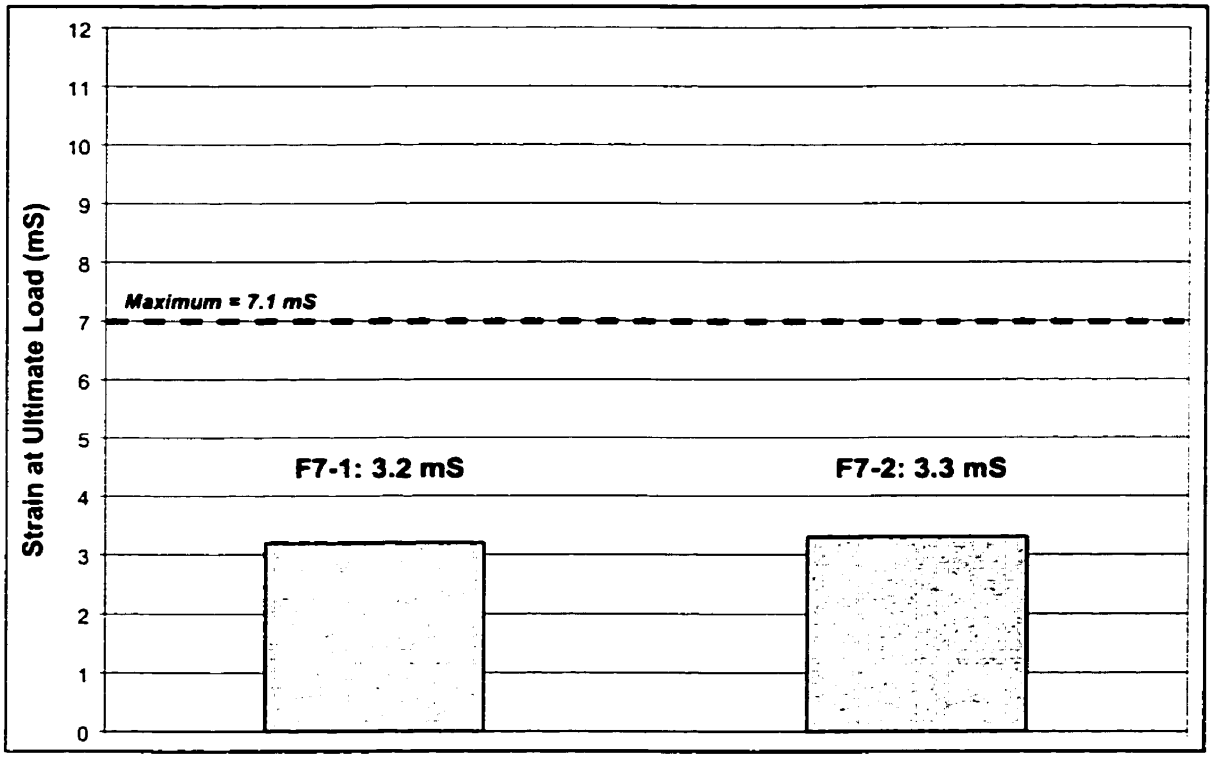

Figure 4.47: Comparison of Strains at Ultimate Load with Maximum Allowable

4.3.2.3 Axial Strain Distribution Across Deck Width

Figures 4.48 through 4.53 show the axial strain distribution across the width of the top and bottom plates.

The strains appear to be uniform across the entire deck width, regardless of location along the span. Strain distribution is nearly uniform at distances of 800 mm from midspan, while distributions right at midspan show some anomalous behaviour. This is most likely attributable to local phenomenon in the close vicinity of the loading plate.

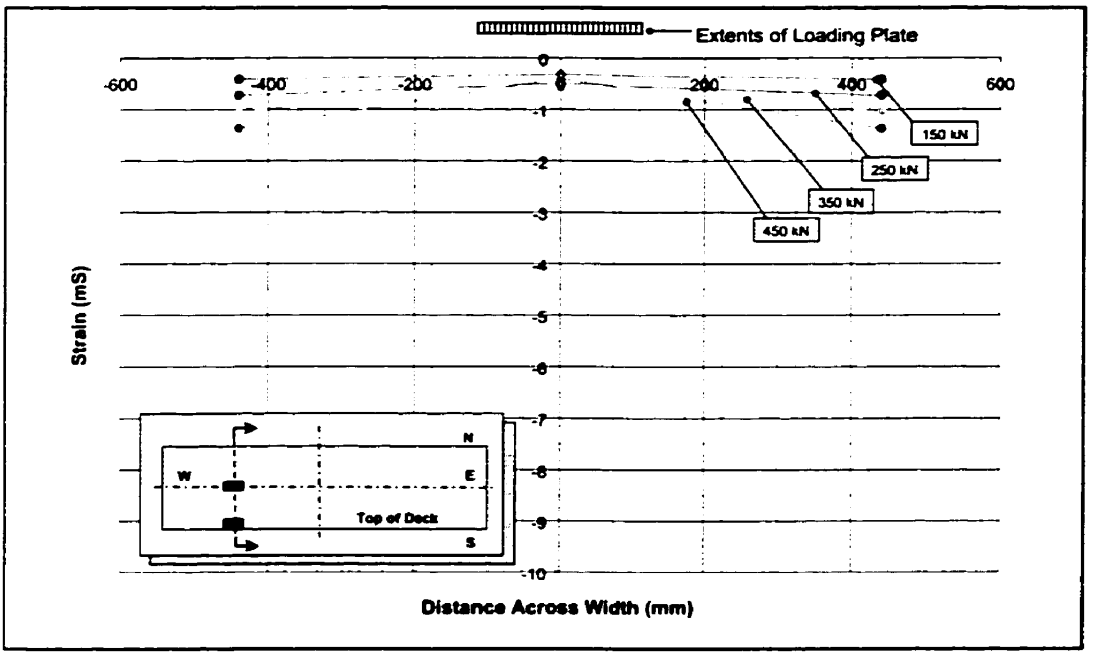

Figure 4.48: Axial Strain Distribution Across Top Deck Plate 800 mm from Centreline – F7-1

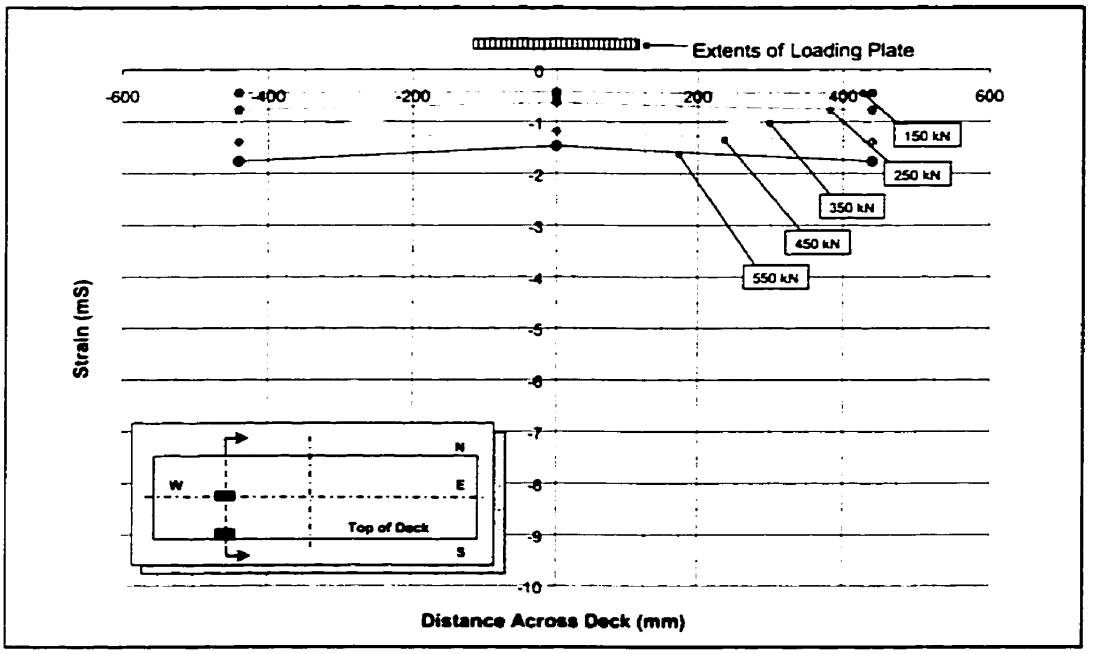

Figure 4.49: Axial Strain Distribution Across Top Deck Plate 800 mm From Centreline – F7-2

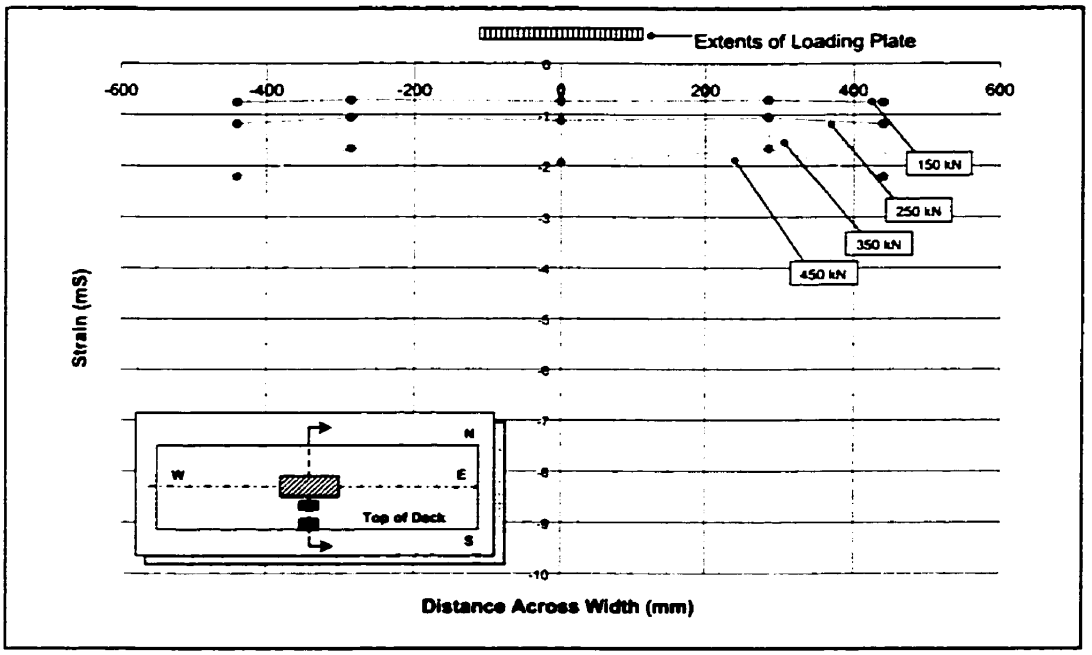

Figure 4.50: Axial Strain Distribution Across Top Deck Plate at Centreline – F7-1

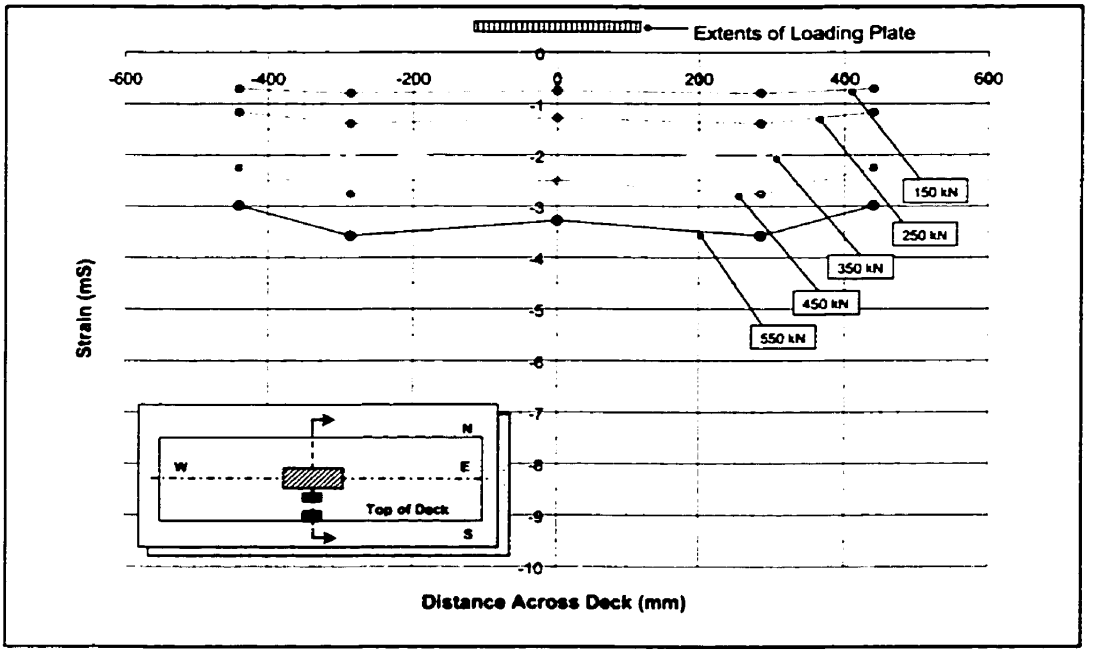

Figure 4.51: Axial Strain Distribution Across Top Deck Plate at Centreline – F7-2

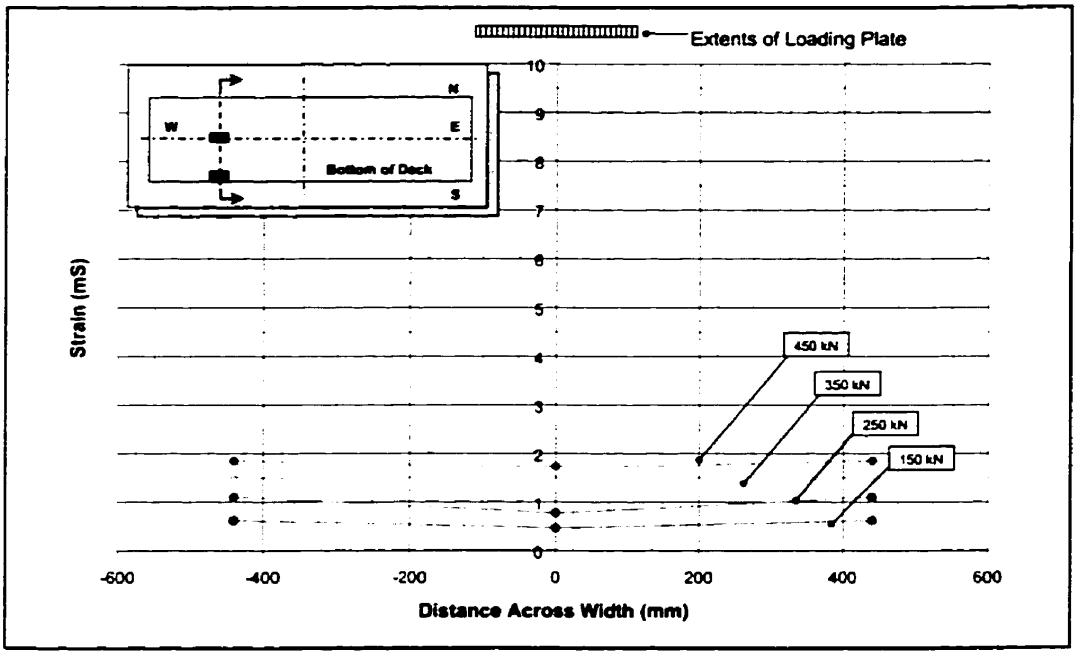

Figure 4.52: Axial Strain Distribution Across Bottom Deck Plate 800 mm From Centreline – F7-1

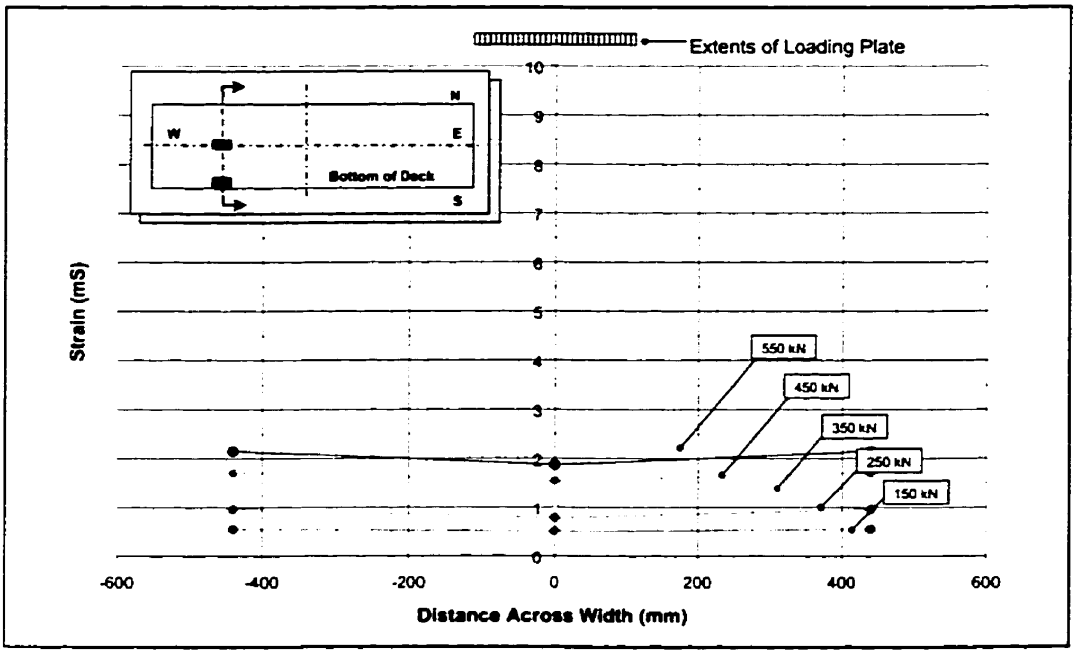

Figure 4.53: Axial Strain Distribution Across Bottom Plate 800 mm From Centreline – F7-2

The uniformity of strain across the deck width indicates good strain transmission across the deck, and efficient use of all components to resist load. Once again, the deck design and manufacturing method seem to have created a high quality, high performance product.

4.3.2.4 Transverse Strain Behaviour

Only one transverse gauge was used on each F7-series deck. The behaviour of each of these gauges is plotted in Figure 4.54.

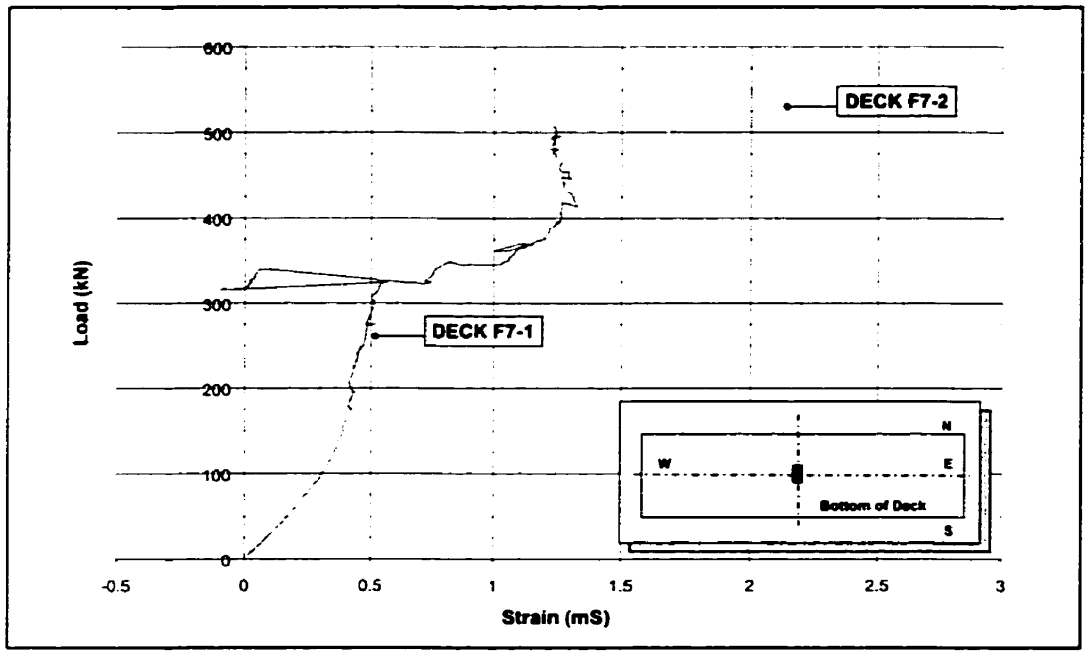

Figure 4.54: Transverse Strain Behaviour at Centreline – Phase II Modules

As was the case with the Phase I decks, the transverse strain data is erratic. As a result, no inferences can be made as to any trends in strain behaviour.

CHAPTER FIVE:

ANALYTICAL MODEL AND VERIFICATION OF THE TEST RESULTS

5.1 Stiffness Model

5.1.1 Model Overview

Prediction of structural behaviour is a very useful tool. Comparison of specimen performance against predicted provides a check on specimen quality. It also allows the designer to change specific design details and determine their effect on performance without extensive experimental testing.

Composite modelling can be a difficult task, especially near failure loads when lamina buckling and delamination occur. Thus, it was endeavoured to predict the load-deflection behaviour of the FRP decks within the service load range only. The model, therefore, assumes an intact section in which no damage has occurred.

The model consists of several steps, shown in Figure 5.1, which eventually lead to a stiffness prediction for the composite deck. It begins with the determination of the effective stiffness of the components of the deck section. This calculation is done using Laminate Plate Theory (LPT). Following this, analysis of the cross section begins. In order to facilitate simple calculations, the cross section is discretized into a series of elements. The area and local moment of inertia are determined for each of these elements. Finally, the overall effective modulus and moment of inertia of the section are computed and used to obtain a theoretical *Load/Deflection* ratio for the deck.

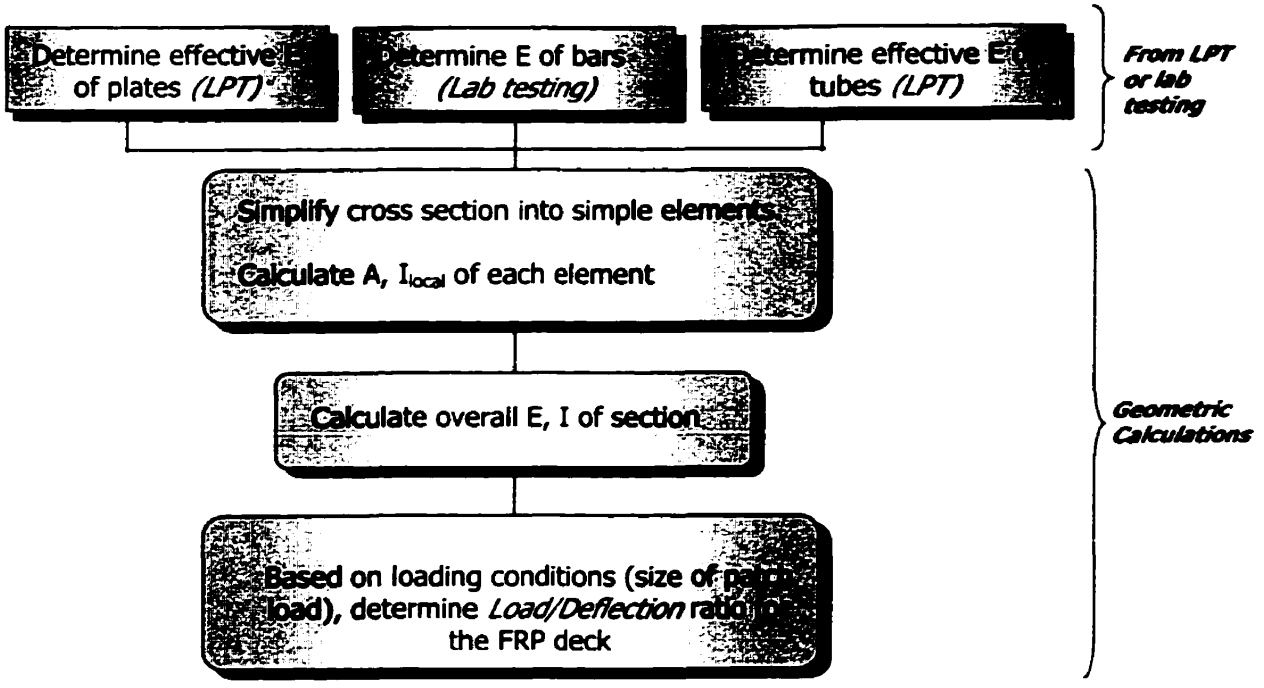

Figure 5.1: Flowchart of Deck Stiffness Modelling Process

The major sections of the model will now be discussed, beginning with the determination of effective stiffness of the plates, bars and tubes.

5.1.2 Effective Component Stiffness

The effective stiffness for the laminate elements (plates and tubes) of the cross section were determined using Laminate Plate Theory (LPT). The essence of LPT is provided in the following section.

LPT applies to laminate structures alone, therefore the stiffness of the pultruded filler bars was determined by a series of simple tension tests in the lab. The resulting stiffness was then entered into the model program.

5.1.2.1 Concept of LPT

Laminated composites consist of a number of laminas, stacked up and bonded in varying orientations. Typically, material properties of individual laminas are known or are easily calculated. LPT takes the properties of each lamina, considers its orientation and position in the laminate structure, and calculates the overall properties of that laminate. In this case, it is the laminate stiffness that is of interest.

Before describing the theory behind LPT, several conventions must be outlined. Within a lamina, the 1-axis is directed along the fibre length, while the 2-axis runs transverse to the fibre direction. The z-axis is directed out of the plane of the lamina. Together, the 1-2-z axis system comprises the principal material directions of the lamina, as shown in Figure 5.2.

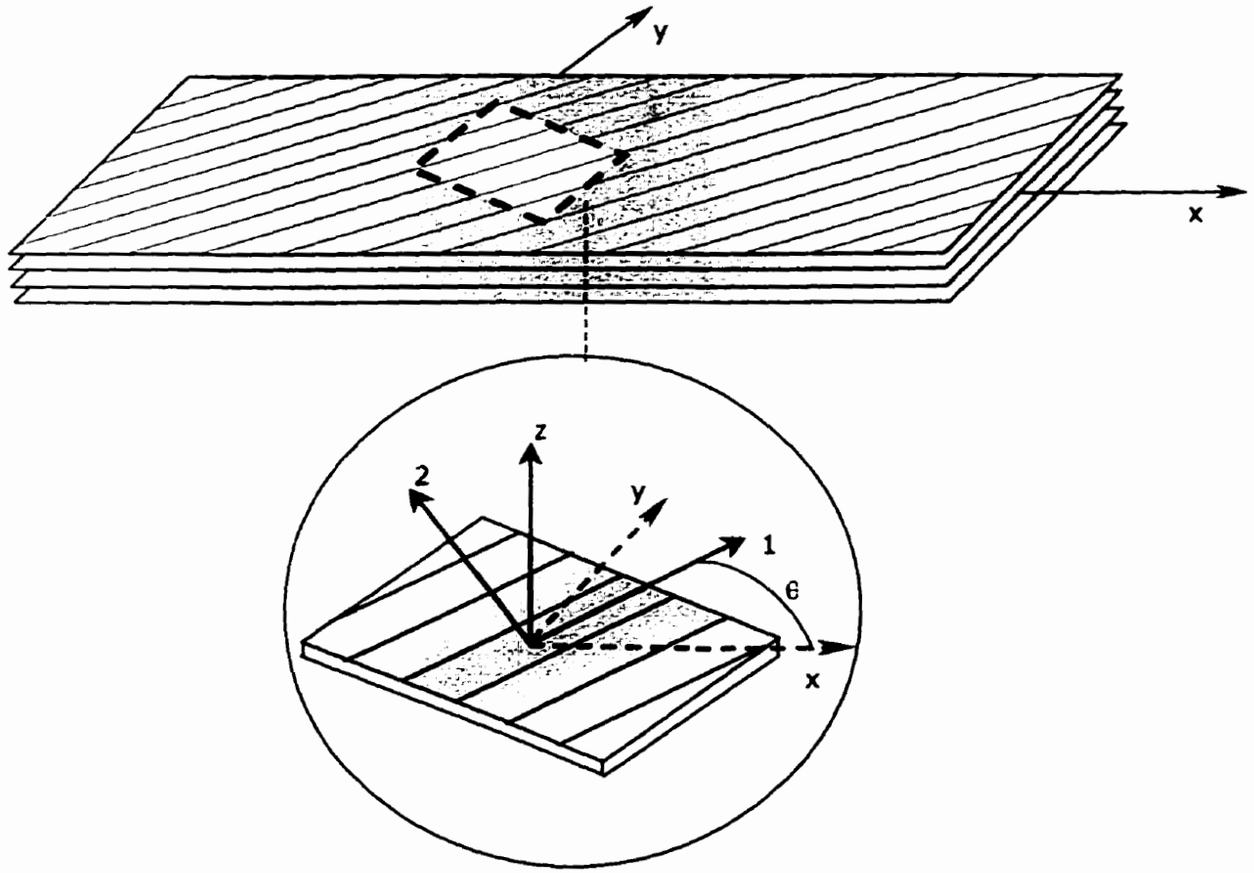

Figure 5.2: Definition of Principal and Loading Axes

The x- and y-axes, on the other hand, are global to the entire laminate structure, and are usually used for referencing load direction.

The angle between the positive x- and 1-axes is called the fibre orientation angle (θ), with its direction determined by the positive right hand rule. This is also shown in Figure 5.2.

There are several assumptions inherent to LPT. These include:

- the laminate is thin and wide (width >> thickness);
- a perfect interlaminar bond exists between various laminas;
- the strain distribution in the lamina thickness is linear; and,
- all laminas are homogeneous and behave in a linearly elastic manner.

Finally, the process involved in LPT is summarized in Figure 5.3's flowchart.

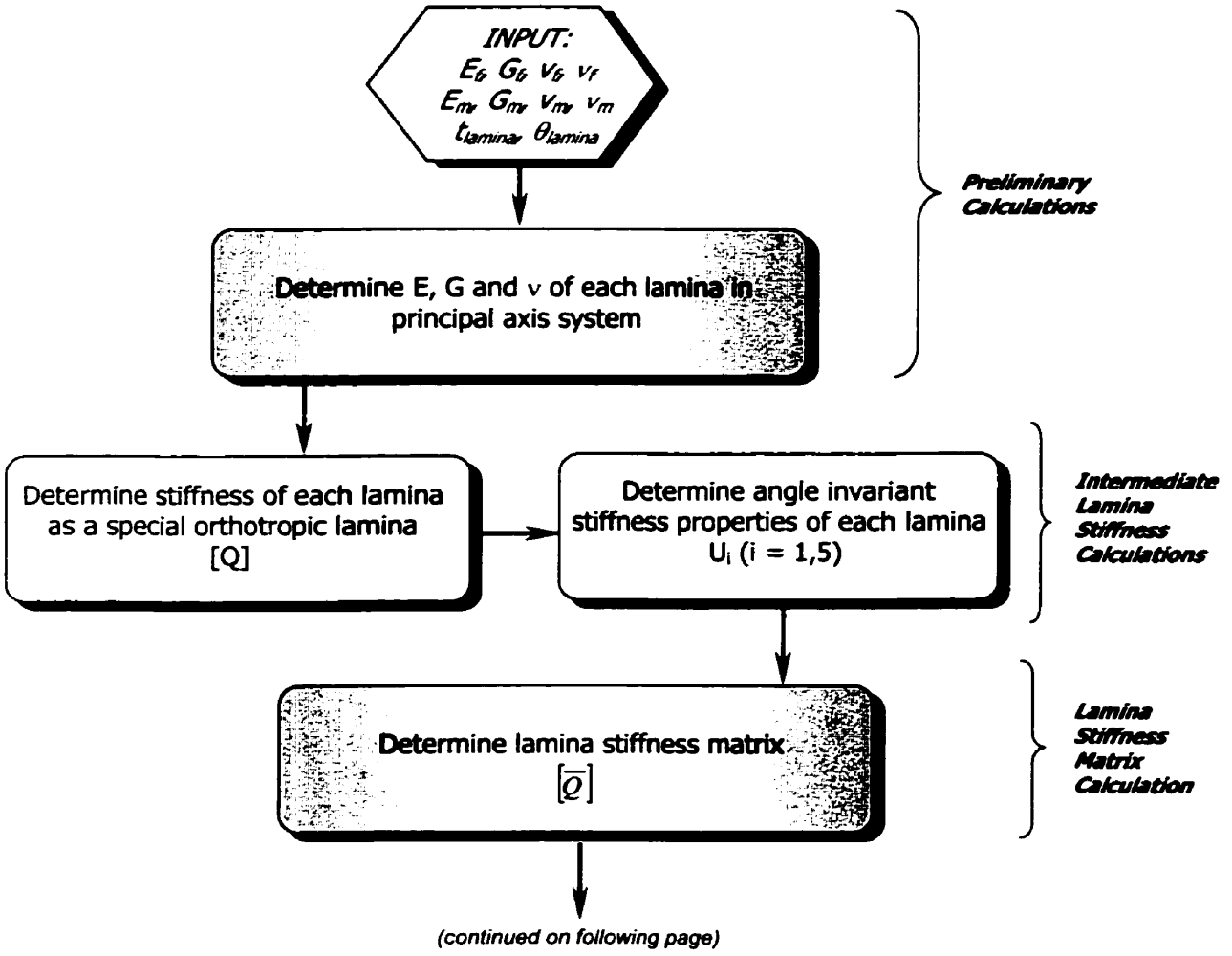

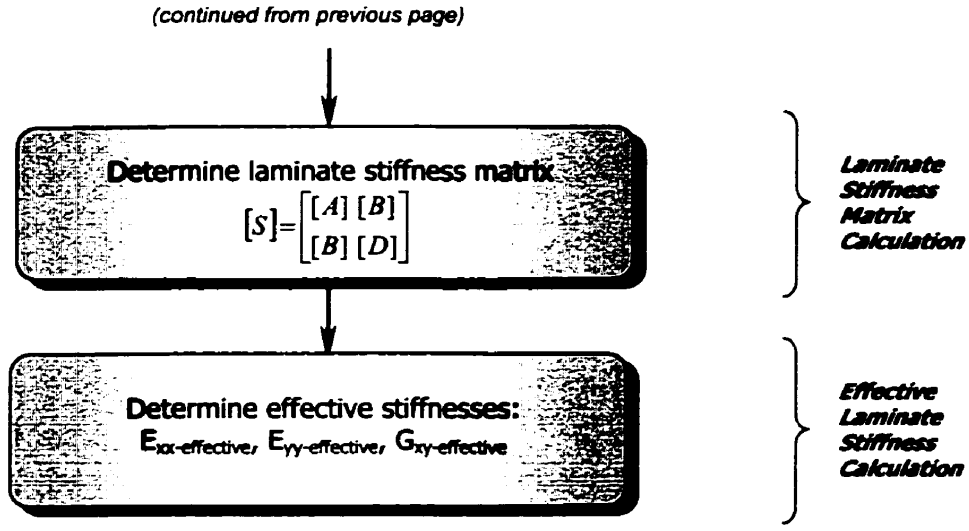

Figure 5.3: Flowchart of LPT Process

5.1.2.2 Lamina Stiffness Matrix

The moduli and Poisson's ratio in the principal material directions (1 and 2) are determined for each lamina using the equations below.

$$E_{11} = E_f v_f + E_m v_m \tag{E5.1}$$

$$\nu_{12} = \nu_f v_f + \nu_m v_m \tag{E5.2}$$

$$E_{22} = \frac{E_f E_m}{E_f - \sqrt{v_f}(E_f - E_m)} \tag{E5.3}$$

$$\nu_{21} = \frac{E_{22}}{E_{11}} \nu_{12} \tag{E5.4}$$

$$G_{12} = \frac{G_f G_m}{G_f - \sqrt{v_f}(G_f - G_m)} \tag{E5.5}$$

where:

E_{11} = *modulus of elasticity of lamina in direction of fibre length*
E_{22} = *modulus of elasticity of lamina in direction transverse to fibre*

E_f = *modulus of elasticity of fibre*
E_m = *modulus of elasticity of matrix*

v_f = *fibre volume fraction*
v_m = *matrix volume fraction = 1 - v_f*

ν_{12} = *major Poisson's ratio of lamina*
ν_{21} = *minor Poisson's ratio of lamina*
ν_f = *Poisson's ratio of fibres*
ν_m = *Poisson's ratio of matrix*

G_{12} = *longitudinal shear modulus of lamina*
G_f = *shear modulus of fibre*
G_m = *shear modulus of matrix*

Since the stiffness computation process can become complex and difficult to understand, a series of intermediate steps are taken that are meant to simplify the process.

The first intermediate step is computation of an intermediate lamina stiffness matrix. This matrix assumes the lamina lies at either 0° or 90° to the global x-axis. However, this assumption is not necessarily a true representation of the composite. The actual orientation of the lamina within the laminate will be accounted for at a later point in the modelling process. The intermediate matrix [Q] takes the form:

$$\begin{bmatrix} Q_{11} & Q_{12} & 0 \\ Q_{21} & Q_{22} & 0 \\ 0 & 0 & Q_{66} \end{bmatrix} = [Q] \qquad \text{[E5.6]}$$

where:

$$Q_{11} = \frac{E_{11}}{1 - \nu_{12}\nu_{21}} \qquad \text{[E5.7]}$$

$$Q_{22} = \frac{E_{22}}{1 - \nu_{12}\nu_{21}} \qquad \text{[E5.8]}$$

$$Q_{12} = Q_{21} = \frac{\nu_{12} E_{22}}{1 - \nu_{12}\nu_{21}} \quad \text{[E5.9]}$$

$$Q_{66} = G_{12} \quad \text{[E5.10]}$$

The [Q] matrix is calculated for each individual lamina.

The next intermediate values calculated are five terms $\{U_i\}$, which depend on the lamina stiffness matrix [Q]. The set of $\{U_i\}$ is termed angle invariant stiffness properties because it do not reflect the orientation of the lamina within the laminate structure. Again, this intermediate calculation is done only to facilitate understanding and make future modification of the model simple. The equations used to obtain the angle invariant properties are given below.

$$U_1 = \frac{1}{8}(3Q_{11} + 3Q_{22} + 2Q_{12} + 4Q_{66}) \quad \text{[E5.11]}$$

$$U_2 = \frac{1}{2}(Q_{11} - Q_{22}) \quad \text{[E5.12]}$$

$$U_3 = \frac{1}{8}(Q_{11} + Q_{22} - 2Q_{12} - 4Q_{66}) \quad \text{[E5.13]}$$

$$U_4 = \frac{1}{8}(Q_{11} + Q_{22} + 6Q_{12} - 4Q_{66}) \quad \text{[E5.14]}$$

$$U_5 = \frac{1}{2}(U_1 - U_4) \quad \text{[E5.15]}$$

A set of {Ui} is calculated for each individual lamina.

Finally, the stiffness matrix of each lamina can be obtained. The values in the lamina stiffness matrix refer to the global xyz axis system.

$$\begin{bmatrix} \overline{Q}_{11} & \overline{Q}_{12} & \overline{Q}_{16} \\ \overline{Q}_{21} & \overline{Q}_{22} & \overline{Q}_{26} \\ \overline{Q}_{16} & \overline{Q}_{26} & \overline{Q}_{66} \end{bmatrix} = [\overline{Q}] \qquad \text{[E5.16]}$$

where:

$$\overline{Q}_{11} = U_1 + U_2\cos(2\theta) + U_3\cos(4\theta) \qquad \text{[E5.17]}$$

$$\overline{Q}_{12} = \overline{Q}_{21} = U_4 - U_3\cos(4\theta) \qquad \text{[E5.18]}$$

$$\overline{Q}_{22} = U_1 - U_2\cos(2\theta) + U_3\cos(4\theta) \qquad \text{[E5.19]}$$

$$\overline{Q}_{16} = \frac{1}{2}U_2\sin(2\theta) + U_3\sin(4\theta) \qquad \text{[E5.20]}$$

$$\overline{Q}_{26} = \frac{1}{2}U_2\sin(2\theta) - U_3\sin(4\theta) \qquad \text{[E5.21]}$$

$$\overline{Q}_{66} = U_5 - U_3\cos(4\theta) \qquad \text{[E5.22]}$$

5.1.2.3 Laminate Stiffness Matrix

The stiffness matrix of the laminate structure actually consists of three submatrices: the extensional stiffness matrix [A] (in N/m), the coupling stiffness matrix [B] (in N) and the bending stiffness matrix [D] (in N-m). The full laminate stiffness matrix is shown below.

$$[S] = \begin{bmatrix} [A] & [B] \\ [B] & [D] \end{bmatrix} = \begin{bmatrix} \begin{bmatrix} A_{11} & A_{12} & A_{16} \\ A_{12} & A_{22} & A_{26} \\ A_{16} & A_{26} & A_{66} \end{bmatrix} \begin{bmatrix} B_{11} & B_{12} & B_{16} \\ B_{12} & B_{22} & B_{26} \\ B_{16} & B_{26} & B_{66} \end{bmatrix} \\ \begin{bmatrix} B_{11} & B_{12} & B_{16} \\ B_{12} & B_{22} & B_{26} \\ B_{16} & B_{26} & B_{66} \end{bmatrix} \begin{bmatrix} D_{11} & D_{12} & D_{16} \\ D_{12} & D_{22} & D_{26} \\ D_{16} & D_{26} & D_{66} \end{bmatrix} \end{bmatrix} \qquad \text{[E5.23]}$$

The terms of the stiffness matrix are based on the sum of individual terms of the lamina stiffness matrices $[\overline{Q}]$.

$$A_{mn} = \sum_{j=1}^{N} (\overline{Q}_{mn})(h_j - h_{j-1}) \quad \text{[E5.24]}$$

$$B_{mn} = \frac{1}{2} \sum_{j=1}^{N} (\overline{Q}_{mn})(h_j^2 - h_{j-1}^2) \quad \text{[E5.25]}$$

$$D_{mn} = \frac{1}{3} \sum_{j=1}^{N} (\overline{Q}_{mn})(h_j^3 - h_{j-1}^3) \quad \text{[E5.26]}$$

where:

$[\overline{Q}_{mn}]_j$ = *elements in the* $[\overline{Q}]$ *matrix of the* j^{th} *lamina*

N = *total number of laminas in the laminate*

h_{j-1} = *distance from midplane of laminate to the top of the* j^{th} *lamina in consideration*

hj = *distance from midplane of laminate to the bottom of the* j^{th} *lamina in consideration*

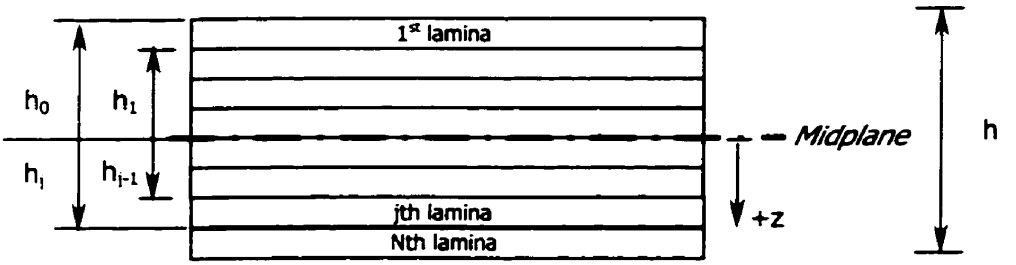

Figure 5.4: Laminate Geometry

Note that in the above coordinate system, h_j is positive below the midplane axis and negative above it.

The laminate stiffness matrix can be used to describe resultant forces and bending moments applied to the laminate structure:

$$\begin{Bmatrix} \{N\} \\ \{M\} \end{Bmatrix} = \begin{bmatrix} [A] & [B] \\ [B] & [D] \end{bmatrix} \begin{Bmatrix} \{\varepsilon\} \\ \{k\} \end{Bmatrix}$$

$$\begin{Bmatrix} N_{xx} \\ N_{yy} \\ N_{xy} \\ M_{xx} \\ M_{yy} \\ M_{xy} \end{Bmatrix} = \begin{bmatrix} [A] & [B] \\ [B] & [D] \end{bmatrix} \begin{Bmatrix} \varepsilon^{\circ}_{xx} \\ \varepsilon^{\circ}_{yy} \\ \gamma^{\circ}_{xy} \\ k_{xx} \\ k_{yy} \\ k_{xy} \end{Bmatrix} \qquad \text{[E5.27]}$$

where:

N_{xx} = *normal force resultant in the x-direction (per unit width)*

N_{yy} = *normal force resultant in the y-direction (per unit width)*

N_{xy} = *shear force resultant (per unit width)*

M_{xx} = *bending moment resultant in the yz-plane (per unit width)*

M_{yy} = *bending moment resultant in the xz-plane (per unit width)*

M_{xy} = *twisting moment resultant (per unit width)*

ε°_{xx}, ε°_{yy} = *midplane normal strains in the laminate*

γ°_{xy} = *midplane shear strain in the laminate*

k_{xx}, k_{yy} = *bending curvatures in the laminate*

k_{xy} = *twisting curvature in the laminate*

5.1.2.4 Effective Laminate Stiffness

Using *[E5.27]*, the effective moduli for a laminate can be determined.

To obtain $E_{xx\text{-effective}}$, a unit force is applied along the x-axis. All other external forces are set equal to zero.

$$N_{xx} = \sigma_{xx} h \quad \textit{(a tensile force along the longitudinal axis of the laminate)}$$

The deformations are isolated by multiplying both sides of *[E5.27]* by the inverse of the laminate stiffness matrix [S].

$$\begin{Bmatrix} \begin{Bmatrix} \varepsilon_{xx} \\ \varepsilon_{yy} \\ \gamma_{xy} \end{Bmatrix} \\ \begin{Bmatrix} k_{xx} \\ k_{yy} \\ k_{xy} \end{Bmatrix} \end{Bmatrix} = [S]^{-1} \begin{Bmatrix} \begin{Bmatrix} \sigma_{xx} h \\ 0 \\ 0 \end{Bmatrix} \\ \begin{Bmatrix} 0 \\ 0 \\ 0 \end{Bmatrix} \end{Bmatrix} \qquad \text{[E5.28]}$$

In order to determine $E_{xx\text{-effective}}$, only the uppermost line of *[E5.28]* is required. Thus, the equation becomes:

$$\varepsilon_{xx} = \left(S^{-1}\right)_{11} (\sigma_{xx} h) \qquad \text{[E5.29]}$$

In typical linear-elastic materials, the following is true:

$$\sigma_{xx} = E_{xx} \varepsilon xx \qquad \text{[E5.30]}$$

Substituting *[E5.30]* into *[E5.29]* gives:

$$\varepsilon_{xx} = \left(S^{-1}\right)_{11} (E_{xx} \varepsilon_{xx})(h) \qquad \text{[E5.31]}$$

Simplifying this equation, it becomes:

$$1 = \left(S^{-1}\right)_{11} E_{xx}\, h$$
$$E_{xx-effective} = \frac{1}{\left(S^{-1}\right)_{11} h} \qquad \text{[E5.32]}$$

The same process can be followed to obtain $E_{yy\text{-effective}}$:

$$E_{yy-effective} = \frac{1}{\left(S^{-1}\right)_{22} h} \qquad \text{[E5.33]}$$

As well, the process applies to obtain $G_{xy\text{-effective}}$:

$$G_{xy-effective} = \frac{1}{\left(S^{-1}\right)_{33} h} \qquad \text{[E5.34]}$$

5.1.3 Cross Section Stiffness

5.1.3.1 Element Area and Moment of Inertia

Upon obtaining the effective stiffness of the plates, tubes and bars, evaluation of the overall deck cross section begins. Due to its geometric complexity, the deck was broken up and evaluated as simplified elements. One spreadsheet was developed to handle the three-tube modules shown in Figure 5.5, while another was developed to work with the seven-tube modules in Figure 5.6.

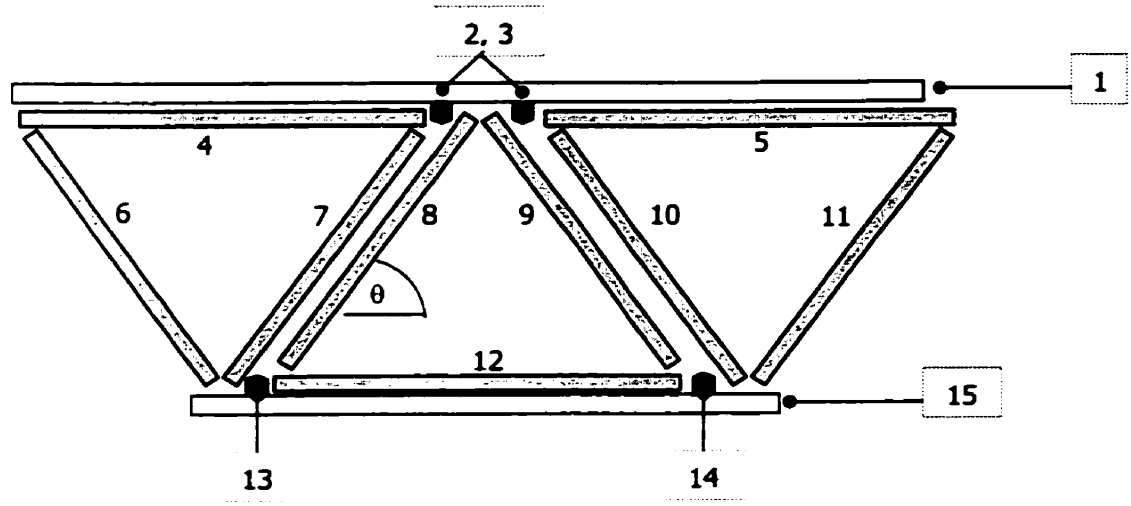

Figure 5.5: Element Numbering for Three-Tube Deck

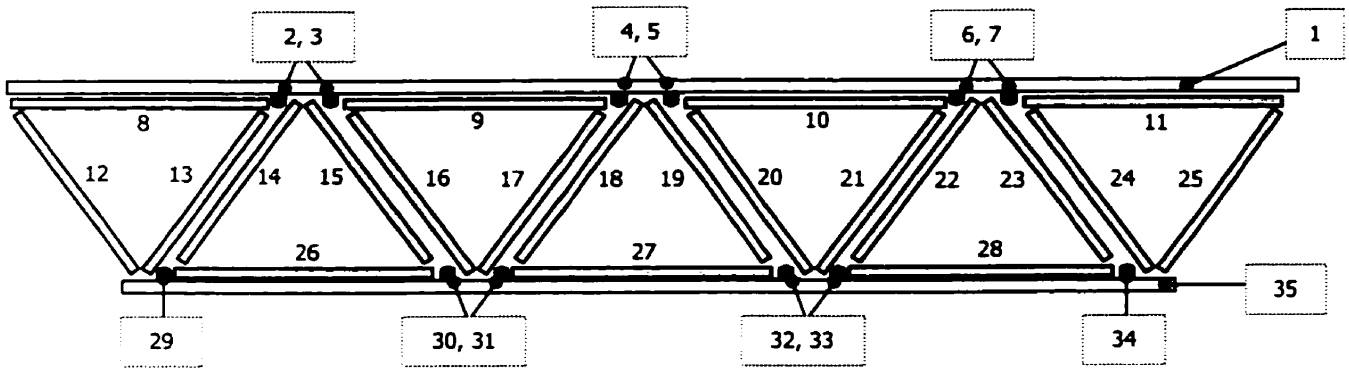

Figure 5.6: Element Numbering for Seven-Tube Deck

A sequence of calculations is then made, leading to the local element values for moment of inertia. The steps followed include:

i.) calculate element area;

ii.) determine distance from bottom of section to element centroid;

iii.) calculate centroid of overall section using:

$$y_{centroid} = \frac{\sum A_i \overline{y_i}}{\sum A_i} \qquad \text{[E5.35]}$$

iv.) calculate the moment of inertia, I_{xx}, of each element about its centroidal axis. Horizontal elements (e.g., elements 4, 5, and 12 in Figure 5.5) use *[E5.36]*, while inclined elements (e.g., elements 6-11 in Figure 5.5) use *[E5.37]* through *[E5.39]*.

$$I_x = \frac{(width)(thickness)^3}{12} \qquad [E5.36]$$

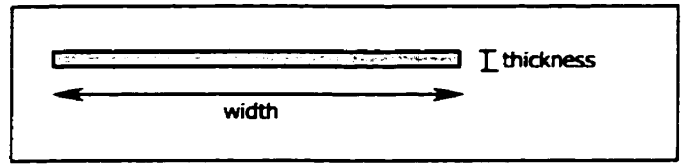

Figure 5.7: Dimensions of Horizontal Elements

$$I_x' = \frac{(thickness)(width)^3}{12} \qquad [E5.37]$$

$$I_y' = \frac{(width)(thickness)^3}{12} \qquad [E5.38]$$

$$I_x = I_x'(\cos^2\theta) + I_y'(\sin^2\theta) \qquad [E5.39]$$

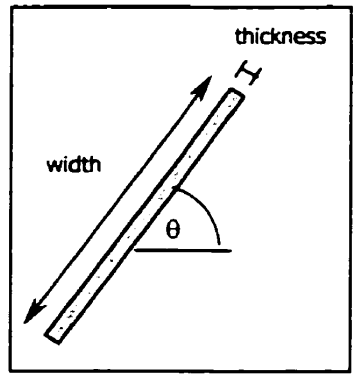

Figure 5.8: Dimensions of Inclined Elements

Bar elements are separated into a rectangle and half-ellipse for computation of their moment of inertia.

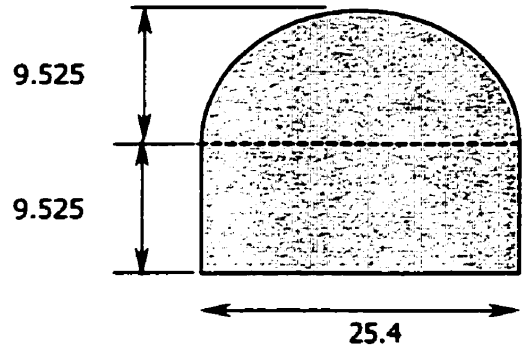

Figure 5.9: Filler Bar Dimensions

First the area of the ellipse and rectangle are computed.

$$A_{ellipse} = \frac{1}{4}\pi h\, w = \frac{1}{4}\pi(9.525)(25.4) = 190.0$$

$$A_{total} = 190.0 + 25.4(9.525)$$

$$= 431.95\, mm^2$$

Next, the location of the centroid of the ellipse is calculated, followed by determination of the location of the section's centroid.

$$\bar{y}_{ellipse} = \frac{4}{3\pi} h = \frac{4}{3\pi}(9.525) = 4.043\, mm\ from\ bottom\ of\ ellipse$$

$$\bar{y}_{bar} = \frac{190(9.525 + 4.043) + 25.4(9.525)\left(9.525/2\right)}{431.95} = 8.64\, mm$$

Finally, the moment of inertia of the ellipse and rectangle are calculated and combined using the parallel axis theorem to produce the filler bar's local moment of inertia.

$$I_{ellipse} = (h^3)(w/2)(\frac{\pi}{8} - \frac{8}{9\pi}) = (9.525^3)(12.7)(\frac{\pi}{8} - \frac{8}{9\pi}) = 1204.6\,mm^4$$

$$I_{rect} = \frac{(w)(h^3)}{12} = \frac{(25.4)(9.525^3)}{12} = 1829.1\,mm^4$$

$$I_{bar} = \left[\left(1204.6 + (190)(13.568 - 8.64)^2\right) + (1829.1 + (25.4)(9.525)(9.525/2 - 8.64)^2)\right] = 11285.4\,mm^4$$

5.1.3.2 Section Moment of Inertia

Since the glass fibre tubes, bars and plates all had a different effective stiffness (E), their geometric properties could not simply be combined without adjustment. An equivalence factor, n, was applied to all elements as defined below.

$$n = \frac{E_{element}}{E_{tube}} \qquad \text{[E5.40]}$$

Therefore, n for the tube elements is always 1, while n for the plate and bar elements will usually be a value other than 1.

In order to calculate the overall moment of inertia of the section, the parallel axis theorem is used as shown in the following equation.

$$I_{global} = \sum_{all\ elements} (n_i I_i + n_i A_i (y_{centroid} - \bar{y}_i)^2) \qquad \text{[E5.41]}$$

5.1.3.3 *Load/Deflection* Ratio

Finally, the loading conditions were evaluated in order to develop an expression for the theoretical *Load/Deflection* ratio. For Phase I modules, the loading plate was 250 by 250 mm producing the following load, shear and bending moment diagrams.

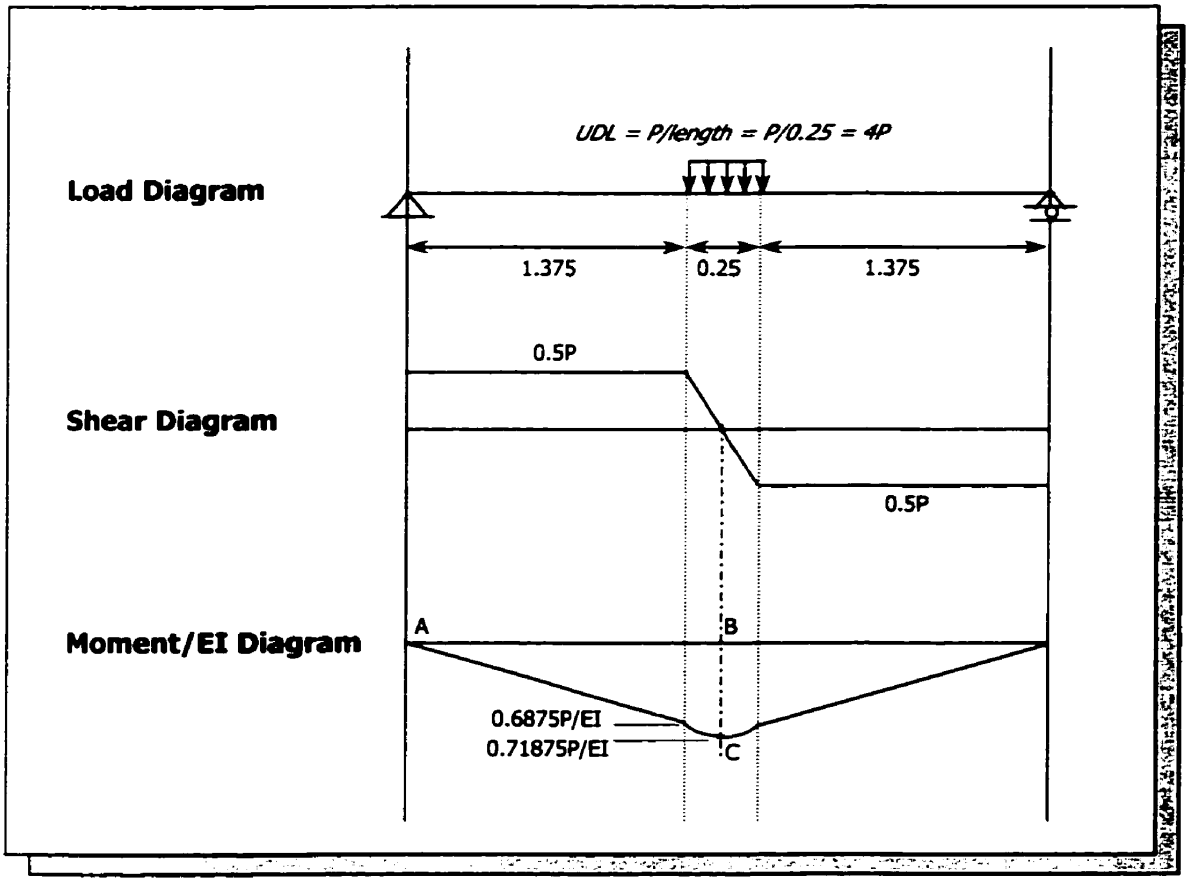

Figure 5.10: Load, Shear and Moment Diagrams for Phase I Decks

By moment-area method, the deflection at midspan can be calculated as:

$$\Delta = Moment\ of\ ABC\ about\ A$$

The area ABC is broken into three subareas as shown in Figure 5.11. The deflection at midspan may then be obtained.

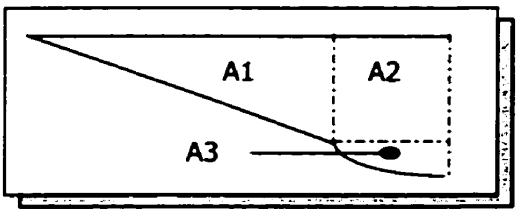

Figure 5.11: Breakdown of Moment Areas

$$\Delta = \tfrac{1}{2}(1.375 \cdot 0.6875P)(\tfrac{2}{3} \cdot 1.375) + (0.6875P \cdot \tfrac{0.25}{2})(1.375 + \tfrac{0.25}{4}) + \tfrac{2}{3}(\tfrac{0.25}{2})(0.71875 - 0.6875)P(1.375 + \tfrac{5}{8} \cdot \tfrac{0.25}{2}) = \frac{0.5606P}{EI}$$

Rearranging, the theoretical load-deflection slope for the Phase I decks is:

$$\frac{P}{\Delta} = \frac{EI}{0.5606} = \left(\frac{Load}{Deflection}\right) ratio \qquad [E5.42]$$

The same argument is true for the Phase II specimens where the loading plate is now 570 mm wide.

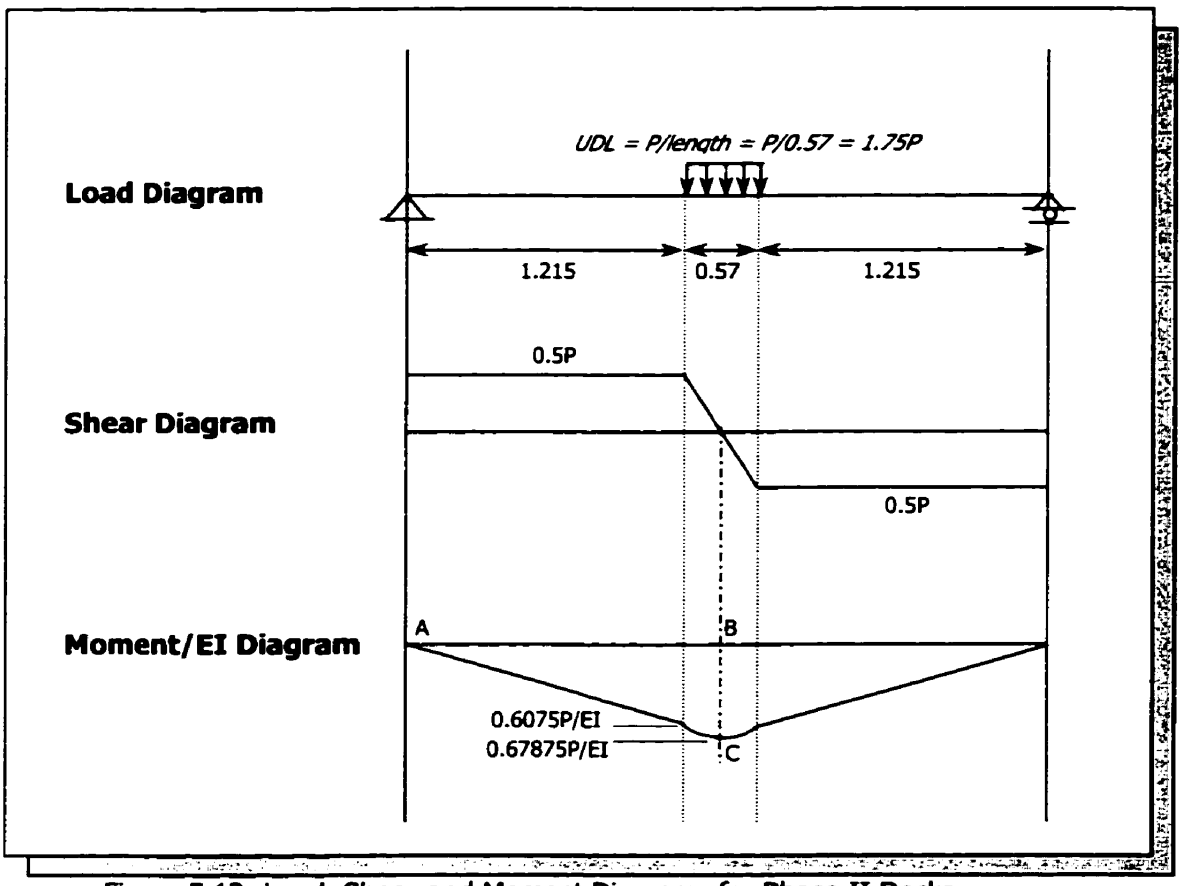

Figure 5.12: Load, Shear and Moment Diagrams for Phase II Decks

$$\Delta = \tfrac{1}{2}(1.215 \cdot 0.6075P)(\tfrac{2}{3} \cdot 1.215) + (0.6075P \cdot \tfrac{0.57}{2})(1.215 + \tfrac{0.57}{4}) + \tfrac{2}{3}(\tfrac{0.57}{2})(0.67875 - 0.6075)P(1.215 + \tfrac{5}{8} \cdot \tfrac{0.57}{2}) = \frac{0.5528P}{EI}$$

Rearranging, the theoretical load-deflection slope for the Phase II decks is:

$$\frac{P}{\Delta} = \frac{EI}{0.5528} = \left(\frac{Load}{Deflection}\right)ratio \qquad [E5.43]$$

5.1.4 Example Calculation

This section details the method by which a user would apply the model to predict deck stiffness. The example deck used is specimen *F7-1*. Important user procedures are highlighted, and the resulting model spreadsheets are provided.

To begin, the following data are input into the '*Effective Plate Stiffness*' and '*Effective Tube Stiffness*' worksheets:

- E_m, ν_m, G_m;
- E_f, ν_f, G_f, ν_f;
- $(t_{lamina})_i$; and,
- $(\theta_{lamina})_i$.

With this data, the '*Effective Plate Stiffness*' and '*Effective Tube Stiffness*' worksheets perform all of the functions detailed in the flowchart of Figure 5.3 and output the following:

- $E_{xx\text{-effective}}$;
- $E_{yy\text{-effective}}$; and,
- $G_{xy\text{-effective}}$.

The above input and output may be found in worksheets provided at the end of this chapter. The user interface of these worksheets consists of the clear data cells on the left hand side of the worksheet, while the matrix calculations are located in shaded cells on the right hand side of the worksheet. The user need only be concerned with the input material properties at the top of the page and the final output at the bottom.

Next, the user moves to the '*Deck Stiffness*' worksheet, which is linked to the previous worksheets. At this point, the user must input the following data:

- $E_{\text{filler bar}}$ (from lab testing);
- top plate width;
- bottom plate width;
- filler bar height;
- filler bar area, A_{bar};
- local centroid of filler bar, $\bar{y}_{bar}$; and,
- total deck section height.

With this input, the worksheet performs the geometric calculations shown in the flowchart of Figure 5.1. Based on this data, the deck moment of inertia and theoretical

Load/Deflection ratio are output at the bottom of the spreadsheet, found at the end of this chapter.

This process was done for each deck specimen in each orientation tested, therefore several models exist. One model predicts deck stiffness for a three-tube specimen tested with the narrow plate facing up, while another model predicts stiffness for a three-tube specimen with the narrow plate facing down. There is also a third model designed to evaluate the stiffness of the seven-tube modules. Should the deck configuration change to a square cross section, as is planned for future development, the seven-tube model will have to be modified in order to accommodate the altered cross section.

5.1.5 Comparison of Theoretical with Measured Behaviour

The model was used to predict the stiffness for each deck test, nine in total. The load deflection diagram for each deck group in Phase I is provided in Figures 5.13 through 5.15.

The model predicted very well the behaviour of all intact decks *F1-TB-a*, *F2-TB-a* and *FR-TB-a*. The predicted stiffness for the retests of the decks was less accurate. This was expected since the model does not take damage from previous testing into account.

The match between predicted and measured stiffness was also very good for the Phase II specimens, as seen in Figure 5.16.

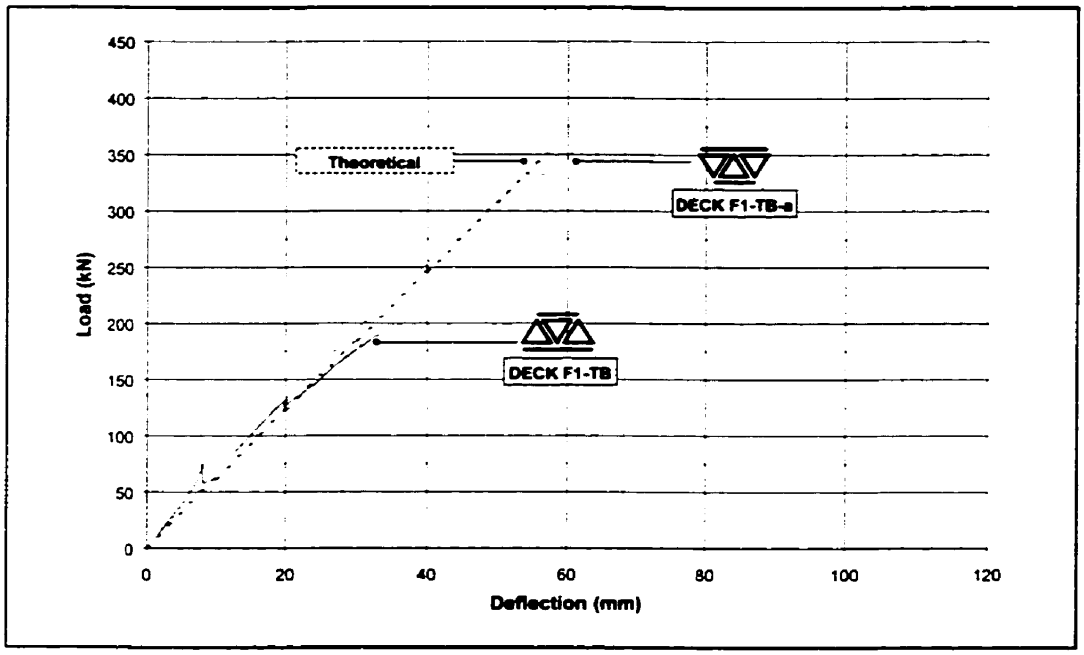

Figure 5.13: Comparison of Predicted with Actual Load-Deflection Behaviour – Group F1

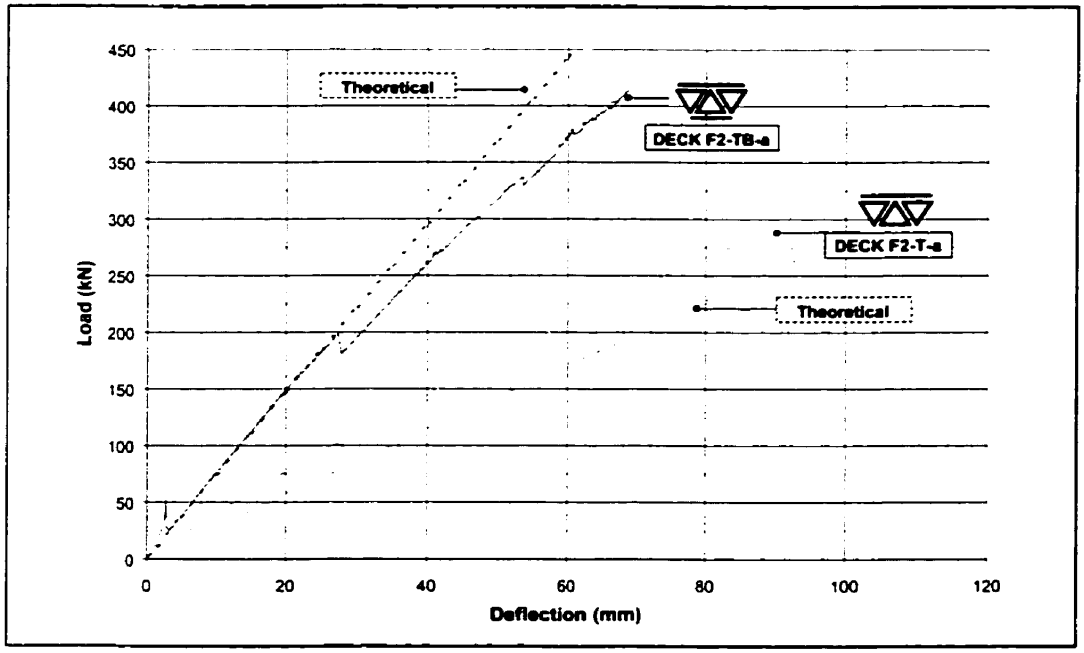

Figure 5.14: Comparison of Predicted with Actual Load-Deflection Behaviour – Group F2

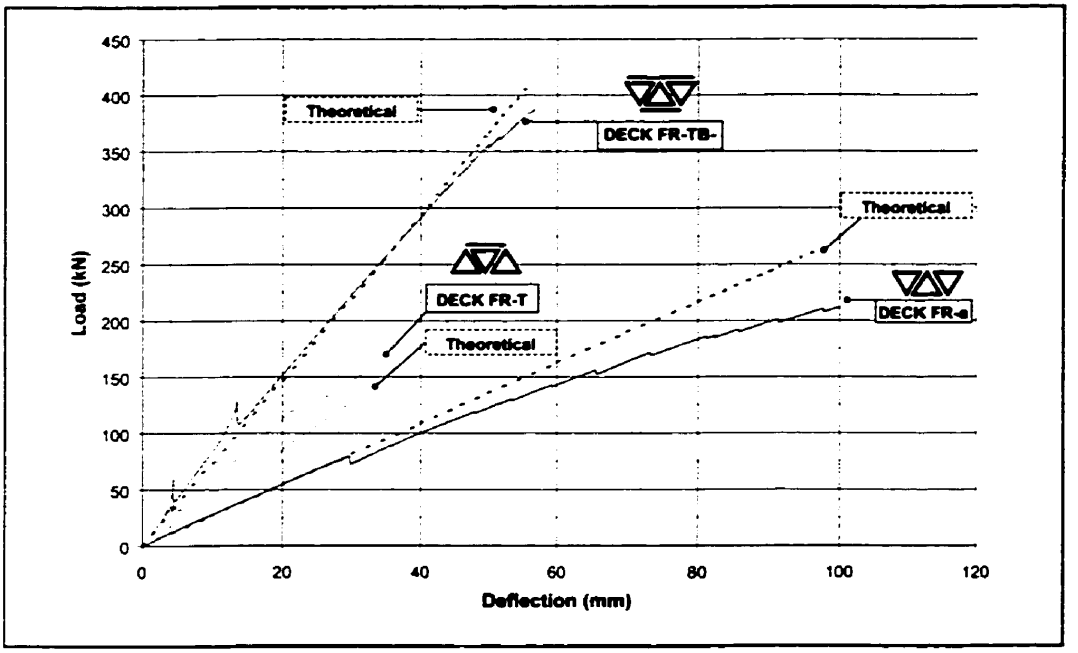

Figure 5.15: Comparison of Predicted with Actual Load-Deflection Behaviour – Group FR

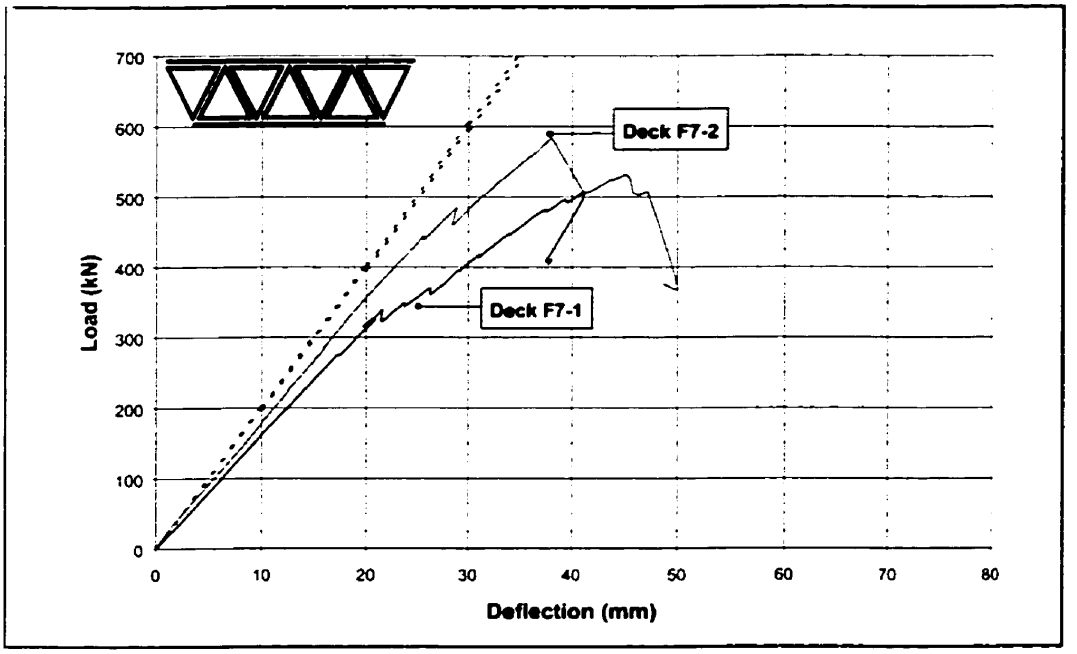

Figure 5.16: Comparison of Predicted with Actual Load-Deflection Behaviour – Group F7

Although the predicted behaviour is plotted through the entire duration of the tests, it should be applied only up to the service load ranges (0 – 139 kN) before any damage could occur. The percent difference between theoretical and actual in this range is shown graphically in Figure 5.17.

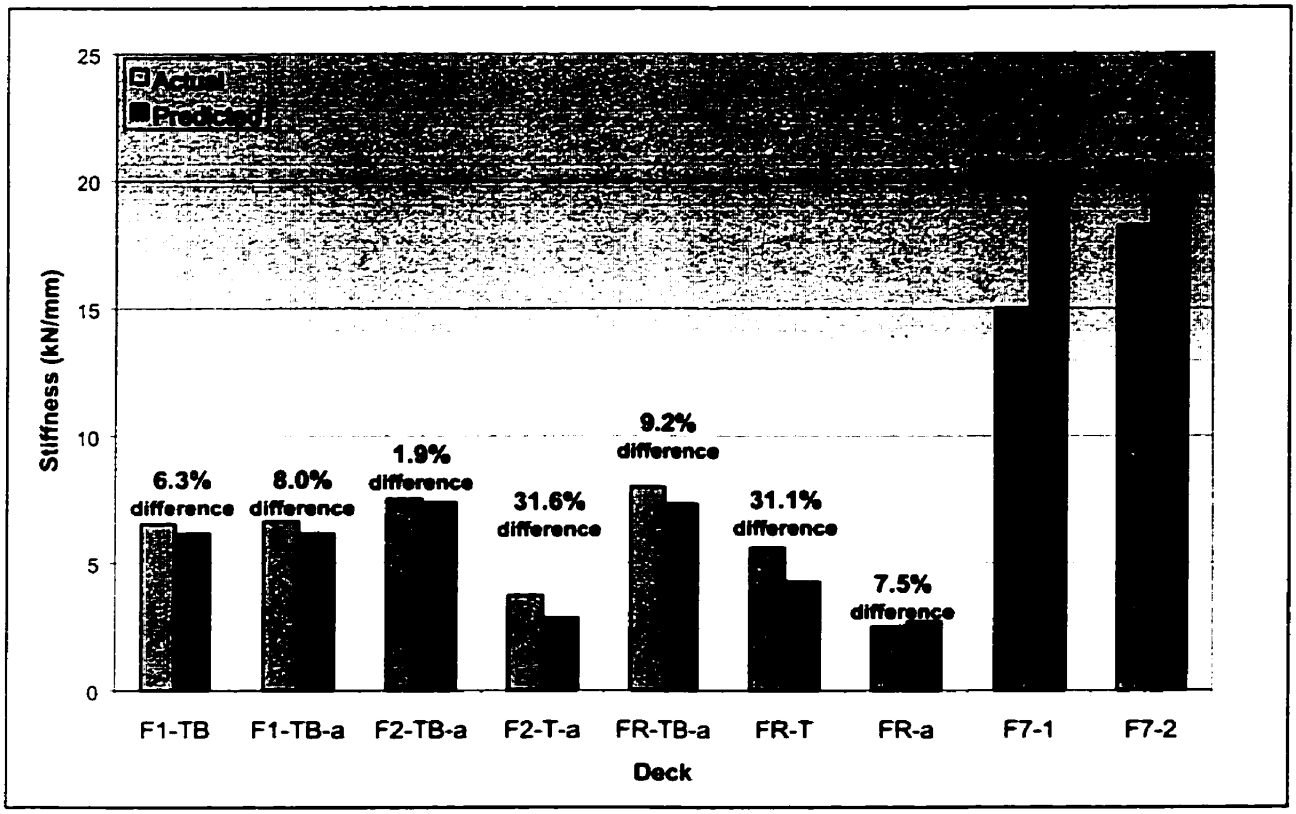

Figure 5.17: Percent Comparison of Predicted and Actual Deck Stiffness

The percent difference between predicted and actual values is reasonable when one considers that the decks are still in the development stage, where manufacturing methods have yet to be perfected. This would account for deviations of the intact decks from expected values. On the whole, the model appears to be a dependable one that may be used to design further phases of deck development in a more efficient and precise manner.

5.1.6 Contribution of Components to Stiffness

Using the derived model, the stiffness contribution of each deck component can be computed. This is achieved by selecting a component to consider (i.e., plates, bars or tubes), and setting the area and moment of inertia of the remaining components equal to zero. The resulting deck stiffness is the contribution of that component to the overall deck stiffness. The results of this analysis are presented in Figures 5.18 and 5.19.

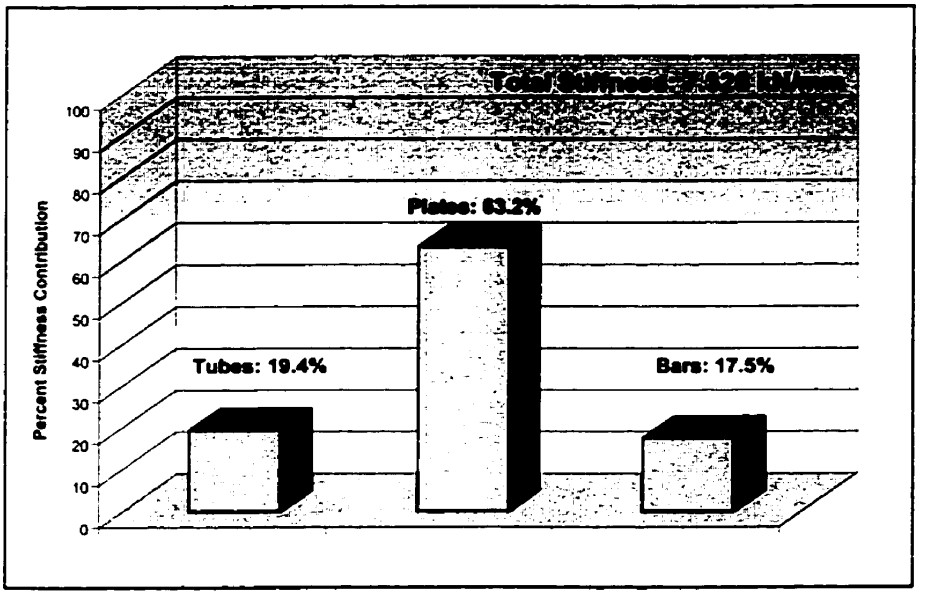

Figure 5.18: Percent Contribution of Each Component in Three-Tube Modules

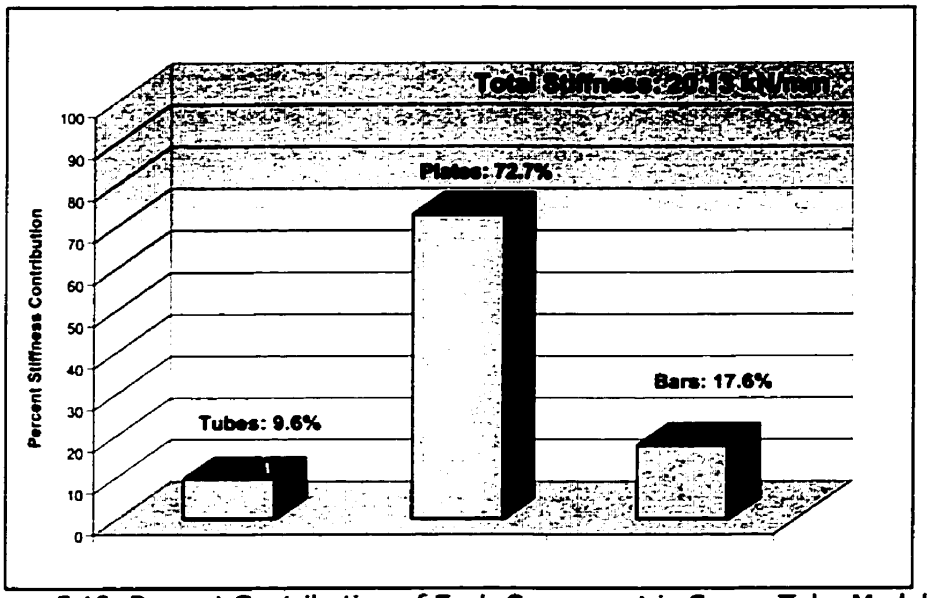

Figure 5.19: Percent Contribution of Each Component in Seven-Tube Modules

It is clear that the majority of the deck stiffness is derived from the deck plates. For this reason, it was warranted to spend the time and money necessary to improve the deck plates in progressing from Phase I to Phase II.

An unexpected discovery is that the bars, intended to be only a filler in the section, actually provide a significant amount of stiffness to the section.

The tubes appear to contribute less to the section stiffness in Phase II than in Phase I. However, in absolute terms, their stiffness contribution is equal in both cases. Therefore, the tubes are not less stiff in the Phase II modules. Rather, their relative contribution is reduced due to the increased overall section stiffness.

5.2 Comparison with Other Decks

The final comparison to be made is that of deck behaviour against other decks being developed.

The first deck to be considered is being developed by Hayes et al (2000) at Virginia Tech. They have produced a module consisting of 12 pultruded square tubes of dimensions 102 x 102 x 6.35 mm. The tubes are connected to each other with Fibrebolt studs and nuts. The plates that are adhered to the top and bottom of the deck are pultruded plates of 9.53 mm thickness. The plates are adhered with epoxy resin, and are cured under pressure. All components are off-the-shelf products available from Strongwell's Extren line.

The modules were tested under a 1.22 m simply supported span, under a single 508 x 305 mm patch load. At a load of 92.5 kN, which corresponds to the service load of an AASHTO HS20 design truck, the deck exhibited 3.81 m of deflection. Since the test span is different from the 3 m used in this project's test program, the two deflections cannot be compared directly. Taking Deck *F7-2*'s deflection at 92.5 kN and multiplying it by an adjustment factor account for test span, the following is obtained.

$$\Delta = \frac{PL^3}{48EI}$$

$$Therefore: \Delta_{Deck\ F7-2\ with\ a\ 1.22m\ span} = 5.08mm\left(\frac{1.22^3}{3^3}\right) = 0.34\,mm$$

Clearly, then deck *F7-2* is superior in service stiffness to the deck in question.

In addition, the achieved *L/270* service deflection ratio of Virginia Tech's deck is surpassed by deck *F7-2*'s corresponding *L/590* ratio at 92.5 kN.

As well, the failure load for Virginia Tech's deck was only 334 kN when a punching shear failure occurred. Deck *F7-2*'s failure load exceeded this as well.

The second deck considered is being developed by Bernetich et al (1996) using SCRIMP. The deck is 2.4 m span, 600 mm wide with triangular tubes as the core. The tubes were wrapped in four layers of stitch bonded glass fabric, while the surrounding plates are made of seven layers of the same material.

This type of deck failed in core shear at a load of 894 kN. This does appear to exceed the failure load of Deck *F7-2*, however the spans under consideration were different. Using the same conversion as previously derived:

$$P = \frac{48EI}{L^3} \text{ therefore } P \text{ is inversely proportional to } L^3$$

$$\text{Then } P_{\text{failure Bernetich et al}} = 894kN\left(\frac{2.4^3}{3^3}\right) = 458\,kN$$

Once again, deck *F7-2* demonstrates superior performance.

The final deck considered is that developed by Zureick (2000) at the Georgia Institute of Technology. It consists of five triangular tubes, pultruded by Creative Pultrusions. Plates were hand layed-up on the top and bottom of these tubes. Under a 2.87 m simply supported span, the modules failed at 425 kN due to tensile failure of the bottom plate. This corresponds to a 372 kN failure load under a 3 m test span.

Larger 3 x 3 m deck panels were also produced that withstood a 635 kN load without failure at only 17.8 mm deflection.

Based on these comparisons, the decks designed and produced by Wardrop Engineering and Faroex Ltd. appear to be equivalent to, or surpass, the performance of other FRP modular decks on the market. With further research and development, this deck technology will be a competitive product when introduced to the market.

Calculation of Laminate Properties
Deck Plates

All input in (N, mm)
50 layer lamina capacity

Resin matrix properties:	
Shell Chemical's EPON Resin 828	
[illegible]	[illegible]
[illegible]	[illegible]
[illegible]	[illegible]
[illegible]	[illegible]
[illegible]	[illegible]
[illegible]	[illegible]
[illegible]	[illegible]

Fibre properties:	
Owens Corning's Type 30 Roving	
[illegible]	[illegible]
[illegible]	[illegible]
[illegible]	[illegible]
[illegible]	[illegible]
[illegible]	[illegible]
[illegible]	[illegible]

Total number of layers 38
Total laminate thickness 15.00

Layer Number	t	θ	Fibre volume	Lamina Density	E11	E22	G12	v12	v21
1	0.39474	90	0.45	1.8215	34312.5	8789.90	3481.96	0.2475	0.063
2	0.39474	-45	0.45	1.8215	34312.5	8789.90	3481.96	0.2475	0.063
3	0.39474	45	0.45	1.8215	34312.5	8789.90	3481.96	0.2475	0.063
4	0.39474	-10	0.45	1.8215	34312.5	8789.90	3481.96	0.2475	0.063
5	0.39474	10	0.45	1.8215	34312.5	8789.90	3481.96	0.2475	0.063
6	0.39474	-10	0.45	1.8215	34312.5	8789.90	3481.96	0.2475	0.063
7	0.39474	10	0.45	1.8215	34312.5	8789.90	3481.96	0.2475	0.063
8	0.39474	-10	0.45	1.8215	34312.5	8789.90	3481.96	0.2475	0.063
9	0.39474	10	0.45	1.8215	34312.5	8789.90	3481.96	0.2475	0.063
10	0.39474	-45	0.45	1.8215	34312.5	8789.90	3481.96	0.2475	0.063
11	0.39474	45	0.45	1.8215	34312.5	8789.90	3481.96	0.2475	0.063
12	0.39474	-10	0.45	1.8215	34312.5	8789.90	3481.96	0.2475	0.063
13	0.39474	10	0.45	1.8215	34312.5	8789.90	3481.96	0.2475	0.063
14	0.39474	-10	0.45	1.8215	34312.5	8789.90	3481.96	0.2475	0.063
15	0.39474	10	0.45	1.8215	34312.5	8789.90	3481.96	0.2475	0.063
16	0.39474	-10	0.45	1.8215	34312.5	8789.90	3481.96	0.2475	0.063
17	0.39474	10	0.45	1.8215	34312.5	8789.90	3481.96	0.2475	0.063
18	0.39474	45	0.45	1.8215	34312.5	8789.90	3481.96	0.2475	0.063
19	0.39474	-10	0.45	1.8215	34312.5	8789.90	3481.96	0.2475	0.063
20	0.39474	10	0.45	1.8215	34312.5	8789.90	3481.96	0.2475	0.063
21	0.39474	-45	0.45	1.8215	34312.5	8789.90	3481.96	0.2475	0.063
22	0.39474	-10	0.45	1.8215	34312.5	8789.90	3481.96	0.2475	0.063
23	0.39474	10	0.45	1.8215	34312.5	8789.90	3481.96	0.2475	0.063
24	0.39474	-10	0.45	1.8215	34312.5	8789.90	3481.96	0.2475	0.063
25	0.39474	10	0.45	1.8215	34312.5	8789.90	3481.96	0.2475	0.063
26	0.39474	-10	0.45	1.8215	34312.5	8789.90	3481.96	0.2475	0.063
27	0.39474	10	0.45	1.8215	34312.5	8789.90	3481.96	0.2475	0.063
28	0.39474	-45	0.45	1.8215	34312.5	8789.90	3481.96	0.2475	0.063
29	0.39474	45	0.45	1.8215	34312.5	8789.90	3481.96	0.2475	0.063
30	0.39474	-10	0.45	1.8215	34312.5	8789.90	3481.96	0.2475	0.063
31	0.39474	10	0.45	1.8215	34312.5	8789.90	3481.96	0.2475	0.063
32	0.39474	-10	0.45	1.8215	34312.5	8789.90	3481.96	0.2475	0.063
33	0.39474	10	0.45	1.8215	34312.5	8789.90	3481.96	0.2475	0.063
34	0.39474	-10	0.45	1.8215	34312.5	8789.90	3481.96	0.2475	0.063
35	0.39474	10	0.45	1.8215	34312.5	8789.90	3481.96	0.2475	0.063
36	0.39474	-45	0.45	1.8215	34312.5	8789.90	3481.96	0.2475	0.063
37	0.39474	45	0.45	1.8215	34312.5	8789.90	3481.96	0.2475	0.063
38	0.39474	90	0.45	1.8215	34312.5	8789.90	3481.96	0.2475	0.063
39	0	0	0	0	0	0.00	0.00	0	0.000
40	0	0	0	0	0	0.00	0.00	0	0.000
41	0	0	0	0	0	0.00	0.00	0	0.000
42	0	0	0	0	0	0.00	0.00	0	0.000
43	0	0	0	0	0	0.00	0.00	0	0.000
44	0	0	0	0	0	0.00	0.00	0	0.000
45	0	0	0	0	0	0.00	0.00	0	0.000
46	0	0	0	0	0	0.00	0.00	0	0.000
47	0	0	0	0	0	0.00	0.00	0	0.000
48	0	0	0	0	0	0.00	0.00	0	0.000
49	0	0	0	0	0	0.00	0.00	0	0.000
50	0	0	0	0	0	0.00	0.00	0	0.000

θ (radians)	[illegible]				Intermediate Angle-invariant Stiffness Properties					Lamina Stiffness Matrix						Thickness	[illegible]
	[illegible]	[illegible]	[illegible]	[illegible]	U1	U2	U3	U4	U5	Qb11	Qb22	Qb12	Qb16	Qb26	Qb66	h	[illegible]
																-7.50	
1.571	[illegible]	[illegible]	[illegible]	[illegible]	16714.8	[illegible]	3100.2	[illegible]	[illegible]	8830.0	34880.5	2210.2	0.0	0.0	3482.0	-7.11	[illegible]
-0.785	[illegible]	[illegible]	[illegible]	[illegible]	16714.8	[illegible]	3100.2	[illegible]	[illegible]	15634.4	15634.4	8670.5	-6482.4	-6482.4	9842.3	-6.71	[illegible]
0.785	[illegible]	[illegible]	[illegible]	[illegible]	16714.8	[illegible]	3100.2	[illegible]	[illegible]	15634.4	15634.4	8670.5	6482.4	6482.4	9842.3	-6.32	[illegible]
-0.175	[illegible]	[illegible]	[illegible]	[illegible]	16714.8	[illegible]	3100.2	[illegible]	[illegible]	33333.6	[illegible]	2964.2	-4261.3	-172.8	4220.0	-5.92	[illegible]
0.175	[illegible]	[illegible]	[illegible]	[illegible]	16714.8	[illegible]	3100.2	[illegible]	[illegible]	33333.6	[illegible]	2964.2	4261.3	172.8	4220.0	-5.53	[illegible]
-0.175	[illegible]	[illegible]	[illegible]	[illegible]	16714.8	[illegible]	3100.2	[illegible]	[illegible]	33333.6	[illegible]	2964.2	-4261.3	-172.8	4220.0	-5.13	[illegible]
0.175	[illegible]	[illegible]	[illegible]	[illegible]	16714.8	[illegible]	3100.2	[illegible]	[illegible]	33333.6	[illegible]	2964.2	4261.3	172.8	4220.0	-4.74	[illegible]
-0.175	[illegible]	[illegible]	[illegible]	[illegible]	16714.8	[illegible]	3100.2	[illegible]	[illegible]	33333.6	[illegible]	2964.2	-4261.3	-172.8	4220.0	-4.34	[illegible]
0.175	[illegible]	[illegible]	[illegible]	[illegible]	16714.8	[illegible]	3100.2	[illegible]	[illegible]	33333.6	[illegible]	2964.2	4261.3	172.8	4220.0	-3.95	[illegible]
-0.785	[illegible]	[illegible]	[illegible]	[illegible]	16714.8	[illegible]	3100.2	[illegible]	[illegible]	15634.4	15634.4	8670.5	-6482.4	-6482.4	9842.3	-3.55	[illegible]
0.785	[illegible]	[illegible]	[illegible]	[illegible]	16714.8	[illegible]	3100.2	[illegible]	[illegible]	15634.4	15634.4	8670.5	6482.4	6482.4	9842.3	-3.16	[illegible]
-0.175	[illegible]	[illegible]	[illegible]	[illegible]	16714.8	[illegible]	3100.2	[illegible]	[illegible]	33333.6	[illegible]	2964.2	-4261.3	-172.8	4220.0	-2.76	[illegible]
0.175	[illegible]	[illegible]	[illegible]	[illegible]	16714.8	[illegible]	3100.2	[illegible]	[illegible]	33333.6	[illegible]	2964.2	4261.3	172.8	4220.0	-2.37	[illegible]
-0.175	[illegible]	[illegible]	[illegible]	[illegible]	16714.8	[illegible]	3100.2	[illegible]	[illegible]	33333.6	[illegible]	2964.2	-4261.3	-172.8	4220.0	-1.97	[illegible]
0.175	[illegible]	[illegible]	[illegible]	[illegible]	16714.8	[illegible]	3100.2	[illegible]	[illegible]	33333.6	[illegible]	2964.2	4261.3	172.8	4220.0	-1.58	[illegible]
-0.175	[illegible]	[illegible]	[illegible]	[illegible]	16714.8	[illegible]	3100.2	[illegible]	[illegible]	33333.6	[illegible]	2964.2	-4261.3	-172.8	4220.0	-1.18	[illegible]
0.175	[illegible]	[illegible]	[illegible]	[illegible]	16714.8	[illegible]	3100.2	[illegible]	[illegible]	33333.6	[illegible]	2964.2	4261.3	172.8	4220.0	-0.79	[illegible]
0.785	[illegible]	[illegible]	[illegible]	[illegible]	16714.8	[illegible]	3100.2	[illegible]	[illegible]	15634.4	15634.4	8670.5	6482.4	6482.4	9842.3	-0.39	[illegible]
-0.175	[illegible]	[illegible]	[illegible]	[illegible]	16714.8	[illegible]	3100.2	[illegible]	[illegible]	33333.6	[illegible]	2964.2	-4261.3	-172.8	4220.0	0.00	[illegible]
0.175	[illegible]	[illegible]	[illegible]	[illegible]	16714.8	[illegible]	3100.2	[illegible]	[illegible]	33333.6	[illegible]	2964.2	4261.3	172.8	4220.0	0.39	[illegible]
-0.785	[illegible]	[illegible]	[illegible]	[illegible]	16714.8	[illegible]	3100.2	[illegible]	[illegible]	15634.4	15634.4	8670.5	-6482.4	-6482.4	9842.3	0.79	[illegible]
-0.175	[illegible]	[illegible]	[illegible]	[illegible]	16714.8	[illegible]	3100.2	[illegible]	[illegible]	33333.6	[illegible]	2964.2	-4261.3	-172.8	4220.0	1.18	[illegible]
0.175	[illegible]	[illegible]	[illegible]	[illegible]	16714.8	[illegible]	3100.2	[illegible]	[illegible]	33333.6	[illegible]	2964.2	4261.3	172.8	4220.0	1.58	[illegible]
-0.175	[illegible]	[illegible]	[illegible]	[illegible]	16714.8	[illegible]	3100.2	[illegible]	[illegible]	33333.6	[illegible]	2964.2	-4261.3	-172.8	4220.0	1.97	[illegible]
0.175	[illegible]	[illegible]	[illegible]	[illegible]	16714.8	[illegible]	3100.2	[illegible]	[illegible]	33333.6	[illegible]	2964.2	4261.3	172.8	4220.0	2.37	[illegible]
-0.175	[illegible]	[illegible]	[illegible]	[illegible]	16714.8	[illegible]	3100.2	[illegible]	[illegible]	33333.6	[illegible]	2964.2	-4261.3	-172.8	4220.0	2.76	[illegible]
0.175	[illegible]	[illegible]	[illegible]	[illegible]	16714.8	[illegible]	3100.2	[illegible]	[illegible]	33333.6	[illegible]	2964.2	4261.3	172.8	4220.0	3.16	[illegible]
-0.785	[illegible]	[illegible]	[illegible]	[illegible]	16714.8	[illegible]	3100.2	[illegible]	[illegible]	15634.4	15634.4	8670.5	-6482.4	-6482.4	9842.3	3.55	[illegible]
0.785	[illegible]	[illegible]	[illegible]	[illegible]	16714.8	[illegible]	3100.2	[illegible]	[illegible]	15634.4	15634.4	8670.5	6482.4	6482.4	9842.3	3.95	[illegible]
-0.175	[illegible]	[illegible]	[illegible]	[illegible]	16714.8	[illegible]	3100.2	[illegible]	[illegible]	33333.6	[illegible]	2964.2	-4261.3	-172.8	4220.0	4.34	[illegible]
0.175	[illegible]	[illegible]	[illegible]	[illegible]	16714.8	[illegible]	3100.2	[illegible]	[illegible]	33333.6	[illegible]	2964.2	4261.3	172.8	4220.0	4.74	[illegible]
-0.175	[illegible]	[illegible]	[illegible]	[illegible]	16714.8	[illegible]	3100.2	[illegible]	[illegible]	33333.6	[illegible]	2964.2	-4261.3	-172.8	4220.0	5.13	[illegible]
0.175	[illegible]	[illegible]	[illegible]	[illegible]	16714.8	[illegible]	3100.2	[illegible]	[illegible]	33333.6	[illegible]	2964.2	4261.3	172.8	4220.0	5.53	[illegible]
-0.175	[illegible]	[illegible]	[illegible]	[illegible]	16714.8	[illegible]	3100.2	[illegible]	[illegible]	33333.6	[illegible]	2964.2	-4261.3	-172.8	4220.0	5.92	[illegible]
0.175	[illegible]	[illegible]	[illegible]	[illegible]	16714.8	[illegible]	3100.2	[illegible]	[illegible]	33333.6	[illegible]	2964.2	4261.3	172.8	4220.0	6.32	[illegible]
-0.785	[illegible]	[illegible]	[illegible]	[illegible]	16714.8	[illegible]	3100.2	[illegible]	[illegible]	15634.4	15634.4	8670.5	-6482.4	-6482.4	9842.3	6.71	[illegible]
0.785	[illegible]	[illegible]	[illegible]	[illegible]	16714.8	[illegible]	3100.2	[illegible]	[illegible]	15634.4	15634.4	8670.5	6482.4	6482.4	9842.3	7.11	[illegible]
1.571	[illegible]	[illegible]	[illegible]	[illegible]	16714.8	[illegible]	3100.2	[illegible]	[illegible]	8830.0	34880.5	2210.2	0.0	0.0	3482.0	7.50	[illegible]
0.000	[illegible]	[illegible]	[illegible]	[illegible]	0.0	0.0	0.0	0.0	0.0	0.0	0.0	0.0	0.0	0.0	0.0	0.00	[illegible]
0.000	[illegible]	[illegible]	[illegible]	[illegible]	0.0	0.0	0.0	0.0	0.0	0.0	0.0	0.0	0.0	0.0	0.0	0.00	[illegible]
0.000	[illegible]	[illegible]	[illegible]	[illegible]	0.0	0.0	0.0	0.0	0.0	0.0	0.0	0.0	0.0	0.0	0.0	0.00	[illegible]
0.000	[illegible]	[illegible]	[illegible]	[illegible]	0.0	0.0	0.0	0.0	0.0	0.0	0.0	0.0	0.0	0.0	0.0	0.00	[illegible]
0.000	[illegible]	[illegible]	[illegible]	[illegible]	0.0	0.0	0.0	0.0	0.0	0.0	0.0	0.0	0.0	0.0	0.0	0.00	[illegible]
0.000	[illegible]	[illegible]	[illegible]	[illegible]	0.0	0.0	0.0	0.0	0.0	0.0	0.0	0.0	0.0	0.0	0.0	0.00	[illegible]
0.000	[illegible]	[illegible]	[illegible]	[illegible]	0.0	0.0	0.0	0.0	0.0	0.0	0.0	0.0	0.0	0.0	0.0	0.00	[illegible]
0.000	[illegible]	[illegible]	[illegible]	[illegible]	0.0	0.0	0.0	0.0	0.0	0.0	0.0	0.0	0.0	0.0	0.0	0.00	[illegible]
0.000	[illegible]	[illegible]	[illegible]	[illegible]	0.0	0.0	0.0	0.0	0.0	0.0	0.0	0.0	0.0	0.0	0.0	0.00	[illegible]
0.000	[illegible]	[illegible]	[illegible]	[illegible]	0.0	0.0	0.0	0.0	0.0	0.0	0.0	0.0	0.0	0.0	0.0	0.00	[illegible]
0.000	[illegible]	[illegible]	[illegible]	[illegible]	0.0	0.0	0.0	0.0	0.0	0.0	0.0	0.0	0.0	0.0	0.0	0.00	[illegible]
0.000	[illegible]	[illegible]	[illegible]	[illegible]	0.0	0.0	0.0	0.0	0.0	0.0	0.0	0.0	0.0	0.0	0.0	0.00	[illegible]

A11
41048.1 8

Exx effective 25761.5 (MPa)
Eyy effective 11353.4 (MPa)
Gxy effective 5663.9 (MPa)
vxy effective 0.364

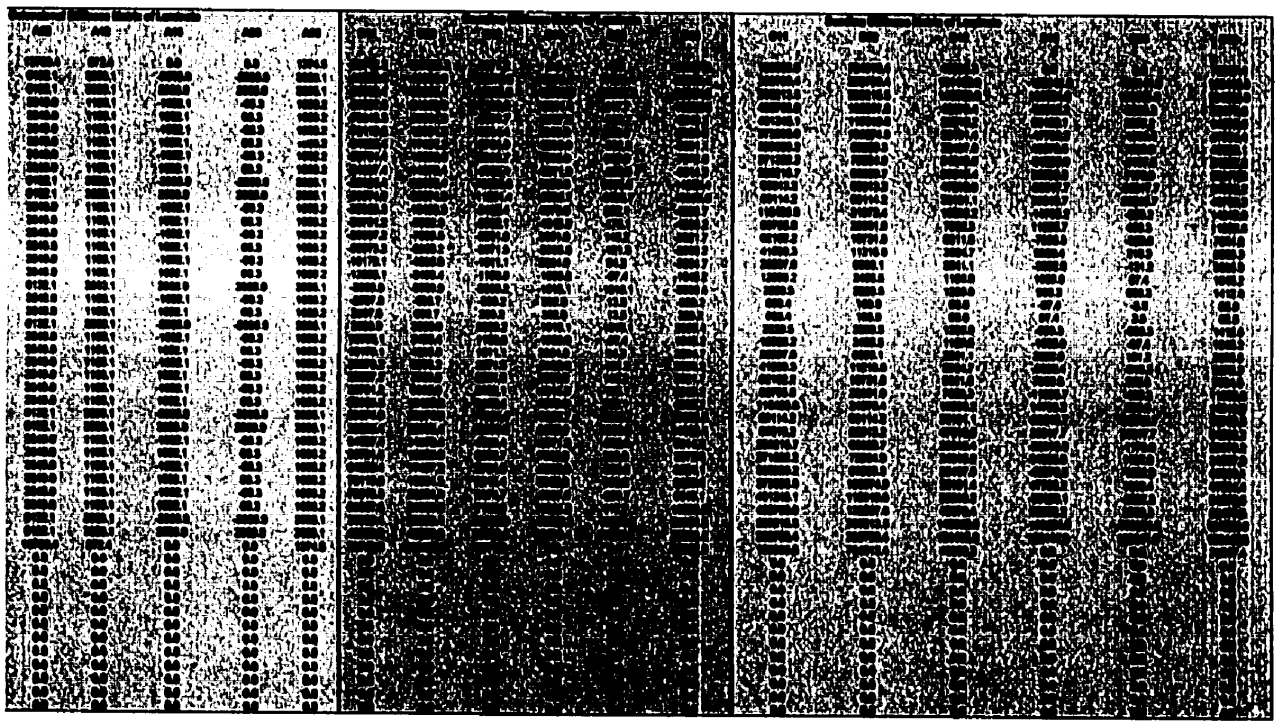

A22	A12	A16	A26	A66	B11	B22	B12	B16	B26	B66	D11	D22	D12	D16	D26	D66
180881.1	65896.8	0.0	0.0	84972.7	0.0	0.0	0.0	8847.0	1360.4	0.0	6718280.8	4213373.8	1313355.2	0.0	0.0	1671062.1

A

410482	65896	0
65896	180881	0
0	0	84973

D

6719281	1313355	0
1313355	4213374	0
0	0	1671052

A'

2.59E-06	-9.43E-07	-1.46E-22
-9.43E-07	5.87E-06	-7.48E-23
-1.46E-22	-7.48E-23	1.18E-05

D'

1.59E-07	-4.94E-08	-9.58E-25
-4.94E-08	2.53E-07	-2.13E-23
-9.58E-25	-2.13E-23	5.99E-07

Calculation of Laminate Properties

Dock Tubes

All input in (N, mm)

50 layer lamina capacity

Resin matrix properties:
Shell Chemical's EPON Resin 828

[illegible]

Fibre properties:
Owens Corning's Type 30 Roving

[illegible]

Total number of layers 8
Total laminate thickness 4.00 [illegible]

Layer Number	t	θ	Fibre volume	Lamina Density	E11	E22	G12	v12	v21
1	0.5	90	0.416	1.75622	32659.5	8384.11	3320.44	0.2467	0.044
2	0.5	45	0.28	1.5716	22540	6378.17	2524.16	0.256	0.072
3	0.5	45	0.28	1.5716	22540	6378.17	2524.16	0.256	0.072
4	0.5	10	0.28	1.5716	22540	6378.17	2524.16	0.256	0.072
5	0.5	10	0.28	1.5716	22540	6378.17	2524.16	0.256	0.072
6	0.5	45	0.28	1.5716	22540	6378.17	2524.16	0.256	0.072
7	0.5	45	0.28	1.5716	22540	6378.17	2524.16	0.256	0.072
8	0.5	90	0.416	1.75622	32659.5	8384.11	3320.48	0.2467	0.044
9	0	0	0	0	0	0.00	0.00	0	0.000
10	0	0	0	0	0	0.00	0.00	0	0.000
11	0	0	0	0	0	0.00	0.00	0	0.000
12	0	0	0	0	0	0.00	0.00	0	0.000
13	0	0	0	0	0	0.00	0.00	0	0.000
14	0	0	0	0	0	0.00	0.00	0	0.000
15	0	0	0	0	0	0.00	0.00	0	0.000
16	0	0	0	0	0	0.00	0.00	0	0.000
17	0	0	0	0	0	0.00	0.00	0	0.000
18	0	0	0	0	0	0.00	0.00	0	0.000
19	0	0	0	0	0	0.00	0.00	0	0.000
20	0	0	0	0	0	0.00	0.00	0	0.000
21	0	0	0	0	0	0.00	0.00	0	0.000
22	0	0	0	0	0	0.00	0.00	0	0.000
23	0	0	0	0	0	0.00	0.00	0	0.000
24	0	0	0	0	0	0.00	0.00	0	0.000
25	0	0	0	0	0	0.00	0.00	0	0.000
26	0	0	0	0	0	0.00	0.00	0	0.000
27	0	0	0	0	0	0.00	0.00	0	0.000
28	0	0	0	0	0	0.00	0.00	0	0.000
29	0	0	0	0	0	0.00	0.00	0	0.000
30	0	0	0	0	0	0.00	0.00	0	0.000
31	0	0	0	0	0	0.00	0.00	0	0.000
32	0	0	0	0	0	0.00	0.00	0	0.000
33	0	0	0	0	0	0.00	0.00	0	0.000
34	0	0	0	0	0	0.00	0.00	0	0.000
35	0	0	0	0	0	0.00	0.00	0	0.000
36	0	0	0	0	0	0.00	0.00	0	0.000
37	0	0	0	0	0	0.00	0.00	0	0.000
38	0	0	0	0	0	0.00	0.00	0	0.000
39	0	0	0	0	0	0.00	0.00	0	0.000
40	0	0	0	0	0	0.00	0.00	0	0.000
41	0	0	0	0	0	0.00	0.00	0	0.000
42	0	0	0	0	0	0.00	0.00	0	0.000
43	0	0	0	0	0	0.00	0.00	0	0.000
44	0	0	0	0	0	0.00	0.00	0	0.000
45	0	0	0	0	0	0.00	0.00	0	0.000
46	0	0	0	0	0	0.00	0.00	0	0.000
47	0	0	0	0	0	0.00	0.00	0	0.000
48	0	0	0	0	0	0.00	0.00	0	0.000
49	0	0	0	0	0	0.00	0.00	0	0.000
50	0	0	0	0	0	0.00	0.00	0	0.000

θ (radians)	[illegible]	[illegible]	[illegible]	[illegible]	U1	U2	U3	U4	U5	Qb11	Qb22	Qb12	Qb16	Qb26	Qb66	h	[illegible]
																-2.00	
1.571	[illegible]	[illegible]	[illegible]	[illegible]	17088.4	[illegible]	[illegible]	[illegible]	[illegible]	46110.4	33177.4	2118.8	0.0	0.0	3320.7	-1.50	[illegible]
-0.785	[illegible]	[illegible]	[illegible]	[illegible]	12727.2	[illegible]	[illegible]	[illegible]	[illegible]	10722.1	10722.1	9873.8	-4116.8	-4116.8	8634.3	-1.00	[illegible]
0.785	[illegible]	[illegible]	[illegible]	[illegible]	12727.2	[illegible]	[illegible]	[illegible]	[illegible]	10722.1	10722.1	9873.8	4116.8	4116.8	8634.3	-0.50	[illegible]
-0.175	[illegible]	[illegible]	[illegible]	[illegible]	12727.2	[illegible]	[illegible]	[illegible]	[illegible]	22000.3	[illegible]	2132.8	[illegible]	-110.2	7003.3	0.00	[illegible]
0.175	[illegible]	[illegible]	[illegible]	[illegible]	12727.2	[illegible]	[illegible]	[illegible]	[illegible]	22000.3	[illegible]	2132.8	[illegible]	110.2	7003.3	0.50	[illegible]
-0.785	[illegible]	[illegible]	[illegible]	[illegible]	12727.2	[illegible]	[illegible]	[illegible]	[illegible]	10722.1	10722.1	9873.8	-4116.8	-4116.8	8634.3	1.00	[illegible]
0.785	[illegible]	[illegible]	[illegible]	[illegible]	12727.2	[illegible]	[illegible]	[illegible]	[illegible]	10722.1	10722.1	9873.8	4116.8	4116.8	8634.3	1.50	[illegible]
1.571	[illegible]	[illegible]	[illegible]	[illegible]	17088.4	[illegible]	[illegible]	[illegible]	[illegible]	46110.4	33177.4	2118.8	0.0	0.0	3320.7	2.00	[illegible]
0.000	0.0	0.0	0.0	0.0	0.0	0.0	0.0	0.0	0.0	0.0	0.0	0.0	0.0	0.0	0.0	0.00	0.0
0.000	0.0	0.0	0.0	0.0	0.0	0.0	0.0	0.0	0.0	0.0	0.0	0.0	0.0	0.0	0.0	0.00	0.0
0.000	0.0	0.0	0.0	0.0	0.0	0.0	0.0	0.0	0.0	0.0	0.0	0.0	0.0	0.0	0.0	0.00	0.0
0.000	0.0	0.0	0.0	0.0	0.0	0.0	0.0	0.0	0.0	0.0	0.0	0.0	0.0	0.0	0.0	0.00	0.0
0.000	0.0	0.0	0.0	0.0	0.0	0.0	0.0	0.0	0.0	0.0	0.0	0.0	0.0	0.0	0.0	0.00	0.0
0.000	0.0	0.0	0.0	0.0	0.0	0.0	0.0	0.0	0.0	0.0	0.0	0.0	0.0	0.0	0.0	0.00	0.0
0.000	0.0	0.0	0.0	0.0	0.0	0.0	0.0	0.0	0.0	0.0	0.0	0.0	0.0	0.0	0.0	0.00	0.0
0.000	0.0	0.0	0.0	0.0	0.0	0.0	0.0	0.0	0.0	0.0	0.0	0.0	0.0	0.0	0.0	0.00	0.0
0.000	0.0	0.0	0.0	0.0	0.0	0.0	0.0	0.0	0.0	0.0	0.0	0.0	0.0	0.0	0.0	0.00	0.0
0.000	0.0	0.0	0.0	0.0	0.0	0.0	0.0	0.0	0.0	0.0	0.0	0.0	0.0	0.0	0.0	0.00	0.0
0.000	0.0	0.0	0.0	0.0	0.0	0.0	0.0	0.0	0.0	0.0	0.0	0.0	0.0	0.0	0.0	0.00	0.0
0.000	0.0	0.0	0.0	0.0	0.0	0.0	0.0	0.0	0.0	0.0	0.0	0.0	0.0	0.0	0.0	0.00	0.0
0.000	0.0	0.0	0.0	0.0	0.0	0.0	0.0	0.0	0.0	0.0	0.0	0.0	0.0	0.0	0.0	0.00	0.0
0.000	0.0	0.0	0.0	0.0	0.0	0.0	0.0	0.0	0.0	0.0	0.0	0.0	0.0	0.0	0.0	0.00	0.0
0.000	0.0	0.0	0.0	0.0	0.0	0.0	0.0	0.0	0.0	0.0	0.0	0.0	0.0	0.0	0.0	0.00	0.0
0.000	0.0	0.0	0.0	0.0	0.0	0.0	0.0	0.0	0.0	0.0	0.0	0.0	0.0	0.0	0.0	0.00	0.0
0.000	0.0	0.0	0.0	0.0	0.0	0.0	0.0	0.0	0.0	0.0	0.0	0.0	0.0	0.0	0.0	0.00	0.0
0.000	0.0	0.0	0.0	0.0	0.0	0.0	0.0	0.0	0.0	0.0	0.0	0.0	0.0	0.0	0.0	0.00	0.0
0.000	0.0	0.0	0.0	0.0	0.0	0.0	0.0	0.0	0.0	0.0	0.0	0.0	0.0	0.0	0.0	0.00	0.0
0.000	0.0	0.0	0.0	0.0	0.0	0.0	0.0	0.0	0.0	0.0	0.0	0.0	0.0	0.0	0.0	0.00	0.0
0.000	0.0	0.0	0.0	0.0	0.0	0.0	0.0	0.0	0.0	0.0	0.0	0.0	0.0	0.0	0.0	0.00	0.0
0.000	0.0	0.0	0.0	0.0	0.0	0.0	0.0	0.0	0.0	0.0	0.0	0.0	0.0	0.0	0.0	0.00	0.0
0.000	0.0	0.0	0.0	0.0	0.0	0.0	0.0	0.0	0.0	0.0	0.0	0.0	0.0	0.0	0.0	0.00	0.0
0.000	0.0	0.0	0.0	0.0	0.0	0.0	0.0	0.0	0.0	0.0	0.0	0.0	0.0	0.0	0.0	0.00	0.0
0.000	0.0	0.0	0.0	0.0	0.0	0.0	0.0	0.0	0.0	0.0	0.0	0.0	0.0	0.0	0.0	0.00	0.0
0.000	0.0	0.0	0.0	0.0	0.0	0.0	0.0	0.0	0.0	0.0	0.0	0.0	0.0	0.0	0.0	0.00	0.0
0.000	0.0	0.0	0.0	0.0	0.0	0.0	0.0	0.0	0.0	0.0	0.0	0.0	0.0	0.0	0.0	0.00	0.0
0.000	0.0	0.0	0.0	0.0	0.0	0.0	0.0	0.0	0.0	0.0	0.0	0.0	0.0	0.0	0.0	0.00	0.0
0.000	0.0	0.0	0.0	0.0	0.0	0.0	0.0	0.0	0.0	0.0	0.0	0.0	0.0	0.0	0.0	0.00	0.0
0.000	0.0	0.0	0.0	0.0	0.0	0.0	0.0	0.0	0.0	0.0	0.0	0.0	0.0	0.0	0.0	0.00	0.0
0.000	0.0	0.0	0.0	0.0	0.0	0.0	0.0	0.0	0.0	0.0	0.0	0.0	0.0	0.0	0.0	0.00	0.0
0.000	0.0	0.0	0.0	0.0	0.0	0.0	0.0	0.0	0.0	0.0	0.0	0.0	0.0	0.0	0.0	0.00	0.0
0.000	0.0	0.0	0.0	0.0	0.0	0.0	0.0	0.0	0.0	0.0	0.0	0.0	0.0	0.0	0.0	0.00	0.0
0.000	0.0	0.0	0.0	0.0	0.0	0.0	0.0	0.0	0.0	0.0	0.0	0.0	0.0	0.0	0.0	0.00	0.0
0.000	0.0	0.0	0.0	0.0	0.0	0.0	0.0	0.0	0.0	0.0	0.0	0.0	0.0	0.0	0.0	0.00	0.0
0.000	0.0	0.0	0.0	0.0	0.0	0.0	0.0	0.0	0.0	0.0	0.0	0.0	0.0	0.0	0.0	0.00	0.0
0.000	0.0	0.0	0.0	0.0	0.0	0.0	0.0	0.0	0.0	0.0	0.0	0.0	0.0	0.0	0.0	0.00	0.0
0.000	0.0	0.0	0.0	0.0	0.0	0.0	0.0	0.0	0.0	0.0	0.0	0.0	0.0	0.0	0.0	0.00	0.0
0.000	0.0	0.0	0.0	0.0	0.0	0.0	0.0	0.0	0.0	0.0	0.0	0.0	0.0	0.0	0.0	0.00	0.0
0.000	0.0	0.0	0.0	0.0	0.0	0.0	0.0	0.0	0.0	0.0	0.0	0.0	0.0	0.0	0.0	0.00	0.0
0.000	0.0	0.0	0.0	0.0	0.0	0.0	0.0	0.0	0.0	0.0	0.0	0.0	0.0	0.0	0.0	0.00	0.0
0.000	0.0	0.0	0.0	0.0	0.0	0.0	0.0	0.0	0.0	0.0	0.0	0.0	0.0	0.0	0.0	0.00	0.0

A11
[illegible]

Exx effective	11946.9	[illegible]
Eyy effective	14039.9	[illegible]
Gxy effective	4806.8	[illegible]
vxy effective	0.252	

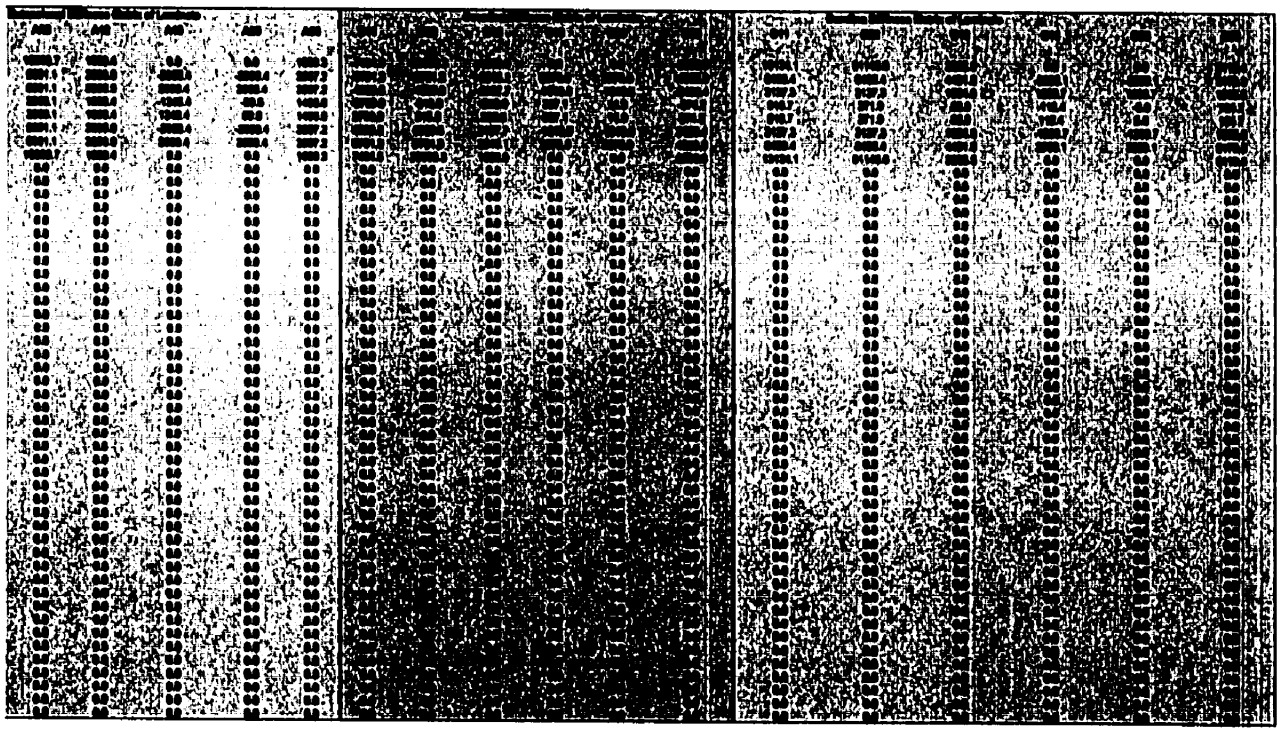

A22	A12	A16	A26	A66	B11	B22	B12	B16	B26	B66	D11	D22	D12	D16	D26	D66
61147.8	15599.2	0.0	0.0	19382.6	0.0	0.0	0.0	2732.8	2099.2	0.0	51332.8	126072.2	19003.8	0.0	0.0	24645.8

A

51984	15599	0
15599	61148	0
0	0	19383

D

51333	19004	0
19004	126072	0
0	0	24646

A'

2.09E-05	-5.27E-06	4.05E-22
-5.27E-06	1.77E-05	-1.56E-21
4.05E-22	-1.56E-21	5.20E-05

D'

2.08E-05	-3.09E-06	5.22E-22
-3.09E-06	8.41E-06	-1.60E-21
5.22E-22	-1.60E-21	4.09E-05

Theoretical Deck Stiffness
Seven-Tube Modules

Material Properties

Plates					
Ef	72400 MPa	Em	3150 MPa	$Ex_{,n}$	25761 5 MPa
Gf	29431 MPa	Gm	1245 MPa	$Ey_{,n}$	11353 4 MPa
vf	0 22	vm	0 27	$v_{,n}$	0 364
vf	0 45				
Unidirectional thickness	0 39 mm				
Design total thickness	15 00 mm				
Filament wound tubes					
Ef	72400 MPa	Em	3150 MPa	$Ex_{,n}$	11946 9 MPa
Gf	29431 MPa	Gm	1245 MPa	$Ey_{,n}$	14099 9 MPa
vf	0 22	vm	0 27	$v_{,n}$	0 252
vf +/-45	0 28				
vf +/-10	0 28				
vf 90	0 426				
thickness +/-45	0 5 mm				
thickness +/-10	0 5 mm				
90 thickness	0 5 mm				
Total thickness	4 00				
Pultruded Filler Bars					
E	50516 MPa				

Geometric Properties

Total height	220 0 mm
Top plate thickness	15 0 mm
Bottom plate thickness	15 0 mm
Tube thickness	4 0 mm
Triangle height	190 0 mm
Triangle width	219 4 mm
Bottom plate width	920 0 mm
Top plate width	1080 0 mm
Filler bar area	432 0 mm
Filler bar height	19 1 mm
Local filler bar centroid	8 6 mm

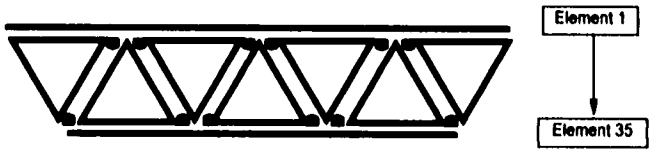

Element Number	Element Description	Width	Height	Area	n_i	Distance to local centroid from bottom	Area*y_i	$\lvert y_{bar}-y_i \rvert$	I_{local}	$I_{global\ n\text{-}equivalent}$
1	Top plate	1080.0	15.0	16200.1	2.156	212.5	3442526.6	96.4	303757.3	325212027.8
2	Filler bar	-	19.1	432.0	4.228	196.4	84817.7	80.2	11285.4	11809896.2
3	Filler bar	-	19.1	432.0	4.228	196.4	84817.7	80.2	11285.4	11809896.2
4	Filler bar	-	19.1	432.0	4.228	196.4	84817.7	80.2	11285.4	11809896.2
5	Filler bar	-	19.1	432.0	4.228	196.4	84817.7	80.2	11285.4	11809896.2
6	Filler bar	-	19.1	432.0	4.228	196.4	84817.7	80.2	11285.4	11809896.2
7	Filler bar	-	19.1	432.0	4.228	196.4	84817.7	80.2	11285.4	11809896.2
8	Horiz. tube	219.4	4.0	877.6	1.000	203.0	178146.9	86.9	1170.1	6626581.6
9	Horiz. tube	219.4	4.0	877.6	1.000	203.0	178146.9	86.9	1170.1	6626581.6
10	Horiz. tube	219.4	4.0	877.6	1.000	203.0	178146.9	86.9	1170.1	6626581.6
11	Horiz. tube	219.4	4.0	877.6	1.000	203.0	178146.9	86.9	1170.1	6626581.6
12	Inclined tube	219.4	4.0	877.6	1.000	110.0	96532.8	6.1	2640312.9	2673083.0
13	Inclined tube	219.4	4.0	877.6	1.000	110.0	96532.8	6.1	2640312.9	2673083.0
14	Inclined tube	219.4	4.0	877.6	1.000	110.0	96532.8	6.1	2640312.9	2673083.0
15	Inclined tube	219.4	4.0	877.6	1.000	110.0	96532.8	6.1	2640312.9	2673083.0
16	Inclined tube	219.4	4.0	877.6	1.000	110.0	96532.8	6.1	2640312.9	2673083.0
17	Inclined tube	219.4	4.0	877.6	1.000	110.0	96532.8	6.1	2640312.9	2673083.0
18	Inclined tube	219.4	4.0	877.6	1.000	110.0	96532.8	6.1	2640312.9	2673083.0
19	Inclined tube	219.4	4.0	877.6	1.000	110.0	96532.8	6.1	2640312.9	2673083.0
20	Inclined tube	219.4	4.0	877.6	1.000	110.0	96532.8	6.1	2640312.9	2673083.0
21	Inclined tube	219.4	4.0	877.6	1.000	110.0	96532.8	6.1	2640312.9	2673083.0
22	Inclined tube	219.4	4.0	877.6	1.000	110.0	96532.8	6.1	2640312.9	2673083.0
23	Inclined tube	219.4	4.0	877.6	1.000	110.0	96532.8	6.1	2640312.9	2673083.0
24	Inclined tube	219.4	4.0	877.6	1.000	110.0	96532.8	6.1	2640312.9	2673083.0
25	Inclined tube	219.4	4.0	877.6	1.000	110.0	96532.8	6.1	2640312.9	2673083.0
26	Horiz. tube	219.4	4.0	877.6	1.000	17.0	14918.8	99.1	1170.1	8621488.0
27	Horiz. tube	219.4	4.0	877.6	1.000	17.0	14918.8	99.1	1170.1	8621488.0
28	Horiz. tube	219.4	4.0	877.6	1.000	17.0	14918.8	99.1	1170.1	8621488.0
29	Filler bar	-	19.1	432.0	4.228	23.6	10211.3	92.5	11285.4	15665365.9
30	Filler bar	-	19.1	432.0	4.228	23.6	10211.3	92.5	11285.4	15665365.9
31	Filler bar	-	19.1	432.0	4.228	23.6	10211.3	92.5	11285.4	15665365.9
32	Filler bar	-	19.1	432.0	4.228	23.6	10211.3	92.5	11285.4	15665365.9
33	Filler bar	-	19.1	432.0	4.228	23.6	10211.3	92.5	11285.4	15665365.9
34	Filler bar	-	19.1	432.0	4.228	23.6	10211.3	92.5	11285.4	15665365.9
35	Bottom plate	920.0	15.0	13800.1	2.156	7.5	103501.7	108.6	258756.2	351588050.6
Sum:				53612.6			6225006.0			931445602.8

y_{bar}	116.11	mm	*(with respect to bottom of section)*
$I_{local\ x\text{-}tube}$	3520027.10	mm^4	
$I_{local\ y\text{-}tube}$	1170.10	mm^4	
$I_{local\ tube}$	2640312.85	mm^4	
$I_{local\ bar}$	11285.38	mm^4	
I_{final}	931445602.8	mm^4	

Theoretical P/Δ

20.130 kN/mm

CHAPTER SIX:

CONCLUSION

A total of nine full-scale modular GFRP bridge decks have been tested in flexure up to failure. The experimental program consisted of two phases. The first phase was a series of tests of three-tube prototype deck modules. Based on the performance and behaviour of these initial tests, a second, large-scale phase was undertaken. In this phase, the manufacturing process was modified to enhance deck behaviour and eliminate problems encountered in the first phase of testing. The modules produced for the second phase were similar to those of the first phase, but incorporated seven filament wound tubes, instead of three, producing a wider module.

Based on the results of the first three-tube GFRP modules, the following conclusions can be made:

1. All decks displayed linear load-deflection behaviour until the initiation of first cracking, which was marked by a loud sound and loss of stiffness.
2. Some of the pultruded GFRP bars used as filler in the decks slipped in most of the tested specimens, causing a sudden load drop.
3. The decks displayed virtually the same stiffness by loading and reloading within the service load range. This behaviour suggests possible good performance under cyclic loading conditions.
4. After complete unloading, the decks experienced small permanent deformation in the range of 2 to 5 mm.
5. All decks failed at load levels exceeding the factored wheel load of an HS30 truck specified by AASHTO specifications.
6. The most prominent mode of failure in the first phase specimens was buckling and delamination of the outer plates.
7. After complete delamination and removal of one or both of the outer plates, the decks maintained considerable load capacity.
8. None of the specimens tested in Phase I satisfied the deflection requirements for bridge decks of *L/360* at service load. The deck that was closest to satisfying these requirements experienced a deflection of *L/163* at a service load of 139 kN.
9. The applied load was well distributed along the width of the deck as evident by the uniform distribution of the measured axial strain along the top and bottom plates.
10. At failure, the bottom plate did not reach the ultimate strain capacity of the material. In all cases, the remaining strain capacity was in the range of 50 to 60 percent of the ultimate strength of the material.

11. The specimens tested in Phase I did not meet the creep rupture requirements. At an equivalent service sustained load, the induced strain exceeded the limits set for creep rupture.

Based on the experience gained from the first phase, which led to significant modification in the fabrication process, the following summarizes the findings of the second phase test results:

1. The decks demonstrated linear behaviour up to much higher loads than those measured for Phase I. Loss of stiffness occurred due to cracking of the resin.
2. Initial failure occurred due to delamination of the tubes between the wet-wound and dry-wound layers, followed by final failure caused by slippage of the tubes at one end of the span.
3. The measured ultimate loads exceeded the 500 kN range. Failure due to buckling of the plates and slippage of the filler bars was prevented.
4. The final deck tested met the maximum deflection limit of *L/360*. Its deflection was *L/380* at service loading conditions.
5. The strain across the width of the deck was well distributed.
6. The maximum axial strain at ultimate load was much less than that measured in the decks of the first phase. The decks of Phase II had at least 85 percent reserve strain capacity in tension at failure. This behaviour indicates that the method of manufacturing used for Phase II specimens produced a more efficient product.

7. The modules displayed strains well under the maximum strain level recommended to avoid the possibility of creep rupture.
8. Axial strain across the width of the deck was consistently uniform, indicating that the entire width of the deck was subject to the same load and that the individual tubes were subjected to equal load levels. This behaviour also demonstrates the efficiency achieved for this second generation of bridge decks.

The analytical model developed was used to predict the load-deflection behaviour of the decks within the service load range. Using this model, the following conclusions can be made:

1. The model predicted the behaviour very well for all of the decks tested in Phase I, with a maximum difference of about 9 percent.
2. The model also predicted the behaviour of the Phase II decks well, with a maximum difference of 25 percent. This difference was due to manufacturing problems experienced in fabricating the first deck, which produced significant void space in the section. The second deck tested in Phase II was within 8 percent of the predicted stiffness value.
3. Manipulation of the model allowed determination of the individual contribution of each component of the deck. The analysis indicated that the plates contributed at least two-thirds of the total stiffness in both Phase I and Phase II specimens.

The behaviour of the decks from this testing program was compared with that of other, similar FRP decks tested elsewhere. This comparison produced the following findings:

1. The F7-series decks provided smaller deflections at HS20 service loads in comparison to a similar deck designed by Virginia Tech. using pultruded products. Ultimate load capacity also exceeded that of the Virginia Tech. deck.
2. The F7-series of decks also surpassed the failure load of a similar deck produced using the SCRIMP method for fabrication of GFRP bridge decks.

Despite the rapid development and achievements made in the course of this project, a considerable amount of research needs to be undertaken prior to field application of this product.

Future research should consider modification of the fabrication process to incorporate a filament wound overwrap around the entire deck section. The testing program should also include cyclic loading conditions to simulate actual load cycles on the bridge.

Based on completion of the deck modules, the research should focus on the development of appropriate connections between the deck modules themselves and between the modules and the supporting girders.

This project has provided a strong foundation for future development of FRP deck technology. It followed a new concept from the design stage to the manufacturing phase,

to full-scale testing in the lab. With the promising results backing this sound product, the progression from lab testing to field implementation should be seriously considered. Upon implementation of FRP deck technology, highway infrastructure's demand for an efficient, durable bridge deck will have been met, and far surpassed.

Internet References:

• "Bridges." Owens Corning. Summer 1999.
http://www.owenscorning.com/owens/composites/applications/infra/bridge.html
June 17, 1999

• "Composite Technology." Martin Marietta Materials. Summer 1999.
http://www.martinmarietta.com/corpsite/about_mmm/technologies/tl_comp_technology.asp,
June 24, 1999

• "New Bridge for Bikers on Ohio to Erie Trail." April 24, 1998.
http://www.creativepultrusions.com/PressRel/042498.htm, September 13, 1999

• Niehaus, John. "NCC Seeking Millions for Bridge Project." *Dayton-Miami Business News*. June 14, 1999.
http://www.amcity.com/dayton/stories/1999/06/14/story3.html, June 17, 1999

• "Superdeck™ Product." Creative Pultrusions Inc. Summer 1999.
http://www.creativepultrusions.com/psprdeck.htm, September 13, 1999

Journal Articles and Texts:

• American Association of State Highway and Transportation Officials, *LRFD Bridge Design Specifications*, 1998, p.2-12;

• Aref, A., Parsons, I.D., "Design and Analysis Procedures for a Novel Fiber Reinforced Plastic Bridge Deck," *2nd International Advanced Composite Materials in Bridges and Structures Conference,* August 1996, pp. 743-750.

• Aref, A.J., Parsons, I.D., White, S. "Manufacture, Design and Performance of a Modular Fiber Reinforced Plastic Bridge," *31st International SAMPE Technical Conference,* October 1999, pp. 581-591.

• Black, Sara, "A Survey of Composite Bridges," *Composites Technology*, April-May 2000, pp. 14-18

• Daniel, Isaac M.; Ishai, Ori, "Engineering Mechanics of Composite Materials," Oxford University Press, 1994, 395 pgs.

• Hayes, Michael D.; Ohanehi, Don; Lesko, John J.; Cousins, Thomas E.; Witcher, Dan, "Performance of Tube and Plate Fiberglass Composite Bridge Deck," *Journal of Composites for Construction*, Vol. 4, No. 2, May 2000, pp. 48-55.

• Karbhari, V.M., "Fiber Reinforced Composite Decks for Infrastructure Renewal," *2nd International Advanced Composite Materials in Bridges and Structures Conference*, August 1996, pp. 759-766

• Mallick, P.K., "Fiber-Reinforced Composites: Materials, Manufacturing and Design," Dekker, 1993, 566 pgs.

• Marshall Industries Composites, "C-BAR Reinforcing Rods: The Future of Reinforcement," Product Data Sheet, Lima, Ohio, www.c-bar.com.

• "Scrimping Saves Money and Time," *Composites Technology,* September-October 1999, pp. 21-28.

• Salim, Hani A.; Davalos, Julio F.; Qiao, Pizhong; Kiger, Sam A. "Analysis and Design of Fiber Reinforced Plastic Composite Deck-and-Stringer Bridges," *Composite Structres*, Vol. 38, No. 1-4, 1997, pp. 295-307.

• Zureick, A.H.; Shih, B.; Munley, E., "Fiber-Reinforced Polymeric Bridge Decks," *Structural Engineering Review*, Vol. 7, No. 3, 1995, pp. 257-266.

• Zureick, A., "Fibre-Reinforced Polymeric Bridge Decks," *ACUN2* (handout from a talk), February 2000.